DEVIATOR BEHAVIOR IN EXTERNALLY POST-TENSIONED BRIDGES

by

LISA LOUISE CARTER, B.S.C.E.

THESIS

Presented to the Faculty of the Graduate School of

The University of Texas at Austin

in Partial Fulfillment

of the Requirements

for the Degree of

MASTER OF SCIENCE IN ENGINEERING

THE UNIVERSITY OF TEXAS AT AUSTIN

August 1987

ACKNOWLEDGEMENTS

This research program was conducted at the Phil M. Ferguson Structural Engineering Laboratory at the Balcones Research Center of the University of Texas at Austin. Funding for the project was provided by the Texas Department of Highways and Public Transportation, Project No. 3-5-85-365. The advice and assistance of Mr. Alan Matejowsky, the Highway Department liason for the project, was greatly appreciated.

Dr. John E. Breen and Dr. and Micheal E. Kreger directed the project. I would like to express my heartfelt gratitude to Dr. Breen, whose great patience and wise counsel contributed not only to my education as an engineer but as a person as well. I would also like to extend warm thanks to Dr. Kreger for his invaluable comments and suggestions plus his helpful ability to balance thoroughness with practicality.

Without the dedication and hard work of all of the staff at Ferguson Laboratory, research activity at the lab would be difficult if not impossible. I would particularly like to thank Mr. Gorham Hinckley, not only for his practical assistance, but for his moral support throughout this endeavor. In addition, I am extremely grateful to Dick Marshall, Blake Stassney, Pat Ball, Sharon Cunningham, Alex Tahmassebi, Laurie Golding and Maxine DeButts for both their technical assistance and their kind consideration.

To Richard Beaupre and Guillermo Ramirez I owe many thanks. They provided tremendous assistance and support throughout the testing phase of the project. I wish them both success with their own studies.

One of the most gratifying rewards of working at the Ferguson Laboratory was the oppurtunity to share the experience with a unique group of diversified, talented and genuinely fine people. The friendships that were made in the process will always be cherished. A few individuals I would particularly like to mention are Leo Linbeck, III, David Sanders, Bob MacGregor, Paul Tikalsky, David Yates and Patty Gaynor. The care and support they offerred me are warmly appreciated and fondly remembered.

Special thanks also goes to Ms. Sandra Pederson, for her support and friendship over the past years. It was her influence that helped me maintain good spirits and a healthy balance of hard work and relaxation.

I will always be grateful to my fiance, David Powell. His love and support were a constant source of strength through a trying period of my life. Thank you, David, for helping me learn that through teamwork, perseverance and faith, the seemingly impossible is well within reach.

Finally, my deepest thanks goes to my parents, Louise and Robert Carter. It is to them that I owe all my acheivements.

Their unrelenting encouragement, support and praise has given me the confidence I needed to pursue my goals. They will always have my deepest love and devotion.

Lisa Louise Carter

July 10, 1987
Austin, Texas

TABLE OF CONTENTS

TABLE OF CONTENTS (continued)

TABLE OF CONTENTS (continued)

TABLE OF CONTENTS (continued)

TABLE OF CONTENTS (continued)

LIST OF TABLES

L I S T O F F I G U R E S

CHAPTER 1

INTRODUCTION

1.1 Background

The development of post-tensioned concrete box girder bridges in the U.S. has progressed at a remarkable rate. The introduction of segmental technology, with its time-saving and economic advantages, has resulted in the predominance of segmental prestressed box girder construction for medium to moderately long span bridges. An important recent development in U.S. box girder bridge construction is the use of external post-tensioning tendons (tendons external to the concrete cross section), as opposed to traditional internal tendons which are contained in ducts within the webs or flanges. The United States' first externally post-tensioned concrete box girder structure, the Long Key bridge, was completed in 1980. Long Key, and three other externally post-tensioned bridges linking the Florida Keys, were designed by Figg and Muller Engineers, Inc. Since 1980, a significant number of these bridges have been built and many more are in design and planning stages. At the present time, the Texas Department of Highways and Public Transportation is involved in a four-part project to construct several miles of elevated highway through San Antonio. A segmental precast box girder with external tendons is being used throughout.

"Internal post-tensioning" refers to the practice of embedding tendon ducts, in straight or draped patterns as required by design, within the webs and flanges of the box girder section. This practice requires time-consuming placing and securing of the ducts inside the box girder reinforcing cage. The presence of multiple ducts often results in congestion and interference with the reinforcing cage (Fig. 1.1). After the concrete is placed and cured, or after precast segments are assembled, the tendons are pulled through the embedded ducts and then stressed. After post-tensioning, the ducts are normally cement grouted. The grout bonds the tendon to the duct and the concrete, and provides corrosion protection for the tendon.

"External post-tensioning" implies that the tendons are removed from the webs and flanges of the concrete section, and are relocated inside the void of the box girder, or between the webs of non-box girders. The draped profile is maintained by passing the tendons through deviation devices cast monolithically with the webs and/or flanges at discrete points along the span. These "deviators" vary in shape and size, though the most common form is a small block or saddle located at the junction of the web and flange of the box girder section. Anchorages for the external tendons are usually placed in thick diaphragms situated over the piers, although blister anchorages are sometimes used at intermediate points within a span. Tendons typically overlap at

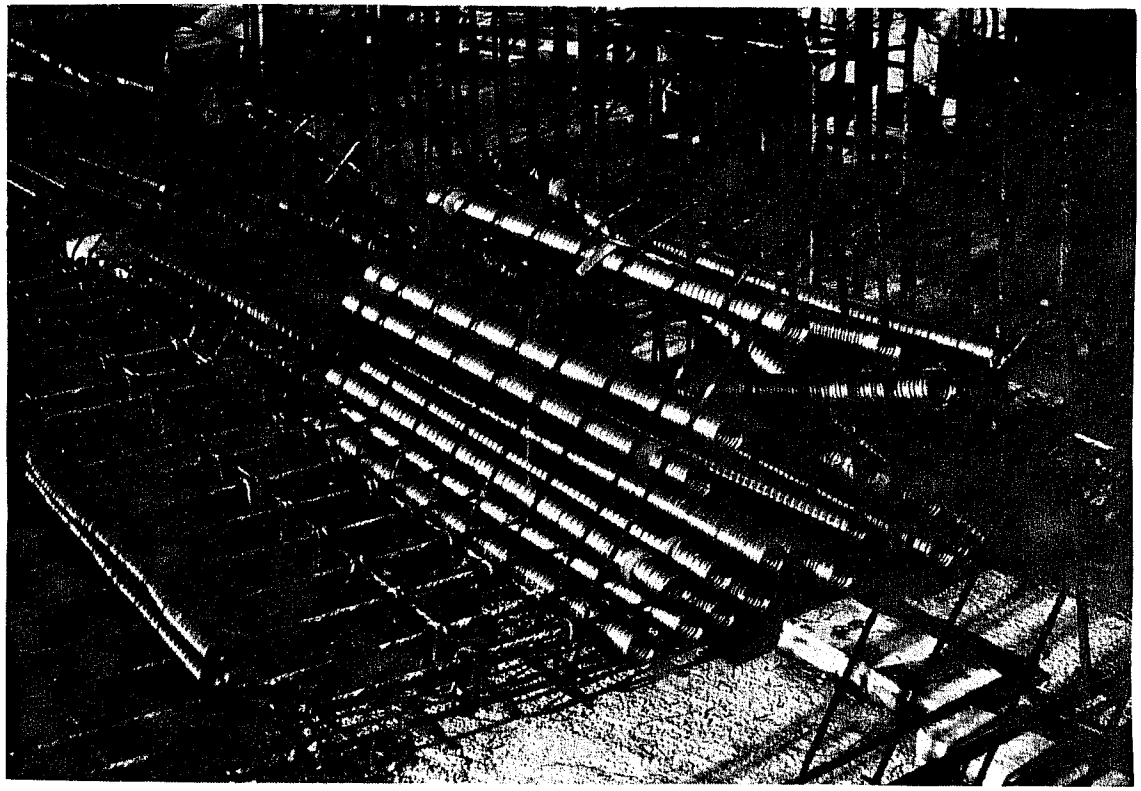

Figure 1.1 Congestion of Ducts for Internal Tendons

diaphragm anchorages for continuity. The cut-away view of the Long Key bridge in Fig. 1.2 clearly illustrates the concept of external post-tensioning. The only positive connection of the external tendon to the concrete section occurs at anchorages and deviators. Between attachment points, the exposed tendon is enclosed in sheathing, typically polyethylene tubing. The tendon is usually grouted along its entire length for protection against corrosion. External tendons are considered unbonded since the majority of the tendon is not bonded to the concrete section and the strains in the tendon are independent of the strains in the adjacent concrete sections.

The behavior of bridges constructed using external tendons and subjected to overload has not been thoroughly documented. Uncertainty also exists concerning the proper design criteria and methodology for deviation details. A study is currently being conducted in the Ferguson Laboratory to explore these topics. The scope includes testing of a scale model of a three-span externally post-tensioned precast segmental box girder bridge. The related program described herein is part of a satellite study to evaluate and test current deviation details and develop design procedures and criteria for deviators.

1.2 Objective and Scope

The primary objectives of the study presented in this report are threefold. The first is to evaluate the current state of the art of external tendon details in order to provide background and direction for the main project as well as the satellite study. The second is to develop testing facilities and procedures for evaluation of deviation details. The third is to explore the mechanisms for load resistance in typical existing deviator details.

1.2.1 Literature Review. Experimental research in the area of external post-tensioning for bridges is just beginning in this country, although research efforts in Europe, especially in France, have been underway for some time. In fact, although external post-tensioning is a very recent development in the United States, the concept has been incorporated in a number of European structures over the last several decades. The object of the literature review is to trace the development of the use of external tendons, citing both successes and problems that have been experienced from inception to the present. Such information provides insight to the current state of the art and points to uncertainties that could benefit from experimental investigation.

1.2.2 Experimental Program. The scope of the experimental program includes the design and construction of a generalized test setup and testing of two representative deviator

specimens. The objective is to provide a launching point for a series of model tests that will eventually result in the refinement of deviator design and detailing, and lead to accurate modelling of deviators for analysis. More immediate objectives are to determine the relative safety of the most typical deviator detail which has already been incorporated in existing bridges and to suggest possible analysis methods based on preliminary results. These objectives are more completely outlined in Chapter 3, Sec. 3.1.

1.3 Summary of Following Chapters

The body of this thesis is organized in the following way:

Chapter 2 contains an extensive review of available literature on the subject of external post-tensioning, with emphasis on deviation details. It includes descriptions of the earliest uses of external tendons, and follows the development through modern structures. Advantages and disadvantages of external post-tensioning are discussed in Sec. 2.3. Sections 2.4 and 2.5 are concerned with deviators only, and include descriptions of typical deviation details and problems that have been experienced in actual structures. The last section in Chapter 2 summarizes all of the completed and ongoing research efforts regarding external tendons that are known to date.

Chapters 3 through 6 cover the experimental program, from inception through execution. Test results are presented in Chapter 6 as well as some preliminary analyses.

The final chapter presents a brief summary of the work contained herein and offers conclusions and interim recommendations based on the results of the two deviator tests.

C H A P T E R 2

STATE OF THE ART

2.1 Introduction

In undertaking an investigation into a new area, the first logical step is to assess the developments that have led up to the current state of the art. Such assessments provide direction for a research program.

An attempt has been made to glean information from all possible sources. This included detailed and in-depth review of all available literature on the subject of external post-tensioning, personal interviews with key figures in the industry and academia who have been directly involved with the subject, and first-hand visits to project sites where external tendons are currently being used. Most of the advancement and development of external post-tensioning technology has originated in France in the short span of a couple decades. The author is fortunate to have had a direct line of communication with the chief engineer for the Service d'Etude Techniques des Routes et Autoroutes (S.E.T.R.A.) and a leading professeur at L'Ecole de Ponts et Chaussees, Monsieur Michel Virlogeux, and also with the laboratory at Saint-Remy-Les-Chevreuse where related research is currently ongoing.

In order to clearly denote sources of information in this chapter, the following system has been devised: Groups of sentences or entire paragraphs that are attributed to one source will be followed by the reference number enclosed in brackets[]. Sources for individual statements will be enclosed in conventional parentheses().

2.2 Historical Development of External Post-Tensioning

In assessing the current state of the art, it is important, as well as interesting, to examine the history of the developments that have taken place. Knowledge of concepts and details envisioned by early engineers, and their subsequent successes or failures, gives a much clearer understanding of the task at hand.

2.2.1 Early German Bridges. The mention of historical developments in the realm of prestressed concrete naturally brings to mind the name of Eugene Freyssinet. Often referred to as the "father of prestressed concrete", Freyssinet in fact patented his invention in 1928 (1). It was not until after the massive destruction of World War II that he actually applied his own patent to prestressed bridges (1).

In pre-war Germany, however, the preeminent engineer Franz Dischinger was pioneering the idea of prestressed concrete (2). Dischinger designed several bridges using prestressing

cables external to the cross section of the structure, perhaps a natural progression of thought from the concept of cables in suspension bridges (3). The prestressing steel was actually large diameter rod with butt welded threaded couplings (7). The rods remained ungrouted and therefore unbonded to the concrete (2).

Dischinger's first attempt, the Saale-brucke, holds claim as the first prestressed bridge in the world. It was also the earliest application of external prestressing. This structure, completed in 1928, spanned 200 feet over the Saale River in Alsleben. Two more bridges of this type followed; one, a highway bridge at Aue in Saxony built in 1936, and a third, the Warthe-Brucke in Poznam. The Warthe-Brucke sported a considerable span (for a concrete bridge of that era) of 245 feet, but it was never finished due to the outbreak of the war in 1939 [2].

The road bridge in Aue, a three-span cantilevered structure, had a main span of 210 feet. Though carefully designed and well constructed, this bridge did not perform satisfactorily because of limitations in the state of the art at that period. The "high-strength" rods that Dischinger used for these early projects had a tensile strength of about 60 ksi, only mild reinforcing steel by modern standards. Creep, shrinkage and relaxation losses were unknown and not considered in design. Consequently, after 25 years in service, the loss in prestress

accumulated to about 75 percent of the original prestress level. The concrete structure underwent large displacements and cracking [7].

The cracking in the Aue bridge made Dischinger aware of the deformation of concrete due to creep and shrinkage, and the considerable effect of those deformations on prestress loss, especially with low strength prestressing tendons. German engineers began to realize the impact of plastic deformation on the structural behavior of concrete. Further development with unbonded prestressing continued without much success for some time to come. It was not until 40 years later that unbonded prestressing was used successfully in Germany, and then with high-strength, highly stressed tendons [7].

2.2.2 Post-War Development in France. The devastation wrought by the war left France with 103 damaged bridges, of which 32 were bridges over the Seine, the Marne, and the Oise rivers which were totally destroyed (4). The tremendous task of reconstruction, plus shortages of essential materials (especially steel) inspired innovation. During this period, Freyssinet was responsible for six major reconstruction projects in prestressed concrete over the Marne (2). Also at this time, interest revived in external post-tensioning, possibly due to a desire to evade the Freyssinet patents (3). Four innovative bridges were built

using external tendons: the Vaux-Sur-Seine in 1951, the Port-a-Binson bridge over the Marne, the bridge at Villeneuve-Saint-Georges and the Can Bia bridge, all three completed in 1953 (3).

In a recent report, French engineers studied these four early examples of external post-tensioning, citing observations made during their construction and also evaluating their performances after 30 years in service (4).

Vaux-Sur-Seine, 1951. The bridge at Vaux-Sur-Seine, (see Fig. 2.1), replaced a reinforced concrete bowstring structure which "disappeared" on June 10, 1940. The construction of the new three span two-celled box girder bridge (main span of 80') employed an interesting technique for stressing the tendons as illustrated in Fig. 2.2. Bundles of prestressing wire, a pair at a time, were pushed apart with relatively low capacity jacks, and held in place by a large concrete chock. Anchorages for the bundles, the subject of a previous study, were relatively cumbersome. Two different systems were employed (see Fig. 2.3); the first wrapped individual wires in a doubled hook fashion around anchor bars. The second configuration, descriptively dubbed "pig tail" anchorages, comprised pairs of wires ending in spirals. Concrete partitions served as deviators to impart a classical draped profile to the tendons. In order to minimize friction at the deviations, the passage holes were fitted with well greased metal pieces curved to the shape of the final tendon

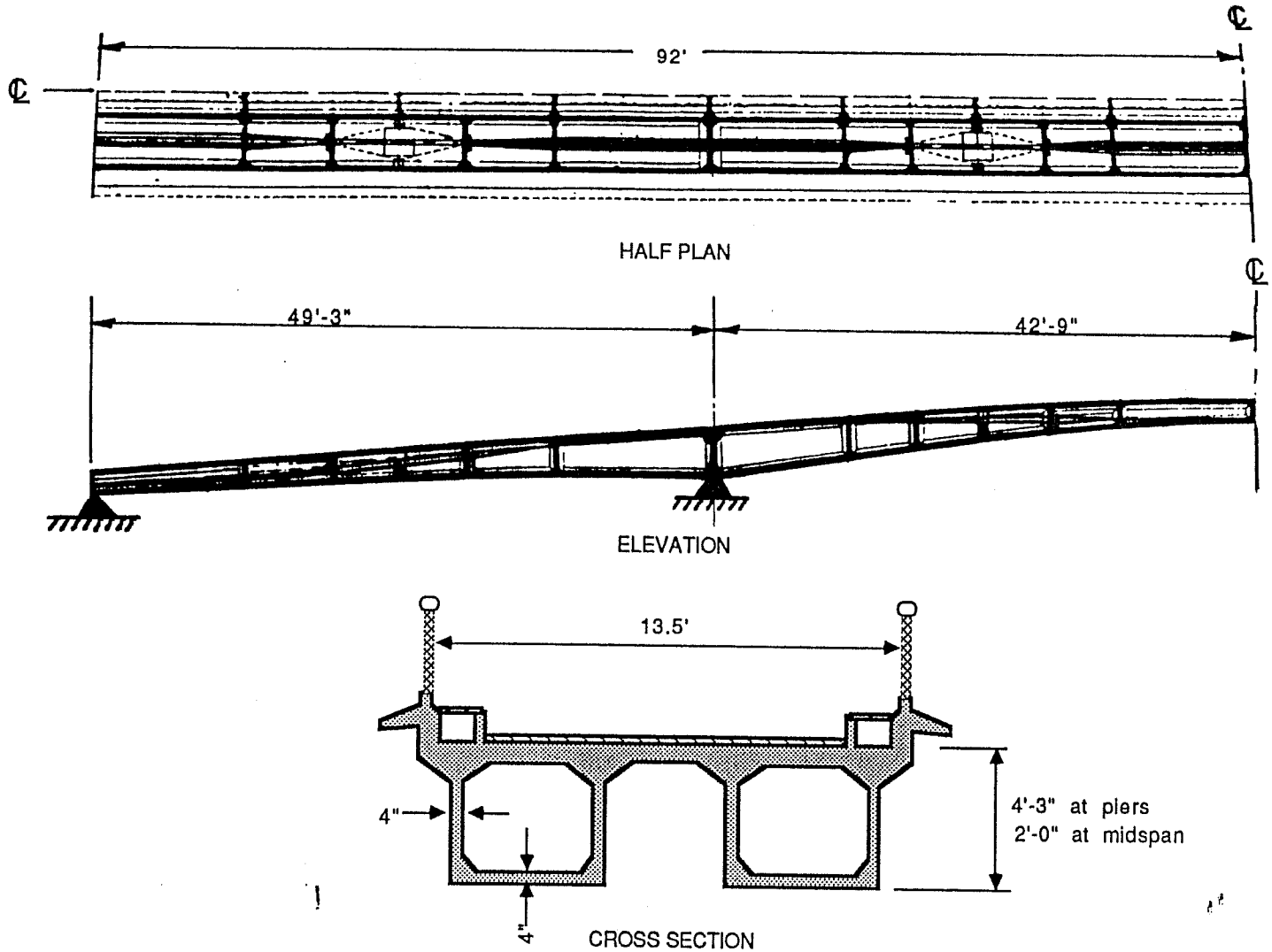

Figure 2.1 Vaux-Sur-Seine Bridge

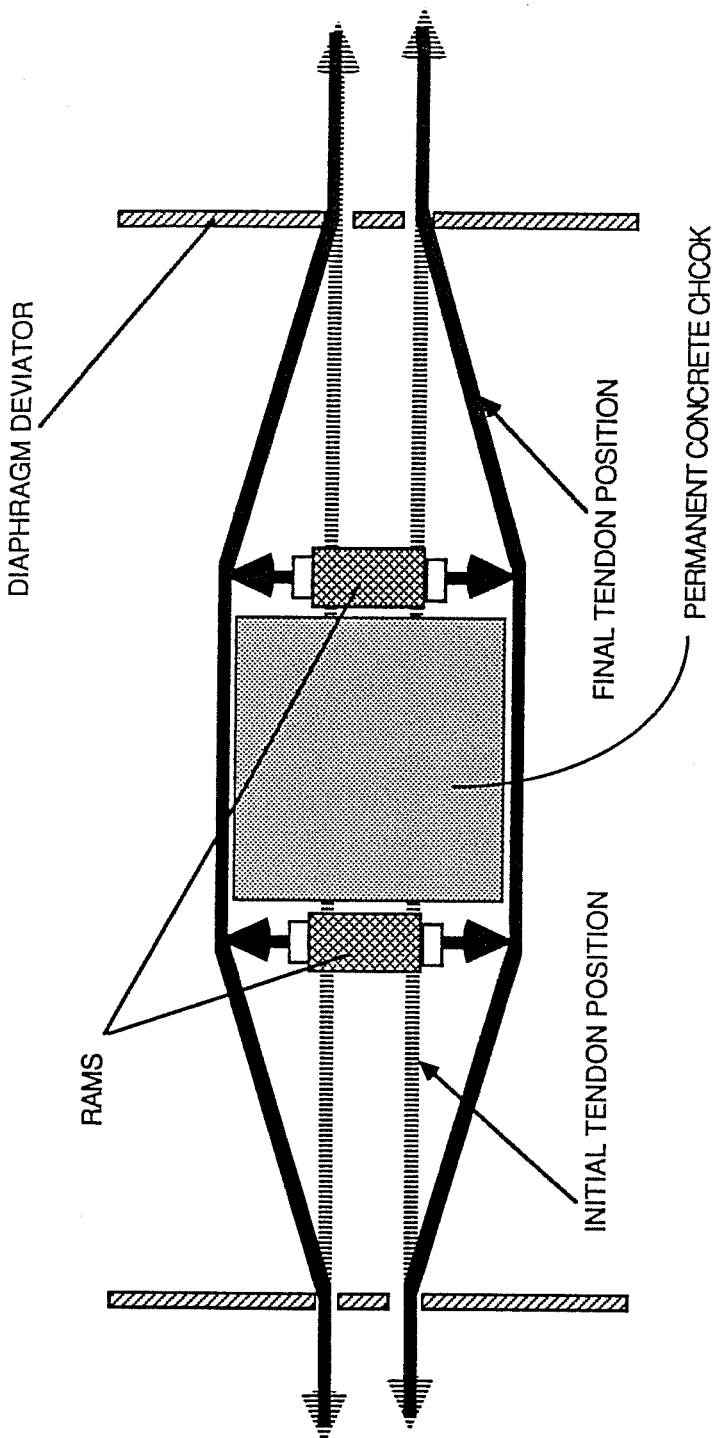

Figure 2.2 Stressing Method for Vaux-Sur-Seine

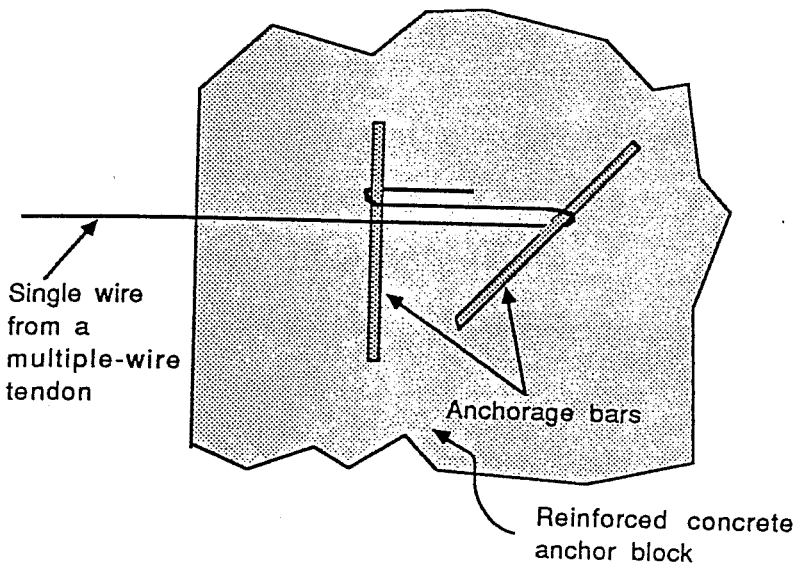

a) Double Hook Anchorage

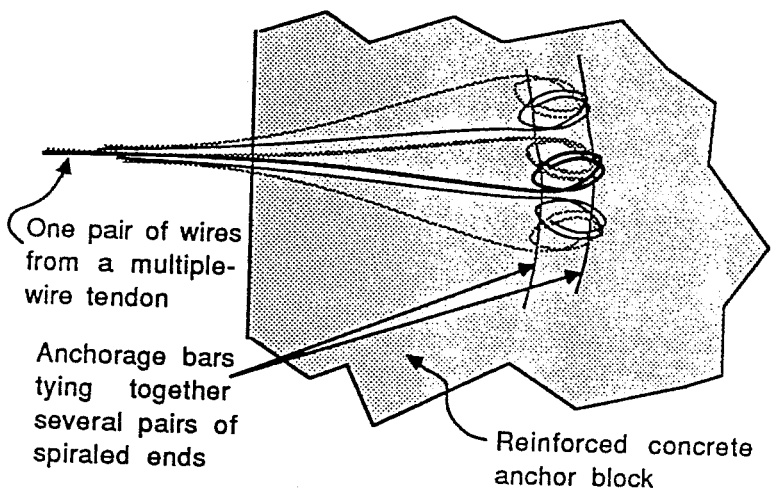

b) "Pigtail" Anchorage

Figure 2.3 Vaux-Sur-Seine Anchorages

profile. Wirope No. 2, a grease product for protecting suspension cables, coated the prestressing steel to prevent oxidation. Observations made during construction revealed that no problems occured with the stressing method. Also noted was the ability to measure loss of prestress by registering the frequency of vibration of the exposed prestressing cables. It was proposed that any losses that should occur could be easily corrected. Some concerns were expressed regarding corrosion of the cables, but since the tendons would be protected from the elements by being enclosed within the box girder, concerns were dismissed [4].

An inspection of Vaux-Sur-Seine in 1981 revealed an absence of cracking in the concrete, but several ruptured wires in the prestressing cables showed evidence of corrosion caused by condensation within the enclosed box. It seems that ventilation had been practically eliminated due to nests built by birds blocking the aeration ports. As a safety measure against further detriment from the corroded wires, additional external post-tensioning, protected in greased PVC ducts, was added shortly after the inspection [4].

Port-a-Binson, 1953. The bridge at Port-a-Binson, a double box girder spanning 125 feet, utilized a prestressing system similar to Vaux-Sur-Seine (Fig. 2.4). Thirty years after construction, the interior of the girder was found to be

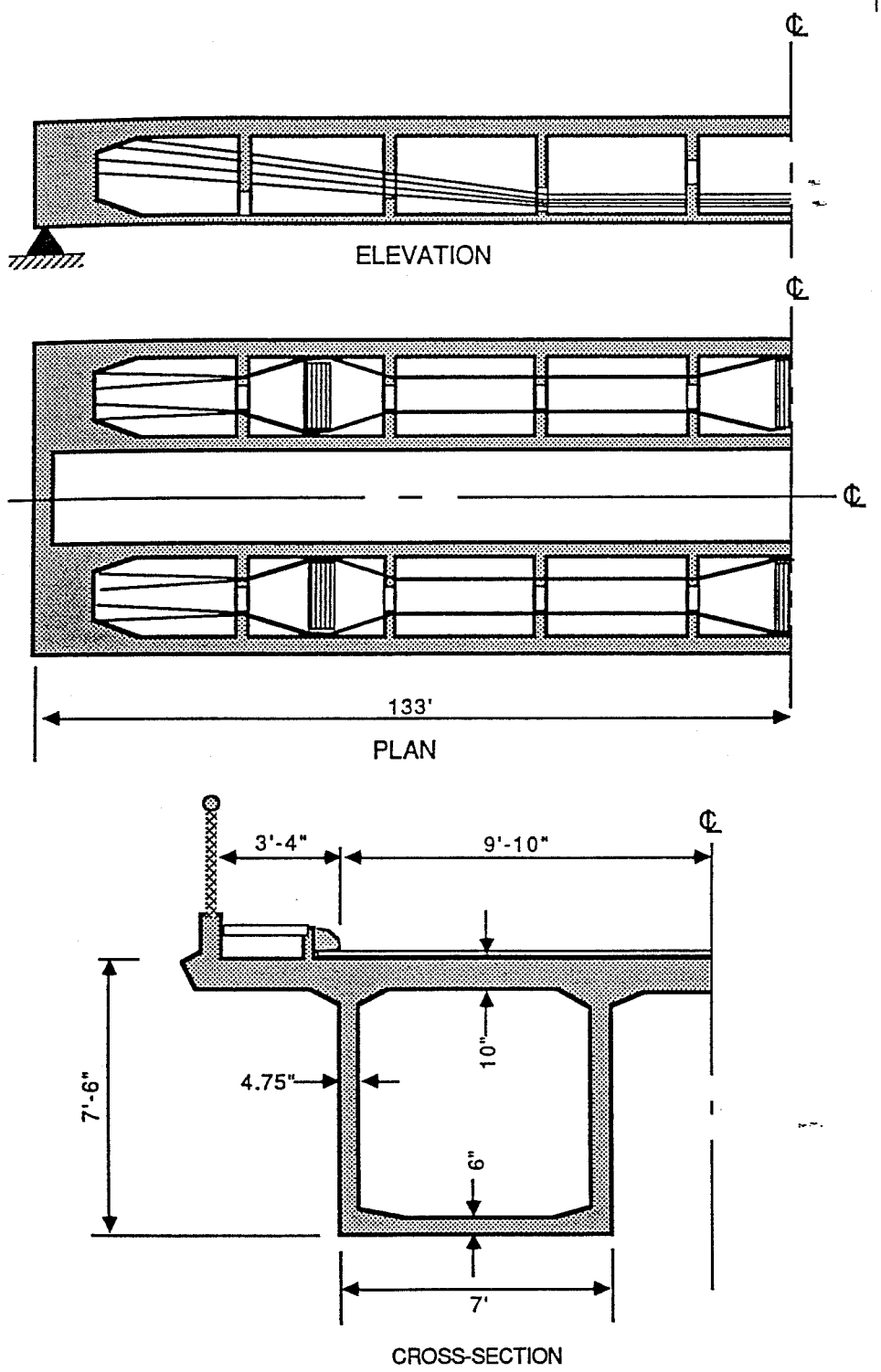

Figure 2.4 Port-à-Binson Bridge

perfectly dry, well ventilated, and the concrete structure free of visible cracking. The bituminous material which had been applied for tendon protection (and reapplied in 1960), had worked well. There was one note of concern: pigeons had roosted inside the box girder, evidently making a perch of the topmost cables since the lower cables were covered with droppings! Simple grills were recommended to resolve the problem [4].

Villeneuve-Saint-Georges, 1953. The bridge at Villeneuve-Saint-Georges, with a cantilevered center span of 250 feet over the Seine, was a three-celled variable depth box girder. The interiors of the cells were equipped with electric lighting systems to facilitate inspection and maintenance of the suspension bridge cables that made up the external tendons. The tendon profile was somewhat complicated (Fig. 2.5). Inclined tendons were deviated by means of specially fabricated hinged rockers supported on reinforced concrete bosses cast monolithically with the bottom flanges (Fig. 2.6a). Anchorages for the cables, composed of 193 spiraled 4.1 mm high-strength wires, consisted of molded steel trumpets filled with a lead-tin alloy. Through the base of the trumpet passed four threaded shafts which were anchored back to the concrete section by means of embedded, hooked reinforcement welded to their extremities (Fig. 2.6b)[6].

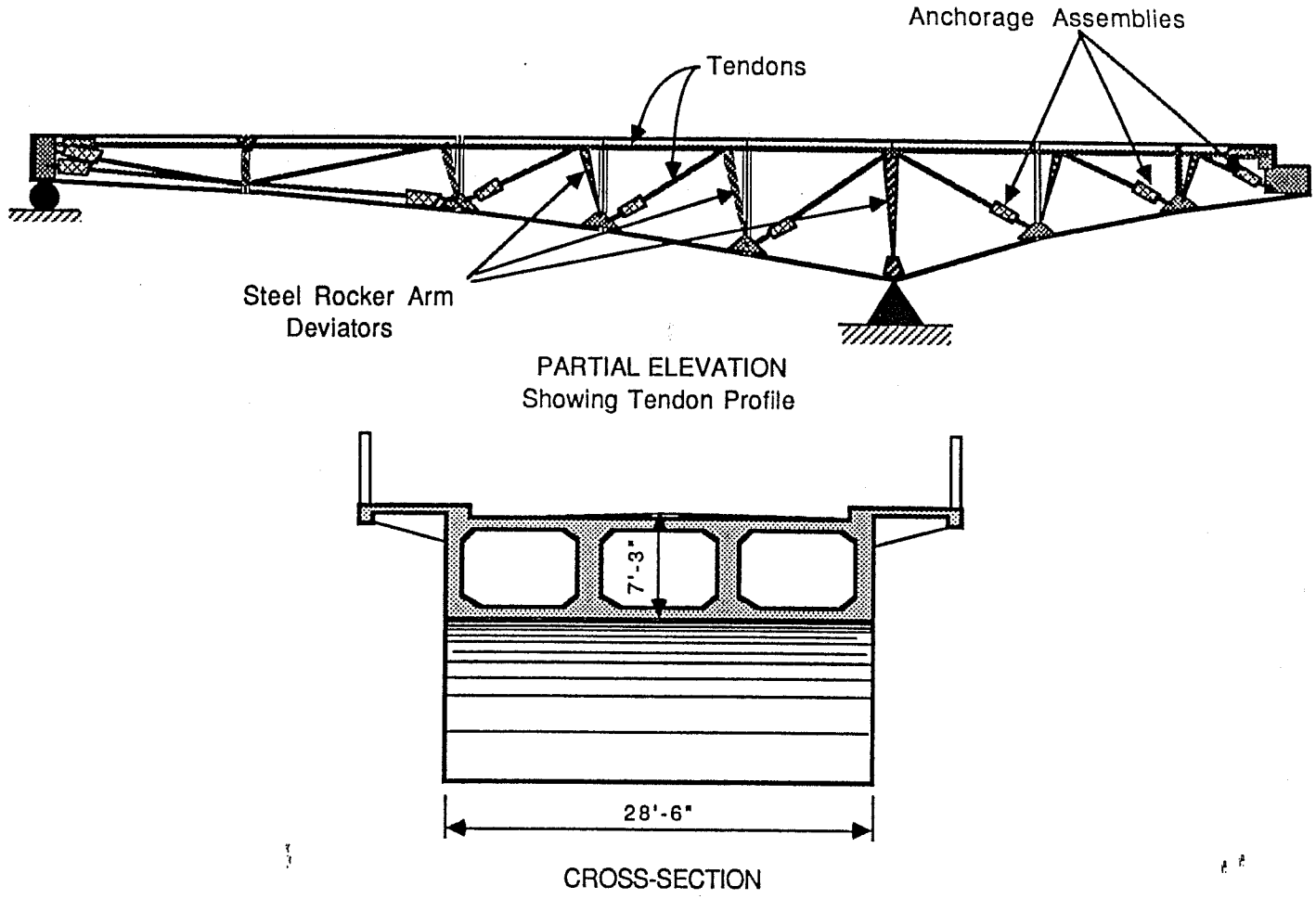

Figure 2.5 Villeneuve-Saint-George Bridge

Though an innovative, pleasing and efficient structure, the Villeneuve-Saint-Georges bridge was uneconomical compared to conventional alternatives due to the complexity of the details envisioned for the external tendons. The post-tensioning method did have the advantage , however, that the stress in the tendons could be easily monitored and corrected if necessary [6].

Can Bia, 1953. The bridge at Can Bia was a box girder structure spanning 190 feet. External tendons were deviated through transverse diaphragms and anchored in the top slab (Fig. 2.7). The tendons were covered with a bituminous paint. Of the four bridges studied, this structure sustained the most deterioration over the 30 year service period. Cracks in the diaphragms and ends of the girder were apparent. More serious, however, was the rupture of several wires, approximately 8 percent of the total area of the post-tensioning tendons. Corrosion was responsible for the damage [4].

In review, after 30 years in service these four pioneering bridges showed few cracks in the concrete. The main problems that were encountered were loss of prestress and failure of tendon protection measures to adequately guard against corrosion.

2.2.3 Other Early Bridges with External Tendons.

Rio Caroni, 1965. In the early sixties, the German structural engineer Fritz Leonhardt designed the bridge at Rio

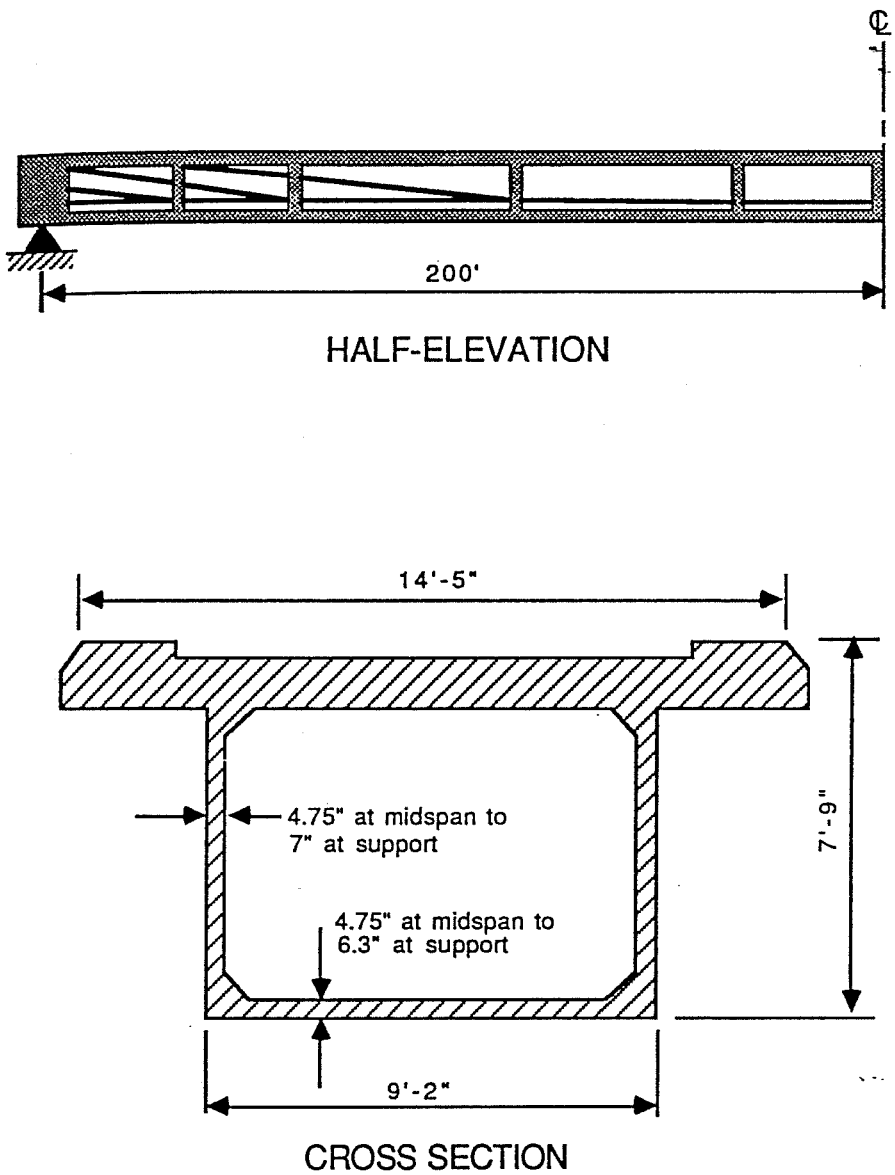

Figure 2.7 Can Bia Bridge

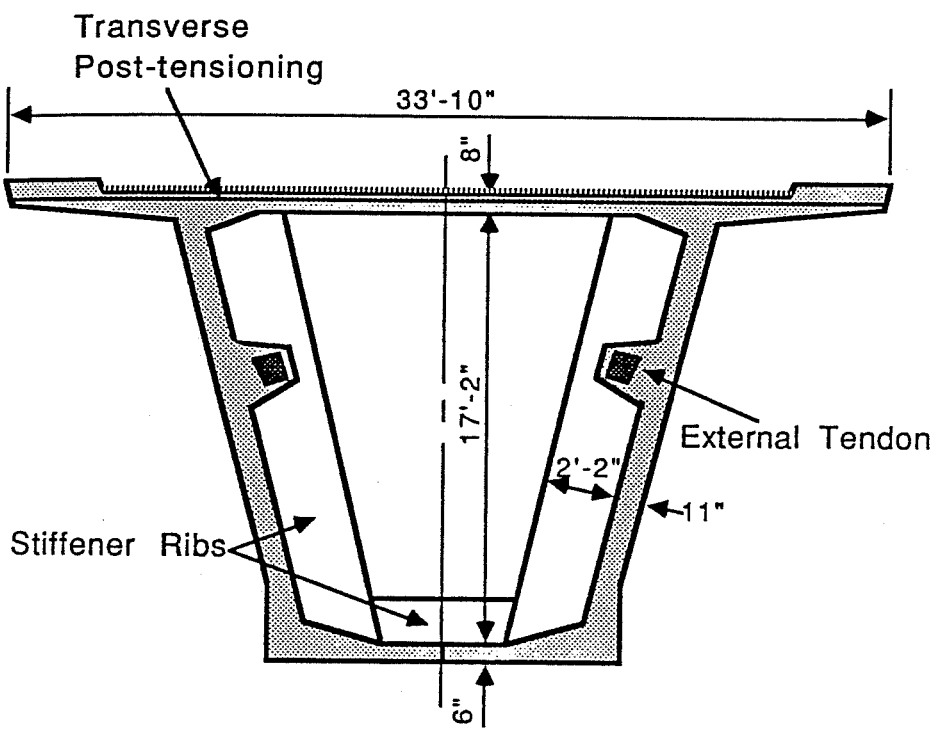

Figure 2.8 Rio Caroni Cross Section

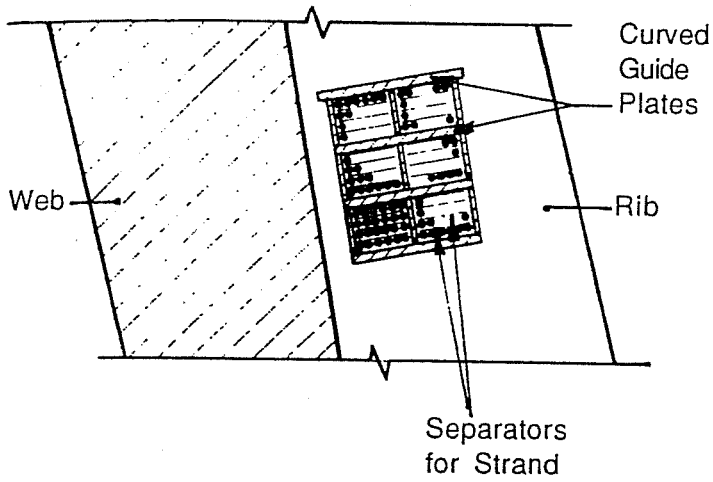

Figure 2.9a Rio Caroni Deviator

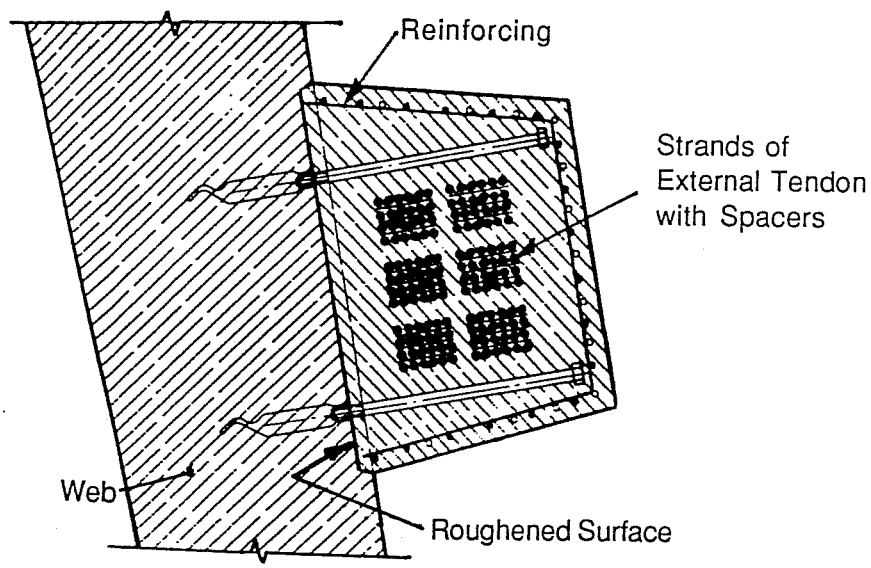

Figure 2.9b Concrete Encasement for External Tendon

local effects. In general, the idea of external post-tensioning did not meet with much success in Great Britain [3].

2.2.4 Experience Gained From Bridge Repairs Using External Tendons. Much of the development of external prestressing technology can be traced to repair and retrofit of prestressed concrete bridges (3). Additional prestressing has proved to be an efficient method for bridge strengthening and repair. Two methods currently prevail: differential jacking of supports, or adding prestressing tendons. The first method has the advantage of being relatively easy, economical and time-saving. The measure is most likely short term, though, since creep induces force redistributions over time. Also, care must be taken to avoid overstressing other parts of the structure. The second method involves additional prestressing with external tendons. While a more permanent solution, it entails several technical problems and considerations concerning tendon layout, deviation devices, anchorages, and choice of duct type and tendon protection scheme [8].

Both straight and draped tendons have been used successfully for retrofit and repair (Fig. 2.10). While straight tendons eliminate the need for deviators and reduce friction losses to practically nil, the result is not efficient for flexural resistance and will not increase shear resistance. A polygonal profile, which follows more closely the moment diagram,

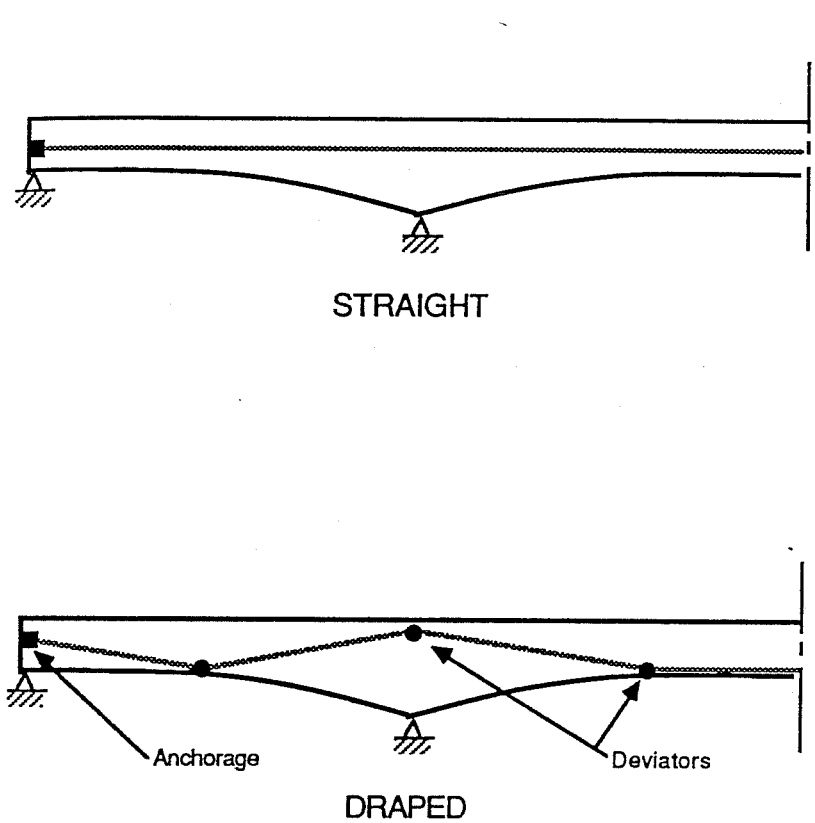

Figure 2.10 Profiles for Retrofit External Tendons

offers more efficient use of prestress plus increased shear resistance from the inclined tendon. However, the deviators required to acheive the tendon profile, which must be somehow clamped to existing webs or flanges, introduce stress concentrations and increase friction losses [8].

Anchoring the added tendons onto the existing structure presents the most difficult problem. Several alternatives have been devised. A large transfer beam may be cast against the ends of the bridge section (Fig. 2.11a). The transfer member can be designed to uniformly distribute concentrated forces to the existing structure. This procedure however, necessitates using tendons as long as the bridge. Also, the abutments must be demolished and reconstructed, a project that will most likely disrupt traffic flow for a considerable period of time [8].

Alternatively, tendons may be anchored at existing diaphragms, if analysis verifies that the diaphragms can provide adequate resistance. A core must be drilled through the diaphragm and anchorage hardware is embedded in a concrete anchorage block cast against the face of the diaphragm (Fig. 2.11b)[8].

In the absence of existing or adequate diaphragms, a concrete boss can be prestressed to the web or flange of the existing section (Fig. 2.11c). This system is advantageous since the prestress from the added external tendons can be distributed

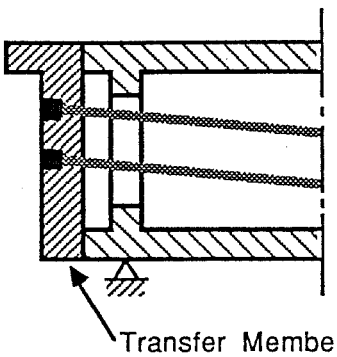

a) Transfer Beam Anchorage

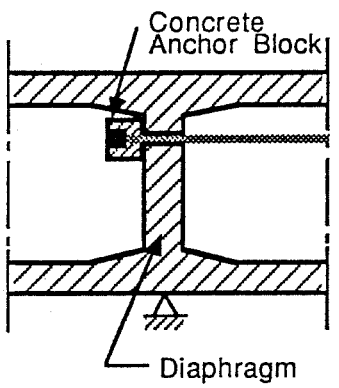

b) Anchorage at Existing Diaphragm

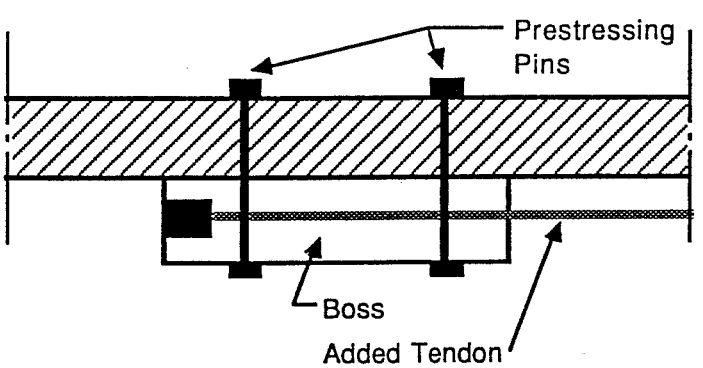

c) "Boss" Type Anchor

Figure 2.11 Anchorage Schemes for Retrofit External Tendons

fairly well over the length of the structure. On the other hand, effects of force diffusion create considerable localized stresses which are additive to the existing state of stress. Localized effects have been reduced by locating anchors in the gusset areas at flange-web junctions [8].

Experience has shown that design of anchorage bosses should be conservative. The clamping force should be at least two times the prestress force. Stressing the boss to the web in two stages can minimize losses in the short prestressing pins. First the pins are stressed to the desired force level. Then, just before stressing the added tendon, the pins are stressed again to recover losses from creep and seating. Tests have shown that the tendon force does not distribute uniformly over the contact surface, but concentrates in two zones at the extremities of the boss. Therefore, pins will be more effective if located in these zones. Light roughening to remove laitance has proven the best contact surface preparation. Application of epoxies may improve bond, but may be a trouble source if the epoxy fails to cure [8].

Similar considerations apply to the design of deviators for draped tendons. The forces on deviators are generally small and no problems have yet been encountered with retrofit deviators. Two alternatives have been developed. The first is similar to the anchor boss (Fig. 2.12a). An alternate scheme,

(Fig. 2.12b), attaches a reinforced concrete rib to the web with epoxied dowels. The benefit of this method is the distribution of the deviation force along the entire web. One inconvenience is that a hole must be cored in the top flange and deck in order to place the concrete [8].

Ducts located within anchorages and deviators serve two purposes. The duct isolates the tendon from the concrete and assures that the tendon is guided properly. Cold bent rigid metal tubes have provided best results. For protection against corrosion between attachment points, several types of sheathing have been used with varying degrees of success. Early repair projects employed corrugated sheathing, such as that typically used for internal post-tensioning tendons. This type of sheathing was found to be insufficiently watertight. Metal conduit and high density polyethylene tubing have both worked well, with polyethylene the most economical choice today. Experience with galvanized cables has disclosed certain problems. It has not been ascertained that galvanized cables under tension are not susceptible to corrosive agents such as salts, bird droppings, etc. [8]. On a particular project, zinc accumulated on the anchorage wedges, resulting in the severe detensioning of a tendon (3).

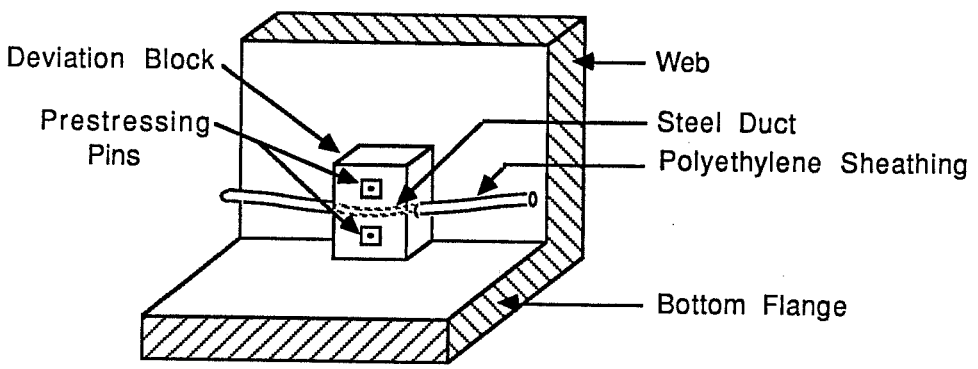

a) "Boss" Type Deviator

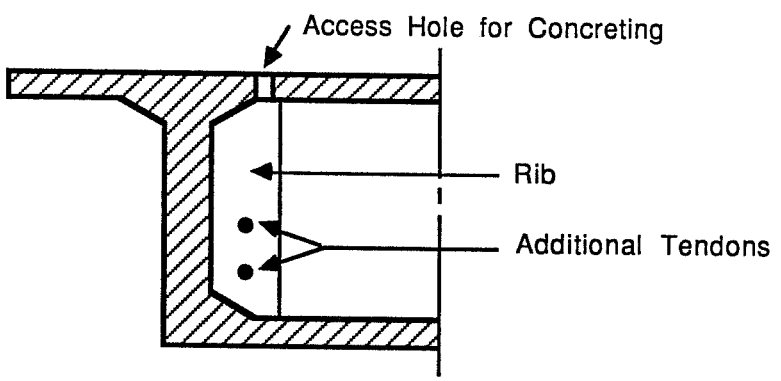

b) Rib Deviator

Figure 2.12 Deviators for Retrofit External Tendons

Another problem exposed by repair with external tendons is vibration of external cables unsupported over extended lengths. Natural frequencies for typical prestressed bridge structures range from 3 to 5 hertz. In comparison, the natural frequency of a 12-0.5 in. diameter strand tendon is about 5 hertz for a free length of about 90 feet. Maximum recommended free length has been about 60 feet. Otherwise, intermediate supports, (Fig. 2.13), which can be very light, have been suggested [8].

2.2.4.1 Repairs to French Bridges - 1970's. A number of prestressed bridges built in France prior to 1975 suffered distress (cracking, excessive deflections) due to deficiencies in design and construction. Several factors can be held responsible. Competition in an open bid market spurred skimping on concrete and steel. Loads were sometimes underestimated or ignored (eg. weights of toppings or hardware). A major source of error was the miscalculation of the effects of plastic deformation of concrete. Redistribution of moments due to creep and shrinkage were not considered and loss of prestress due to creep deflections was underestimated. The effects of thermal gradients were ignored. Friction losses of internal tendons in curved or misaligned ducts were underestimated [3]. In some of the later bridges, a possible need for future additional prestress was forseen, and empty ducts and extra anchorages were added during construction for this purpose (8). Still, in some

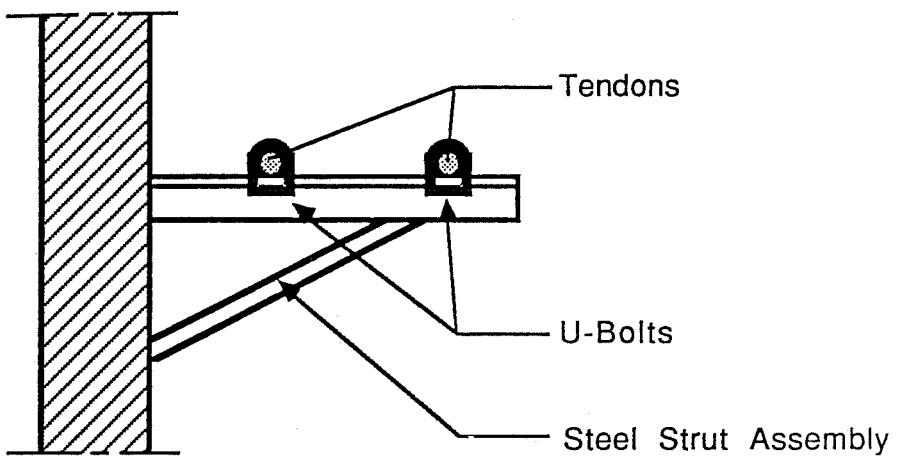

Figure 2.13 Antivibratory Device

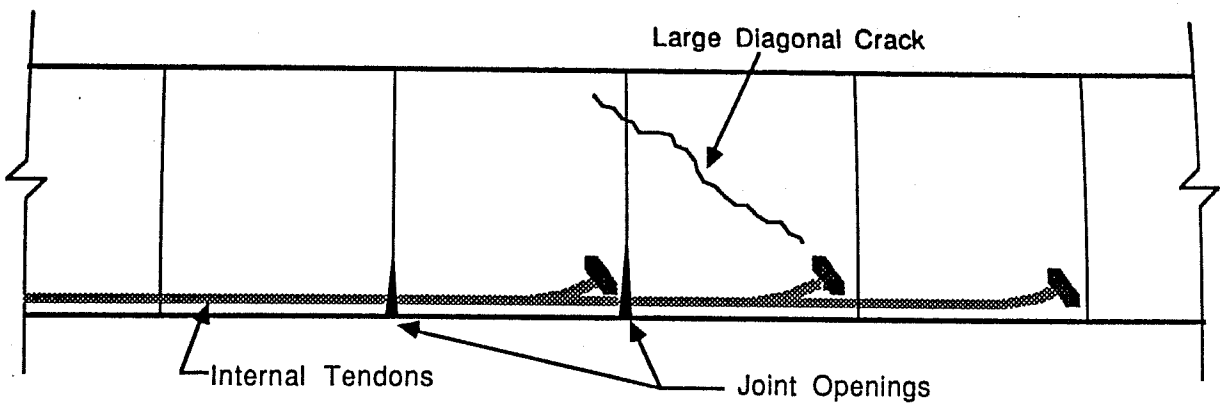

Figure 2.14a Distress in a French Bridge

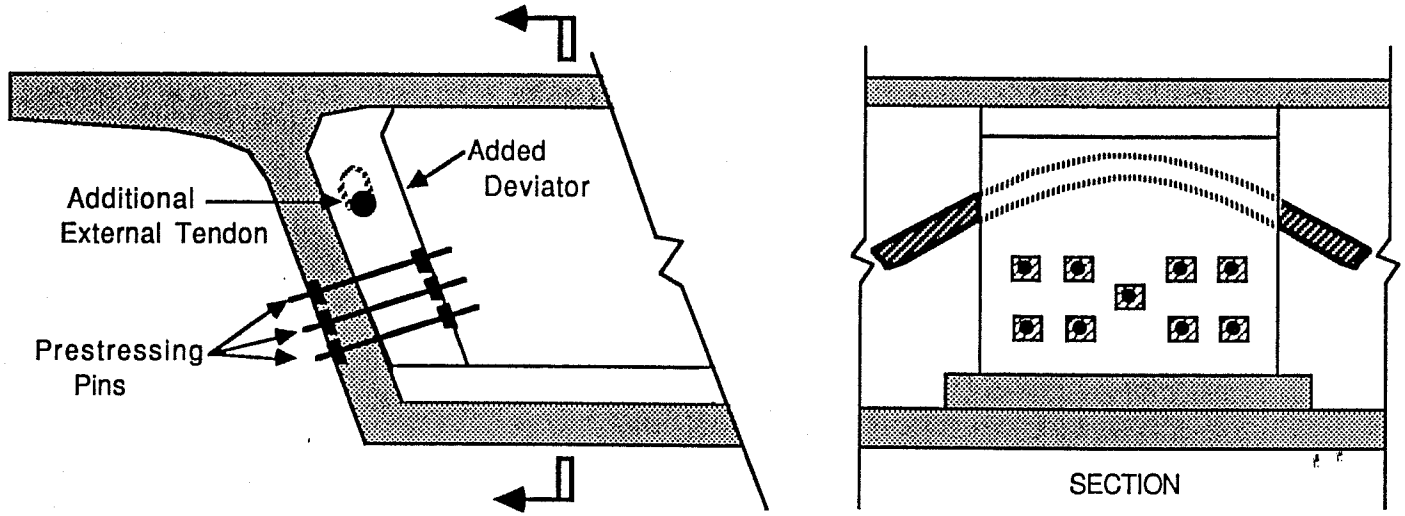

Figure 2.14b Repair Scheme

Remedial measures included the addition of 19-0.6 in. diameter strands per web in external tendons, corresponding to an augmentation of prestressing steel area of 37 percent. The draped tendons were deviated and anchored in wide ribs that were cast against and prestressed to the existing webs (Fig. 2.14b). The total cost of the repair was reported to amount to about 12 percent of the original cost.

The importance of prestress loss due to friction was well illustrated during the construction of the viaduct at Marne-La-Vallee, the first precast segmental railroad bridge. Using jacks equipped with pressure gages to measure applied force at both extremities of a tendon, the considerable friction loss over the length of the tendon became apparent. Additional prestressing steel was required to make up for losses. The French railroad commission, SNCF, had forseen a possible future need to augment the prestress force, and had requested that provisions be made (extra ducts, anchorages, etc.) to add a supplementary 20 percent. Unfortunately, an increase in prestress force beyond that figure was required. Six external tendons of 12T15 (metric equivalent to 12-0.6 in. diameter strands) per web were deviated through existing diaphragms over the piers and through attached "boss" type deviators. In light of the repairs made, the effiency of external prestressing with regard to friction losses was recognized [3].

During load tests on the completed viaduct at Marne-La-Vallee it was observed that the external tendons were easily set to vibrating, necessitating the addition of antivibratory devices. It was also this project that precluded further use of traditional corrugated sheathing for external tendons, as it became apparent during grouting procedures that this type of sheathing was not sufficiently watertight. The Marne-La-Vallee Viaduct was completed in 1977 [3].

2.2.4.2 Repair of North American Bridges. The North American continent's first precast segmental bridge, an internally prestressed structure with a main span of 260 feet over the Lievre River in Quebec, Canada, dates to 1967 (9). The Lievre bridge was plagued by the same problems experienced by the french bridges, notably the effect of plastic deformation of the concrete and neglect of thermal gradient effects. In addition, insufficient development length contributed to a lack of fixity at the piers. The structure eventually suffered noticeable cracking in the positive moment regions, joint openings, and deflections.

The repair scheme, shown in Fig. 2.15, consisted of straight external tendons, located in the positive moment regions only, anchored in bosses prestressed to the outsides of the webs of the box girder. An intermediate support was required in the long center span.

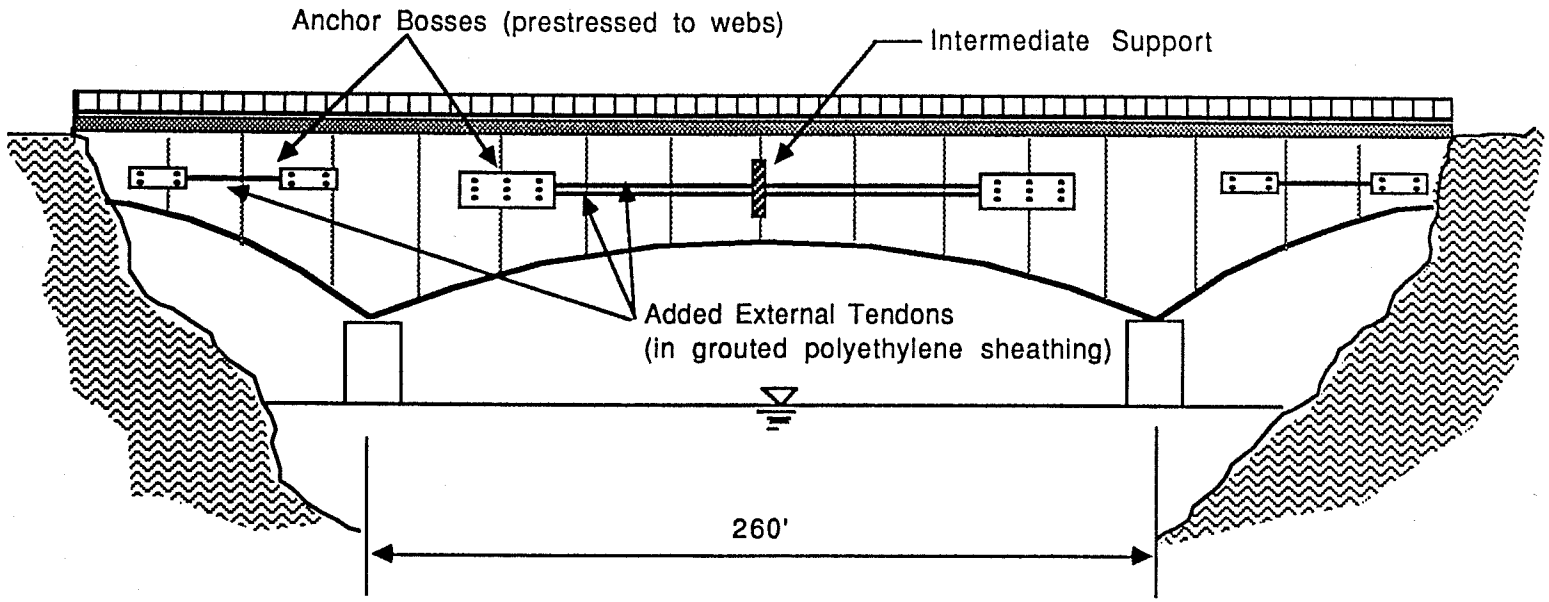

Figure 2.15 Repair Scheme for the Lièvre Bridge

Several other Canadian bridges required similar reinforcement as have the cast-in-place segmental bridges at Vail Pass in Colorado.

2.2.5 Modern Bridges with External Tendons. Within the last decade, a number of bridges with external tendons have been built in various parts of the world. These structures have been built with rapid construction times and very competitive costs. To illustrate the diversity of cross sections, tendon profiles, construction methods, etc. of modern externally post-tensioned bridges, this section provides a brief description of several notable structures which have been recently completed or are still in progress.

2.2.5.1 Florida Keys, U.S.A. The first modern bridges to employ external tendons exclusively were a string of four structures linking the Florida Keys: Long Key, Seven Mile, Channel Five, and Niles Channel bridges, all designed by the consulting firm of Figg and Muller Engineers, Inc. (3). Long Key Bridge, comprising 11,960 total feet of roadway, is of precast segmental construction erected by the span-by-span method. The structure is continuous over eight spans with expansion joints at the pier segments and slender precast V-piers. In addition to the two-lane roadway, the structure was designed to carry a 30 inch diameter water main within the void of the box section [9].

An underslung erection truss was utilized to support the 65 ton segments in a typical span of 118 feet, until the entire span could be post-tensioned. Anchorages are located in thick diaphragms within the pier segments. A typical span could be erected in two working days. Joints between the the typical match-cast segments were left dry [9].

Figure 2.16 shows a schematic of the tendon layout for Long Key. Multi-strand external tendons pass through ducts embedded in small reinforced conrete deviation blocks or saddles cast monolithically with the single-cell box girder. The tendons overlap at anchorage diaphragms for continuity. Corrosion protection provided for the tendons between anchorages and deviators consists of grouted polyethylene sheathing [9].

The Seven Mile Bridge is a similar structure with a cross section almost identical to Long Key. The alignment includes both horzontal and vertical curvatures. A different pier design employs hollow box segments post-tensioned together. The erection scheme was changed to include an overhead erection truss instead of the underhung truss used previously. A total of 264 spans of 135 feet were erected in record time [9].

2.2.5.2 Bubiyan, Kuwait. The French firm of Bouygues proposed the design for the Bubiyan bridge in Kuwait. The Bubiyan superstucture incorporates an interesting space truss configuration in which an open lattice system of concrete truss

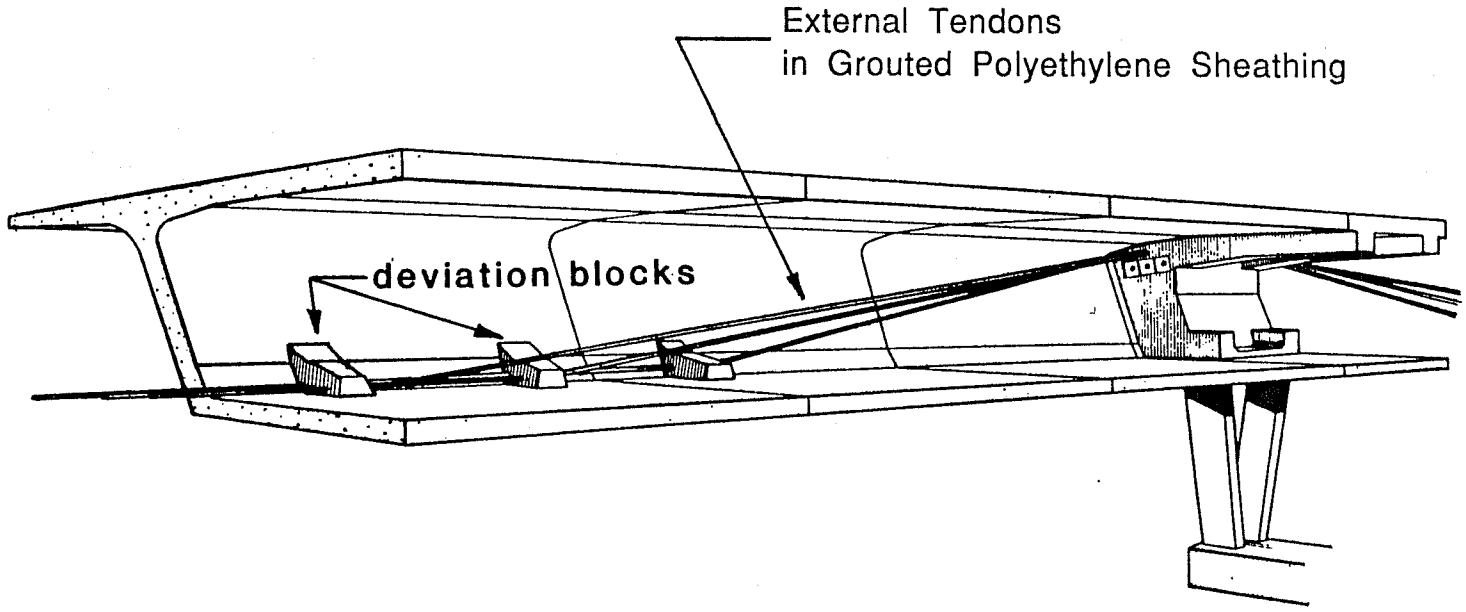

Figure 2.16 Cut-Away View of Long Key Bridge

elements replaces the long solid webs of conventional concrete box girders (Fig. 2.17a). The advantages of this open system include a reduction of dead weight and an ability for load redistribution in the unlikely event of a member failure [9].

The external longitudinal post-tensioning is strung in four vertical planes with couplers at the pier segments for continuity. Between anchorages and couplings, tendons are enclosed entirely in polyethylene sheathing. Deviations are accomplished by means of grooves cast in the underside of the bottom ribs (Fig. 2.17b). To avoid damage to the polyethylene in the deviations, the sheathing was reinforced on the inside with flexible metal tubing [3].

2.2.5.3 Banquiere and Vallon-des-Fleurs Viaducts, France. The aforementioned structures all were constructed using span-by-span techniques. French consultants, Campenon-Bernard, wished to utilize the method of progressive placement with provisory cable stays for the construction of two similar viaduct structures. Experience had shown that large friction losses are encountered when traditional internal post-tensioning is used in conjuction with progressive placement construction, due to the complex tendon profile required. The Banquiere and Vallon-des-Fleurs viaducts are both precast segmental parallel box girders post-tensioned solely with external tendons. The tendons are anchored in pier segment diaphragms and deviated in large

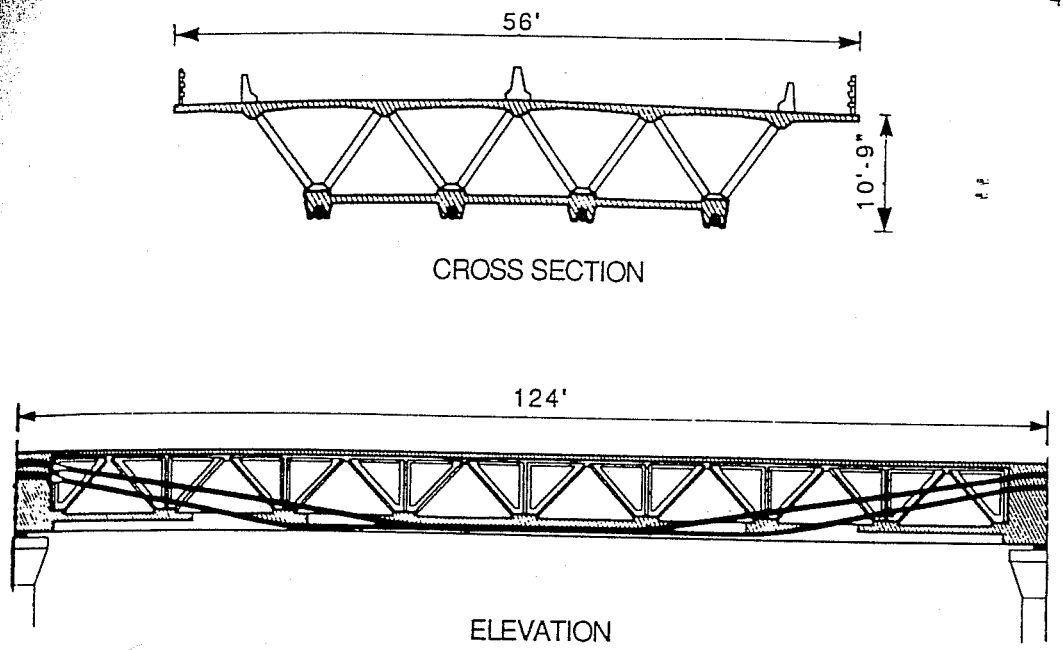

Figure 2.17a Bubiyan Bridge

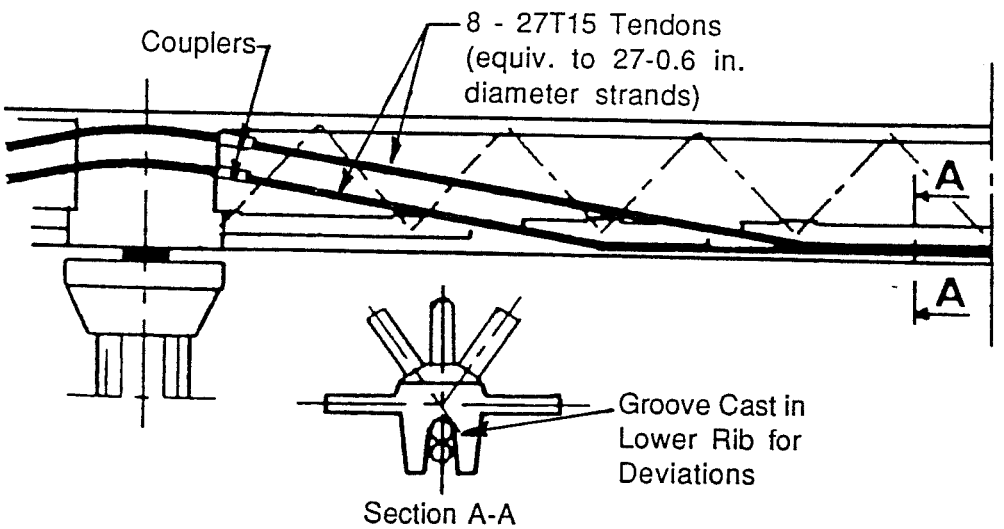

Figure 2.17b Bubiyan Details

deviation blocks cast monolithically with the lower web-flange gussets in the center of each segment (Fig. 2.18). Projections at the upper gussets serve as anchorages for temporary dywidag bars used during construction. Between attachment points, tendons are enclosed in high density polyethylene sheathing injected with grease. This practice allows possibility of future tendon replacement [3].

2.2.5.4 Saint-Agnant Viaduct, France. In an effort to maximize efficient use of precast segmental technology applied to short-span bridge structures, Campenon-Bernard devised an open cross section for the Saint-Agnant viaduct (Fig. 2.19a). The open profile was designed to facilitate forming, casting and stripping procedures, as well as economize use of materials. The relatively light segments (less than 16 tons) resulted in substantial savings for the erection appurtenances and equipment required for span-by-span construction. Aiming at a standardization of elements, an external post-tensioning scheme was adopted and a new concept for deviators was devised (Fig. 2.19b)[10].

2.2.5.5 Sermanez Viaduct, France. The Sermanez Viaduct crosses the Rhone River just east of Lyon. Five spans of two parallel variable depth box girders were proposed for the project. The peculiarity of the Sermanez bridge lies in the use of external tendons in conjunction with a cantilever method of

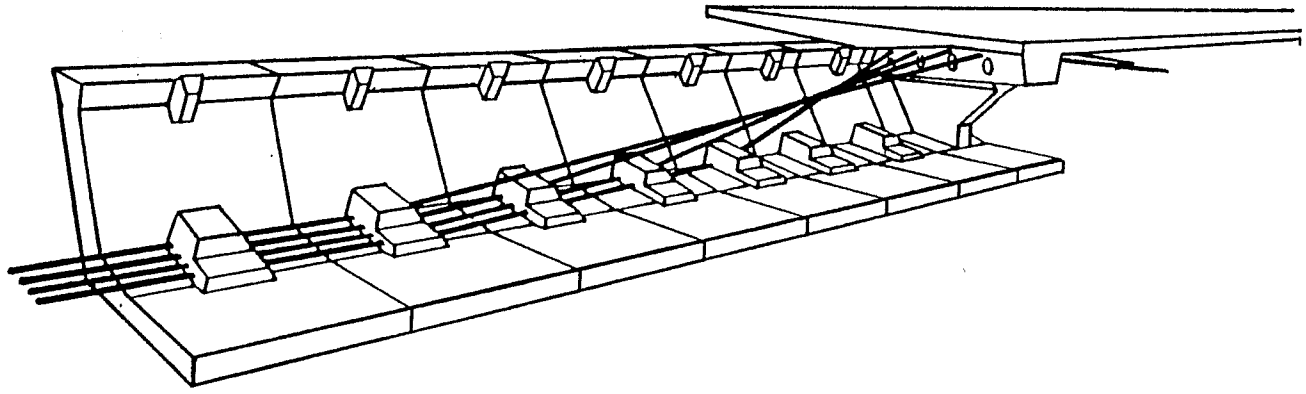

Figure 2.18 Vallon-des-Fleurs Viaduct

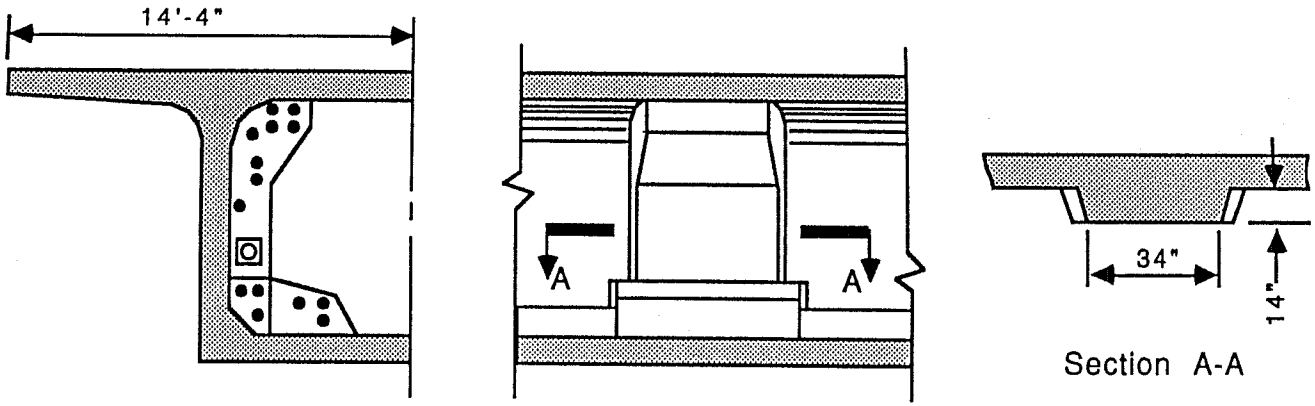

CROSS SECTION

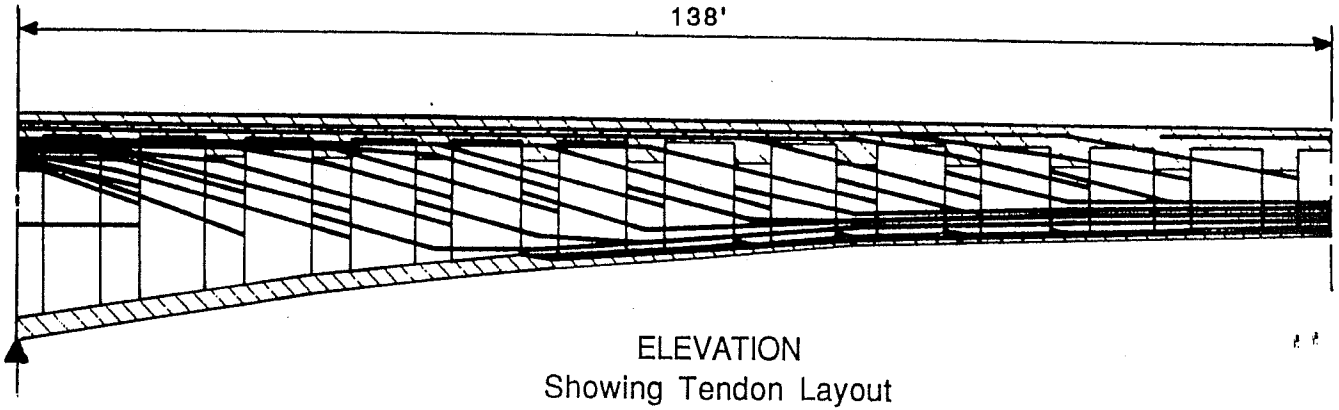

ELEVATION
Showing Tendon Layout

Figure 2.20 Sermanez Viaduct

previous project due to accumulations of zinc in the wedges, a procedure was devised so that fresh wedges would always be used for final seating of the strands. Anticorrosive measures for anchorages included galvanized trumpets and anchor plates, and chrome plated wedges. The anchorage hardware and tendons were left bare, so that the tendons are completely replaceable [11].

2.2.5.6 French Bridges with Mixed Tendons. The span-by-span method of construction lends itself particularly well to the exclusive use of external post-tensioning. For other methods of construction such as balanced cantilever, progressive placement, or incremental launching, however, internal tendons are advantageous to support the weight of the structure during construction. In France, a synthesis of these two ideas has resulted in a number of projects with "mixed tendons", a combination of internal and external post-tensioning. In general, three separate "families" of tendons can be distiguished (Fig. 2.21). First, internal tendons in the cantilever are proportioned to carry only the self weight of the structure and construction loads. These tendons are typically straight and are anchored in the upper gusset areas of the box girder section. The second set is comprised of draped external tendons for continuity. These tendons carry most of the live and superimposed dead loads and the inclination of the tendons increases shear resistance. Typically, the external tendons are

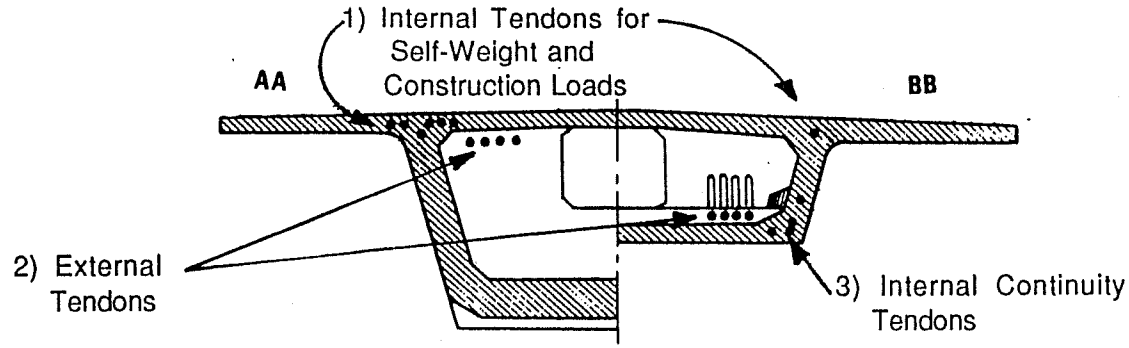

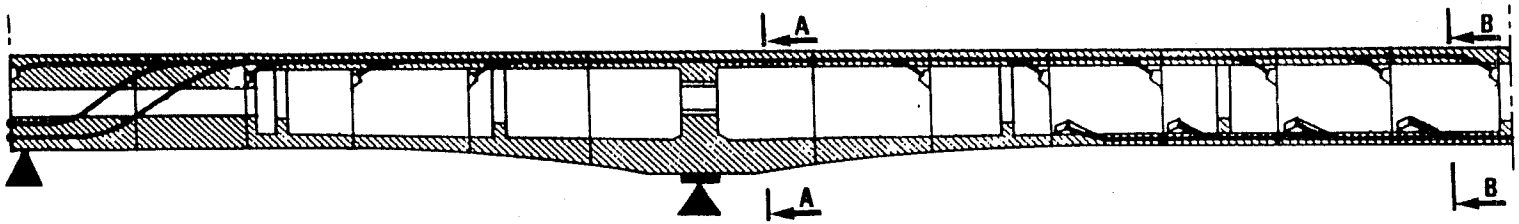

1) and 3) Internal Tendons

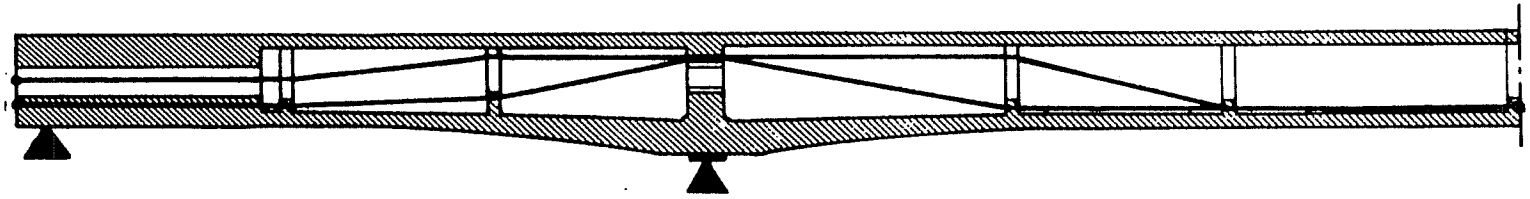

2) External Tendons

Figure 2.21 Mixed Tendon Layout - Example

stressed near completion of the structure. The final set consists of internal continuity cables, ususally straight, anchored in the lower gussets. Three prominent examples of mixed tendon construction, each built using a different construction technique, are the Fleche Bridge, the viaduct at Pont-a-Mousson, and the Cergy-Pointoise Bridge [3].

2.2.5.7 Recent U.S.A. Projects. The newly opened Sunshine Skyway bridge crosses over four miles of Tampa Bay in Florida. The precast segmental structure has cable stayed main spans, the largest of which is 1200 feet. The externally post-tensioned approaches consist of 8 and 10 span continuous twin box girder units with 135 ft. spans. The designers are Figg and Muller Engineers, Inc. [20].

San Antonio Y is a four part project which will add an upper deck to interstate highways that pass through the downtown section of San Antonio, Texas. Figg and Muller's design for Phase I of the project includes a precast segmental single-cell box girder superstructure (Fig. 2.22a). The 90 to 100 foot spans are erected span-by-span using underhung erection trusses, and are post-tensioned with external tendons. Tendons are deviated with full-height diaphragms (Fig. 2.22b). Construction of this first phase of the project is presently underway.

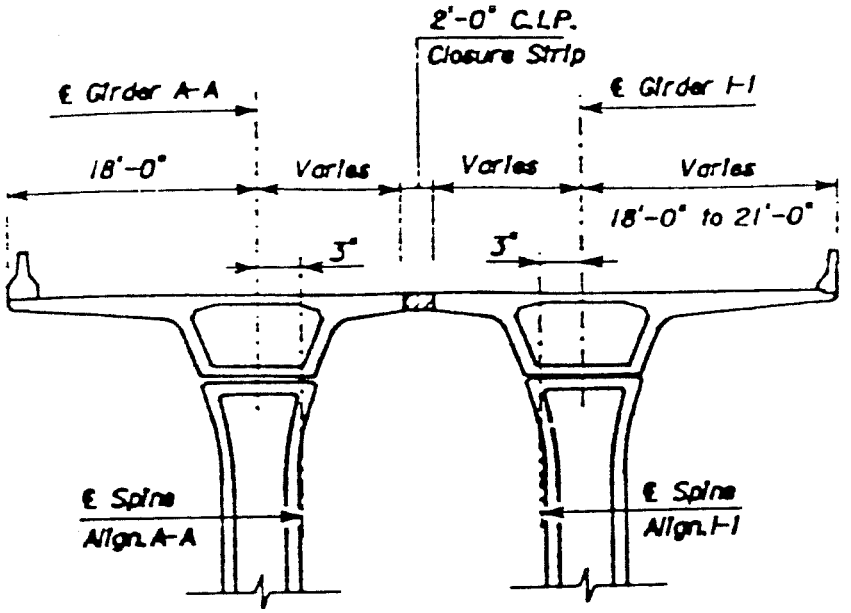

Figure 2.22a San Antonio Y Cross Section

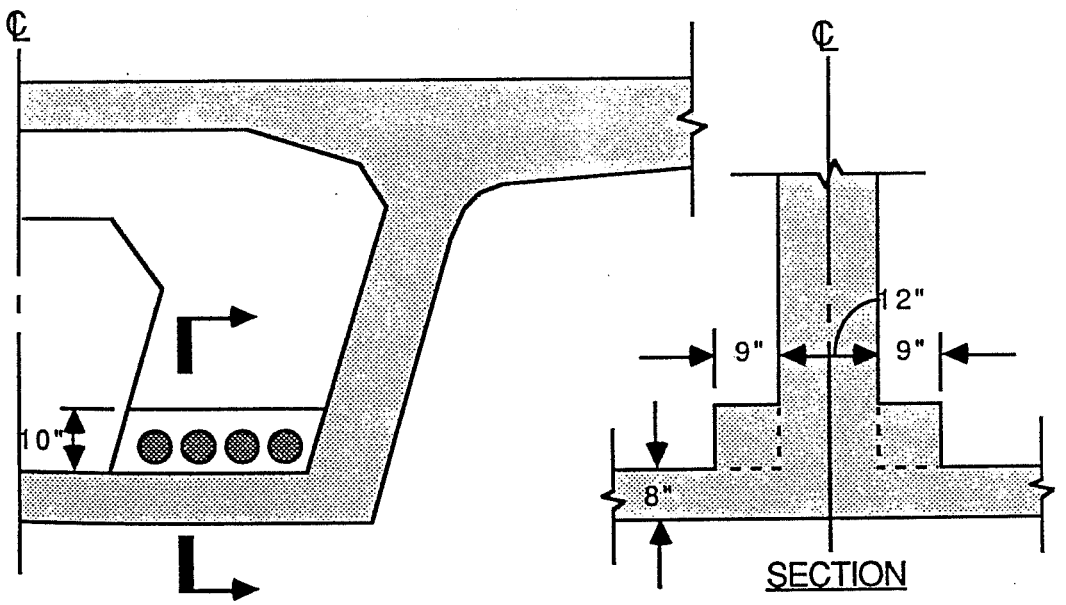

Figure 2.22b San Antonio Y Diaphragms

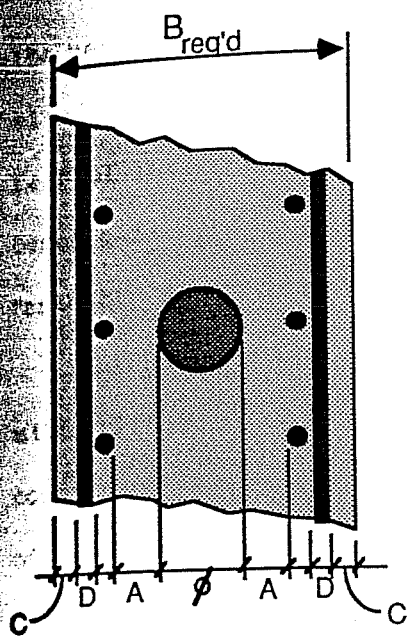

$$B_{req'd} \cong 2xC + 2xA + 4xD + \phi$$

Figure 2.23a Web Thickness for Sections Containing Ducts

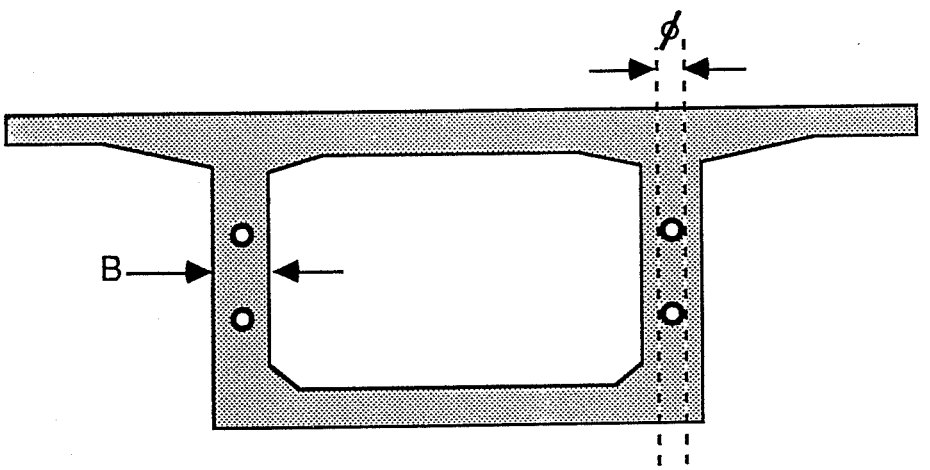

$$B_{eff} = B - \phi/2$$

Figure 2.23b Effective Web Thickness for Shear

the reinforcing cage. Interference with passive reinforcement is eliminated. Mild reinforcing cages can be assembled without fear of later interference with post-tensioning ducts. This benefit has the greatest impact in segmental construction since "assembly line" efficiency can be acheived.

Reduced Congestion. The absence of ducts within the mild reinforcing cage relieves congestion, resulting in better conditions for concrete placement and consolidation. Incidents of poorly consolidated concrete occur routinely when ducts are grouped together in closely spaced bundles, which is often the case with traditional internal tendons.

Accessibility of Tendons. The ease of access to external tendons facilitates installation of the tendons and sheathing. Open access to the full length of the tendons ameliorates grouting conditions. Preplaced grout ports become unnecessary, and danger of obstructed, collapsed, or otherwise damaged ducts disappears.

Replaceability of Tendons. The issue of replaceability of post-tensioning tendons has not been addressed much in this country. In France, however, there is considerable concern regarding this subject. The French federal transportation administration has taken the position that all external tendons should be replaceable (3). The French have patented a method of "double ducts" that allow removal and replacement of tendons,

even if they are grouted (Fig. 2.24)(12). The accessability of external tendons means that, with a few precautions and relatively little additional cost, tendons can be replaced without major effort or disruption of the use of the bridge (3).

Reduced Friction Losses. The use of external tendons reduces overall loss of prestress due to friction. Since the tendon is straight between attachment points and the duct is unrestrained, the effect of wobble is effectively nullified. Since the minimum acceptable radius of curvature for post-tensioning ducts is about the same for both internal and external tendons, curvature friction remains about the same.

Fatigue Advantages. Risk of fatigue failure of external tendons is, for all practical purposes, nonexistent. Since an unbonded tendon undergoes very little fluctuation in stress, even under the very worst loading conditions, fatigue poses no problem, except perhaps at the grips and from fretting in the deviators.

Particular Advantages for Segmental Construction. In segmental construction with internal tendons, the tendon ducts are interrupted at each joint. The continuous sheathing (between attachment points) used for external tendons can possibly result in better corrosion protection.

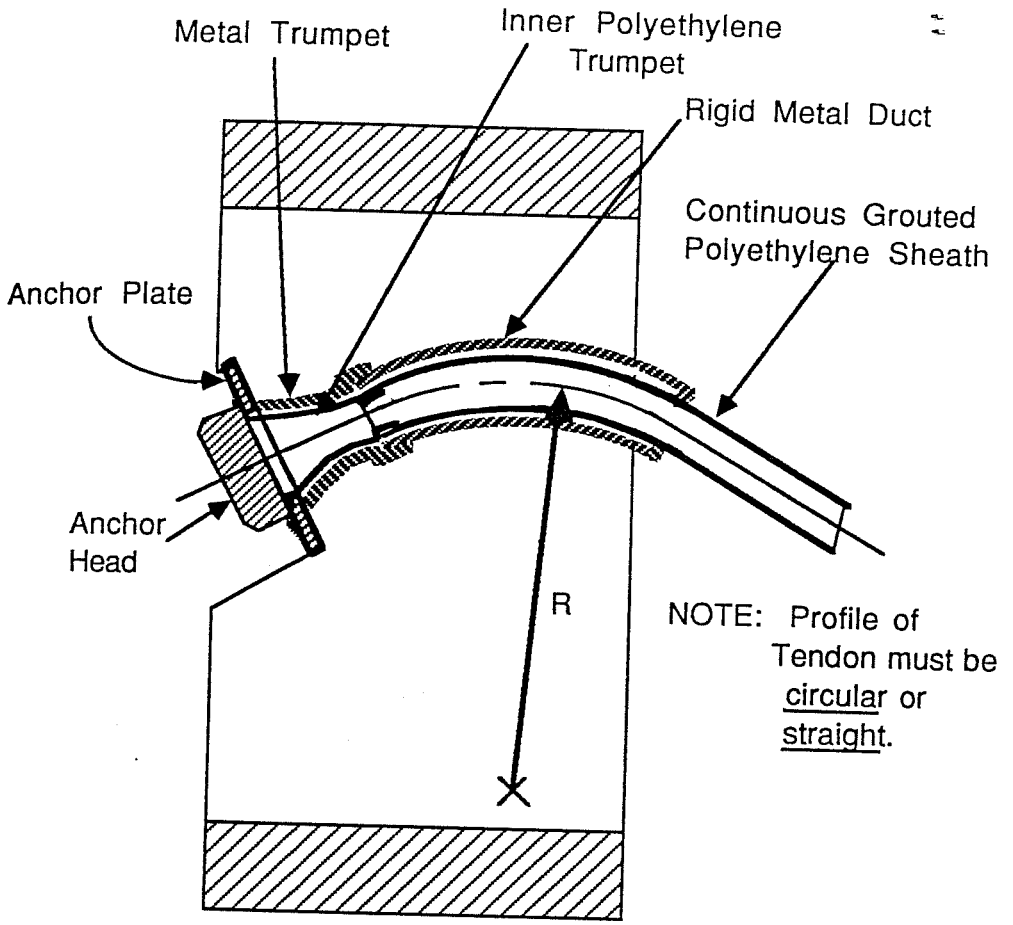

Figure 2.24 "Double Duct" for Replaceable Tendons

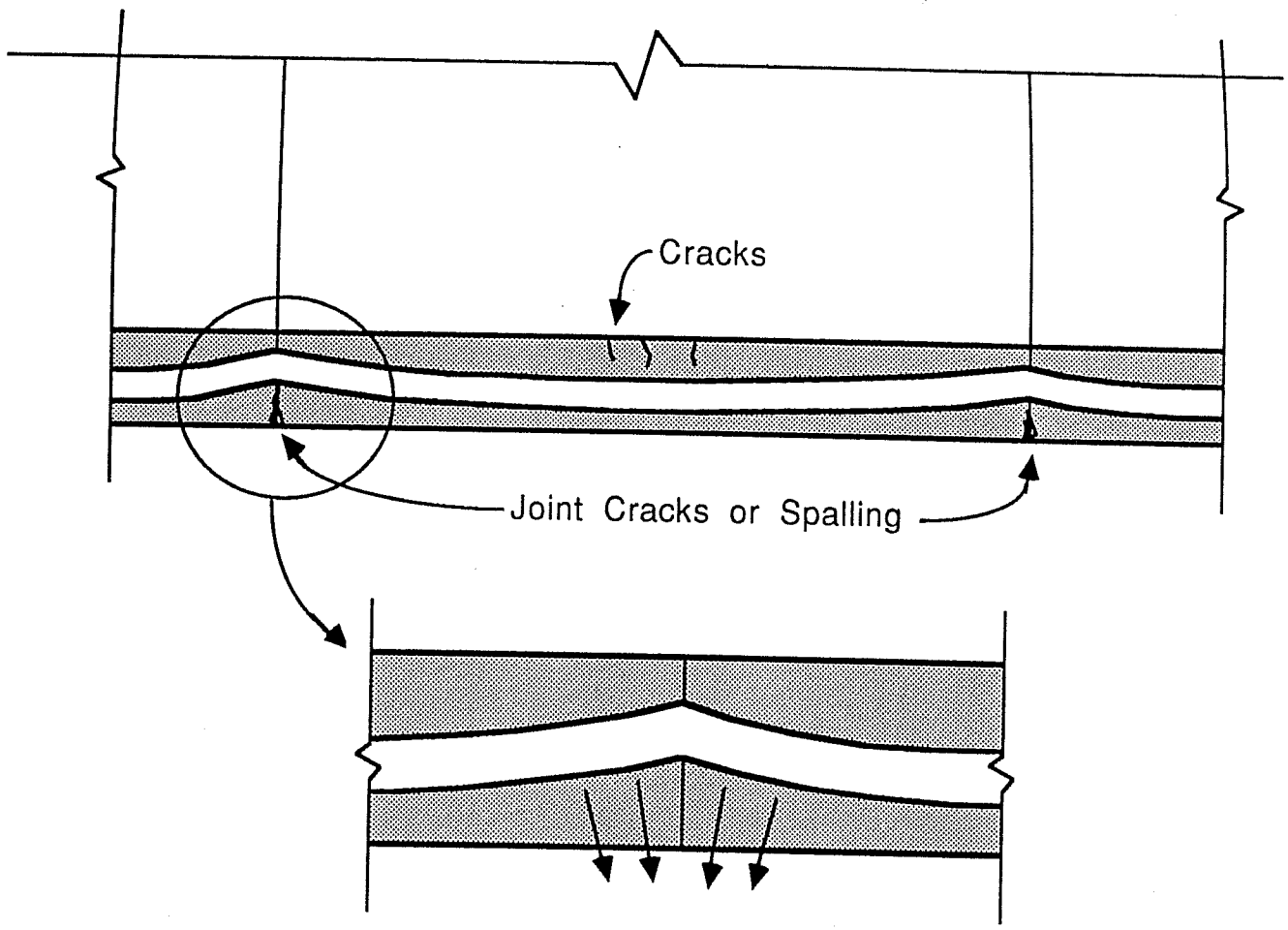

Figure 2.25 Misalignment of Ducts at Segment Joints

post-tensioning can also work to their disadvantage. Since tendons are external to the concrete cross section, eccentricity may be decreased and the free tendons can vibrate. External tendons are considered unbonded tendons, which behave differently from internal, bonded post-tensioning. Lack of bond can result in a reduction in efficiency and ductility, and a concentration of forces at attachment points.

Vibration of Unrestrained Tendons. Attachments of external tendons to the concrete section are often spaced quite far apart. The problem of vibration of long expanses of free cable has been experienced several times. Special precautions are required in these cases.

Reduced Eccentricity. Reduction in available eccentricity of prestress force is another negative aspect of external post-tensioning. For the typical closed box girder section, the tendon ususally lies inside the inner surfaces of the flanges. The limited eccentricity decreases flexural efficiency.

Reduced Efficiency of Unbonded Tendons. Reduced efficiency at ultimate is characteristic of beams with unbonded tendons. Instead of the large numbers of small, well-distributed cracks which occur with internal bonded tendons, a few large cracks appear in unbonded beams [15]. Tendon strain is averaged over the length of the tendon, so the stress in the tendon at

ultimate is only slightly above stressing levels. The concentration of rotation at a single crack often results in an early compressive type failure (Fig. 2.26). The absence of passive reinforcement across these large cracks (or the open joints in the case of segmental bridges) worsens the condition.

In addition, there may be a reduction of shear transfer for external tendons due to the absence of dowel action in the web. This is probably a minor effect, though.

Reduced Ductility. The loss of ductility for externally post-tensioned bridges is currently the subject of experimental and analytical study. A comparison of theoretical moment-deflection curves for a simple model analyzed first with internal bonded tendons, then with external unbonded tendons, illustrates the loss of ductility in the external tendon case (Fig. 2.27)(3). Experimental studies have confirmed this trend (16,17).

Concentrated Forces at Attachments. Another area under experimental investigation concerns the diffusion of concentrated forces at anchorages and deviations. These elements represent the only physical attachment of the external tendon to the concrete girder. Distress or failure of such elements could be catastrophic.

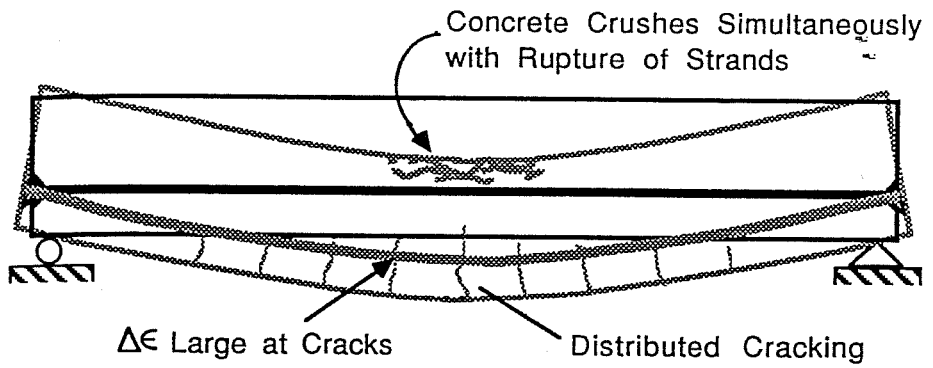

BONDED TENDON

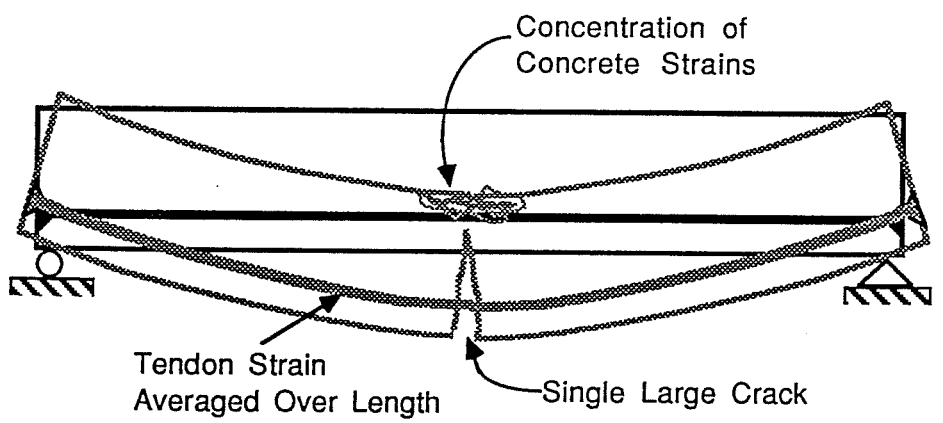

UNBONDED TENDON

Figure 2.26 Reduced Efficiency for Unbonded Tendons

Fig. ~~2.1~~ 1.2 out →

hurry report

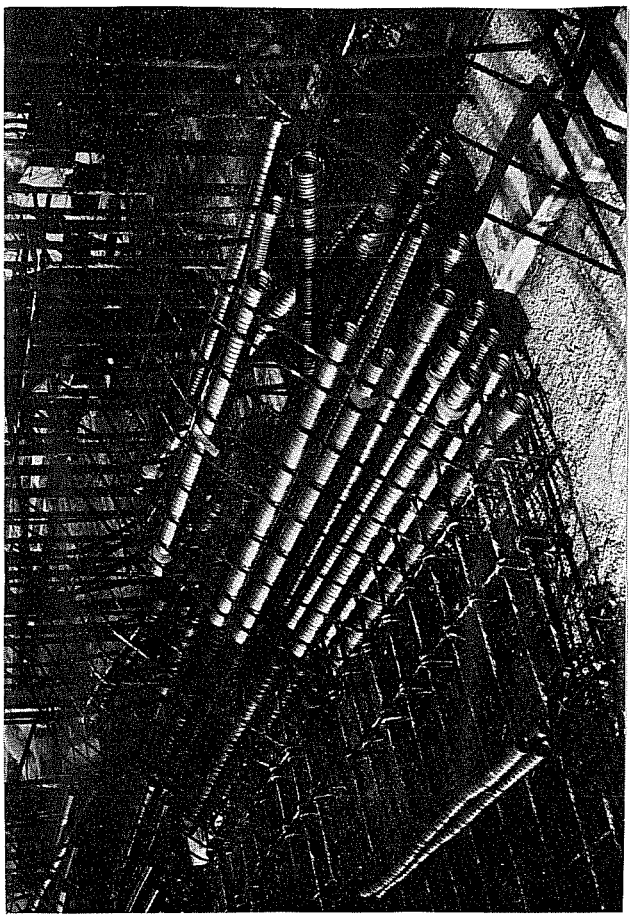

Figure 1.1 Congestion of Ducts for Internal Tendons

What we have to work with ↑.
Enlargements w/ different
amts of light follow. Take
your pick.

2.1

2.2

2.3

2.4

$2.5 + 2.6$

2.7 4

2.8

25 + 26

2.9 a

2.9 b

2.10

2.11

2.14

2.15

47 & 48

2.18

2.19

2.20

2.21

2.17

๒.๒๐

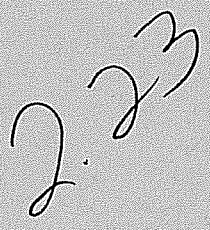

2.24

J.26

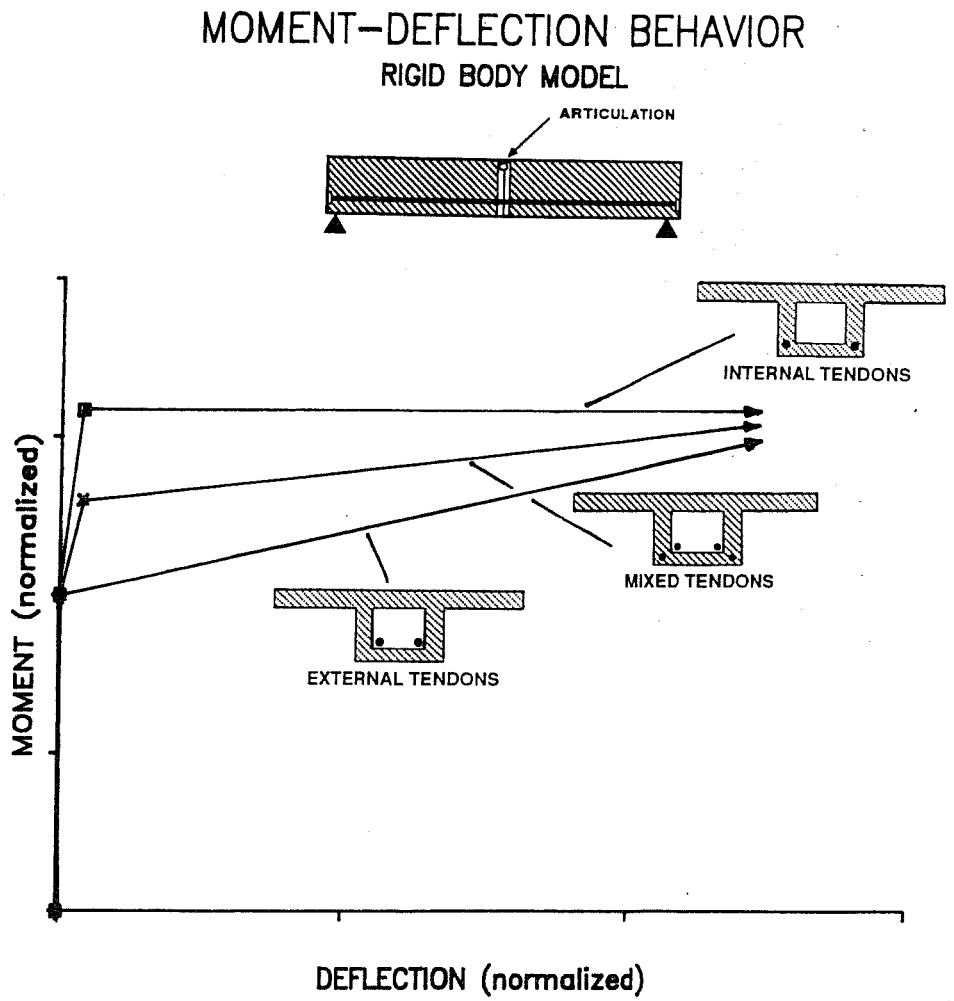

Figure 2.27 Reduced Ductility for External Tendons

2.4 Deviators

One detail that is unique to external post-tensioning is the deviation device. The deviator is a critical detail since, other than at anchorages, it is the only positive attachment of the external tendon to the concrete section. Deviators provide the hold-down points necessary to achieve the draped tendon profiles required by flexural and shear design, and by geometry. Since the first externally post-tensioned structures were built, designers have devised a variety of alternatives for deviation devices.

2.4.1 Types of Deviators. The most common configurations of deviation devices for external tendons can be categorized by shape into three basic types: (1) the diaphragm (see Fig. 2.28), (2) the rib or stiffener (see Fig. 2.29), and (3) the saddle of block (see Fig. 2.30). Each is comprised of a reinforced concrete projection cast monolithically with the bridge section which contains curved rigid ducts through which pass the external tendons. Block, rib or diaphragm deviators work well with the box girder cross section typically used for bridges with external tendons. Departures from the box-shaped section can require innovative conceptions for deviators. The Bubiyan bridge and the Saint-Agnant viaduct deviators, for example, include grooves cast strategically into the lower parts of the girder segments.

2.26

2.29

2.36

2.4.1.1 Diaphragm. Diaphragm type deviators are usually "U"-shaped, (Fig. 2.28a), or the "U" may be inverted. The opening allows passage through the void of the girder. The thickness of the diaphragm, typically ranging from 12 to 30 inches, is normally dictated by the length required to achieve a particular deviation. In some cases the upper part of the diaphragm is thinner; the lower section containing the deviated tendon extends out from either side, as in Fig. 2.28b.

2.4.1.2 Rib. The stiffener or rib shape is normally employed for retrofit measures where external tendons are added, although it has also been incorporated in new bridge designs. The ribs are typically somewhat shallow, extending perhaps a foot or so from the web of the box section. The depth is usually increased at the toe and the head of the rib (Fig. 2.29).

2.4.1.3 Block. Jean Muller is credited with the conception of the saddle or block type deviator (3). This relatively small block is located at the junction of the web and lower flange of the box section. Figure 2.30 illustrates some typical shapes for deviation blocks.

2.4.2 Ducts. Ducts located within deviators guide the external tendons and separate them from the concrete. Typically, the duct is formed by embedding a smooth, curved, rigid metal pipe (usually standard steel pipe) in the concrete section of the deviator.

2.4.2.1 Duct Details. Detailing the ducts requires care to minimize friction between the tendon and the duct and to avoid problems due to misalignment of the duct. Since the deviation of an external tendon usually involves both horizontal and vertical components, precise positioning of the curved pipe within this spatial geometry is often difficult.

Usually, the ends of the embedded pipe extend four to eight inches beyond the face of the deviator. This extension provides a place for attaching the protective sheathing that is generally used for external tendons. Figure 2.31 shows a typical detail for attaching polyethylene pipe to metal duct. The sheathing and duct are typically injected with cement grout (conventional American practice) or with grease or wax (European practice). If cement grout is used, the tendon is effectively bonded at the deviator. Grease or wax injection is used when the possibility of tendon replacement is to be retained. Extending the metal duct can also ameliorate slight misalignment problems since the duct can deform (see Sec. 2.5.2).

A "double duct" configuration has been used in several French bridges. In this case, the tendon sheathing remains continuous over the full length of the tendon (Fig. 2.32). This detail enables replacement of the tendon.

2-31

2.32

Another type of metal duct which has been used in some externally post-tensioned bridges has a flared or "bugle" shape. This shape avoids misalignment problems (refer to Sec. 2.5.2).

2.4.2.2 Duct Size. The minimum nominal duct area for a multiple-strand post-tensioning tendon is specified as two times the area of the tendon (21,22,23). For external tendons, however, a desirable criteria of 2-1/2 times the area of the tendons has been recommended (24).

2.4.2.3 Radius of Curvature. Rigid metal ducts are cold-bent to a radius required to conform to the geometry of the external tendon profile. The radius is chosen to achieve the total deviation angle within the length of the deviator. Ordinarily, the duct is actually bent to a slightly smaller radius in order to avoid misalignment problems (refer to Sec. 2.5.2). If the radius of curvature is small, however, the friction loss due to curvature can be considerable. This must be taken into consideration during the conception of the tendon profile and the design of the deviator. Neither AASHTO nor PTI specify a minimum radius of curvature for post-tensioning ducts (22,23). In standard American practice 15 feet is normally the smallest radius used for internal tendons. The 15 foot dimension corresponds to the minimum radius that traditional corrugated post-tensioning duct can be bent without kinking (25). For external tendons, the following has been recommended as a

desirable criteria:(24)

Minimum radius at piers: 20 ft. for 19-strand tendons
15 ft. for 12-strand tendons
10ft.for 7-strand tendons
and smaller

Minimum radius at deviators: 10 ft. for all tendon sizes.

Pending results from tests to be conducted at the Saint Remy Laboratory, the French federal transportation administration specifies a minimum radius for external post-tensioning ducts of 3 meters (9.2 ft.) for smaller tendons, and 4 meters (12.3 ft.) for larger tendons (eg. 19-0.6 in. diameter strands or larger). The same requirements apply to conventional internal tendon ducts [3].

2.4.3 Reinforcing Schemes. To illustrate the types of typical reinforcement currently being used in deviators, several reinforcing diagrams from existing structures are shown.

2.4.3.1 Saddle or Block - Typical Reinforcement. Reinforcement for deviation blocks is usually mild reinforcing steel in the form of links and bent bars anchored back to the web and bottom flange of the box girder section. Figures 2.33a-c present several examples from existing bridges.

2.4.3.2 Diaphragm - Typical Reinforcement. Diaphragm type deviators typically include a mesh of horizontal and vertical reinforcing bars which tie into the flanges and webs of

2,339

p. 336

2 33c

the box girder section. Additional bent bars provide confinement in the region of the deviation ducts. Transverse post-tensioning has also been used. Figure 2.34 shows some examples of diaphragm reinforcement.

2.4.3.3 Design Criteria and Procedures. The exact criteria that have been utilized for the design of deviation devices in existing bridges are not well known. That is to say, no open literature has been found where such criteria have been published. Regarding deviation saddles, personal conversations with engineers in the industry have revealed that deviators are designed to resist direct tension and shear friction using basic ACI Building Code procedures. The service load is taken as the deviated force component of the tendon at a stress level of 80 percent of ultimate, and the maximum service stress of the mild reinforcement is taken as 40 percent of yield stress.

A recently published document from the Florida Department of Transportation cites similar criteria (18). The following is an excerpt from Chapter 4 (Design Criteria for Segmental Bridges) of that document, Section 10. Deviation Saddles:

> "10.2 Design
> Reinforcement shall be provided in the form of links and bent bars to take the full resultant pullout force from the deviated tendon(s) at a service stress of 0.4 fy. Additional reinforcement shall be provided to take any out of balance longitudinal forces by shear action according to the latest A.C.I. Standard 318,

2.34

Article 11.7. Reinforcement shall also be provided to take any localized bending effects transmitted from the deviation saddles to the webs and/or flanges.

10.3 Detailing
All reinforcement shall have a full effective development length measured from the tendon axis or shall otherwise be fully mechanically anchored around longitudinal reinforcement located at the outside of the (box) section. Consideration shall be given to constructability and clearances between reinforcement for adequate concrete compaction. As a guide, not more than two reinforcing bars shall be bundled and the clear distance between reinforcement should be at least one-half inch (1/2") greater than the maximum aggregate size and in no case less than 1-1/2"."

2.5 Problem Areas Concerning Deviators

2.5.1 Deviator Type. The configuration of deviators has been a controversial issue (3). One design philosophy advocates the use of deviation blocks. The other more conservative school of thought prefers the full height diaphragm for deviating external tendons. The rib type deviator represents a compromise between the block and the diaphragm. Each of the solutions has definite advantages as well as disadvantages.

One point of contention between the design philosophies is the relative strength of each deviator type. Clearly, the strength of any design depends to a large extent on the detailing of the reinforcement. Even with adequate detailing, however, it is reasonable to expect a greater risk of catastrophic failure for a deviation block than for the rib or diaphragm deviators. Generally, in a diaphragm or rib, a compression strut forms above

the deviated tendon. This compression strut contributes to the post-cracking strength of the deviator. (This is not always the case, however, as evidenced by the problems with the Pont-a-Mousson diaphragms; reference Sec. 2.5.4). In a cracked deviation block, there is no compression strut. The deviator reinforcement must resist the pullout forces with little contribution from the concrete.

The block or saddle deviator has seen more prevalent use in U.S. bridges. Long Key, Seven Mile, Glenwood Canyon, Dauphin Island, and Sunshine Skyway bridges all include this type of deviation detail. Two french structures, the Banquiere and Vallon-des-Fleurs viaducts, included a slightly larger version of the typical American deviation block. With regard to construction, the saddle or block configuration presents considerable advantages. The formwork can be greatly simplified, since only a small blockout in the interior form is required. When casting a segment without a deviator, the blockout is simply sheathed over. In addition, the small block adds an almost insignificant amount to the self-weight of the superstructure [3].

On the other hand, the use of deviation blocks imposes limitations on the tendon profile. The points of deviation are, in effect, predetermined by the geometry of the structure. The

external tendons cannot be aligned in a single vertical plane; the profile must therefore include otherwise unnecessary horizontal displacements [3].

Full-height diaphragms allow the designer complete freedom when laying out the tendon profile (3). Ordinarily, efforts are made to reduce the number of diaphragms required since the diaphragms add substantial weight to the structure. Reducing the number of deviations increases the magnitude of the deviation angles, creating larger deviation forces on the diaphragm. The resulting diaphragm required usually has a "U" shape. The bottom part of the "U" is designed to stiffen the lower flange to carry localized bending from the deviation forces.

From a construction point of view, the full-height diaphragm is cumbersome. Obviously, the formwork becomes more complicated. For segmental construction, segments with diaphragms must often be made shorter, due to weight restrictions for segment handling. This results in further modification of forms. Alternatively, the diaphragms may be placed in a second stage cast, in which case dowels must be provided and an opening left in the upper flange for subsequent concreting (3). Moreover, the diaphragms can add considerably to the dead load, easily offsetting the savings offered by web reduction.

2.5.2 Geometry Errors of Ducts Embedded in Deviator. The difficulty of properly aligning the ducts within the deviator has caused recurrent problems. There are three principal sources of error: bending of the duct to an incorrect radius of curvature, improper positioning of the ends of the duct at the faces of the deviator, and pivoting of the duct around the axis joining the points of exit. Care must be taken to ensure that the duct is adequately secured so that it will not shift during concreting [12]. The misaligned duct creates angular bends or kinks in the tendon at the point of exit from the concrete. The kink, in turn, creates concentrated forces which are applied to the unreinforced cover at the face of the deviator. Damage, in the form of cracking or spalling, is usually noticed during stressing procedures when deviation forces are highest. Repair measures may become necessary. Undetected damage may lead to corrosion of the mild reinforcement in the deviator, possibly resulting in further distress or disfunction of the deviator.

Not only the concrete deviator, but the tendon as well, is subject to damage. Localized bending of strands in the tendon, and rubbing under the action of loading, can result in wear and fatigue of the tendon.

Several preventive measures have been devised to alleviate problems due to geometry errors of ducts in deviators. Extending the duct a few inches beyond the face of the concrete

allows the metal duct to deform somewhat, softening the kink. In addition, the duct is made larger than necessary and bent to a slightly smaller radius than that required for the exact geometry of the tendon profile. Under these conditions, the tendon is less likely to bear against the face of the concrete (Fig. 2.35a). Another method inserts some flexible material around the end of the duct at the face of the concrete. This isolates the duct from the unreinforced cover and transfers the concentrated force to the reinforced concrete (Fig. 2.35b)[12]. A different idea used in some French bridges employs a bugle shaped rigid metal duct (Fig. 2.36). The radius of the flare is smaller than that required by the tendon geometry for all deviators in the bridge. In this manner, the same duct can be used for all deviators, and location of the ducts is simplified.

2.5.3 Force Diffusion at Deviator. There are two areas of uncertainty concerning force diffusion at the deviators: How do the concentrated force components from the deviated tendon distribute within the deviator? How does the deviator transfer forces to the box girder section? The second question is of less interest; there have been no reports of damage to the concrete in the girder section. Most of the problems that have occurred have involved cracking or spalling of the deviator itself.

2.35

2.36

2.5.4 Damage to Deviators in Existing Structures. Several incidences of damage to deviators in existing structures have occurred. Most of the problems that have been published have originated from errors in geometry of the ducts within the deviators. Other problems, more structural in nature, have also been reported. Unfortunately, when problems occur, parties involved with the distressed structure are naturally reluctant to publicly disclose information about the problems, so as not to call attention to them. The author has learned of the following accounts through published reports, personal conversations with eyewitnesses, and from first-hand observations.

The Sermanez viaduct (reference Sec. 2.2.5.5) is one of the few externally post-tensioned bridges built by the cantilever method. The complicated tendon profile required a large number of ducts in each of the closely spaced deviation ribs. Imperfections in the alignment of several ducts (the ends of which were flush with the face of the concrete) provoked minor spalling around the ducts. The galvanized external tendons were carefully checked, fortunately revealing no damage to the galvanized coating at the kinks [11].

A similar incident involved a segmental box girder bridge with deviation saddles. During stressing of the first few spans, the concrete around the ducts in several deviators spalled and cracked. The spalled concrete was chipped away and patched.

For the remaining segments which were waiting for erection, the contractor rechecked the alignment of each duct using surveying equipment. Unacceptable deviators were repaired by chipping away the concrete around the end of the duct, bending the duct to the proper position, and then patching.

The Pont-a-Mousson bridge (reference Sec. 2.2.5.6) incurred more serious cracking in the diaphragm type deviators. The external tendon profile included some sharp horizontal deviations which were directed inward toward the void of the box section (Fig. 2.37a). Interferences with anchorages for internal continuity tendons necessitated these horizontal deviations. Large cracks and spalling appeared during stressing operations (see Fig. 2.37b), requiring extensive repairs [12].

In another case, deviation diphragms were highly congested with reinforcing steel and ducts of multiple tendons which were deviated or passing through the diaphragm. A combination of the shape of the diaphragm and congestion in the reinforcing cage resulted in poor consolidation in the area of the deviations. For a large number of segments, the deficient concrete had to be chipped away and repaired with an epoxy-based cement patch.

In other structures, there have been reports of structural cracking in the deviation saddles. One such report

involved a large number of relatively small cracks in several deviation blocks. Most of these cracks appeared on the top faces of the blocks and ran perpendicular to the tendons.

2.5.5 Lack of Consistent Design Philosophy. Because little is known about the behavior of deviators under overload, universally accepted models for designing deviators do not exist. When using design procedures for proportioning direct tension and shear friction reinforcement, the load path of the deviation forces is left up to the designer. Where complete reinforcement details and tendon layouts have been available, the author has attempted to back-calculate from the given loads and areas of steel, in order to determine the rationale used for designing a particular deviator. In most cases, a rational approach for distributing forces to the appropriate reinforcement was not apparent. One objective of this research program is to establish a representative model for behavior of deviation blocks.

2.6 Related Research

Experimental research with external post-tensioning may be regarded as in its infancy. The most significant projects known are briefly described below.

2.6.1 Girder Studies with External Tendons.

Laboratory at Saint-Remy, France. Under the combined auspices of the French organizations SETRA (Service d"Etude

Technique des Routes et Autoroutes) and CEBTP (Centre Experimentale de Recherce et D'Etudes du Batiment et des Travaux Publics), engineers at the laboratory at Saint-Remy conducted tests of four externally post-tensioned segmental box girders. The primary objective of the study was to examine the ultimate behavior of girders with external tendons in order to furnish or justify the assumed criteria used for ultimate strength calculations [16].

The test girders were match cast and erected with dry joints. The reduced-scale cross section used for all four tests was a simple, compact prismatic box girder (Fig. 2.38). The girders differed in tendon profile and type of tendon protection (grouted, hot wax injected). The fourth test girder also included some internal tendons. The behavior of the deviators, and their effect on overall behavior, was not a parameter in this study [16].

The simply supported girders were loaded symmetrically with point loads at outer quarter points. All girders experienced the same failure mode, independent of tendon profile or protection. First, the central joints opened and continued to open up to the level of the bottom surface of the top flange. At the same time, diagonal cracks propogated upward from the shear keys in the compressed region. The stress in the tendons did not rise significantly until the applied load was within

2.38

2.39

subsequently unloaded and, in attempt to simulate an anchorage loss in the case of an earthquake, the wedges for some of the strands were burned and removed. The girders were then reloaded incrementally to failure [17].

The failure mode for the bonded tendon girder was flexural; concrete in the compression zone crushed simultaneously with the fracturing of strands in the tensile zone. The unbonded and modified bonded tendon girders both experienced a shear-compression failure in the top flange. Joints opened and shear keys progressively broke, concentrating strain in the top flange [17].

Ferguson Structural Engineering Laboratory. An experimental program involving external tendons is presently underway at the University of Texas at Austin's Ferguson Laboratory. Sponsored by the Texas Department of Highways and Public Transportation, the program includes construction and testing of a quarter-scale three span continuous bridge model. A computer program is concurrently being developed to analyze externally post-tensioned systems. As with the other girder studies, behavior of the deviators is not a parameter in the bridge test.

2.6.2 Deviator Studies. The only other known experimental program involving deviators is currently ongoing at the laboratory at Saint-Remy-Les-Chevreuse in France. Sponsored

by SETRA-CEBTP, this study concerns not the behavior of the deviator itself, but the behavior of the deviated tendons. Parameters in the study include characteristics of the deviation (e.g. radius of curvature, deviation angle, duct type and size, etc.), nature of the tendon (e.g. number of strands, degree of entanglement of the strands), tendon protection (duct material and injection product), and loading. The Saint-Remy laboratory does have future plans to study the deviator itself, using the same test setup used in the tendon tests [19].

CHAPTER 3

TEST AND SPECIMEN DESIGN

3.1 Test Objectives

To begin a program of deviator research, a representative prototype was chosen from existing U.S. structures. Based on that prototype a scale model was constructed for testing. For this first set of tests, the basic objectives were to:

1) Investigate the behavior of the deviator through a full range of loading. Is the mode of failure of the deviator relatively brittle or ductile? Is the failure zone confined to the deviator itself, or are there significant local effects in the web and flange surrounding the deviator?

2) Evaluate the design of the prototype deviator with respect to details and overall performance. Is adequate anchorage provided for tying the deviator to the concrete section? Do splices and laps develop? How much reserve capacity over service load level is provided by this typical design? Are similar current designs safe?

3) Determine a generalized model of behavior for this particular case. How does each type of reinforcement contribute to the overall load carrying system? What are important

considerations (e.g. shear friction, local bending, confinement) for design and detailing of this type of deviator?

4) Suggest a safe, rational design approach. If a reasonable model can be established from the limited test data, a more rational approach for design than currently exists can be suggested. Pending further study, a set of design procedures can be refined.

5) Evaluate the test setup. Does it function well? Can it be modified to facilite testing, or to improve test conditions?

6) Provide a starting point for further study. What are the important parameters that affect behavior? Can these parameters be isolated, or instrumented more effectively?

3.2 Test Specimens

3.2.1 Basis for Models. A thorough survey of existing externally post-tensioned bridge structures revealed that the deviation block is the most prevalent type of deviation detail. Common sense dictates that the block type deviators are generally weaker than diaphragms or rib deviators. But the deviation block also has advantages over other alternatives (reference Section 2.5.1), and could have even more appeal if testing confirms the safety of this type of detail. Several of the structures that were examined had very similar deviator reinforcing details. One

structure from this set was chosen as a prototype for the scale model.

The model comprised a typical segment of the single-cell box girder bridge, excluding the cantilever wing portions. The two deviators in the model segment were tested one at a time. Both deviators had identical reinforcement, but were taken from adjacent segments in the span. While one block deviated two tendons, the other contained three. This was done to see how a change in the relative magnitude and direction of the total force component on the deviator would affect its behavior.

The basic box section of the specimen had several advantages. It eliminated torsional problems and was easy to anchor. The single cell box is a typical section and makes an adaptable basis for future testing. Reinforced according to AASHTO minimum requirements, the basic box can remain the same regardless of the type of deviator to be tested. Only the deviator reinforcement and the inside forms need to be replaced.

3.2.2 Scale Factor. Several considerations influenced the choice of scale factor. On one hand, the specimen needed to be large enough so that scaling would not appreciably alter local effects. In addition, too small a specimen would complicate construction, since tolerances for placement of reinforcing bars and ducts would be critical. On the other hand, too large a specimen would require unrealistically large test appurtenances

and equipment in order to develop the tendon reactions. Safety was also a factor in limiting the size to a reasonable level. Finally, a linear scale factor of 1/3 was chosen.

3.2.3 Dimensions of Prototype and Model. The prototype cross section is shown in Fig. 3.1a-b. For modelling, the shape of the box and of the deviation block were simplified somewhat. The total width of the prototype box as well as the length of the segment were reduced by 2/3 before applying the 1/3 scale factor to facilitate anchorage and handling of the specimen. Fig. 3.2 shows the model cross section and dimensions.

3.2.4 Tendon Layouts. The prototype tendon layout, and resulting deviation angles, are presented in Fig. 3.3. The modelled deviations are denoted as "Block A" and "Block B" in the figure. Figures 3.4a-c show the tendon layouts used for each test. Geometry constraints of the test setup prohibited exact reproductions of the prototype deviation angles for each tendon. However, the layouts were manipulated in such a way that the total relative horizontal and vertical components on the deviator are approximately the same.

3.2.5 Choice of Materials.

3.2.5.1 Concrete. The specimen concrete strength of 6000 psi is representative of strengths used for segmental post-tensioned construction. The availability of 3/8" pea gravel for

3.1a &

3.1b

3.2

3.3

3.4 a b & c

coarse aggregate precluded the need for micro-concrete. ACI proportioning guidelines were followed to obtain mix designs for several trial batches. Retarder was added since the construction of the specimen took place during summer in Austin, where temperatures routinely reach 100 degrees. Workability was an important criteria since good consolidation in and around the deviation block was very important. From the trial batches a suitable mix was selected. A local ready-mix plant supplied the concrete.

3.2.5.2 Mild Reinforcing Steel. The smallest conventional reinforcing bars (No. 3's) were too large for the third scale model. Undeformed wire was unacceptable, as it was felt that bond characteristics might play an important role in the behavior of the deviator. Fortunately, deformed microbars (No. 1's, 1.5's and 2's) were located. When tested, the microbars demonstrated a relatively brittle behavior so the bars were annealed to produce a stress-strain behavior very similar to conventional GR 40 reinforcing steel. The range of available sizes allowed a close representation of the prototype deviator reinforcement; in most cases the same number of bars were used. The microbars also had the advantage of being easy to bend, a desirable quality since much of the reinforcing in the deviator had complex shapes.

3.2.5.3 Ducts. A smooth walled duct with a representative scaled wall thickness was desired. Thin-walled galvanized metal conduit was chosen for this purpose.

3.2.5.4 Tendons. Seven-wire strand with a nominal diameter of 3/8 inches was a convenient choice for the multi-strand tendons, since this size was compatible with standard anchorage hardware and stressing equipment. The low relaxation strand had a nominal ultimate strength of 270 ksi.

3.3 Test Setup

The primary concerns governing the design of the test setup were safety and adaptability. In any application, the concentrated energy stored in highly stressed post-tensioning tendons presents a potentially dangerous situation which must be carefully and concientiously controlled. The danger is magnified tenfold with external tendons, since, after stressing, the tendon is not contained inside a beam or slab of concrete, but is exposed. Several precautions were taken to ensure the safety of the testing crew and general laboratory personnel.

Since it was difficult to foresee the direction and scope that the deviator research program would take, adaptability was important. Adaptability of the setup meant incorporating in the test structures and equipment the means to test a variety of

specimens including flexibility in specimen size, the number of tendons, the layout of the tendons and the loading method.

3.3.1 General Layout. Figure 3.5a illustrates the basic testing concept while Figures 3.5b-c show the structures and equipment that make up the testing assembly. Two large concrete reaction buttresses are anchored to the structural laboratory floor with high-strength post-tensioned threaded rods. The normal clamping force from the tensioned rods provides shear friction resistance capable of developing a total horizontal reaction of up to 460 kips from the post-tensioning tendons.

Heavy steel lever frames are pin-connected to the end of each buttress. Restraining arms at the sides of the frames fasten to the buttresses to hold the frames in position between tests. The external tendons anchor at the back side of each frame. Anchor plates for the post-tensioning tendons bolt to the frame members. Located at the north end of the setup, frame "A" is designed to accomodate anchorages in a number of positions along a horizontal line (Fig. 3.6). Stressing operations take place at this end. The tendons run from the "A" frame, pass through the specimen deviator, and are deviated to the "B" frame, located at the south end of the setup. The "B" frame is designed as a sort of "grillage" of deep vertical members (Fig. 3.7). Anchor plates can be bolted to the vertical members in a number

3.5a, b, and

3.5c

3.6

3.7

of positions in order to achieve the desired deviation angle at the deviator.

A pair of 100-ton capacity hydraulic rams supply the upper reaction between the lever frame and the buttress. The rams are suspended by ajustable rods from small cantilever frames fixed to the tops of the buttress uprights. Spherical heads attached to the rams ensure good bearing between the ram pistons and the steel frame members (Fig. 3.8).

Between the two buttresses, the specimen is anchored to a long concrete pedestal (Fig. 3.9). Like the buttresses, the pedestal is also prestressed to the structural floor. The pedestal serves two purposes. First, it elevates the specimen to the appropriate height. Secondly, a set of open steel moment frames bolted to the pedestal provide vertical and horizontal (i.e. east-west) restraint for the specimen. Additional devices attached to the pedestal provide restraint in the longitudinal (i.e. north-south) direction.

Additional equipment includes pumps for the hydraulic rams, the data acquisition computer system, surveying instruments for reading dial gages and remote monitoring of the specimen, and a video camera for recording the tests. This equipment is located on the east side of the setup. Large concrete barriers were installed at the extremities of the setup as a safety precaution.

3.8

3.9

3.3.2 Safety Features. As previously mentioned, safety of the laboratory personnel was of utmost importance during this test program. The main concern was to provide a system of containment for the stressed tendons in the event that a wire or strand should break or an anchorage should fail. Large concrete barriers are situated directly behind the anchorage zones. Plywood boxes designed to deflect or at least slow down possible projectiles are secured to the barriers (Fig. 3.10). Each external tendon is encased in a 3-1/2 in. diameter standard pipe. Several steel cables, looped around the pipes and anchored to the structural floor or to the buttresses, provide restraints for the tendons (Fig. 3.11).

The entire test area was roped off to general lab traffic during the tests. Surveying equipment provides a remote optical system for monitoring cracking in the deviatior and for reading dial gages located around the specimen.

3.3.3 Specimen Restraints. A system of restraints to anchor the specimen within the test setup was designed to limit as much as possible the rigid body motion of the box section, while keeping the deviation zone unrestrained. The restraint system is also fully adjustable to accomodate changes in the positioning of the specimens from test to test and the possibility of different sizes of specimens.

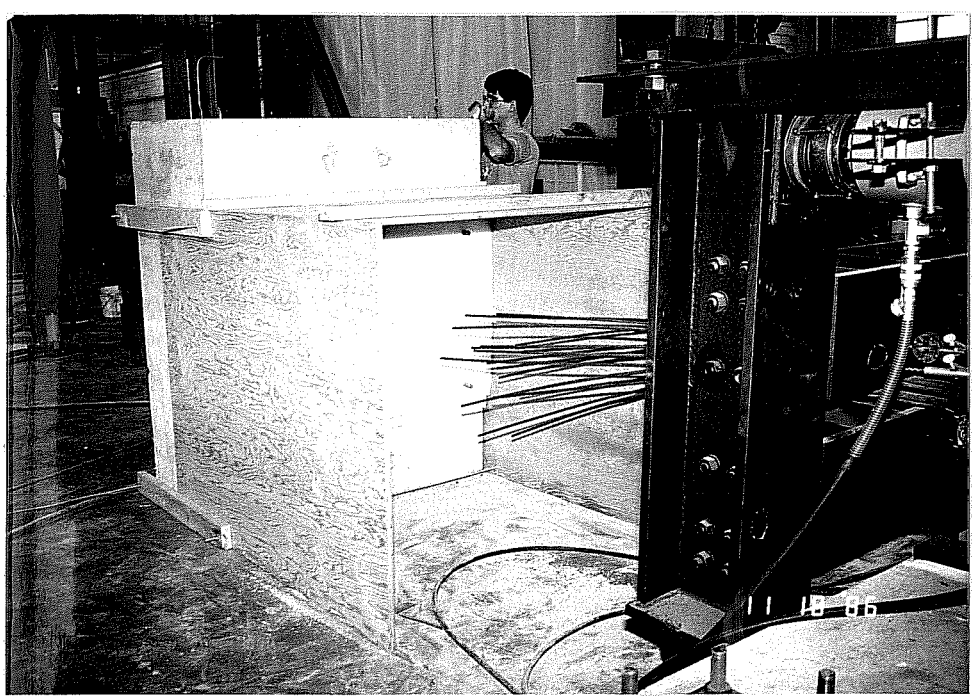

Figure 3.10 Concrete Safety Barrier with Plywood Containment Box

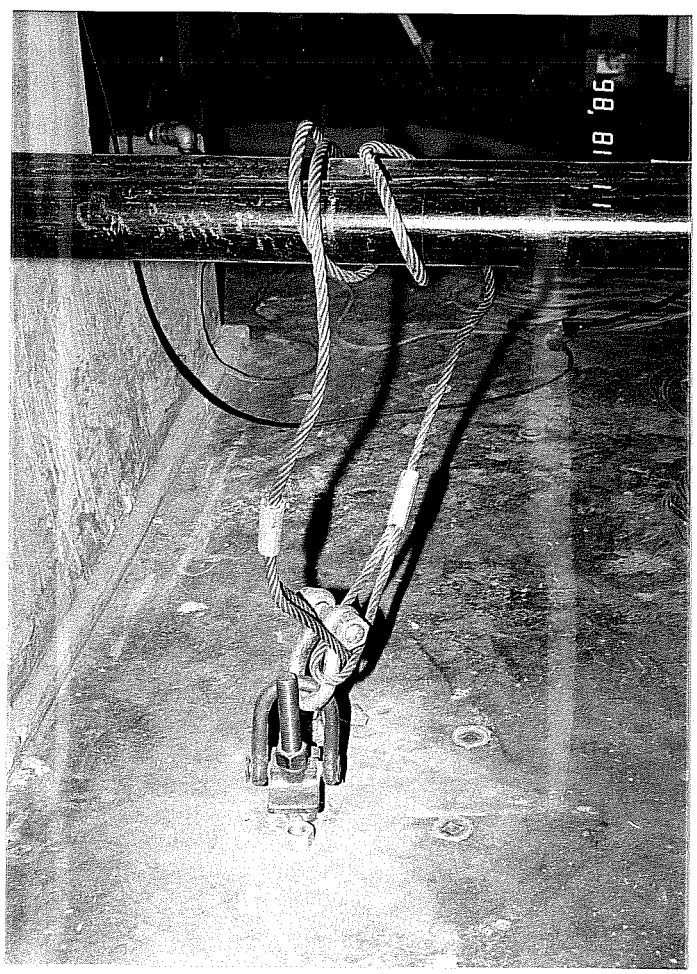

Figure 3.11 Tendon Restraint

The pair of moment frames which are fixed to the pedestal were designed to carry the maximum foreseeable deviation force components. Attached to these frames are a set of small adjustment assemblies. The adjustment assemblies bear on neoprene pads at the upper corners of the specimen box section. The base of the specimen rests on four small neoprene pads located at each corner of the base. By tightening the adjustment assemblies against the outside of the box the specimen is clamped into position (Fig. 3.12).

During the first test it became apparent that the longitudinal forces on the specimen were greater than had been anticipated. Slight damage to the pedestal required a more substantial system for longitudinal restraint. Figure 3.13 shows the revised detail, a double channel section which is prestressed to the pedestal. Steel spacer plates driven between the channel flanges and the bottom flange of the specimen ensure a tight fit.

3.3.4 Loading Concept. Forces on the deviator are increased by increasing the stress in the deviated tendons. This may be accomplished in a variety of ways. By adjusting the piston extensions on the pairs of 100-ton rams, then tightening the bolts on the frame restraining arms, the frames can be locked in any desired position (vertical, or inclined in or out). Then, using a standard jack for multi-strand tendons, any one tendon can be stressed incrementally to load the deviator. Or, for

3.12

3.13

multiple tendons, the tendons can be stressed, one at a time, to a desired preliminary stress level. Then, the stress in all tendons can be increased as the 100-ton rams are activated, pushing out the lever frames thereby extending the tendons. In this manner, the force in the tendons can be increased from one side only, by pushing out on only one frame. Or, the force can be increased from both sides, by alternately or simultaneously pushing out both lever frames. The movement of the frames can be controlled by monitoring either the deformation of the frame or the pressure in the hydraulic rams. Retracting the rams unloads the deviator. The variability in the loading scheme allows the test setup to be used to model many possible prototype loading scenarios. In addition, with some modification to the hydraulic system, the setup can be used for dynamic as well as static loading.

3.3.5 Anchorages. A combination of standard and specially fabricated hardware was utilized to anchor the multi-strand tendons at each lever frame. Freyssinet-type multi-strand anchor blocks were donated by Prescon Corp. The forged steel anchor blocks, type 12 K 5 P, have 12 tapered holes, drilled at correct angles to eliminate unwanted kinks in the strands, to accomodate up to 12-0.5 in. diameter strands and wedges. For the 3/8 in. diameter strands used in the tests, Prescon also supplied

special conversion wedges that allow anchorage of the smaller strand in the holes for 0.5 in. diameter strands. Anchor plates for "A" end anchorages consist of 1 inch thick rectangular steel plates with center holes for the the tendons, and bolt holes spaced to correspond with the holes drilled in the horizontal members of the "A" frame. Bevel welded to the anchor plate are 1 inch long sections of 5 in. nominal diameter double extra strong steel pipe. The surface of the 3/4 inch thick pipe wall serves as the bearing surface for the anchor block (Fig. 3.14).

Anchorages at the "B" frame posed a special problem. The tendons deviated to the "B" frame are inclined vertically and horizontally at the anchorage point. A bearing surface perpendicular to the direction of the tendon is required. To accomplish this, a section of the 5 in. nominal diameter double extra strong pipe was flame cut at an angle calculated to correspond to the angle of the tendon, and bevel welded to the 1 inch thick rectangular steel plate. Bolt holes, drilled in the plate, match holes in the vertical members of the "B" frame.

3.3.6 Instrumentation Concept. Several types of electronic and mechanical instrumentation are utilized to collect key information during the tests. The most important measured quantity is the force in the external tendons from which the deviation force components are calculated. Two different systems were selected to measure tendon force. Pressure transducers

3.14

connected to the 100-ton rams read hydraulic pressures that are converted to force units. The total force in the tendons is calculated from equilibrium canditions. For tests with only two tendons, equilibrium equations give the relative force in each tendon as well, since the point of application of the loads from the tendon and the geometry of the statically determinate frame are well known. A second system uses strain gages on several strands in each tendon.

Strain gages were placed on selected reinforcement within the deviation block. The objective of measuring strains in the reinforcement is to try to determine the participation of each reinforcing bar.

Linear potentiometers and dial gages monitor the rigid body motion of the concrete box and the displacement of the deviation block relative to the box. Potentiometers and dial gages are also used to monitor the movement of the lever frames.

A Hewlett-Packard data acquisition/control unit, hooked to an IBM XT PC collects and stores the electronic data.

CHAPTER 4

SPECIMEN DETAILS AND CONSTRUCTION

4.1 Details

4.1.1 Reinforcing Cage - Basic Box. Reinforcement for the specimen box section was proportioned to produce a basic box that would be adequate, not only for this particular specimen, but for future specimens as well. AASHTO minimum requirements for post-tensioned box girders (22) served as a guideline to arrive at a reinforcing scheme which is representative of segmental post-tensioned box girder construction. Maximum spacing restrictions were scaled from 18 inches to 6 inches. In most cases, slightly more than the minimum required reinforcement was used so that a convenient spacing could be obtained. The available reinforcing bars were No. 1.25 (A_s=0.019 sq.in.), No. 1.5 (A_s=0.028 sq.in.) and No. 2 (A_s=0.050 sq.in.) deformed microbars. Table 4.1 reviews the steel percentages used for the flanges and webs of the box. Figure 4.1 illustrates the resulting layout of reinforcement and the reinforcing schedule is given in Fig. 4.2.

4.1.2 Deviation Zone Steel. Prototype deviation reinforcement (Fig. 4.3) was scaled with respect to area and yield strength. For complete prototype deviator reinforcement details, refer to Fig. A.1 in the Appendix. Table 4.2 presents a

BOX REINFORCEMENT REQUIREMENTS

		% Steel req'd	Base Area	As required	As provided
TOP FLANGE	*LONGIDUDINAL*	0.4%	60"X3.5"= 210 in^2	0.84 in^2	11-#2 @ 6" o.c. top and bottom =1.09 in^2
	TRANSVERSE	0.5%*	24"x3.5"= 84 in^2	0.42 in^2	6-#2 @ 4.5 " o.c. top and bottom =0.595 in^2
BOTTOM FLANGE	*LONGITUDINAL*	0.4%*	40"x3.0"= 120 in^2	0.48 in^2	8-#2 @ 6" o.c. top and bottom =0.79 in^2
	TRANSVERSE	0.5%*	24"x3.0"= 72 in^2	0.36 in^2	6-#2 @ 4.5": o.c. top and bottom =0.595 in^2
WEBS	*LONGITUDINAL*	0.2%**	30"x3.5"= 105 in^2	0.125 in^2	5-#1.25. evenly spaced, e.f. =0.192 in^2
	PARALLEL TO WEB INCLINATION	0.5%***	24"x3.5"= 84 in^2	0.42 in^2	6-#2 @ 4.5" o.c., e.f. =0.595 in^2

* AASHTO Minimum requirement

** ACI Minimum for shrinkage and temperature

*** Usually governed by shear design. Use same as top flange transverse requirement.

Table 4.1

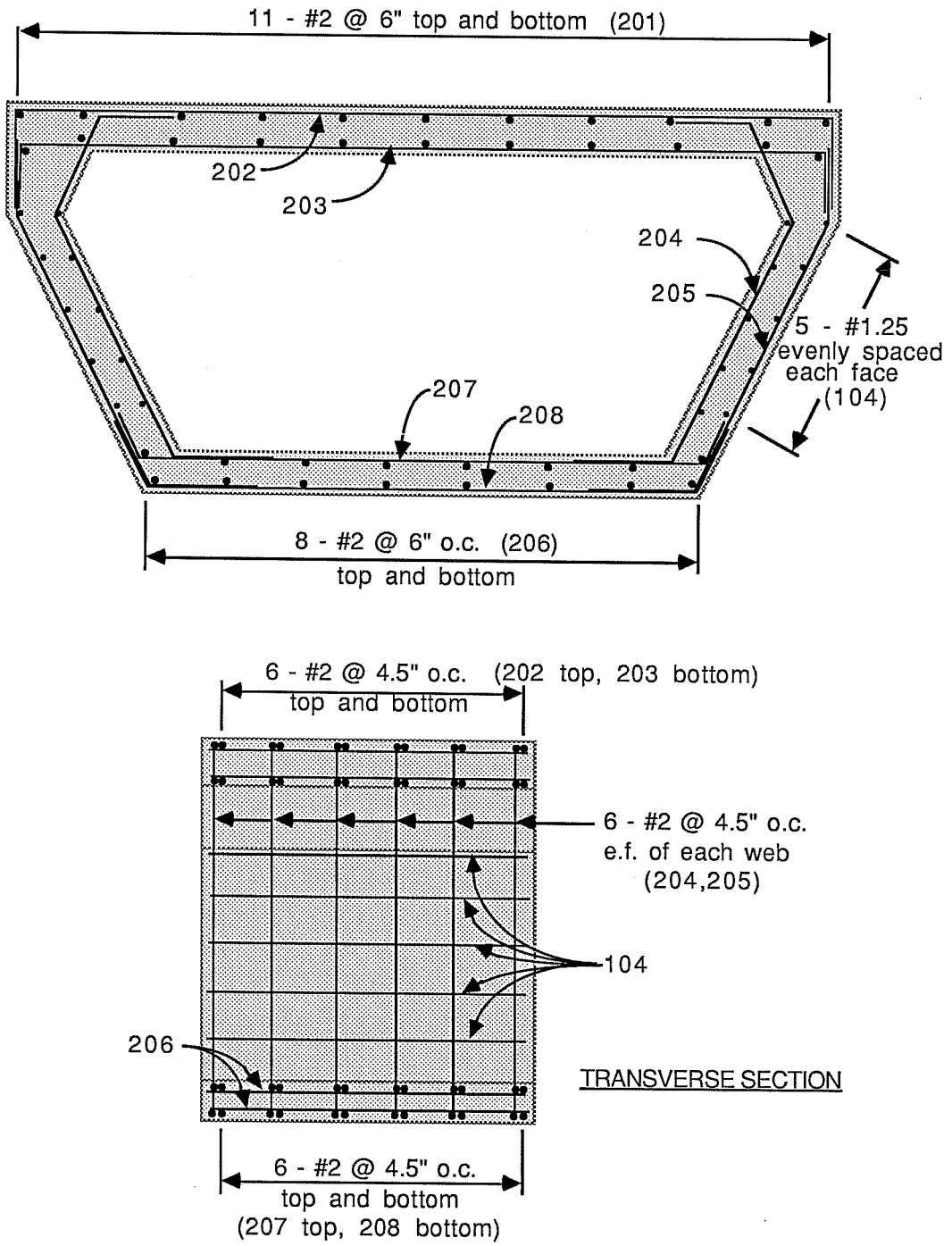

Figure 4.1 Box Reinforcement

Schedule No.	Bend Type	Bar Size	Length	Pieces required
201	straight	#2	23"	22
206	straight	#2	23"	16
104	straight	#1.25	23"	20
202	A	#2	72"	6
203	B	#2	66"	6
204	C	#2	39.25"	12
205	D	#2	36.25"	12
207	E	#2	59"	6
208	F	#2	57"	6

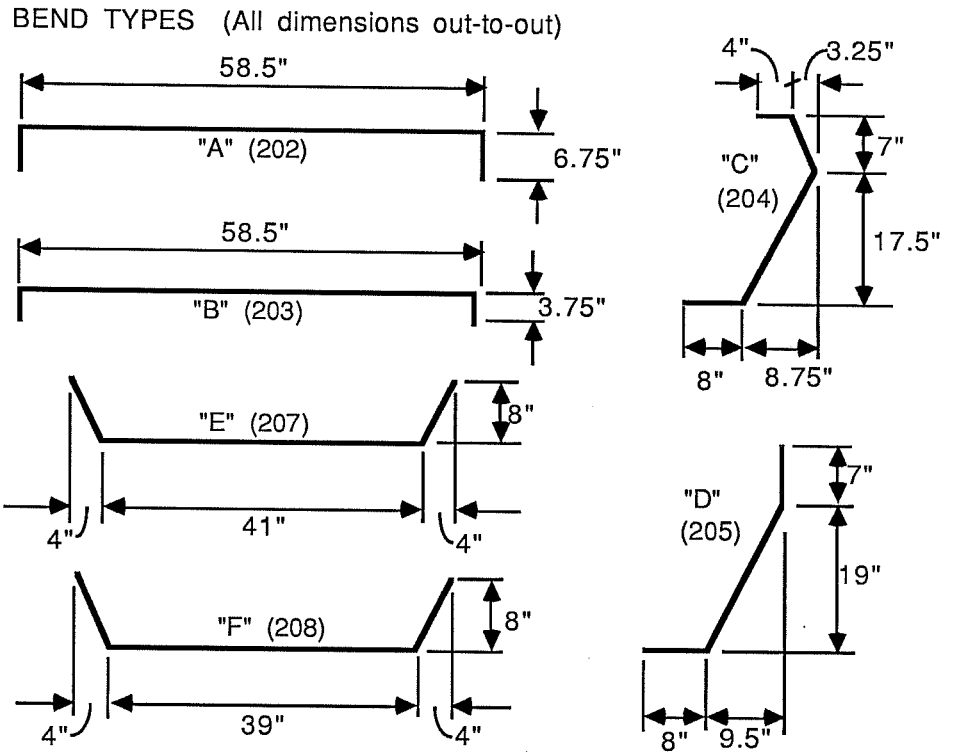

Figure 4.2 Box Reinforcement Schedule

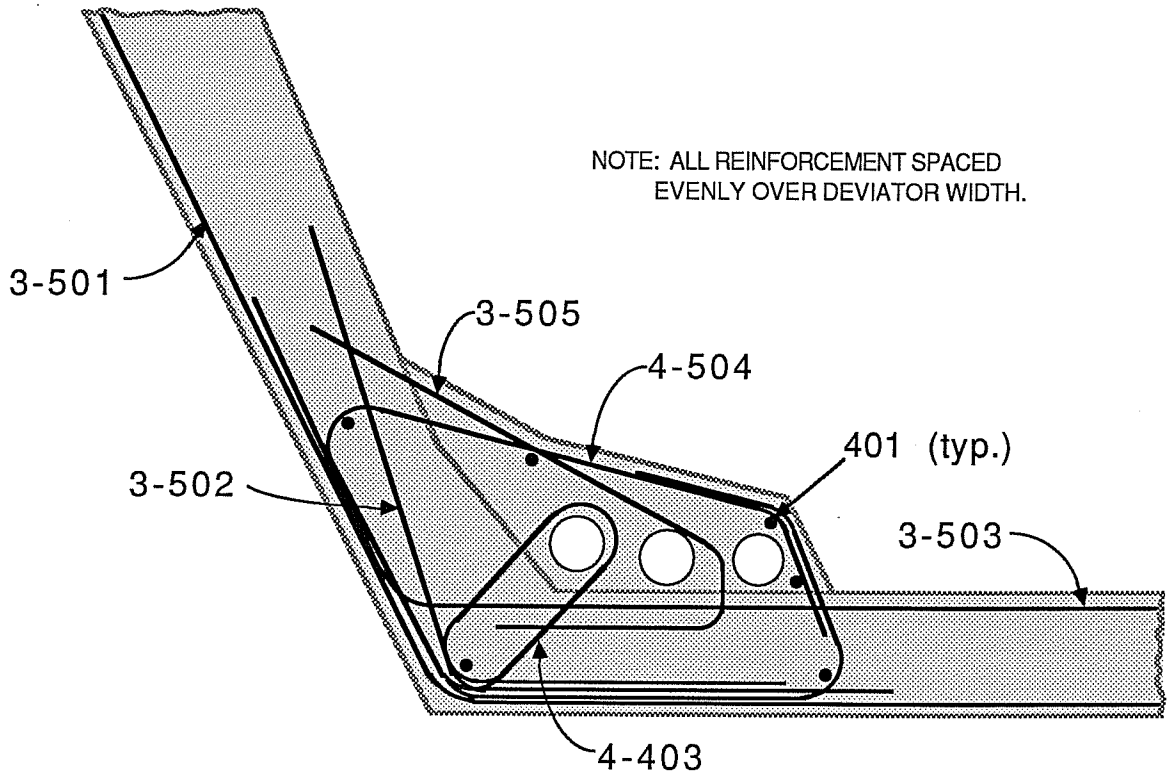

Figure 4.3 Prototype Deviator Reinforcement

SCALING PROTOTYPE DEVIATOR REINFORCEMENT

PROTOTYPE			EXACT MODEL	ACTUAL SPECIMEN		
I.D.	#, bar size	As total	$As_{prototype} x(1/9)x(60/45)$	#, bar size	As total	I.D.
501	3- #5	$0.93 in^2$	$0.93 in^2 x0.111x1.333=0.138 in^2$	3 - #2	0.149	201
502	3 - #5	$0.93 in^2$	$0.93 in^2 x0.111x1.333=0.138 in^2$	3 - #2	0.149	202
503	3 - #5	$0.93 in^2$	$0.93 in^2 x0.111x1.333=0.138 in^2$	3 - #2	0.149	203
504	4 - #5	$1.24 in^2$	$1.24 in^2 x0.111x1.333=0.184 in^2$	4 - #2	0.198	204
505	3 - #5	$0.93 in^2$	$0.93 in^2 x0.111x1.333=0.138 in^2$	3 - #5	0.149	205
403	4 - #4	$1.60 in^2$	$1.60 in^2 x0.111x1.333=0.237 in^2$	4 - #1.5	0.221	1.503

Table 4.2

summary of steel areas in both prototype and specimen. The specimen deviator reinforcing scheme is shown in Fig. 4.4 and Fig. 4.5 gives bending details.

4.1.3 Deviation Ducts. Based on the tendon layouts, a total angle change was calculated for each duct. To insure a better fit and to reduce the possibility of kinks in the tendons at the face of the deviator, the calculated angle was increased two degrees. Equipment for bending the ducts at variable radii was not available. An alternate procedure was devised in which the ducts were bent at three points by one third of the total working angles (i.e. the calculated angle plus two degrees). For the short lengths of duct, the result was a fairly smooth curve. The hydraulic pipe bending apparatus which was used is shown in the photo in Fig. 4.6. The thin-walled galvanized metal conduit which was used for ducts had an outer diameter of 1-11/16 inches and a wall thickness of 1/16 inch.

4.2 Construction and Formwork

4.2.1 Formwork Design and Function. The formwork was greatly simplified by constructing the specimen on its side. The forms consist of several units which assemble and dissassemble easily (Fig. 4.7). The two units which constitute the outside forms lag-bolt together at joints and are fastened with lag bolts to a flat base. The preassembled specimen reinforcing cage was

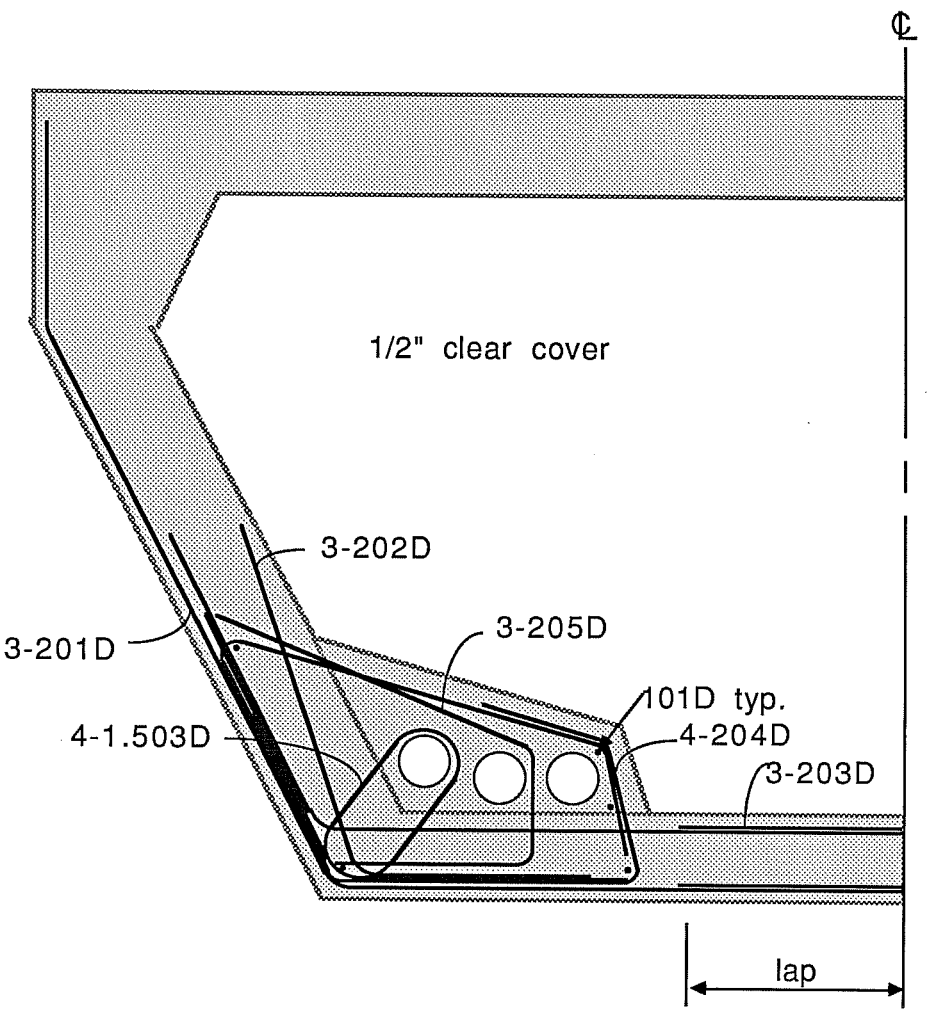

NOTE: Refer to Fig. 3.2 for physical dimensions of deviator.

Figure 4.4 Specimen Deviator Reinforcement

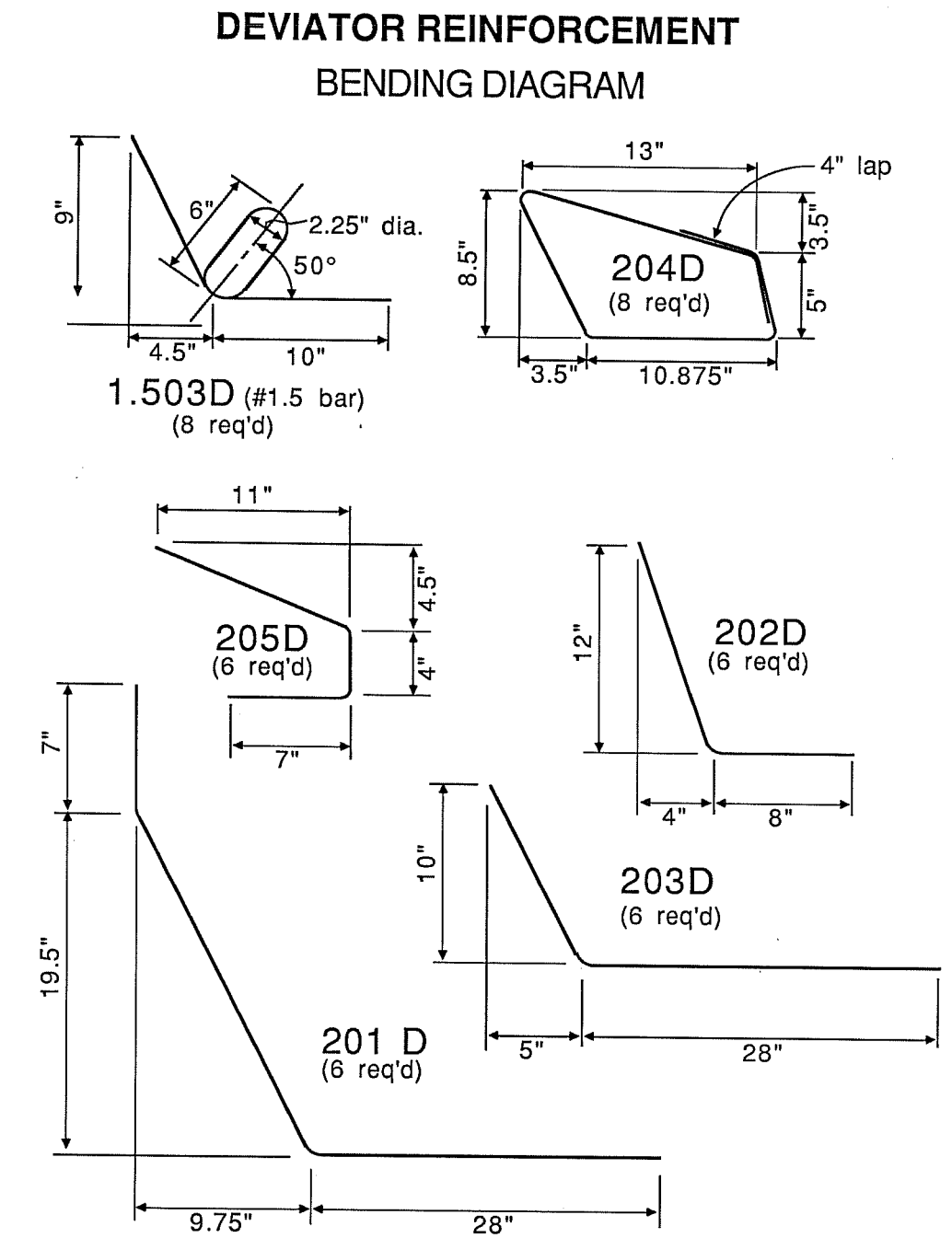

NOTE: Diameter of bends = 1" unless otherwise noted.

Figure 4.5 Deviator Reinforcement Bending Diagram

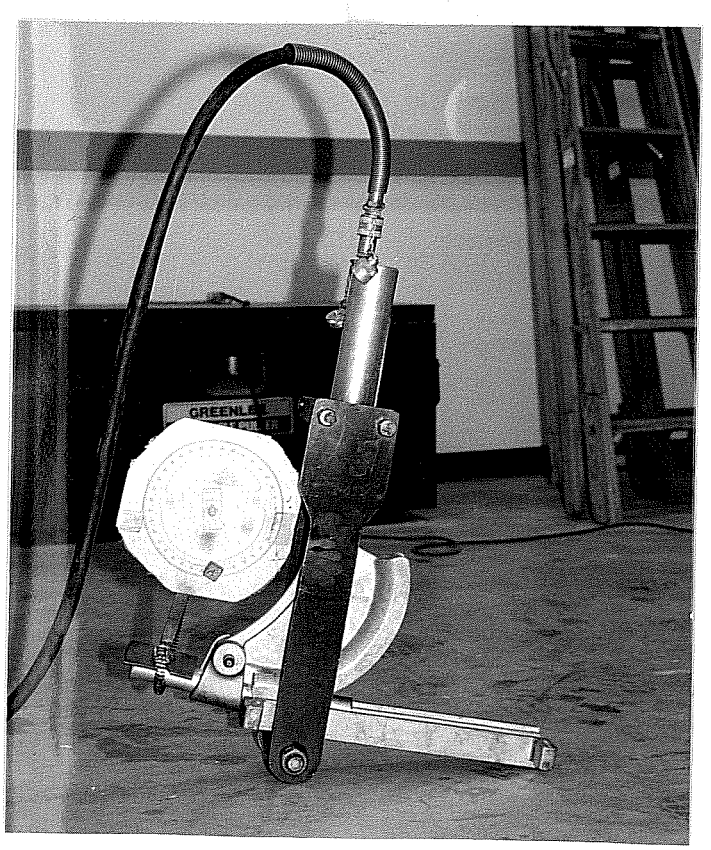

Figure 4.6 Duct Bending Equipment

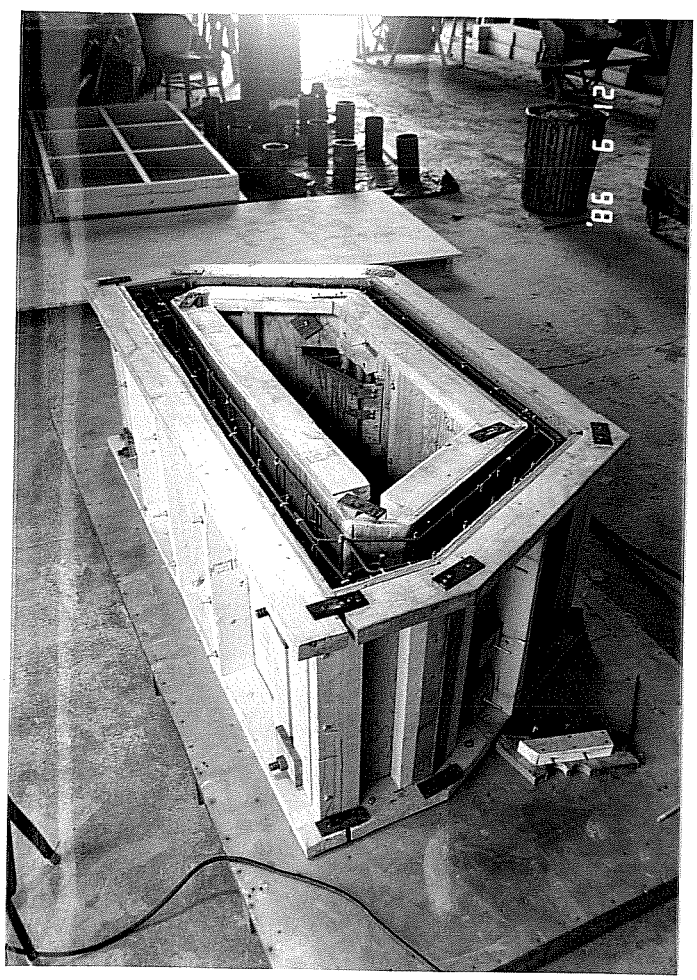

Figure 4.7 Specimen Forms

dropped in place inside the outer forms. Then the four units comprising the inside forms were slid or rotated into place around the cage. Lag bolts fasten the inside units to the base. Spacers were fabricated from threaded rod and nuts to maintain correct web and flange thicknesses. The plywood block-outs forming the deviation blocks were then constructed around the deviator reinforcing. To ensure proper compaction of the concrete, a port left on the upper faces of each deviation block allowed insertion of vibrators (Fig. 4.8). Sheet metal, lining the inside face of the forms, facilitates stripping and makes multiple reuse of the forms feasible.

4.2.2 Construction of Reinforcing Cage. All specimen reinforcement was bent by hand in the laboratory. Special bending jigs were fabricated for the different bending patterns. Dimensional accuracy was checked by comparing each piece of reinforcement against a full scale drawing during the bending process. After the bars making up the box section were bent, the box cage was completely assembled (Fig. 4.9a). The deviator steel was prepared and instrumented and inserted into the box cage (Fig. 4.9b).

4.2.3 Instrumentation of Deviator Reinforcement. Light grinding removed bar deformations at locations for strain gages on selected deviator reinforcing bars. Final smoothing was accomplished by hand sanding with very fine grit sandpaper. The

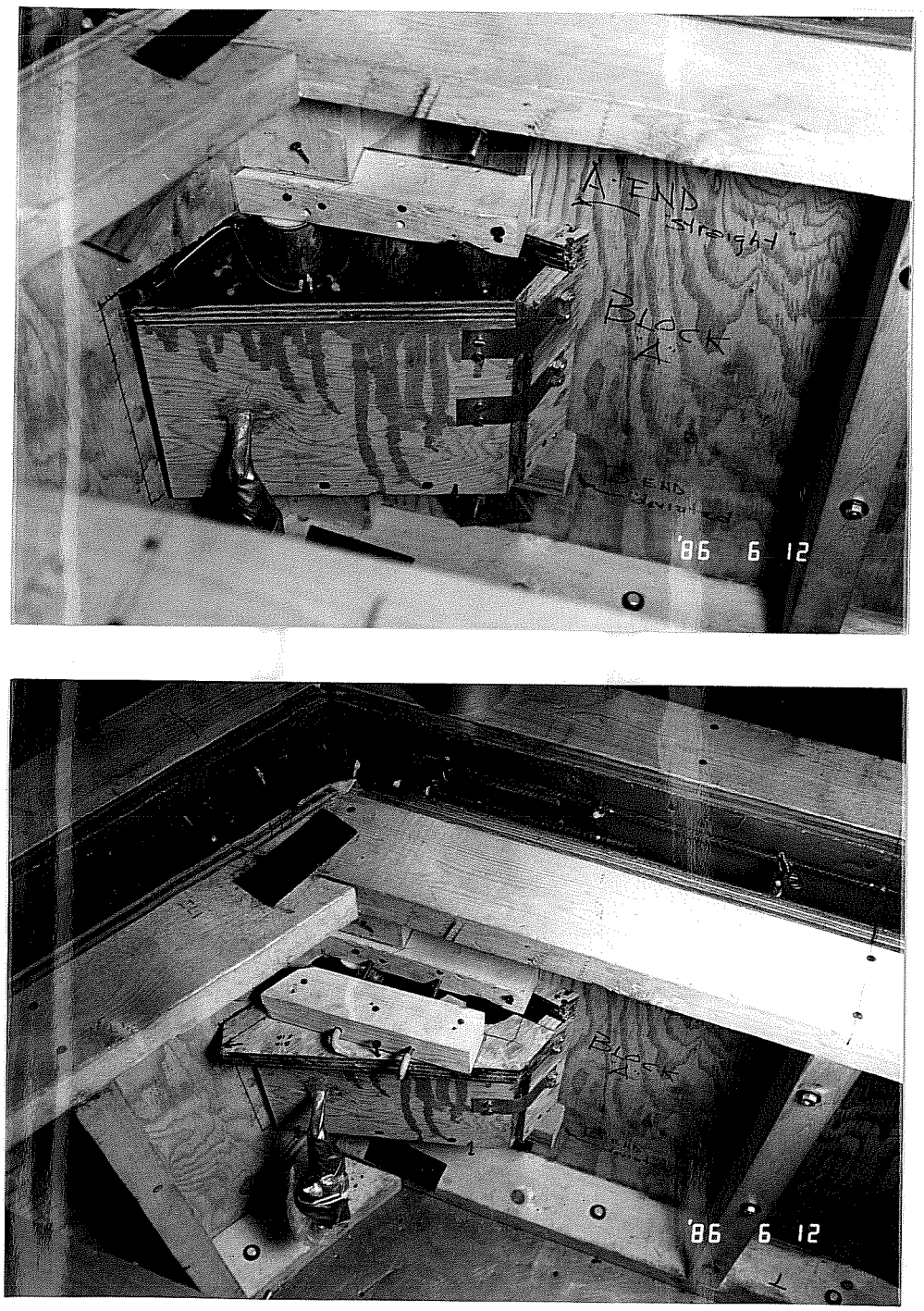

Figure 4.8 Specimen Forms Showing Vibration Port in Deviator

Figure 4.9a Box Reinforcing Cage

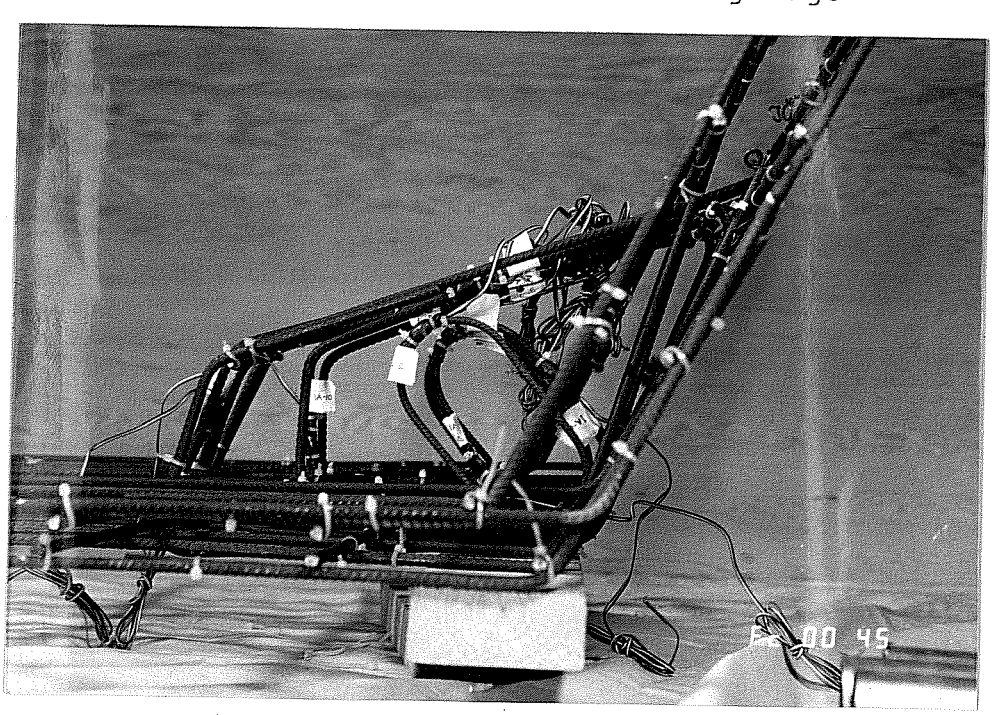

Figure 4.9b Deviator Reinforcement

grinding and sanding were executed with great care to limit as much as possible the reduction in cross-sectional area of the small bars, while assuring a good contact surface for the gages. The surfaces were cleaned with acetone, prepared with acid and neutralizer, then cleaned once more. M-Bond, a high-strength adhesive, affixed the gages to the bars. Lead wires were connected and soldered. An insulating coating, then a black plastic patch, Barrier E, were applied to the entire gage regions to waterproof the gages. A final outer layer of thin rubber encased the gage areas to provide further protection during concreting. The photo in Fig. 4.10 shows examples of the instrumented deviator bars. After tying the deviator bars into the box cage, the lead wires were attached to reinforcing steel with very light gage wire to minimize the danger of leads being ripped from the gages during concrete placement and vibration. The leads were fed through a small port in the formwork.

4.2.4 Concreting. A local ready-mix supplier delivered two yards of concrete to the laboratory with a slump of 2-1/4 inches. One gallon of water was added on site to bring the slump up to 3-1/4 inches. The fresh concrete was hand shoveled into the forms in several lifts (Fig. 4.11). One inch diameter stick vibrators were used to consolidate the concrete. After concrete was placed up to the level of the deviator ports, and the

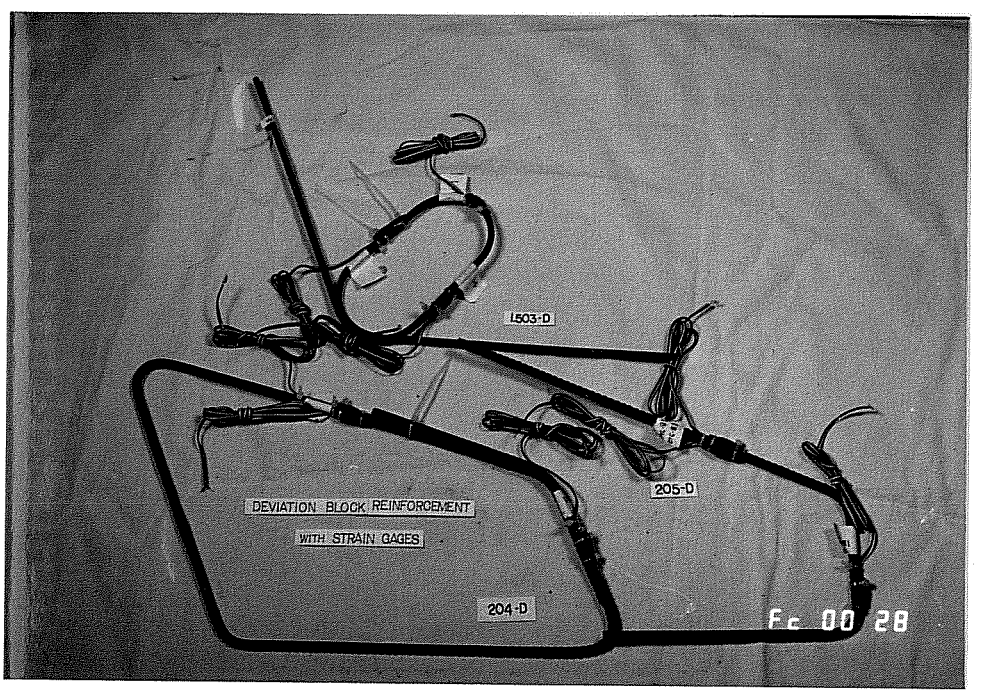

Figure 4.10 Instrumented Deviator Reinforcement

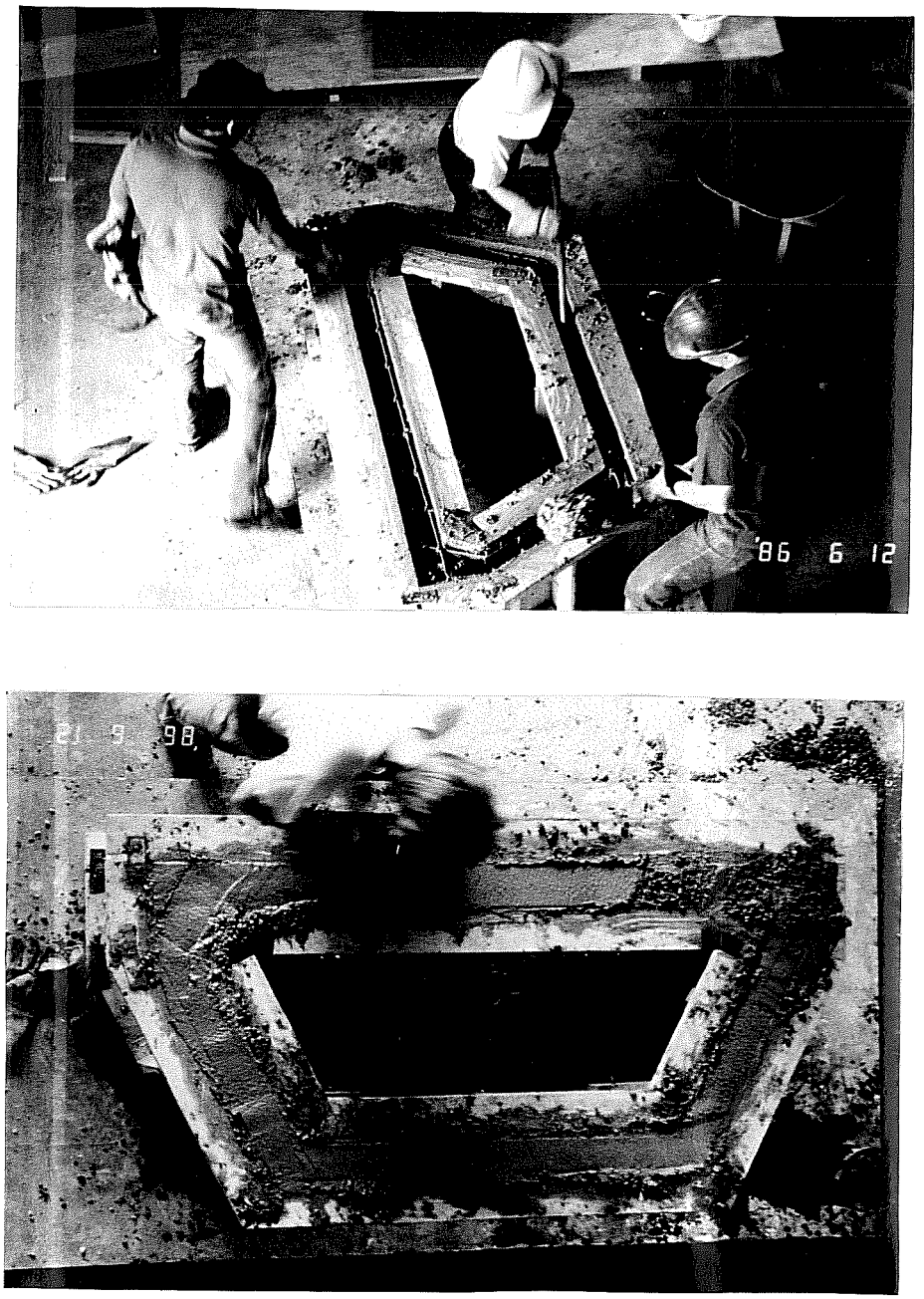

Figure 4.11 Placing Specimen Concrete

deviator blocks had been well vibrated, the ports were sealed and the remaining concrete was placed. The exposed concrete at the top of the forms was trowel-finished. Several test cylinders were also prepared.

4.2.5 Curing. After initial set, the specimen forms were covered with wet burlap and enclosed in a layer of plastic sheeting. Forms were stripped after 48 hours, but to ensure that no shrinkage cracking would occur, moist curing was continued for 5 more days. The specimen was then stored in the laboratory until testing. Test cylinders received identical treatment.

4.3 Material Properties

4.3.1 Concrete. Mix proportion information for the non-air entrained concrete used for the specimen are given in Table 4.3. The target 28-day compressive strength for the 6 sack mix was 6000 psi. The concrete cylinders were tested under uniaxial compression at several key ages (a sample of three cylinders per test) and at the time of each deviator test. Figure 4.12 shows the compressive strength verses age relationship for the specimen concrete. Average 28-day compressive strength was 5350 psi and the strength at the time of tests 1A and 1B had leveled off to 5650 psi.

4.3.2 Mild Reinforcing Steel. The specimen reinforcing microbars were annealed to obtain a well defined yield plateau.

MIX PROPORTION INFORMATION

MIX DESIGN INFORMATION

MATERIAL QUANTITIES (per yard, with dry aggregates)	
Cement (Type I)	564 lbs.
Fine Aggregate	1355 lbs.
Coarse Aggregate (3/8" max.)	1700 lbs.
Water	33 gal.
Retarder Dosage (Spec. 494)	24 oz.
W/C	0.49

BATCH PLANT INFORMATION

Batch Volume = 2 cu.yds.
Measured Moisture Content in Sand = 8%

CORRECTED MIX PROPORTIONS

MAT'L QTY'S	AS PER DESIGN	AS BATCHED
Cement	1128 lbs.	1140 lbs.
F. A.	2927 lbs.	2950 lbs.
C. A.	3400 lbs.	3525 lbs.
Water	40 gal.	40 gal.
Retarder	48 oz.	48 oz.
W/C	0.50	0.50

ON SITE INFORMATION

Slump as delivered = 2-1/4 in.
Slump after adding 1 gal. water = 3-1/4 in.
Final W/C = 0.51
Entrained Air Content = 3.2%

Table 4.3

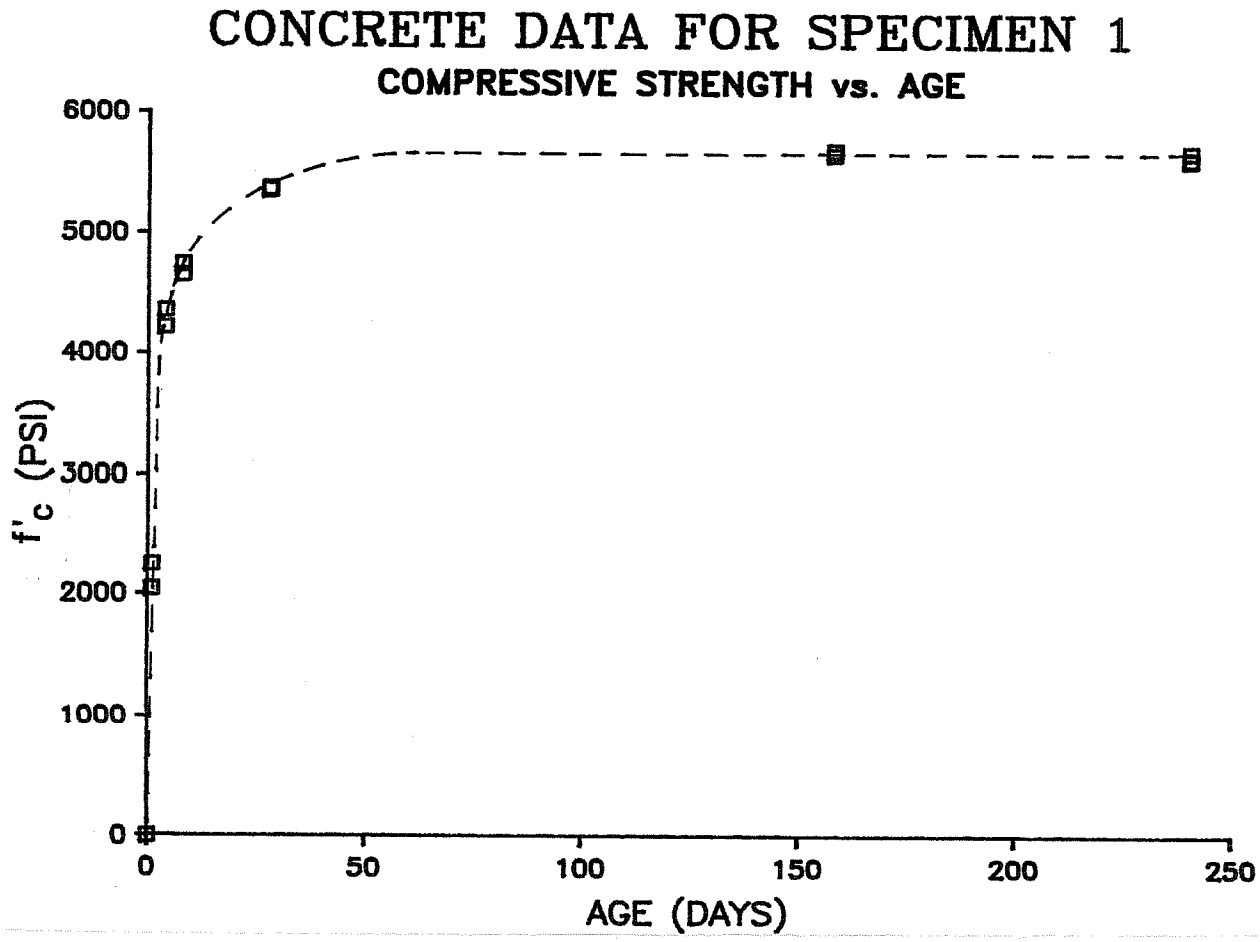

Figure 4.12 Concrete Data for Specimen 1

The heat treatment procedure included subcritical annealing at 1150 degrees fahrenheit for one hour. Uniaxial tension tests performed on 20 heat-treated microbar specimens (including all sizes) revealed ductile behavior with an average yield strength of 45 ksi and an average ultimate strength of 63 ksi. The modulus of elasticity was assumed as 29,000 ksi which results in a yield strain of 1550 micro inches/inch.

4.3.3 Prestressing Strand. Material properties for the prestressing strand used in the tests were supplied by the manufacturer. Tests of the 3/8 inch diameter low-relaxation strand showed an ultimate strength of 279 ksi and a modulus of elasticity of 28,400 ksi.

CHAPTER 5

INSTRUMENTATION AND TESTING

5.1 Instrumentation

Several types of electronic and mechanical measuring devices were used to monitor forces and displacements on the specimen (Fig. 5.1), and on the loading frame. Section 3.3.6 outlines the philosophy behind the various measurements. This section provides specific information regarding instrumentation locations and descriptions. Tables 5.1a-b and 5.2a-b list the designations and locations of the instrumentation used in each deviator test.

5.1.1 Strain Gages. The resistance type strain gages which were applied to both the specimen reinforcing steel and tendon strands were made of constantan foil with polymide backings (Micro Measurements Type EA-06-062AP-120 Option L). The small gages had a gage length of 0.062 inches, a gage factor of 2.005 and a resistance of 120 ohms. (Refer to Sec. 4.2.3 for details regarding application of gages.)

Each deviation block had 15 gages attached to selected reinforcing bars. The gage locations for blocks 1A and 1B are shown in Fig. 5.2a-b. Only "primary deviator reinforcement" was instrumented, i.e. the bent bars that reinforce the deviation

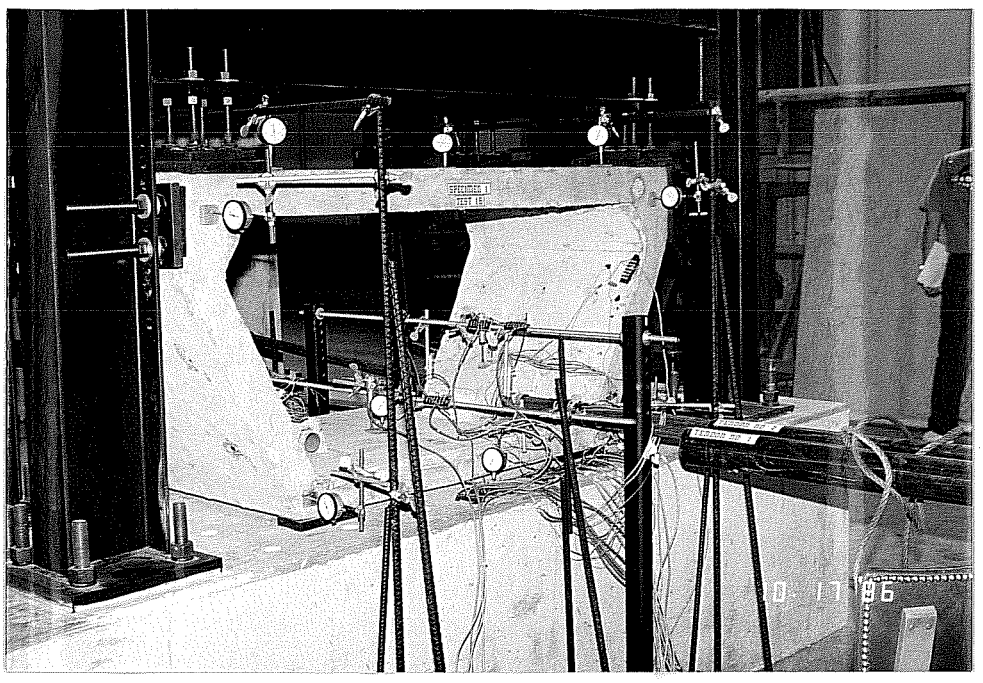

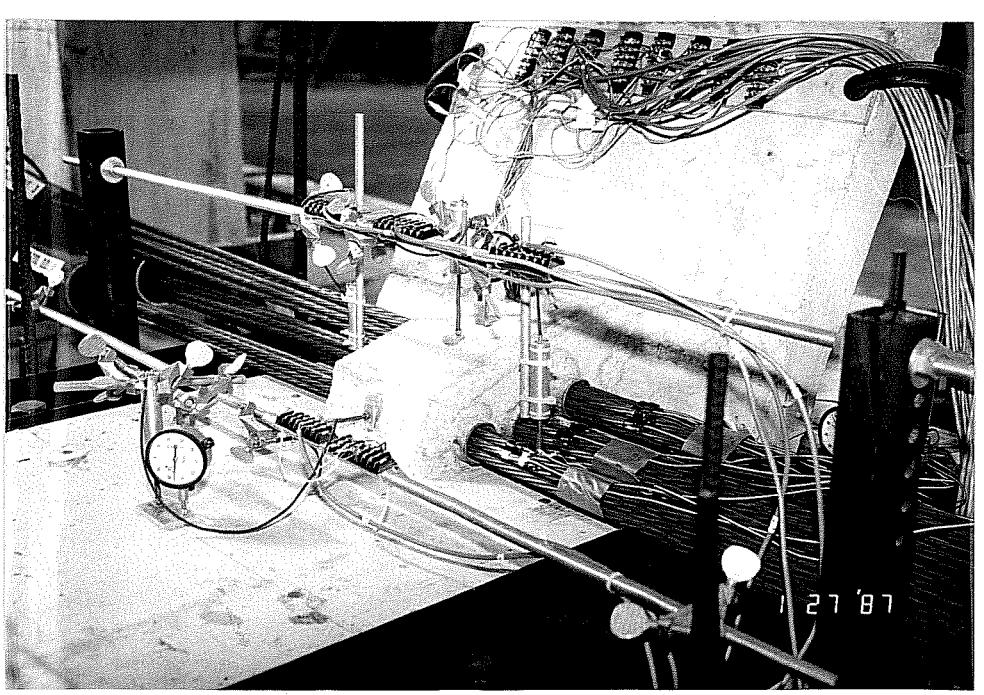

Figure 5.1 Specimen: Instrumented for Testing

TEST 1A ELECTRONIC INSTRUMENTATION

ID	DESCRIPTION	LOCATION
PT-A1	Pressure transducer	@ Ram AI
PT-A2	"	@ Ram AII
PT-B1	"	@ Ram BI
PT-B1	"	@ Ram BII
P-A1	6 in. linear pot	@ East side of "A" frame
P-A2	"	@ West side of "A" frame
P-B1	2 in. linear pot	@ East side of "B" frame
P-B2	"	@ West side of "B" frame
P-1A-H	2 in. linear pot	front center of deviator -horizontal
P-1A-V	"	top center of deviator - vertical
P-1A-S	"	on bottom flange south of deviator
P-1A-N	"	on bottom flange north of deviator
P-1A-C	"	on bottom flange at center of specimen
1A-1UP	strain gage - dev. reinf.	refer to Figure 5.2a
1A-1LO	"	
1A-2	"	
1A-3UP	"	
1A-3LO	"	
1A-4	"	
1A-5	"	
1A-6	"	
1A-7	"	
1A-8	"	
1A-9UP	"	
1A-9LO	"	
1A-10	"	
1A-11	"	
1A-12	"	
1A-1.1S	strain gage - strand	Tendon 1
1A-1.2S	"	"
1A-1.3S	"	"
1A-2.1S	strain gage - strand	Tendon 2
1A-2.2S	"	"
1A-2.3S	"	"
1A-3.1S	strain gage - strand	Tendon 3
1A-3.2S	"	"
1A-3.3S	"	"
1A-3.4S	"	"

Table 5.1a

TEST 1B ELECTRONIC INSTRUMENTATION

ID	DESCRIPTION	LOCATION
PT-A1	Pressure transducer	@ Ram AI
PT-A2	"	@ Ram AII
PT-B1	"	@ Ram BI
PT-B1	"	@ Ram BII
P-A1	6 in. linear pot	@ East side of "A" frame
P-A2	"	@ West side of "A" frame
P-B1	2 in. linear pot	@ East side of "B" frame
P-B2	"	@ West side of "B" frame
P-1B-H	2 in. linear pot	front center of deviator -horizontal
P-1B-V	"	top center of deviator - vertical
P-1B-S	"	on bottom flange south of deviator
P-1B-N	"	on bottom flange north of deviator
P-1B-C	"	on bottom flange at center of specimen
1B-1UP	strain gage - dev. reinf.	refer to Figure 5.2b
1B-1LO	"	
1B-2	"	
1B-3UP	"	
1B-3LO	"	
1B-4	"	
1B-5	"	
1B-6	"	
1B-7	"	
1B-8	"	
1B-9UP	"	
1B-9LO	"	
1B-10	"	
1B-11	"	
1B-12	"	
1B-1.1S	strain gage - strand	Tendon 1
1B-1.2S	"	"
1B-1.3S	"	"
1B-1.4S	"	"
1B-2.1S	strain gage - strand	Tendon 2
1B-2.2S	"	"
1B-2.3S	"	"
1B-2.4S	"	"
1B-2.5S	"	"
1B-2.6S	"	"

Table 5.1b

TEST 1A DIAL GAGES

ID	LOCATION
DG-1A-V	back-up for pot P-1A-V on top face of deviator
DG-C	back-up for pot P-1A-C at center of specimen
DG-A1	back-up for pot P-A1 at frame "A" near ram AI
DG-A2	back-up for pot P-A2 at frame "A" near ram AII
DG-T1	top flange of specimen - northwest corner
DG-T2	top flange of specimen - northeast corner
DG-T3	top flange of specimen - southwest corner
DG-T4	top flange of specimen - southeast corner
DG-NF1	north face of specimen - top west corner
DG-NF2	north face of specimen - bottom west corner
DG-NF3	north face of specimen - top east corner
DG-NF4	north face of specimen - bottom east corner
DG-EF	east side of specimen - horizontal

Table 5.2a

TEST 1B DIAL GAGES

ID	LOCATION
DG-P1	@ center of pedestal on north side of specimen
DG-P2	@ northwest corner of pedestal
DG-1B-V	back-up for pot P-1B-V on top face of deviator
DG-C	back-up for pot P-1B-C at center of specimen
DG-A1	back-up for pot P-A1 at frame "A" near ram AI
DG-A2	back-up for pot P-A2 at frame "A" near ram AII
DG-B1	back-up for pot P-B1 at frame "B" near ram BI
DG-B2	back-up for pot P-B2 at frame "B" near ram BII
DG-T1	top flange of specimen - northwest corner
DG-T2	top flange of specimen - northeast corner
DG-T3	top flange of specimen - southwest corner
DG-T4	top flange of specimen - southeast corner
DG-NF1	north face of specimen - top west corner
DG-NF2	north face of specimen - bottom west corner
DG-NF3	north face of specimen - top east corner
DG-NF4	north face of specimen - bottom east corner
DG-EF	east side of specimen - horizontal

Table 5.2b

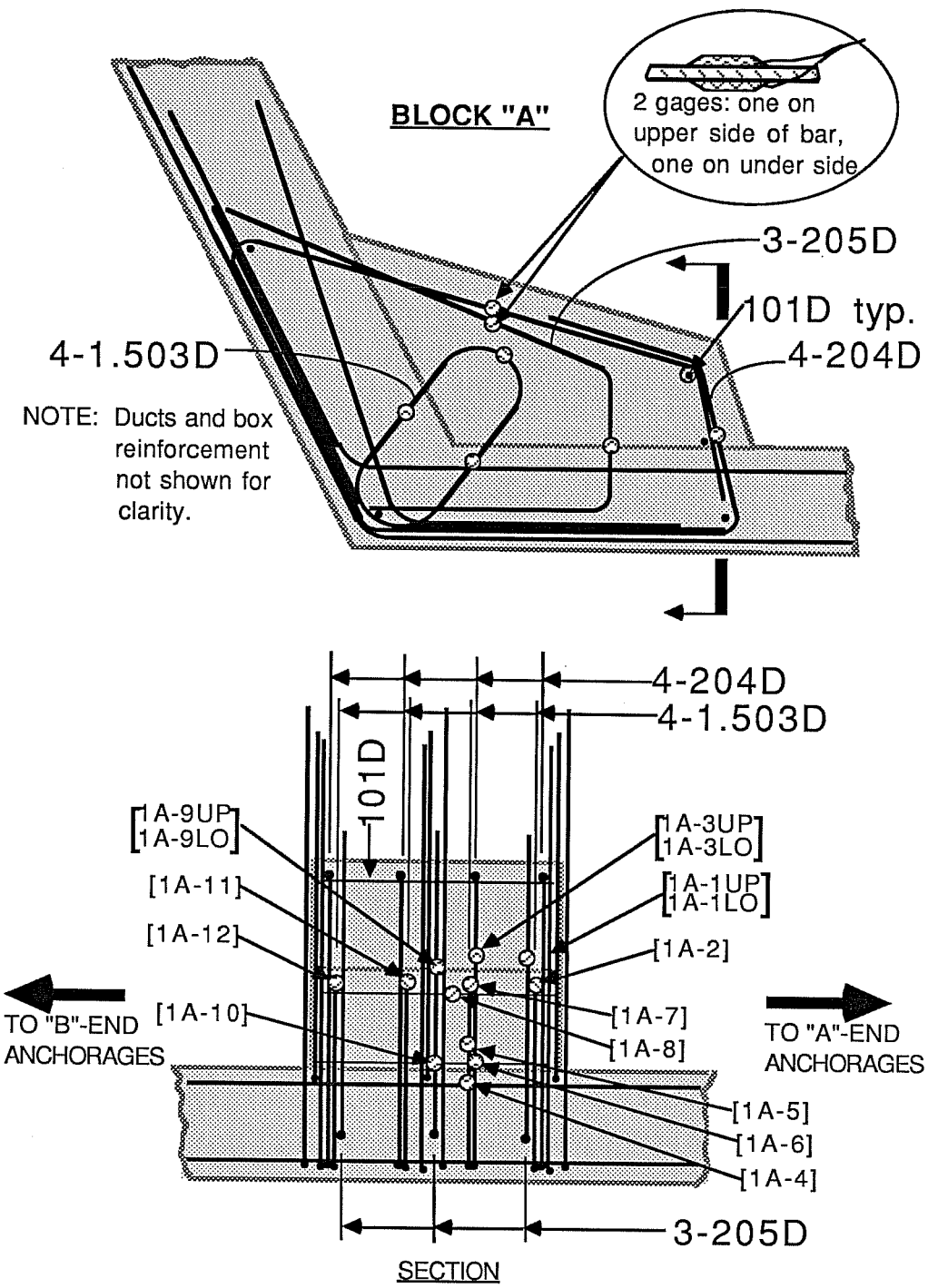

Figure 5.2a Deviator Reinforcement Strain Gage Locations, TEST 1A

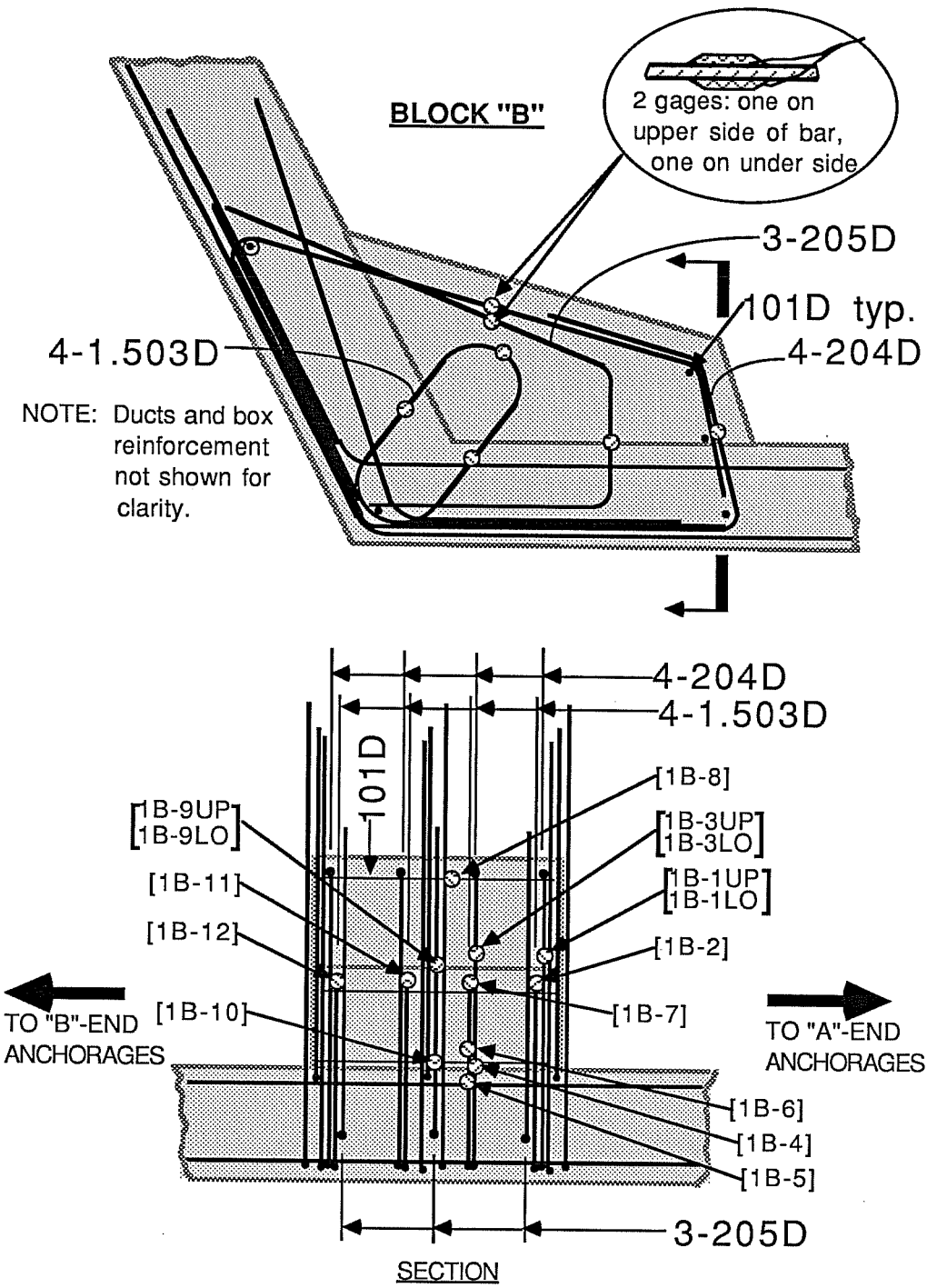

Figure 5.2b Deviator Reinforcement Strain Gage Locations, TEST 1B

block itself, not the auxiliary reinforcement located in the bottom flange and webs of the box section.

Ten strain gages affixed to selected wires of several strands furnished a supplementary method for measuring tendon force. The ten gages were divided proportionately among the tendons. (Refer to Tables 5.1a-b for tendon strain gage designations.)

5.1.2 Potentiometers and Dial Gages. Five 2-inch linear potentiometers located inside the specimen box measured the deformations of the deviation block. At some locations, dial gages provided back-ups for the potentiometers. Additonal dial gages, positioned at points around the outside of the specimen, assessed the rigid body motion of the box. The cut-away view of the specimen in Fig. 5.3 shows the relative positions of the dial gages and pots around the specimen. Stands for these instruments were supported on the lab floor. Potentiometers and dial gages also monitored the movement of each lever frame. Prior to each test, all potentiometers and gages were checked by application of a known displacement.

5.1.3 Pressure Transducers. A 10,000 psi precision pressure transducer with 10 mv/v output was connected to each 100-ton ram. A similar 5000 psi capacity transducer was used in combination with the stressing ram. Before connecting the transducers into the hydraulic system, they were checked for

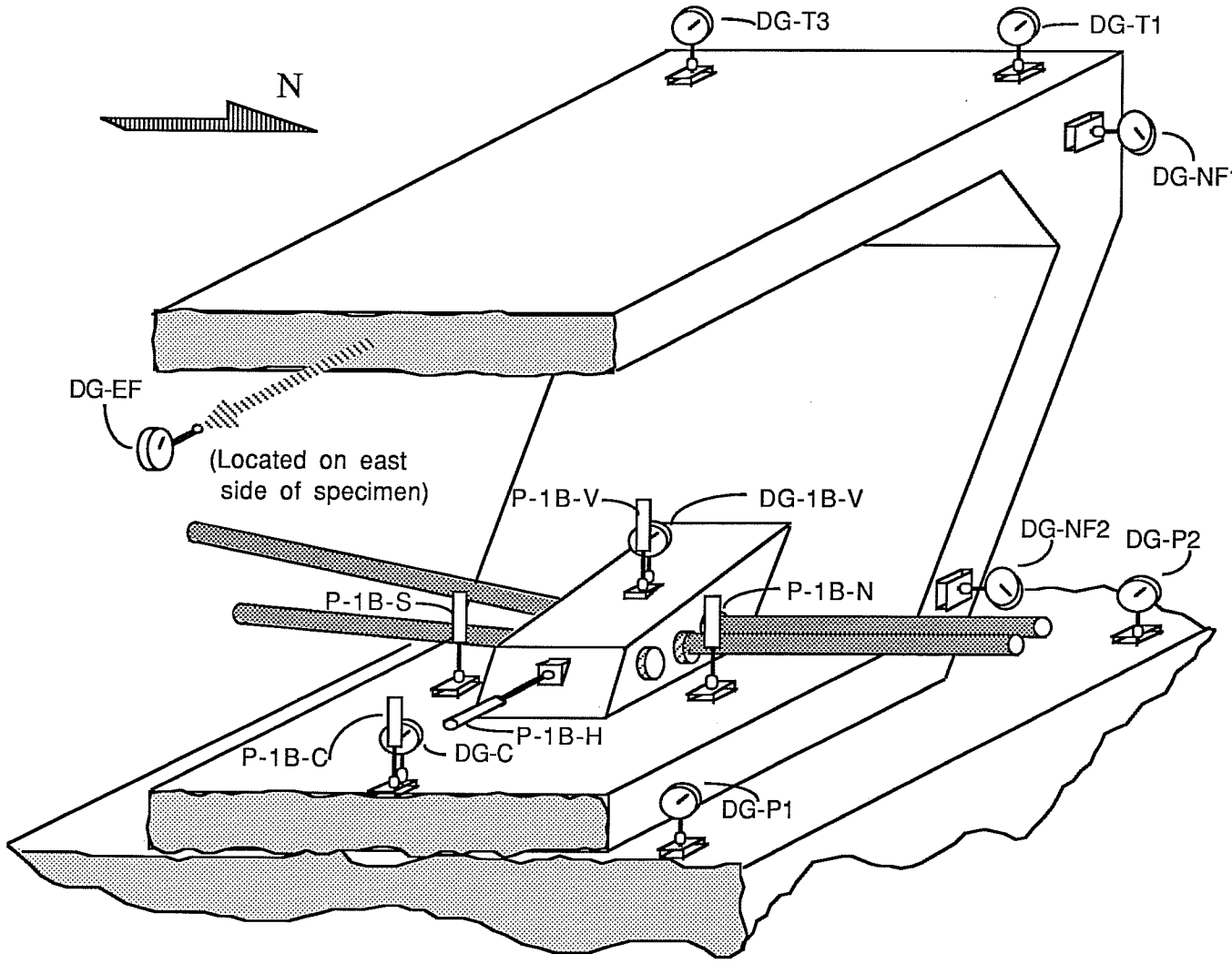

Figure 5.3 Potentiometer and Dial Gage Locations

linearity using a dead weight calibrator. All pressure tranducers were certified accurate to plus or minus 0.5 percent.

5.1.4 Data Acquisition. Data from the strain gages, potentiometers and pressure transducers were read electronically through a Hewlett-Packard scanner. An input voltage of ten volts was applied across full bridge connections (potentiometers, transducers), and two volts was applied across quarter bridges (strain gages). Scanning was controlled by data acquisition software using an IBM AT personal computer. The software, a program called HPDAS which was developed at the laboratory, incorporated a testing routine which was used to check the entire electronic system prior to each test.

5.2 Test Procedures

5.2.1 Load Checks and Accuracy. Before beginning the deviator tests, the load apparatus itself was tested to ensure that it was functioning properly and to eliminate all possible sources of error in assessing the forces that were being applied to the deviator. The first step in this program was to perform precise calibrations of each pump/ram/transducer combination used in the setup. This included the four 100-ton capacity rams, the stressing ram, hydraulic pumps, and the transducers mentioned above. Once reliable calibration data were obtained a series of "statics checks" were performed to ensure that the equations of

statics could be applied to calculate the tendon forces within a reasonable margin of error.

5.2.1.1 Ram/Transducer Calibrations. Precise calibrations were required in order to obtain reliable force determinations from pressure readings on the 100-ton rams and the Prescon stressing ram. The accuracy of the transducer/ram system is affected by the frictional characterstics of the ram packing (teflon in this case). The pressure-load relationship is generally linear, but a hysteresis is obtained when the direction of travel of the ram piston is reversed.

The calibrations were performed using a 600-kip SATEC test machine. Each calibration was done twice, using the same combination of pump, hydraulic lines, pressure transducer, ram, and method of data collection in the calibration as would be utilized in the test. The calibration procedures were devised to simulate each of the loading conditions that the rams would undergo during the deviator tests. The loading conditions were defined by the load range and by the direction and range of ram piston travel. Pressure transducers connected to the 100-ton rams were read electronically by the data acquisition system. Load in the Prescon ram was controlled by readings on a strain indicator box which was connected to the pressure transducer. Figure 5.4 shows an example calibration curve obtained for a

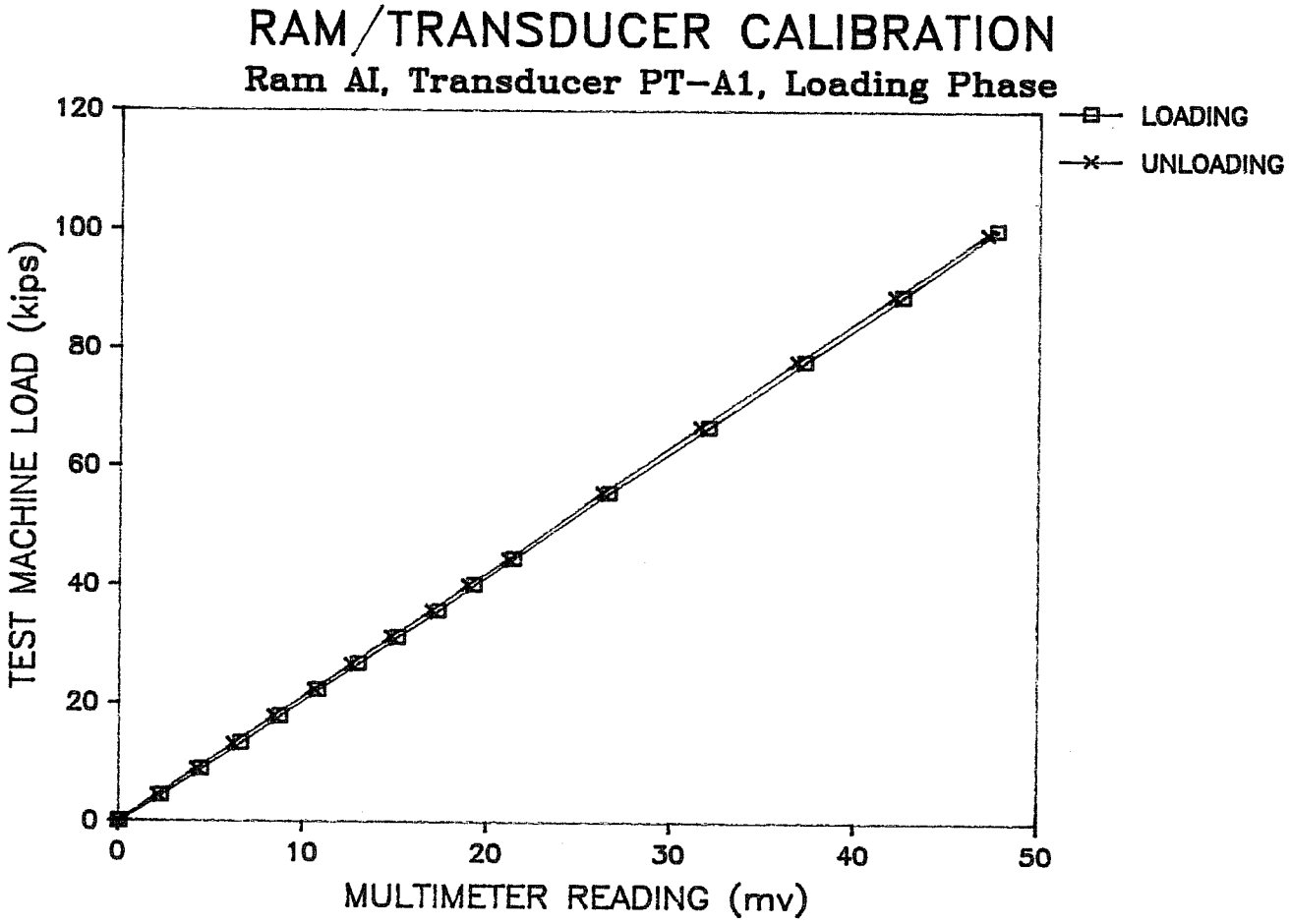

Figure 5.4 Example Calibration Curve

100-ton ram/transducer combination. This particular calibration applies to a loading phase of the test, in which the 100-ton rams are being pumped, with the pistons extending as they push out the lever frame to load the tendons. Unloading is accomplished by slow, controlled bleeding of the rams, which retracts the pistons. The figure illustrates the narrow friction reversal hysteresis loop and the general linearity of the load-pressure relationship, in this case expressed in terms of force versus millivolt reading. This force-voltage relationship could not be input directly into the data acquisition program, however. Input parameters for the HPDAS program include the transducer capacity (10,000 psi), its output rating (10mv/v), and the bore area of the ram (21.2 sq. in.). From this information, the program automatically calculates the force in the ram based on a linear relationship. The calibration curves were used to calculate a correction factor, based on the deviation of the calibration curve from the theoretical line, to be applied to the data force values. A plot of force versus correction factor (i.e. the calibration curve value divided by the HPDAS value), representing data from duplicate calibrations of the Ram AI/Transducer PT-A1 combination, appears in Fig. 5.5. A bilinear (for the loading case) or linear (for the unloading case) approximation was taken from the sets of points to correct the data force values.

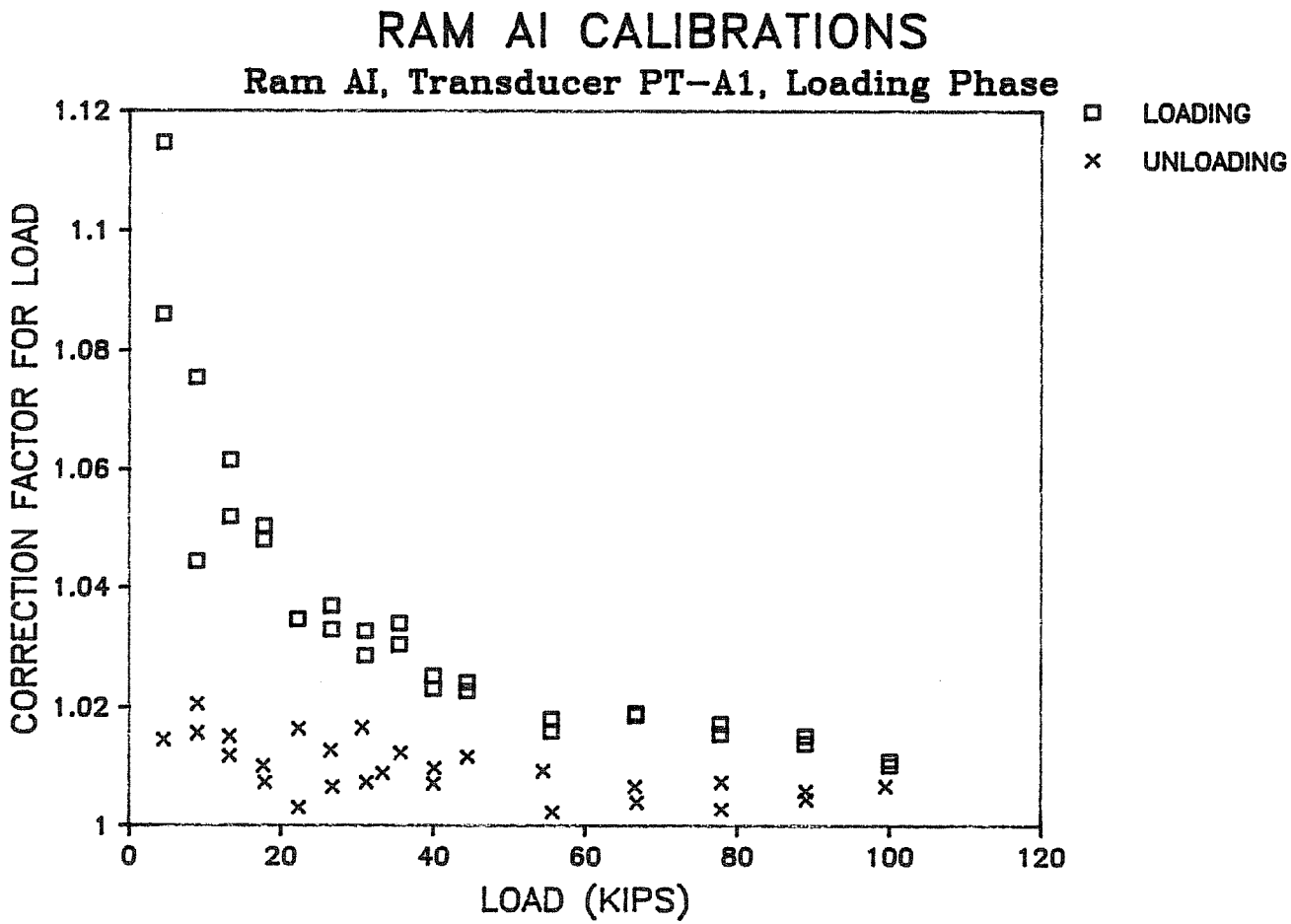

Figure 5.5 Example Correction Factor Plot

The calibration curve for the stressing ram was used directly to control the stress of the tendon during stressing. For a given force in a particular tendon, the corresponding value for microstrain was taken from the curve. The strain indicator box was then set to that reading and the ram was pumped until the needle came to the zero postition.

5.2.1.2 Statics Checks. The "A" frame at the stressing end of the setup was designed as a statically determinate grid. It has simple connections at the ends of the horizontal members and pin connections at the base (Fig. 5.6). For the case of two tendons, since the reactions at the top of the frame, i.e. the ram forces, are known, the force in each tendon can be found given the following assumptions:

1. Tendon forces P1 and P2 distribute equally to the two W10x88 horizontal members.

2. The two W10x88 horizontal members act as pure simple beams, i.e. the clip angle connections allow free rotation.

3. Reactions from the horizontal members act symmetrically on the vertical W10x88 members, i.e. the reaction at the pin equals the reaction at the ram.

To check these assumptions, a statics test was devised in which only one tendon (denoted Tendon No. 1) was stressed. During stressing, the forces in Tendon No. 1, Ram AI and Ram AII were known. These forces are denoted P1, AI, and AII respectively. P1 was taken from the calibration curve for the stressing ram.

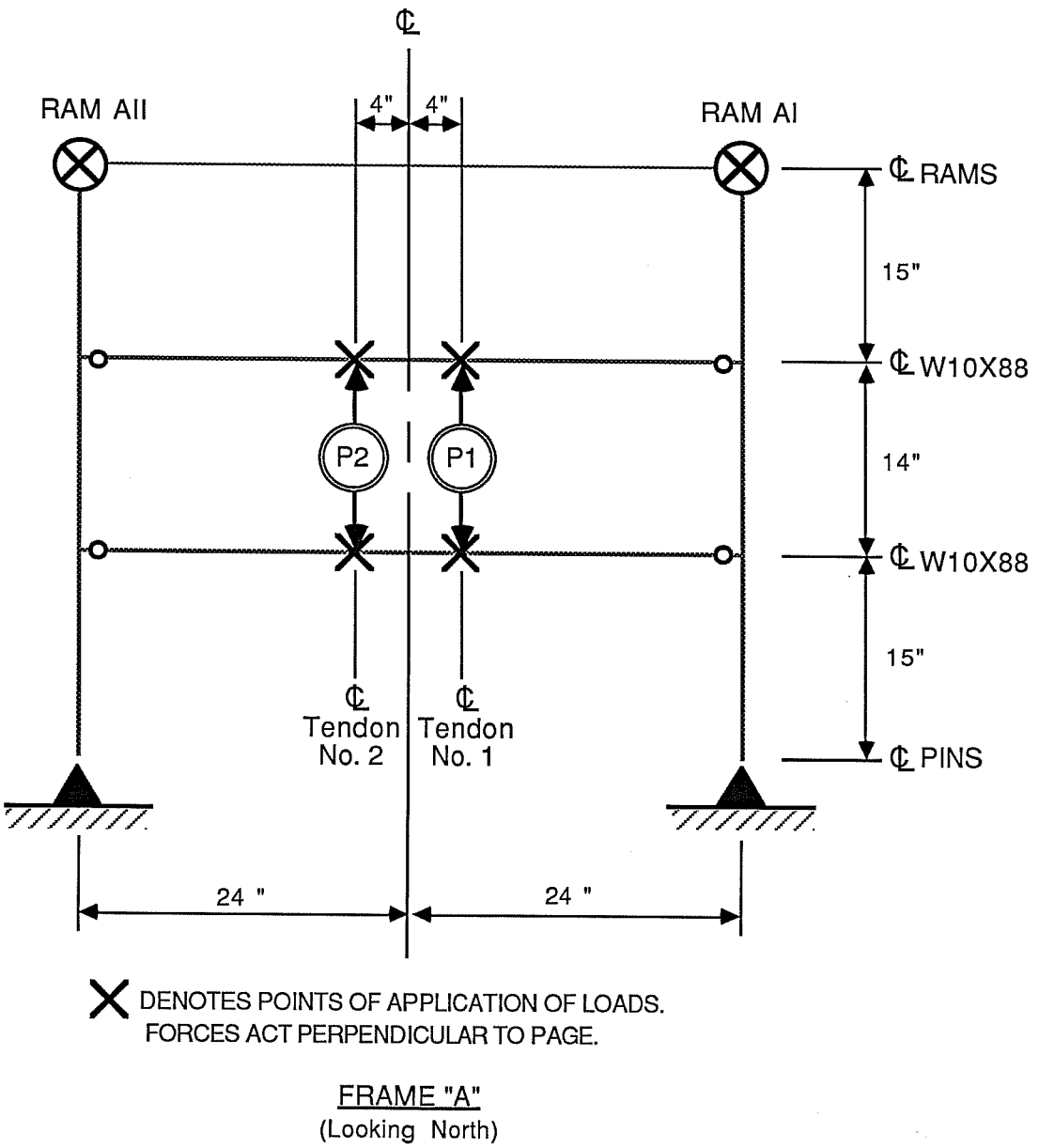

Figure 5.6 Frame "A" Model for Equilibrium Calculations

Ram forces AI and AII were determined by the data acquisition system and adjusted by the correction factor calculated from the calibration curve. If the following conditions hold true, then assumptions 1. through 3. are valid:

i) $AI + AII = (P1)/2$

and

ii) $AI = 0.5833 \times (P1)/2 = 0.2917 \times P1$
$AII = 0.4167 \times (P1)/2 = \underline{0.2083 \times P1}$
$0.5 \times P1$

The first few statics checks revealed a disparity between the left and right sides of the above equations which varied from 10 to 25 percent. However, upon closer inspection of the test setup, "hidden" sources of restraint were detected. The restraining arm bolts had not been loosened completely, causing the restraining arms to pick up some of the force that supposedly had gone into the pair of 100-ton rams. The internal seating mechanism that was originally incorporated into the stressing ram also accounted for misreadings of the tendon force. In addition, operating all three rams at very low load levels (less than 5 percent of their capacities) contributed to considerable error. After these problems had been resolved, the statics checks came within three to four percent agreement. The remaining error could be attributed to less than perfect distribution of bearing force at the points of application of the loads. This small margin of error was deemed acceptable.

The final results of the statics checks showed that the equations of statics could be used to adequately determine the force in the tendons. Applying the conditions of equilibrium to the two-tendon system in Test 1B, expressions for the tendon forces reduce to a system of two equations with two unknowns:

$$P1 = 7AI - 5AII \text{ and}$$
$$P2 = -5AI + 7AII$$

5.2.2 General Test Procedures. The information that follows outlines the generalized procedure that was selected for testing the deviation blocks. Each test comprises three distinct phases. During the stressing phase, the tendons are stressed to a preliminary level determined to be less than cracking load for the deviator. The next phase, called Phase I, may be construed as service load testing. While actual load levels on the deviator may exceed true service loads, the damage to the deviator during this phase is what might be expected in the service life of a bridge. Phase II follows as an ultimate loading phase in which the tendon stress is increased until the deviator fails.

5.2.2.1 Stressing the Tendons. Stressing procedures used in the deviator tests were more complicated than normal stressing operations for multi-strand tendons. Ordinarily, the Prescon ram incorporates an internal self-seating mechanism that automatically seats the wedges. However, this mechanism was

removed during the statics checks because it caused too much friction at the anchorage which resulted in false indications of the tendon force for the relatively short tendons. Instead, a chair was fabricated and the wedges were seated manually. The photos in Fig. 5.7 show some of the hardware and equipment required for stressing. The top photo shows the Prescon stressing ram and the temporary anchor block at the back of the ram. The ram bears against a chair which fits over the permanent anchor block and bears on the anchor plate attached to the "A" frame. The bottom photo shows the implements fabricated to facilitate seating the wedges. A two pound hammer was used to strike the square stock which drove the wedges into the anchor block. Not shown in the photos is the pressure control system for the ram which included a Simplex manually operated hydraulic pump and the 5000 psi capacity pressure transducer which was connected to a strain indicator box. The steps involved in stressing are listed below.

1. The permanent anchor heads are threaded onto the strands at both ends of tendon. Care is taken to ensure that the strands of the tendon remain parallel.

2. The wedges at "B" end are seated by driving them into the anchor block holes.

3. The chair at the stressing end is positioned. Shims are inserted to align the chair and ram with the direction of the tendon at the anchorage.

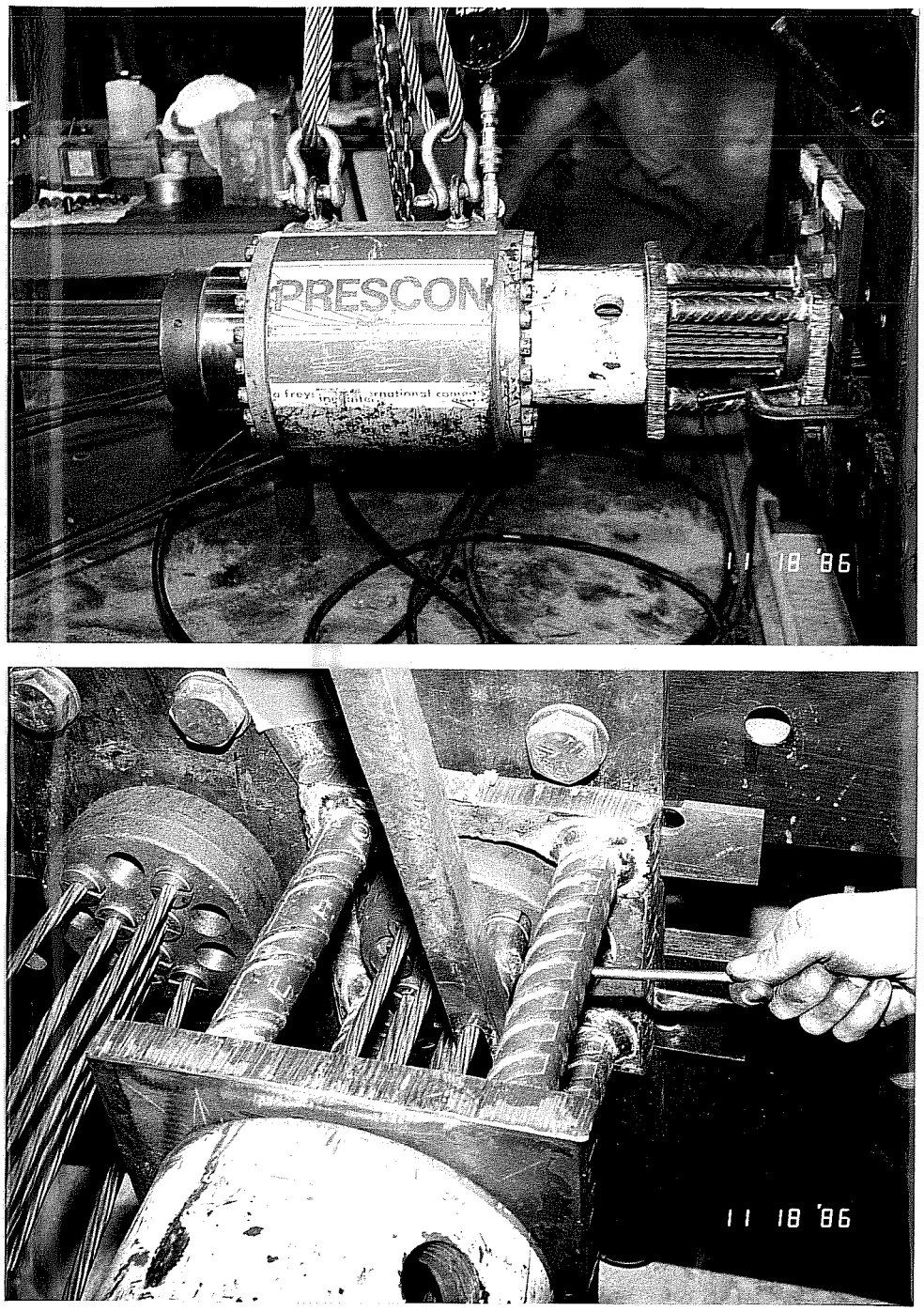

Figure 5.7 Stressing Equipment and Hardware

4. The ram is positioned on the chair. The ram is suspended from a hoist so that the height and position are adjustable.

5. The temporary anchor block at the back side of the ram is placed. The hole pattern in the temporary block is aligned with the pattern in the permanent anchor block so that no strands cross each other. Wedges are then inserted and seated in the temporary anchor block.

6. The ram is pumped to the desired pressure in stages. The data acquisition system takes readings after each increment for statics checks.

7. The desired pressure is maintained while the wedges are seated in the permanent anchor block.

8. The pressure is relieved in the stressing ram and the tendon is released. Readings are taken just before and immediately after release.

9. The stressing equipment is detached and the process is repeated for the remaining tendons.

5.2.2.2 Test Phase I. This phase begins after all tendons are stressed. The pair of 100-ton rams, AI and AII, are activated to push out the lever frame. Dial gages set up at each side of frame "A" monitor the movement of the frame. Synchronized pumping of the hydraulic pumps controlling Rams AI and AII advances the frame equally at both sides. Displacement increments are chosen to generate appropriate tendon force increments. At the end of each load stage, the data acquisition system scans all channels of instrumentation and dial gages are read. Tendon force is calculated as the test progresses. A plot of tendon force versus strain in some of the key deviator

reinforcement strain gages is maintained to monitor the response of the deviator after each load stage. Displacement increments are adjusted if necessary. Cracks are marked, documented and photographed. After a well developed crack pattern is established, the specimen is unloaded by slowly bleeding the rams in controlled increments. The system is unloaded only until the stress in the tendons reaches the original seating level. This marks the end of the first load cycle and the end of Phase I of the deviator test.

5.2.2.3 Test Phase II. Phase II begins by reloading the deviator to the peak level attained in Phase I in a few large increments. Then smaller dispacement intervals are resumed. Documentation and marking of cracks continues until cracks begin to grow significantly in size and number. At this point, safety dictates that further monitoring be conducted remotely using the surveying equipment. Loading continues until the deviator fails.

5.2.3 Test 1B. Test 1B was actually the first test conducted. Since Block B deviated only two tendons, it presented the simpler case for stressing and loading. At this point, it was still necessary to verify that the test setup and loading system would function as expected.

Based on a conservative direct tension model, a lower bound for first cracking was determined as 36 kips for Tendon 2.

Failure was estimated at a force of 92 kips for Tendon 2, based on the same simple model.

The "A" frame was initially inclined two degrees to provide more travel for the lever frame. This also reduced the maximum angle of kink at the anchorage that the tendons would experience as the lever frame rotated about its pins.

Tendon No. 1, which had only a small horizontal deviation, was stressed first. Then Tendon No. 2 was stressed. It should be noted that Tendon 1 initially had 7 - 3/8 in. diameter strands, and Tendon 2 had 10 - 3/8 in. diameter strands (more strands were added to each later in the test). A combination of seating loss and relaxation (24 hours passed before Phase I began) contributed to total losses of 30 percent for Tendon 1 and 55 percent for Tendon 2, which was considerably more than had been anticipated.

Phase I began with Tendon 1 at a load level of about 12 kips and Tendon 2 at 8.5 kips. Displacement intervals of 0.1 inches to 0.25 inches at the level of the loading rams resulted in load increments of total tendon force of 5 to 10 kips. At the fifteenth load stage, microcracking was evidenced by a significant jump in the strain levels of the deviator reinforcing steel. Force levels at Load Stage 15 were 64 kips for Tendon 1 and 78 kips in Tendon 2, giving a combined tendon force of 142 kips. Loading continued for three more load stages when it

became apparent that the lever frame would soon run out of travel. Total tendon force had reached roughly 170 kips. The decision was made to stop the test at this point and unload until the total tendon force dropped to about 40 kips. To gain more travel at the "A" frame, the lever frame at the "B" end of the setup was pushed out about two degrees. This brought the total tendon force back up to approximately 95 kips with Tendon 2 recovering proportionally more force since it was inclined. Rams AI and AII were again activated and loading resumed. Visible cracking appeared in the deviator when the total tendon force reached 200 kips. The cracks were traced with markers and photographed. Loading continued for three more load stages. The final tendon forces for Phase I of Test 1B were 80 kips in Tendon No. 1 and 143 kips in Tendon No. 2, which added to a total tendon force of 223 kips.

It was obvious at this point that the deviator was much stronger than had been anticipated. Clearly, factors other than the direct tension capacity of the link reinforcement were contributing to the behavior of the deviator. Since a safety limit of 70 percent of ultimate (189 ksi, or 160 kips for Tendon 2) had been set for the test tendons, it became apparent that existing tendon steel was more than likely insufficient to fail the deviator. These considerations led to the decision to unload

the system completely, deseat the tendons and add more strands to each tendon. Augmentation to 9 - 3/8 in. diameter strands for Tendon 1 and 12- 3/8 in. diameter strands for Tendon 2 furnished an additional 30 percent of safe tendon capacity. A decision was also made at this time to deviate further from the general test procedures in order to expedite and facilitate the completion of Test 1B. A new loading scheme was adopted in which Tendon 1 would be stressed to a target stress level after release of about 160 ksi (122 kips). Then Tendon 2 would be stressed incrementally until the deviator failed. This procedural change eliminated one stressing procedure, saving considerable time and effort. Controlling only one ram (the stressing ram), instead of two would facilitate testing as well. Since the deviation angle of Tendon 1 was small compared with Tendon 2, it was felt that the difference in loading would have an insignificant effect on the overall behavior of the deviator.

Phase II began by restressing Tendon 1, this time to a level of 170 ksi (130 kips). Seating losses reduced the force in Tendon 1 to 118 kips. The Prescon stressing ram was mounted on Tendon 2 and stressing began. The force in Tendon 2 was increased, first in 10 kip increments, then in 5 kip increments, until the deviator failed explosively just before completing Load Stage 16. The force levels at failure included 100 kips in

Tendon No. 1, 166 kips in Tendon No. 2, or a total tendon force of 266 kips.

5.2.4 Test 1A. With the benefit of experience gained from Test 1B, Test 1A proceeded as planned with no major deviations from the general test procedures. The initial stress in the tendons was increased since Test 1B had better defined the cracking capacity of the deviator. Tendons for Test 1A consisted of 9 - 3/8 in. diameter strands in Tendon 1, and 12 - 3/8 in. diameter strands each in Tendon 2 and Tendon 3. All tendons were stressed to a level of 60 ksi. At the start of Phase I, seating and relaxation losses had accounted for a force reduction in Tendon 1 from 46 kips to 24 kips (48 percent), in Tendon 2 from 61 kips to 40 kips (34 percent) and in Tendon 3 from 61 kips to 41.5 kips (32 percent).

Phase I included 14 load stages in which the total tendon force was increased from 105.5 kips to 304 kips. All loading increments were applied by pushing out the "A" lever frame. Microcracking occurred at 210 kips and the first visisble crack appeared two stages later when the total tendon force reached 246 kips. The final force levels in the tendons were 82 kips in Tendon 1, 113 kips in Tendon 2 and 109 kips in Tendon 3. The system was then unloaded in steps until the total tendon force had decreased to 95 kips, approximately the seating level at the beginning of the load cycle.

The system was reloaded for Phase II. The deviator finally failed after 34 load stages at a total tendon force of 437 kips. The force was divided among Tendon 1 with 119 kips, Tendon 2 with 153 kips and Tendon 3 with 165 kips.

CHAPTER 6

TEST RESULTS

6.1 Deviator Forces

Discussion of the test results will be facilitated by the introduction of a reference frame by which force levels in the specimen deviators can be compared to each other and to those in the prototype structure. All forces which were applied to each deviator specimen will therefore be presented relative to the scaled maximum forces on the corresponding prototype deviator. The maximum force on the prototype deviator occurs at stressing, when the maximum tendon stress allowed by AASHTO is 80 percent of the guaranteed ultimate strand stress. After seating and relaxation losses have occurred the tendon force drops and, except for excessive overload approaching failure, would never again attain the original stress level at jacking, since the unbonded external tendon distributes strain globally over the length of the tendon. Maximum force components on the prototype deviator at jacking are termed the nominal forces and are computed by multiplying 80 percent of the ultimate tendon force by the sines of the horizontal and vertical deviation angles. An equivalent force on the model is found by applying the scale factor for force ($S_F=S_L^2=1/3^2=1/9$) to the prototype value. The total scaled force on the deviator, D, is computed as the vector

sum of all the scaled horizontal and vertical force components (see Fig. 6.1). This vector sum of maximum service level forces (nominal force) is defined by a magnitude, denoted D_o, and a direction, denoted θ_o. Similarly, the total scaled nominal horizontal force component is denoted H_o, and the nominal vertical component, V_o. Figure 6.1 summarizes the scaled prototype force components and gives the sign convention adopted for these forces. Positive vertical force components act upward on the deviator and positive horizontal components are directed inward toward the center of the specimen box. θ is measured counterclockwise from the positive horizontal axis. Figure 6.2 illustrates the reference quantities D_o, V_o, H_o, and θ_o. Corresponding test result quantities are denoted D, V, H, and θ repectively.

6.1.1 Test 1B. Figures 6.3a-b show the history of the forces seen by Block B as Test 1B, Phase I progressed. In Fig. 6.3a, the magnitude and direction of the total force vector on the deviator are shown, as well as the reference quantities D_o and θ_o. The relative contributions of forces from each tendon to the total force vector are illustrated in Fig. 6.3b. The contribution of force from Tendon 1 was slight since the deviation angle for Tendon 1 was small as compared to that of Tendon 2. Figures 6.4a-b show similar information for Phase II.

PROTOTYPE DEVIATION ANGLES/FORCES

SIGN CONVENTION:

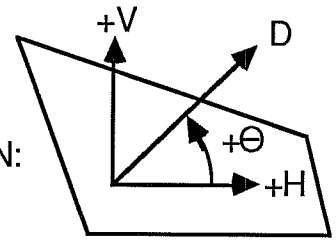

BLOCK A

TENDON	Aps	.8fpuAps/9	HORIZONTAL		VERTICAL	
			dev. angle	force	dev. angle	force
1	1.836 sq.in.	44.06 kips	-3.68°	-2.83 kips	0	0
2	2.907 sq.in.	69.77 kips	-3.68°	-4.48 kips	0	0
3	2.907 sq.in.	69.77 kips	+0.82°	+1.00 kips	+6.41°	7.79 kips

Vo = 7.79 kips
Ho = -6.31 kips
Do = 10.02 kips
Θo = 129.01°

BLOCK B

TENDON	Aps	.8fpuAps/9	HORIZONTAL		VERTICAL	
			dev. angle	force	dev. angle	force
1	1.836 sq.in.	44.06 kips	+1.84°	+1.41 kips	0	0
2	2.907 sq.in.	69.77 kips	+2.93°	+3.57 kips	+8.22°	9.98 kips

Vo = 9.98 kips
Ho = 4.98 kips
Do = 11.15 kips
Θo = 63.48°

Figure 6.1 Prototype Deviation Angles and Forces

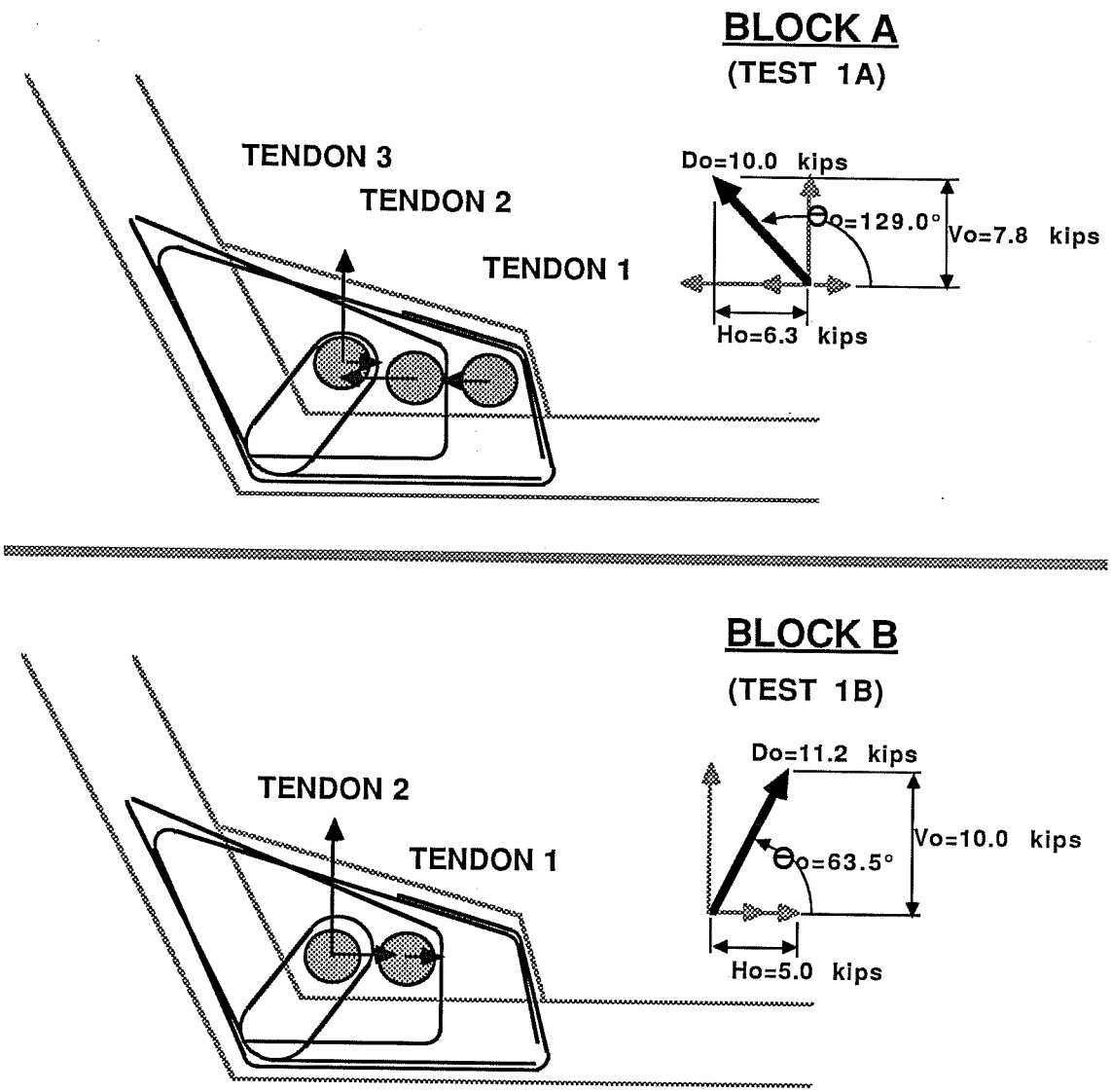

SCALED FORCE COMPONENT =
.8FpuAps x sin(deviation angle) x scale factor
Do = Vector Sum of Force Components
Ho = Total Horizontal Force
Vo = Total Vertical Force

Figure 6.2 Reference Forces

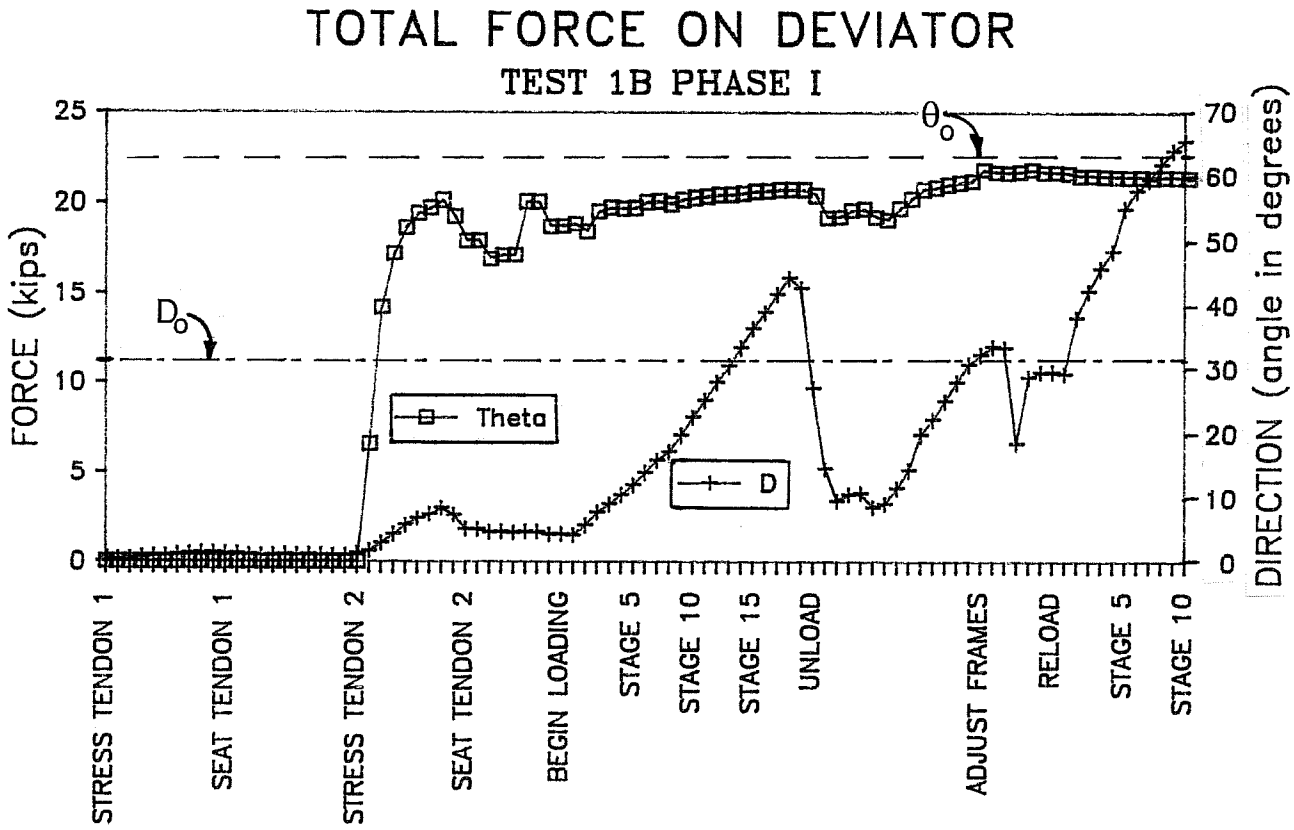

Figure 6.3a Test 1B Phase I Force Vector History

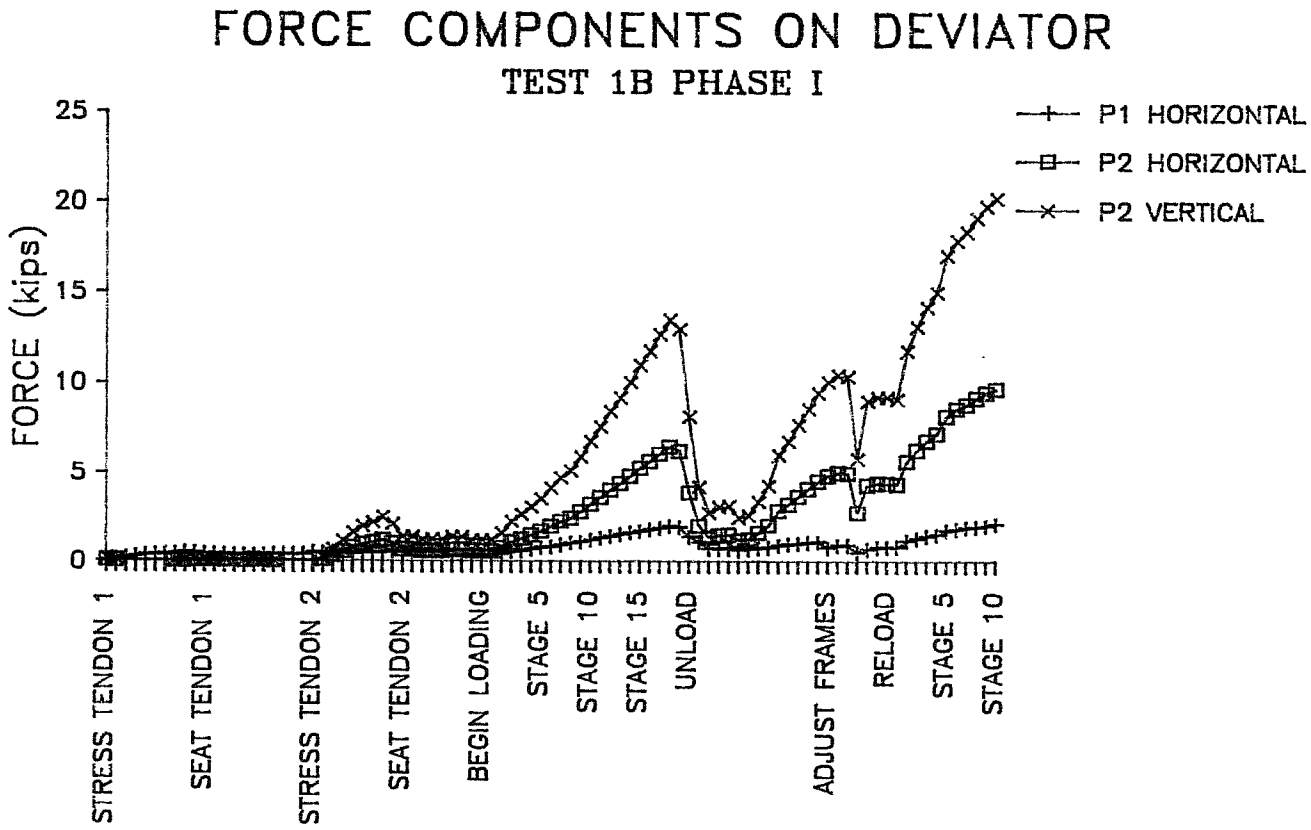

Figure 6.3b Test 1B Phase I Force Components

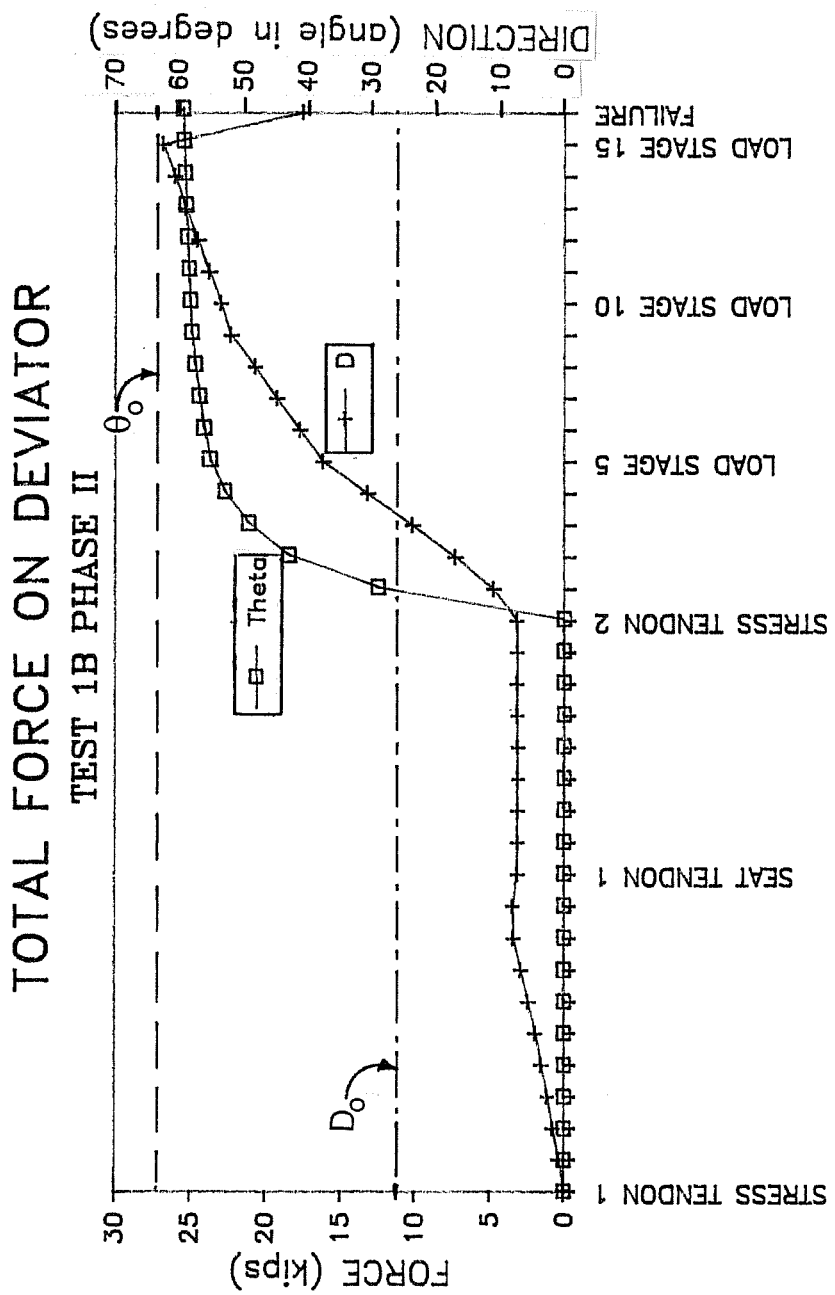

Figure 6.4a Test 1B Phase II Force Vector History

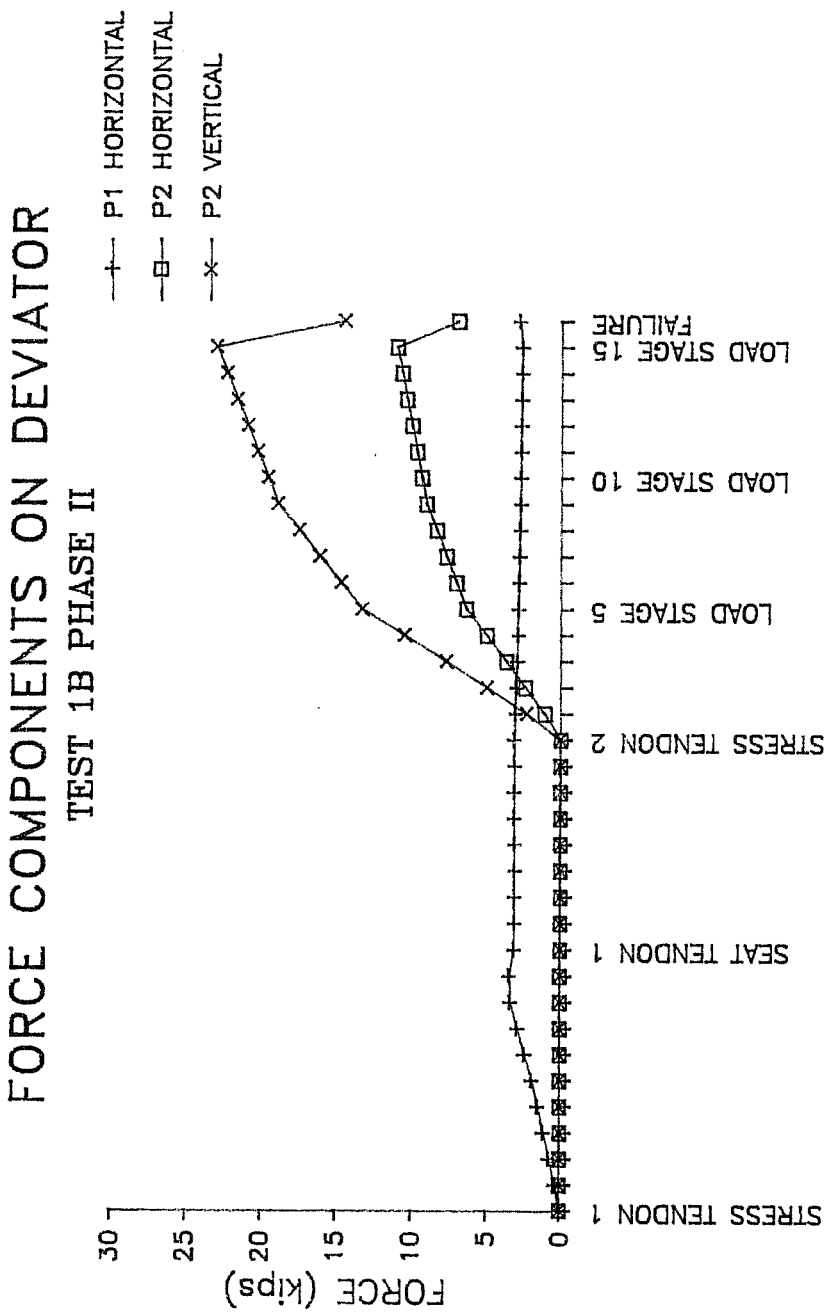

Figure 6.4b Test 1B Phase II Force Components

Load levels at critical stages of behavior are presented relative to the scaled maximum force on the prototype deviator in Fig. 6.5. This figure illustrates the fact that, although the total force on the deviator at failure was more than twice D_o, this force was not appreciably higher than the force on the deviator when the first cracks appeared or at first yielding of the deviator reinforcement. This points to a lack of ductility which will be addressed further in Section 6.2.

6.1.2 Test 1A. Figures 6.6a-b and 6.7a-b show the forces applied to Block A during Test 1A, Phase I and Phase II respectively. Note that the horizontal components of deviation force in Tendons 1 and 2 are negative, in keeping with the sign convention presented in Fig. 6.1. Total force vectors at significant stages of behavior are again related to the reference quantities D_o and θ_o in Fig. 6.8. As in Test 1B, the force on the deviator at failure was more than twice D_o, yet in this case there was significantly more reserve capacity after first visible cracking although the ratios of D/D_o are comparable for both tests at final failure. The modes of failure for each deviator and their relative ductilities will be discussed in detail in the following section.

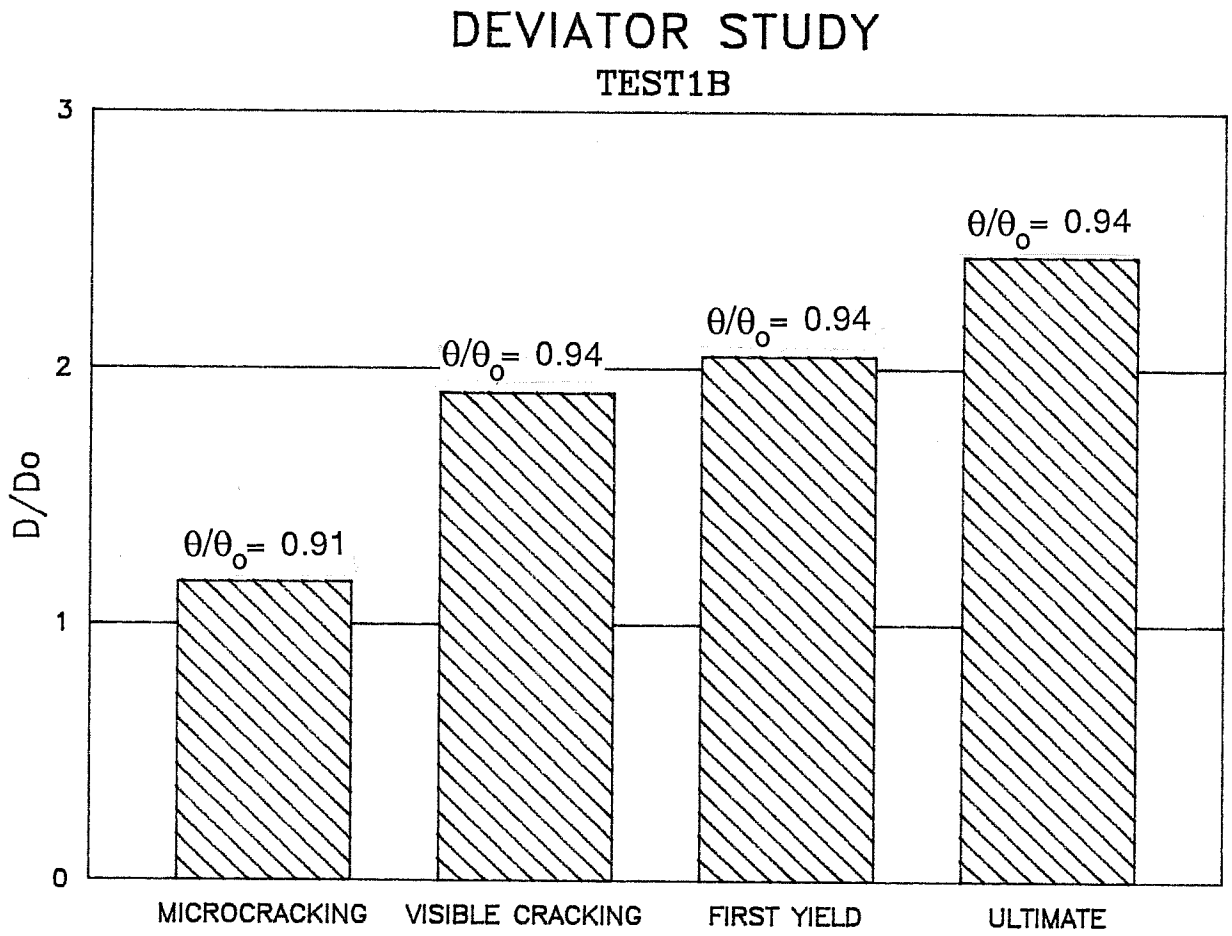

Figure 6.5 Test 1B Force Comparisons

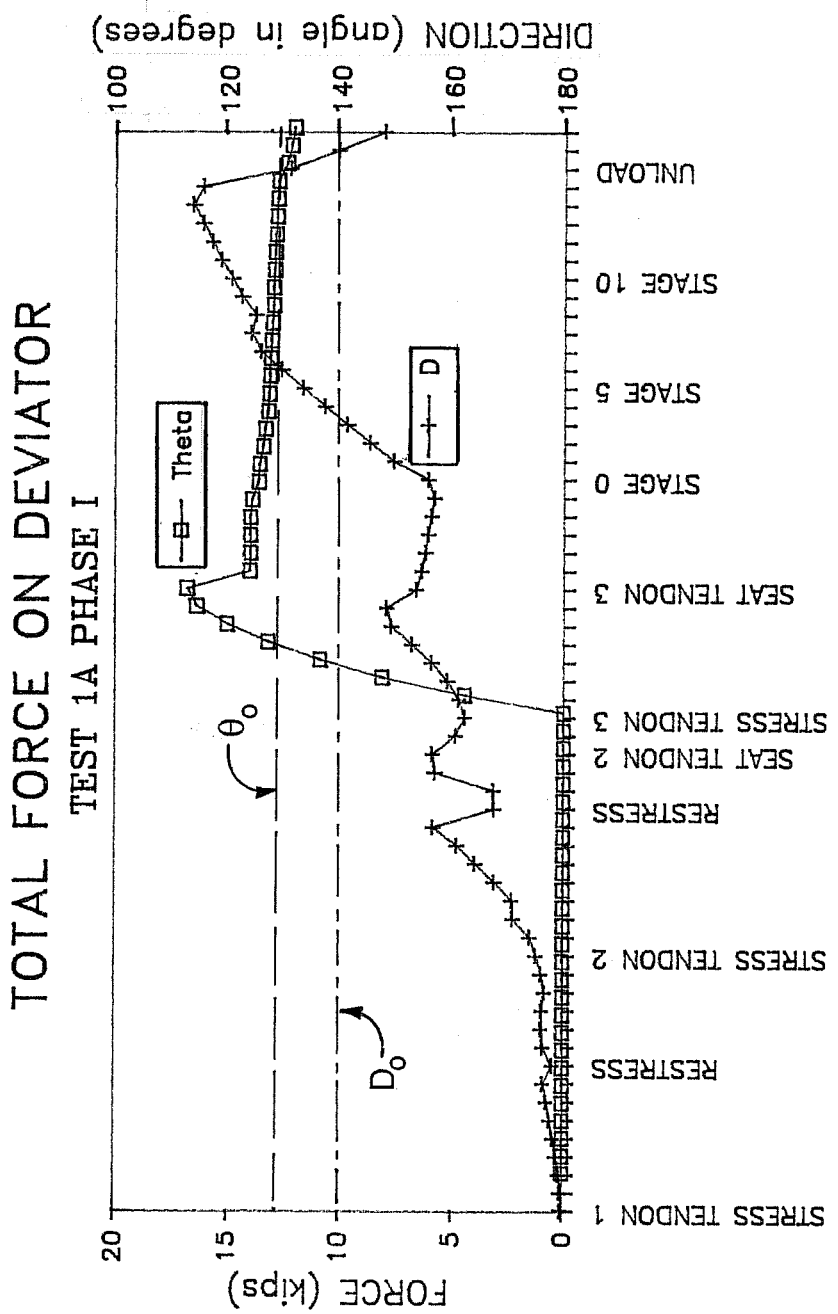

Figure 6.6a Test 1A Phase I Force Vector History

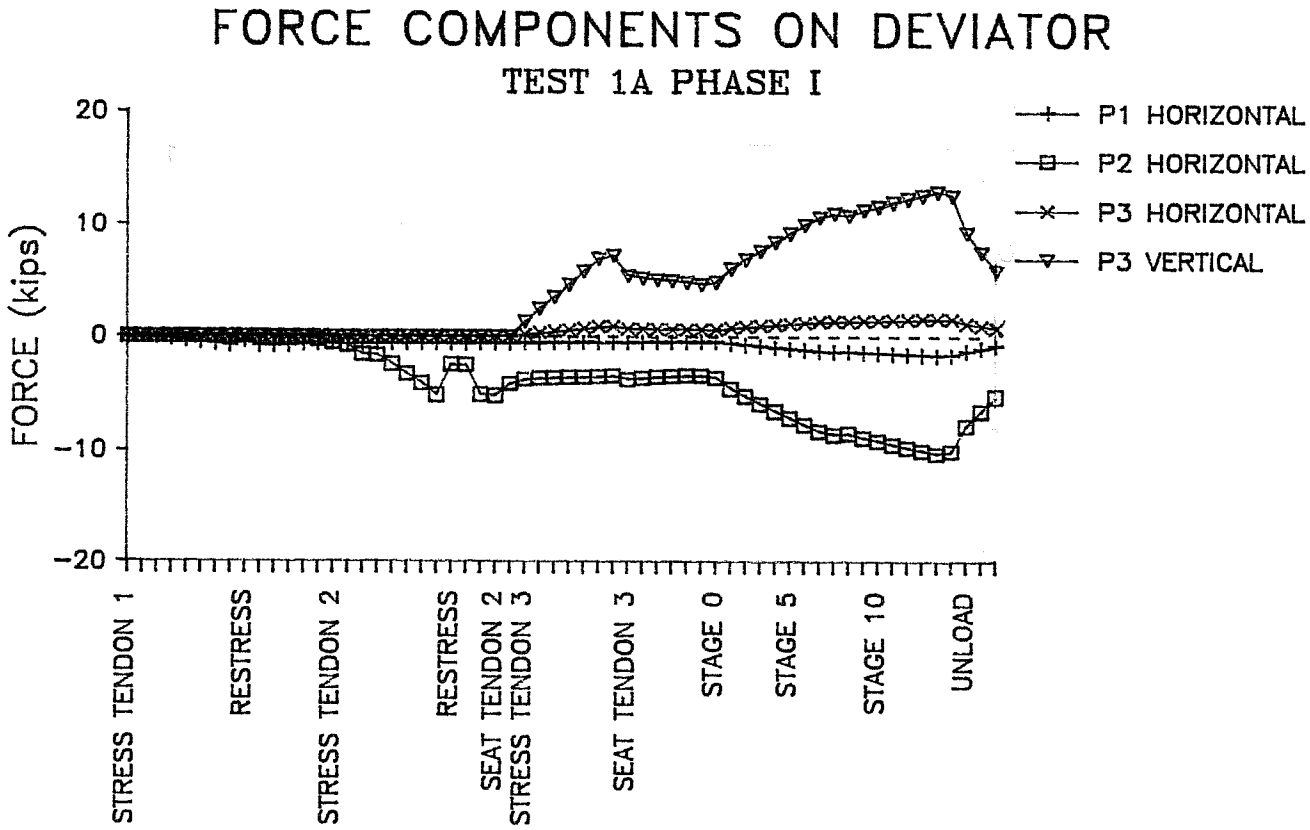

Figure 6.6b Test 1A Phase I Force Components

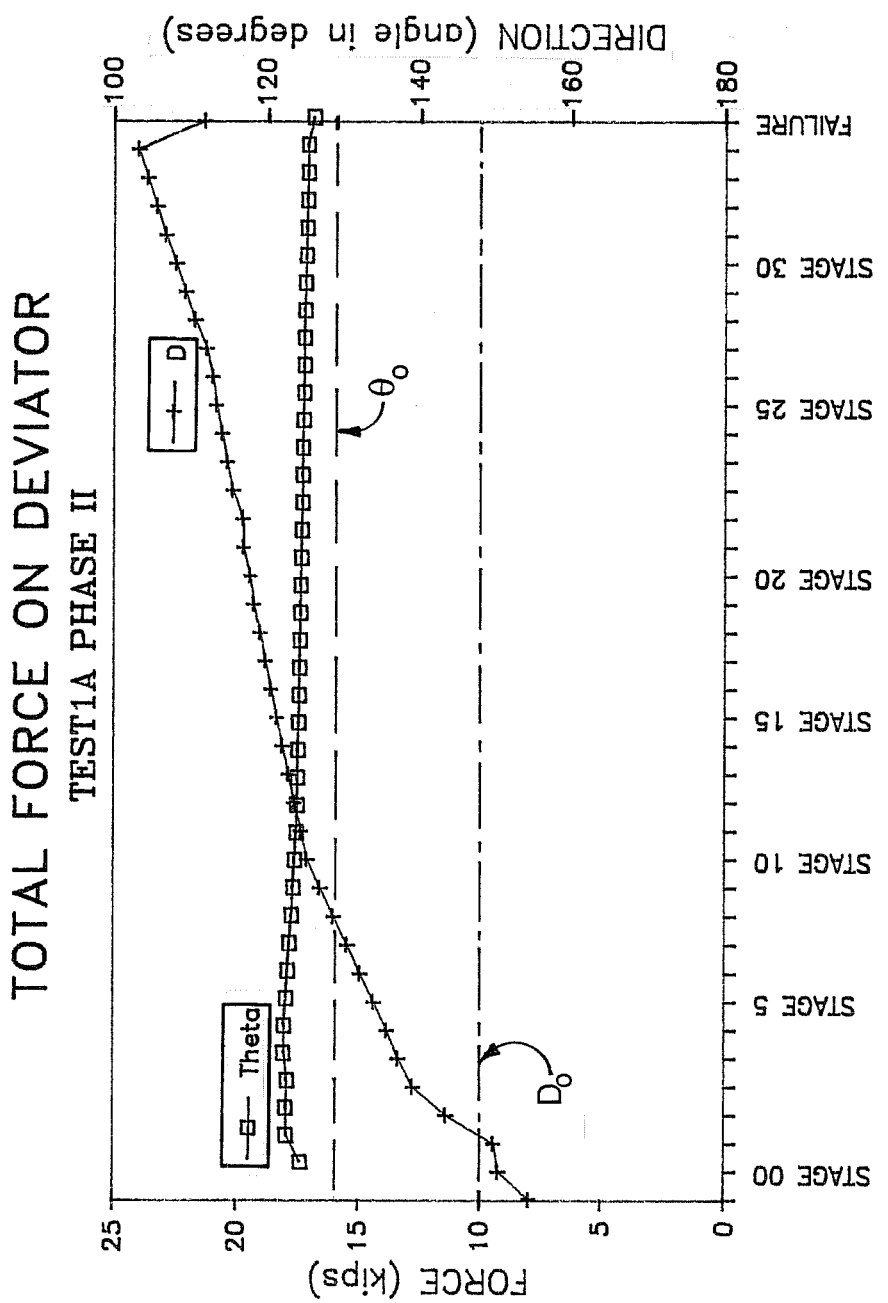

Figure 6.7a Test 1A Phase II Force Vector History

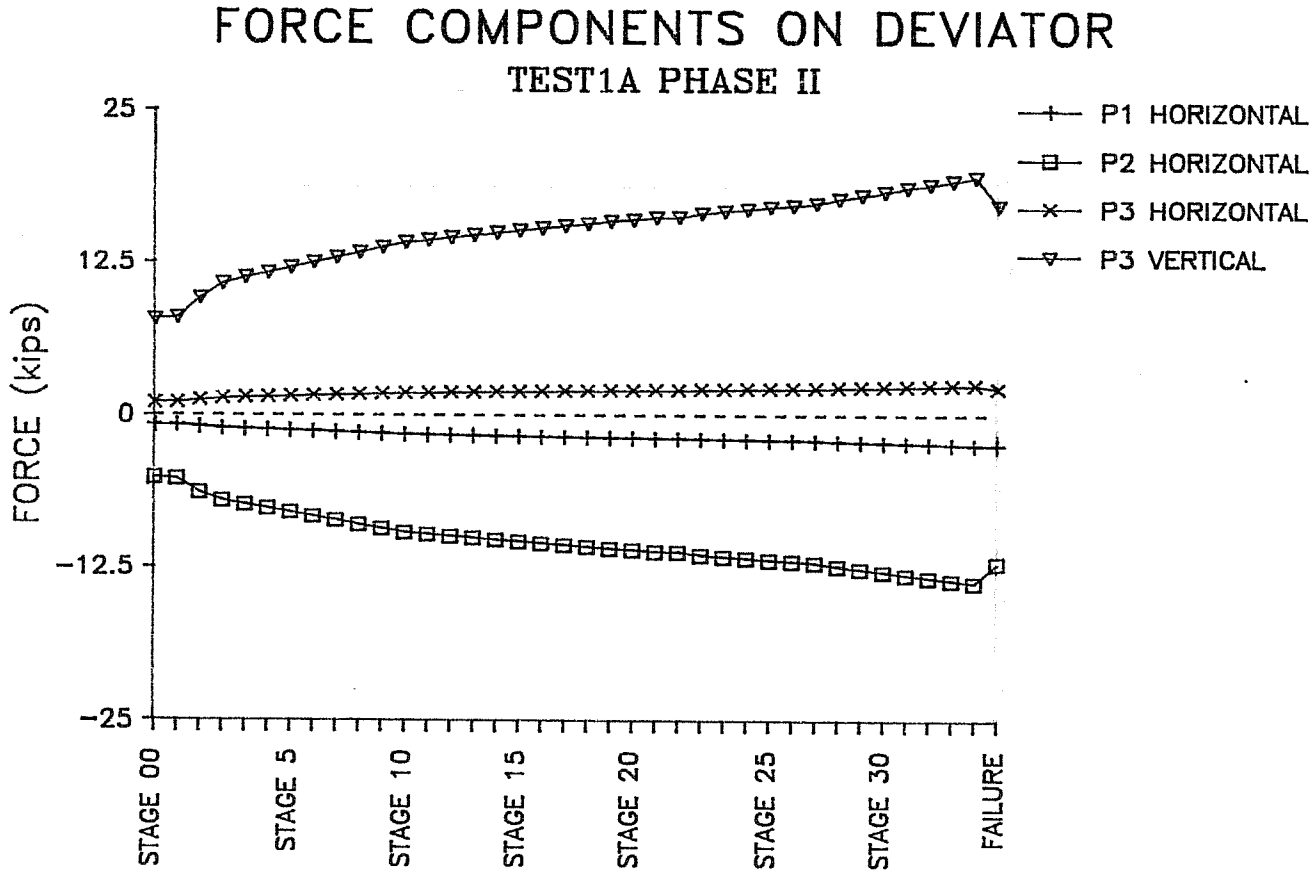

Figure 6.7b Test 1A Phase II Force Components

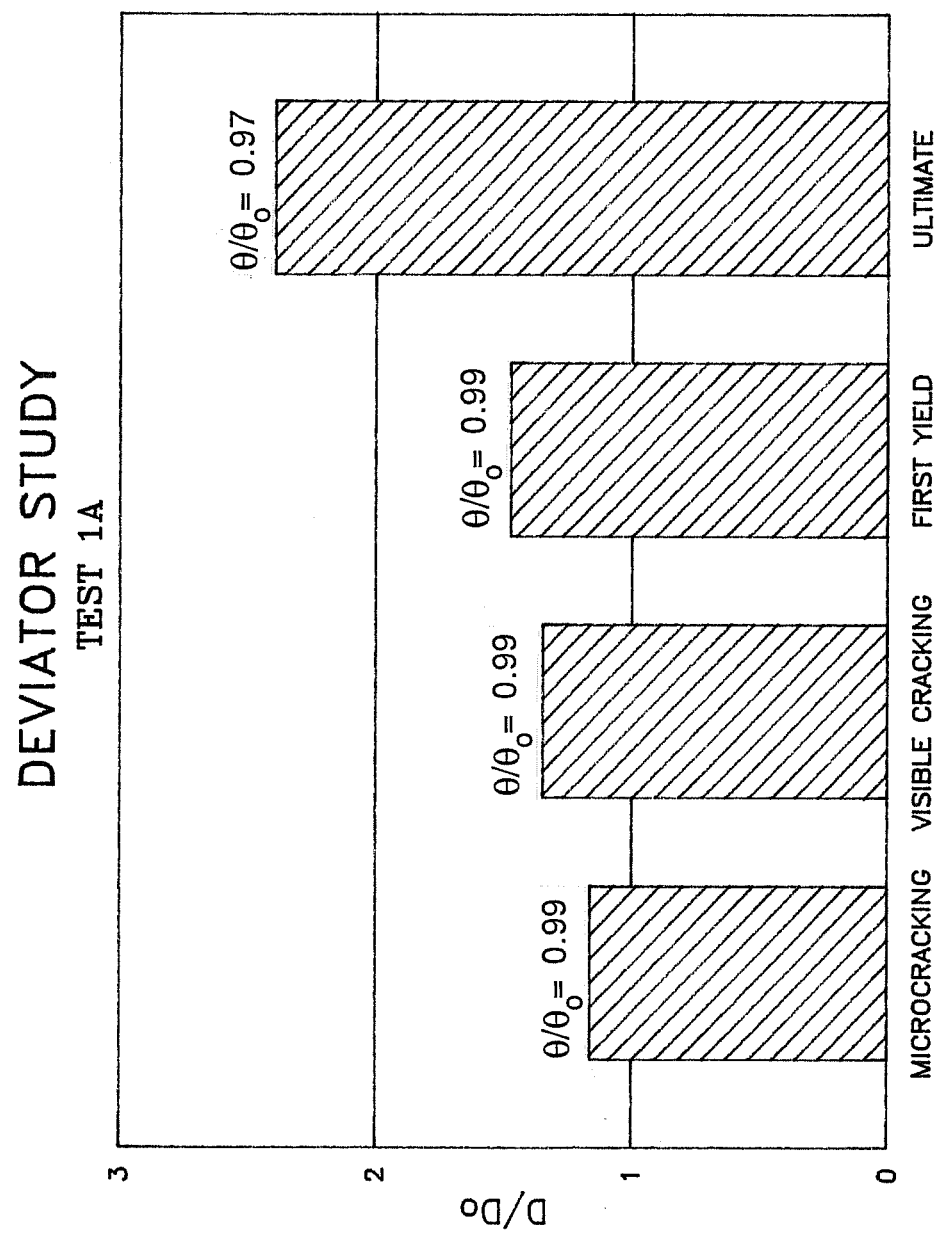

Figure 6.8 Test 1A Force Comparisons

6.2 General Observations

Aspects of deviator behavior which were observed and noted during the tests included the appearance and location of cracking and the failure mode for each deviator. Videotapes of the tests allowed slow-motion playbacks of the failures. Cracks which appeared early in the test were marked on the deviator and later stages of cracking were monitored remotely for safety reasons. All cracks were mapped as accurately as possible on a scale drawing of the deviator as they appeared. A plot of tendon force versus strain in some of the key gages on the deviator reinforcement was maintained throughout each test. These plots provided useful information which helped in controlling the tests. Strain gage data will be presented and discussed in Section 6.3.

For the purpose of discussion, the three components of principal deviator reinforcement will be denoted as shown in Fig. 6.9. The effectiveness of each of these components (link reinforcement, outer loop, and inner loop) will be discussed in Section 6.5.

6.2.1 Test 1B. Phase I of Test 1B began with both tendons at a very low stress level. The original test plan had been to stress the tendons to a level which would produce forces on the deviator that would be just below a conservative estimate of the cracking load. This estimate assumed the concrete would

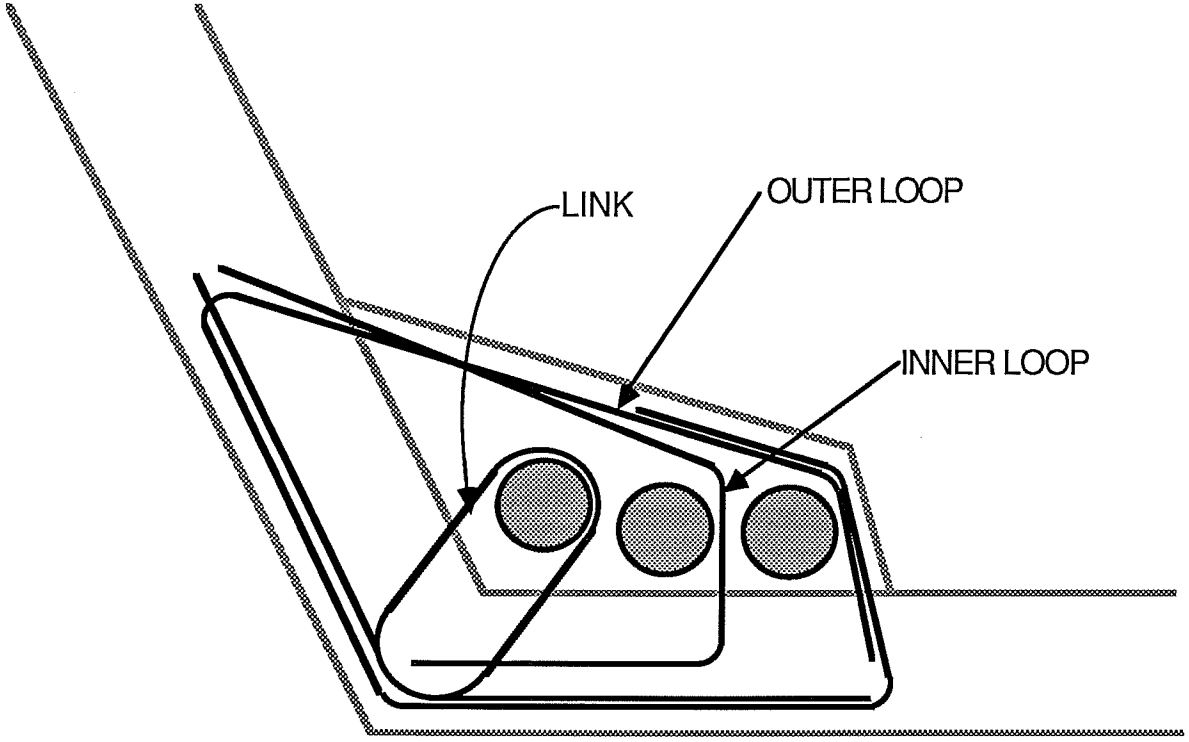

Figure 6.9 Principal Deviator Reinforcement

crack when the direct tension reinforcement attained a level of strain equal to the modulus of rupture of the concrete. This condition would occur when the force in Tendon 2 reached approximately 36 kips. Assuming equal stress in both tendons, the corresponding value of D was roughly 6 kips (D/D_o=0.54). Loading continued far beyond this level with no sign of visible cracking in the concrete and no significant response in the embedded strain gages on the deviator reinforcement. Finally, at Load Stage 15, a distinct jump in strain levels in nearly every strain gage indicated internal microcracking. There was no external cracking visible to the naked eye. The tensile capacity of the concrete had been exceeded and the reinforcement was beginning to pick up force. At this point D had reached about 13 kips (D/D_o=1.16), more than twice the anticipated cracking level. This was the first indication that factors other than the direct tension action of the reinforcement were significantly affecting the behavior of the deviator.

Loading continued for three more load stages. Faint "crackling" noises eminated from the deviator, but thorough inspection revealed no visible cracks. At this point it became apparent that the lever frame would run out of travel before any perceptible damage would occur in the deviator. Both the "A" and

"B" lever frames were subsequently manipulated to allow further loading from the "A" end.

The second cycle of Phase I began the next day. The starting point for this cycle, called Stage 0, corresponded to D of approximately 10 kips (D/D_o=0.89). Loading resumed, and after the load level surpassed that of the previous day, "crackling" noises were again heard. An occasional loud "ping" was presumably caused by the tendons sliding and re-situating inside the duct. The first cracks appeared just after Load Stage 6, when D had increased to slightly over 21 kips (D/D_o=1.88). This level of total force on the deviator represented an increase of over 60 percent above the level of D at microcracking. The first visible distress was a hairline crack on the north face or "A" side of the deviator. (Refer to Fig. 6.10.) The crack propagated at an angle from the Tendon 1 duct, above the Tendon 2 duct, and toward the top corner of the deviation block. Closer inspection revealed that the crack also extended from the other side of Duct 1 toward the front face of the deviator. Two other cracks which were barely visible were detected at this time. One of these was on the top face of the deviator, directly above and running parallel to Tendon 2. The third crack started at the top of Duct 2 on the south face or "B" side of the deviator, and ran along a slight incline to the top face of the deviator. After these first cracks became visible, a decrease in stiffness was

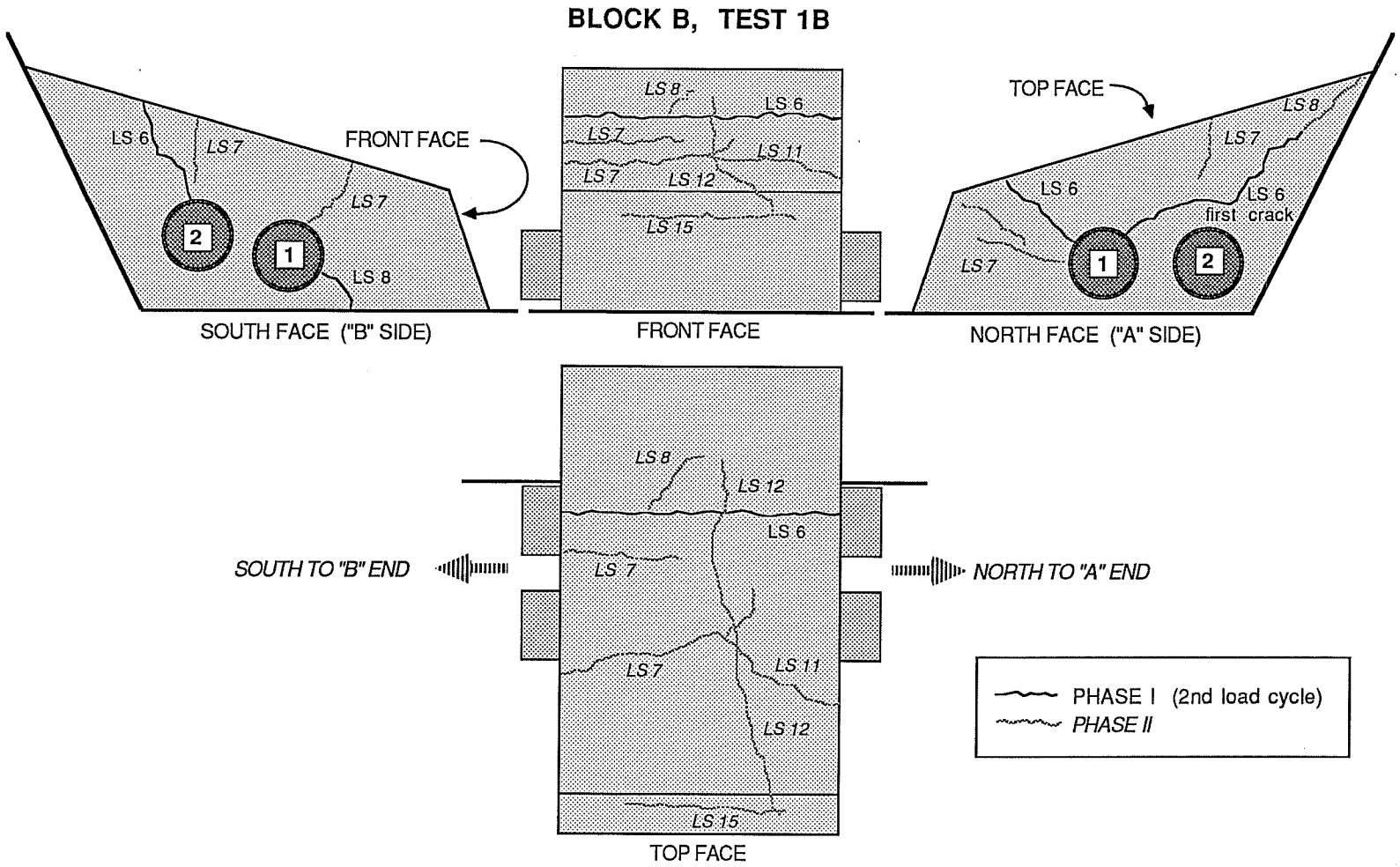

Figure 6.10 Test 1B Crack Patterns

evidenced by a decreasing slope in the tendon force versus strain plot.

Figure 6.10 is a complete map of all the cracks that appeared on the deviator up to failure. Phase I cracks are drawn with solid lines accompanied by the load stage number at which they first appeared. Only one other crack appeared before the end of Test 1B Phase I. This crack was noticed at Load Stage 8, and began at the underside of Duct 1 and ended at the junction of the deviator and the bottom flange of the specimen box. At the end of Phase I, the specimen was completely unloaded and prepared for Phase II as described in Chapter 5.

When the specimen was reloaded in Phase II of Test 1B, new cracks began to appear on the deviator at load levels lower than the maximum attained in Phase I. Phase II cracks are represented by the shaded lines in Fig. 6.10. Corresponding load stage numbers are italicized. Several cracks appeared at Load Stage 7 (see Fig. 6.10) at a value of D of 19.2 kips (D/D_o=1.72), and two more became noticeable at Load Stage 8 when D was 20.7 kips (D/D_o=1.85).

It is of interest to note at this point that the direct ultimate tensile capacity of the link reinforcement corresponded to a value of D of approximately 16 kips (D/D_o=1.43). Clearly, other factors were influencing the deviator capacity. The

general pattern of cracking suggests the possible influence of flexural behavior in the top portion of the deviation block. This top portion of the block can be thought of as a beam element, with the top face of the block forming the tension face of the beam. The crack map in Fig. 6.10 shows cracks perpendicular to the top face of the block near the center of the "beam". These can be construed as vertical flexural cracks. Away from the center, toward either end of the "beam", inclined cracks appear. These cracks resemble inclined shear cracks for a simple beam loaded at the center. Although the cracking in the deviator was extensive, no crack was very wide. Safety precautions prohibited measuring crack widths at this late stage in the test, but the maximum crack width was estimated to be 0.2mm.

Before Load Stage 12, all cracks on the top face of the deviator ran more or less parallel to the direction of the tendons. At Load Stage 12 (D = 24.5 kips, D/D_o=2.19), however, a relatively large crack (probably 0.1mm to 0.2mm wide) developed on the top face, perpendicular to the tendons. This crack originated in the upper third of the top face of the deviator and propagated in subsequent load stages down into the front face. The last crack to appear before failure was a hairline crack which ran horizontally across the front face of the deviator. It is likely that this crack formed when the laps in

the outer loops at that front edge of the deviator began to fail. Propagation of the cracks was observed through a theodolite as the load was being increased on the deviator.

As the force in the tendons was being increased to the predetermined level for Load Stage 16, the deviator failed explosively with very little warning. Slow-motion playback of the video tape revealed a sudden bulging at the top of the block occurring simultaneously with the formation of a large crack at the corner of the front face of the block. The elapsed time between the first perceptible bulging and the failure was 1.0 second. Tendon 2, which had been deviated vertically and horizontally, tore free, virtually ripping the entire deviation block from the box. All of the reinforcement that had been above Tendon 2 necked down and broke. In three of the four closed outer loops, which were lapped at the top front edge, the lap splices had failed. The fourth lap, which had been tied with a wire, developed and the bar broke just above the lap.

The series of photographs in Figures 6.11 and 6.12 attest to the catastrophic nature of the failure. In Fig. 6.11, Tendon 2 is seen to have ripped free entirely from the block. Tendon 1 remained wedged against the unbroken concrete in the bottom of the block. Figure 6.12 shows the ends of the failed lap splices in the outer loops and the necked down break points

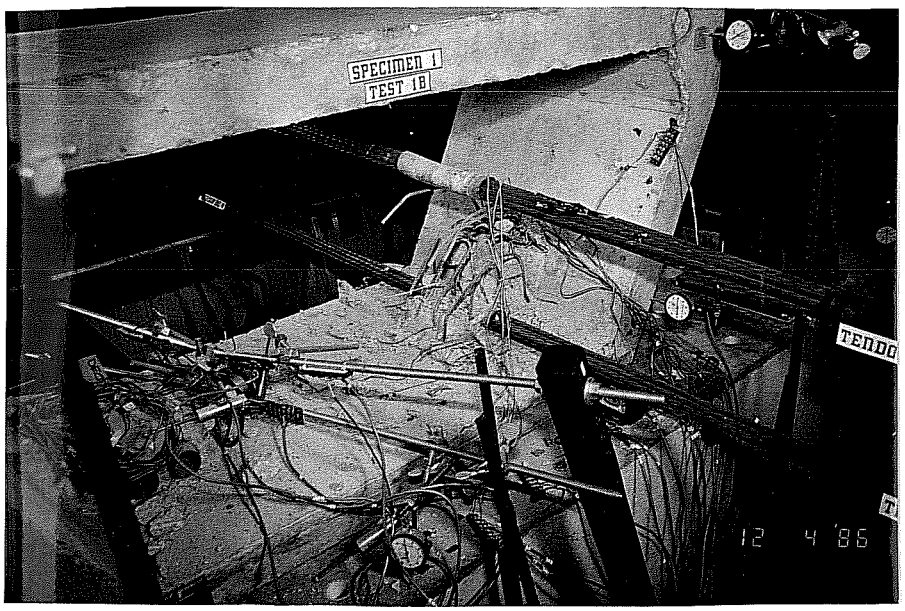

Figure 6.11 Block B: Immediately After Failure

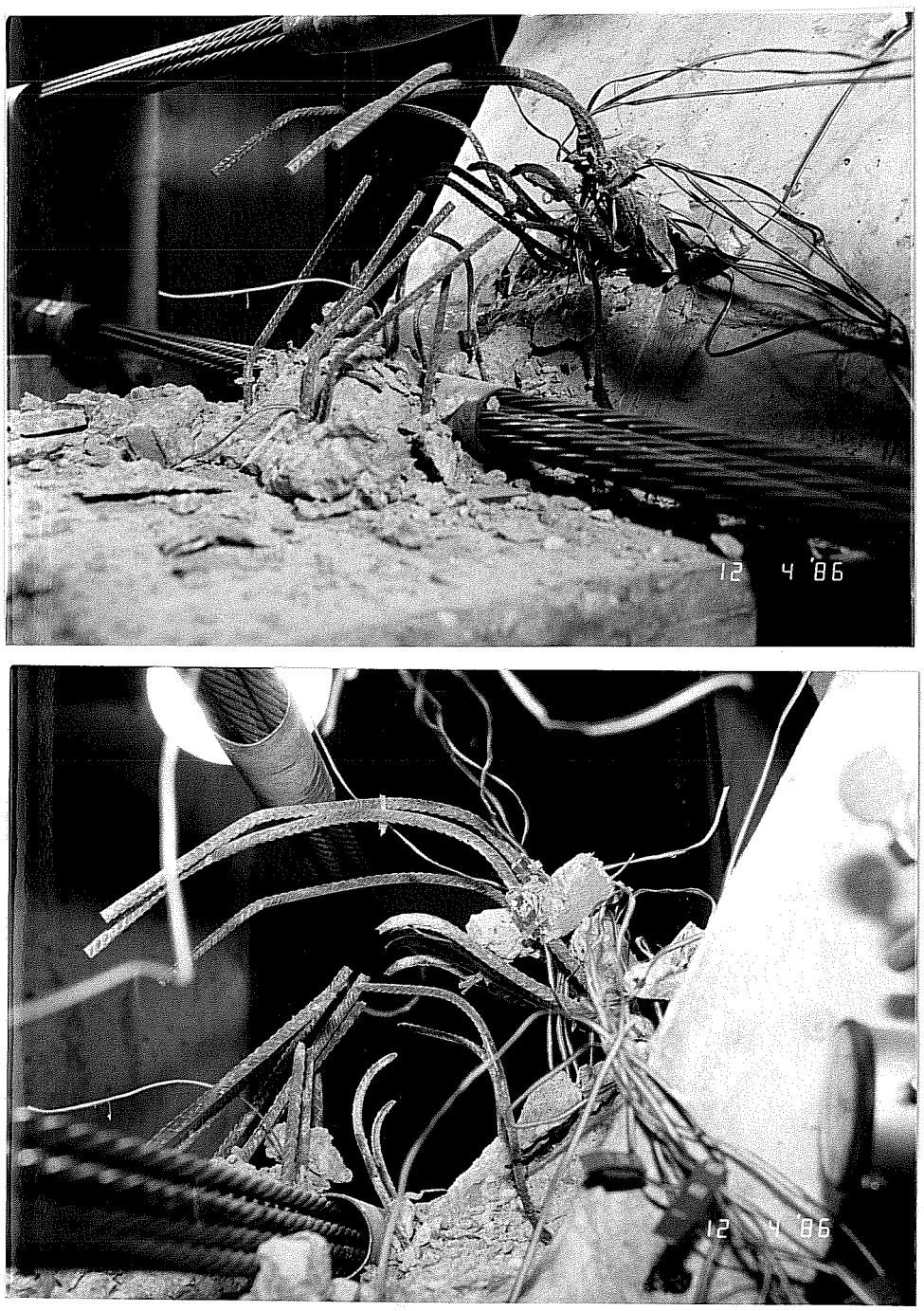

Figure 6.12 Block B Failure: Details

on the link bars and inner loops. The break points for the bars are indicated in Fig. 6.13. Even though the deviation block itself was completely destroyed, the test specimen box girder webs and bottom slab surrounding the deviator remained intact.

6.2.2 Test 1A. After stressing the three tendons which were deviated by Block A, loading began at a significantly higher level than the starting point for Test 1B for reasons discussed in Section 5.2.4. At Load Stage 0 in Test 1A Phase I, the total force, D, on the deviator was 6.0 kips (D/D_o=0.60). At load stage 5 (D/D_o=1.17), microcracking was evidenced by a significant increase in the deviator reinforcement strain. This jump in strain levels was not as pronounced as that observed in the previous test. At Load Stage 7, the first visible crack was noticed. At this point D was 13.5 kips (D/D_o=1.35), representing an increase of 16 percent above the force level at microcracking. The first crack, located on the north face of the deviator (see Fig. 6.14) began at one side of Duct 2 and ran horizontally to the edge of the duct containing Tendon 3. Continuing on the opposite side of Duct 3, the crack turned upward and extended diagonally toward the top corner of the deviator. This first visible crack on Block A was, when first noticed, already as wide (approximately 0.2mm) as any of the cracks in Block B just before failure.

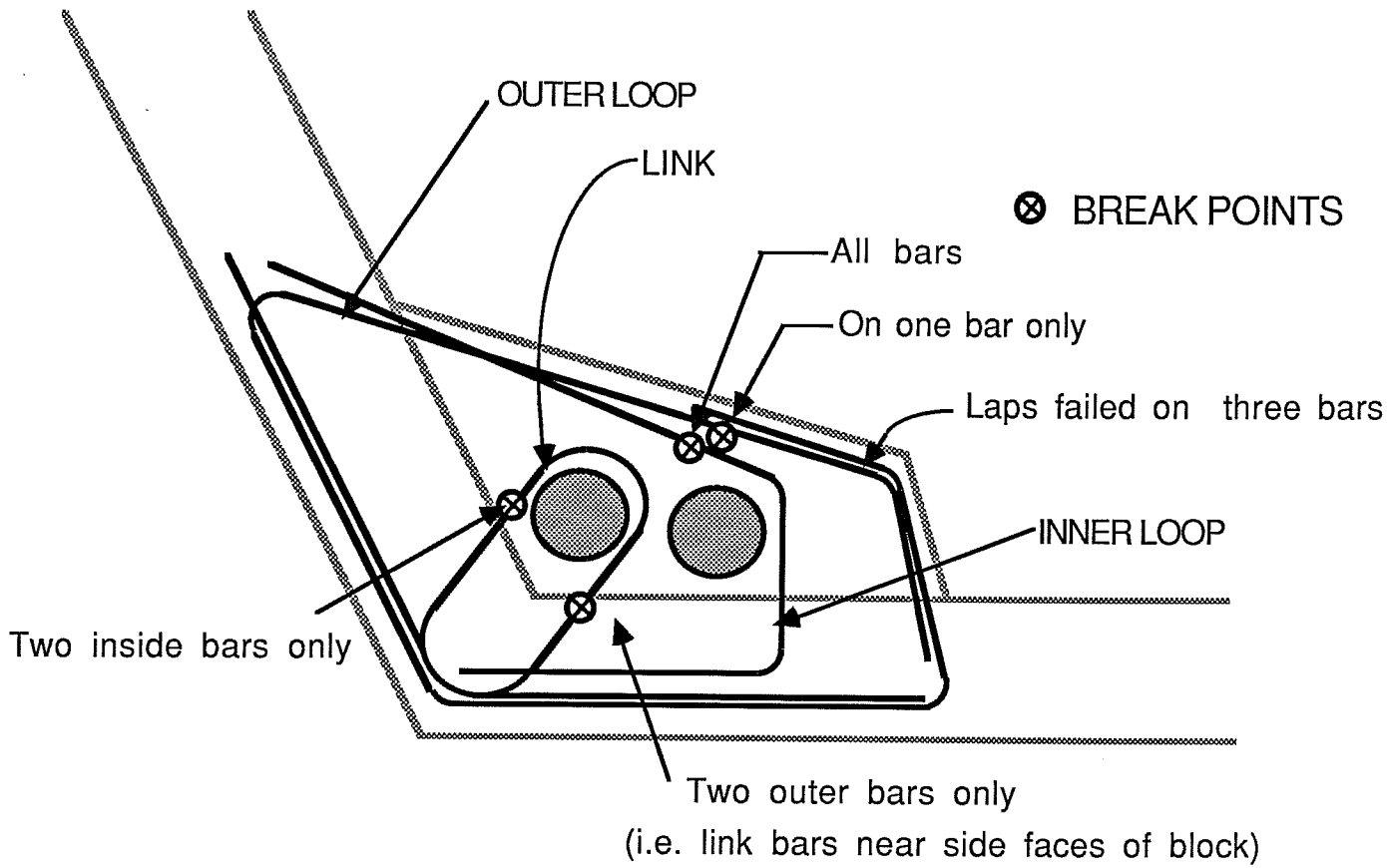

Figure 6.13 Test 1B Deviator Reinforcement Break Locations

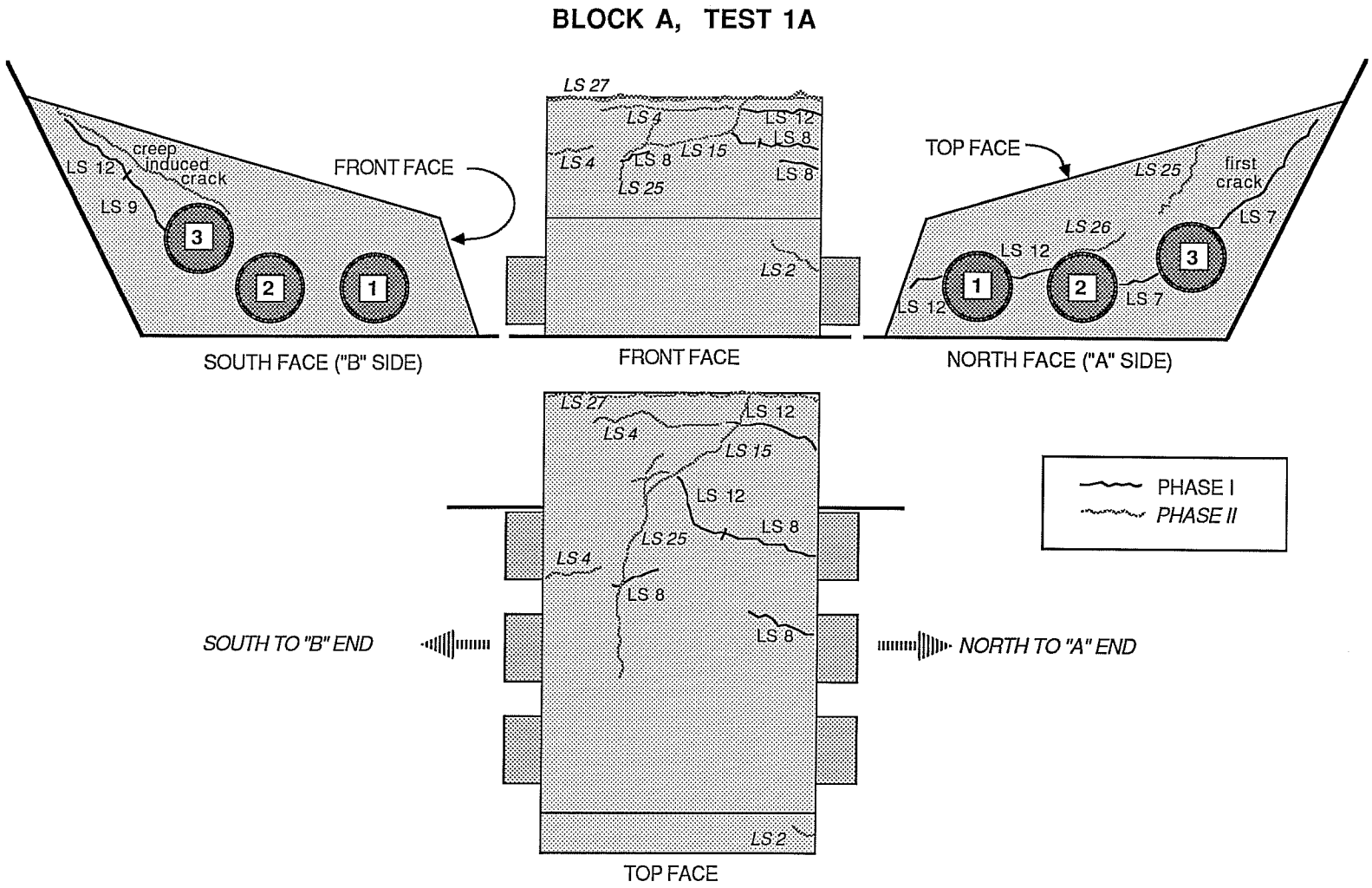

Figure 6.14 Test 1A Crack Patterns

The crack patterns for Block A are presented in Fig. 6.14. Phase I cracks are represented by solid lines next to the corresponding load stage at which they first appeared. Several scattered hairline cracks appeared on the top face of the deviator at Load Stage 8 (D/D_o=1.40), and a diagonal crack originating from Duct 3, on the south face of the deviator, was noticed at Load Stage 9 (D/D_o=1.44). First yield of the deviator reinforcement occured at the next load stage, at which time the total force, D, had increased to approximately 15 kips (D/D_o=1.50). The last cracks to form in Phase I of Test 1A occurred at Load Stage 12. As shown in Fig. 6.14, the cracking pattern on the north face of the deviator appeared to define a wedge of concrete that was being pushed toward the web by the force of the Tendons 1 and 2, which were deviated in that direction.

At the completion of Phase I, the specimen was unloaded until D had decreased to roughly 8 kips (D/D_o=0.80). It should be noted that very few of the cracks closed very much after this partial unloading.

The second loading cycle began the following day in Phase II with D at a level of 9 kips (D/D_o=0.90). (Slight adjustment of the loading ram pressures resulted in the 1 kip increase.) Before loading began, however, a new crack was noticed on the south face or "B" side of the deviator.

Apparently, this crack was induced by creep. Except for the appearance of a small crack at the corner of the front face of the deviator at Load Stage 2 (see Fig. 6.14), further cracking did not develop until the load regained the level at which first cracking appeared in Phase I. After Load Stage 4, more cracks appeared on the top face, parallel to and about one inch from the intersection of the deviation block and the web. The value of D at Load Stage 4 was 13.8 kips (D/D_o=1.38).

No new cracks appeared until D had reached 17.6 kips (D/D_o=1.76) at Load Stage 12, but the existing cracks had widened considerably. The crack which ran diagonally upward from Duct 3 on the north face of the deviator (the first crack) became especially large. At Load Stage 10 some slight spalling occured at this crack, indicating relative movement at the crack interface. The width of the crack, measured at Load Stage 11, was 0.4mm. Two load stages later, the width had increased to 0.6mm. All of the cracks began to widen, especially those on the side faces of the deviator. Dial gage and potentiometer readings on the deviator began to show significant displacements. At later stages, a full separation of the deviator from the web at the top face of the deviator became evident as the wedge formed by the top portion of the block continued to be pushed toward the

web (Fig. 6.15). This very ductile behavior contrasted markedly with the brittle failure seen in the previous test.

The deviator failed after completing Load Stage 34, at which point the total force, D, was 24 kips (D/D_o=2.40). The deviator held this load for several minutes, while dial gage readings and photographs were being taken. The bottom photo in Fig. 6.15 shows the deviator just after completing Load Stage 34. During loading to Stage 34, the only new sign of damage was a slight widening of existing cracks. Two minutes after reaching this load, however, the concrete at the interface of the large crack on the south face began to spall. At the same time, the top face of the block began to bulge and new cracks formed in several locations. Sixty seconds after this spalling and cracking, the deviator block failed. The failure was explosive, but less so than in Test 1B. Again the force of the deviated tendons tearing out destroyed the concrete of the deviation block, but only the link reinforcement broke. Breaks in three of the link bars occurred at the junction of the deviation block and the bottom flange of the box. The remaining link, which was located close to the "B" face of the deviator, broke near the web of the box. The laps in the outer loops remained bonded and both the outer loops and the inner loop bars stayed anchored in the remaining concrete. The box section was unharmed. Figure 6.16 shows photographs of the deviator immediately after failure.

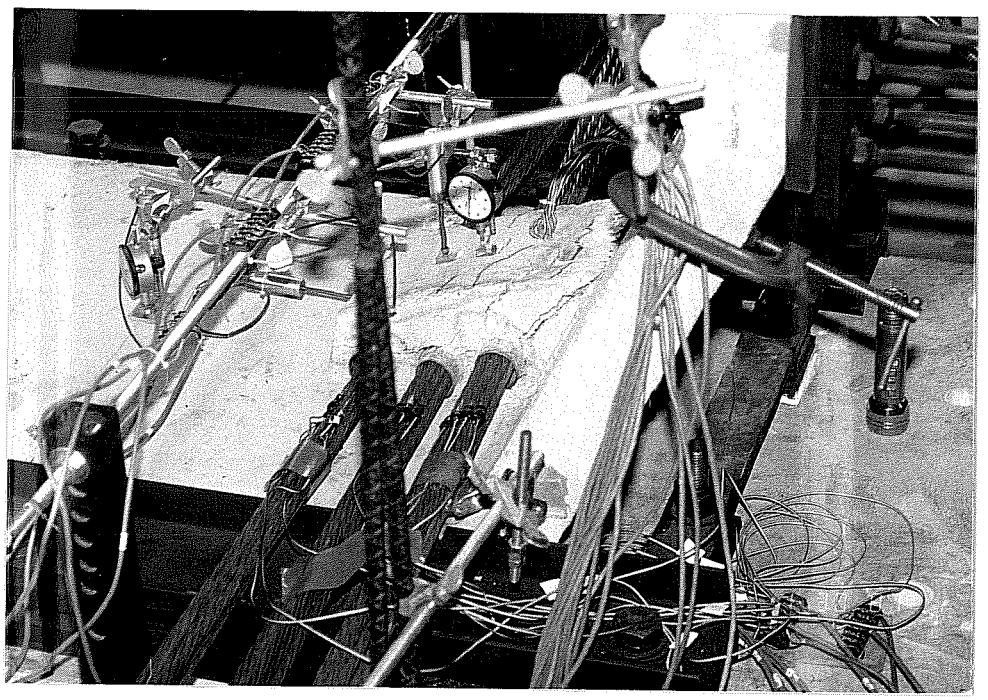

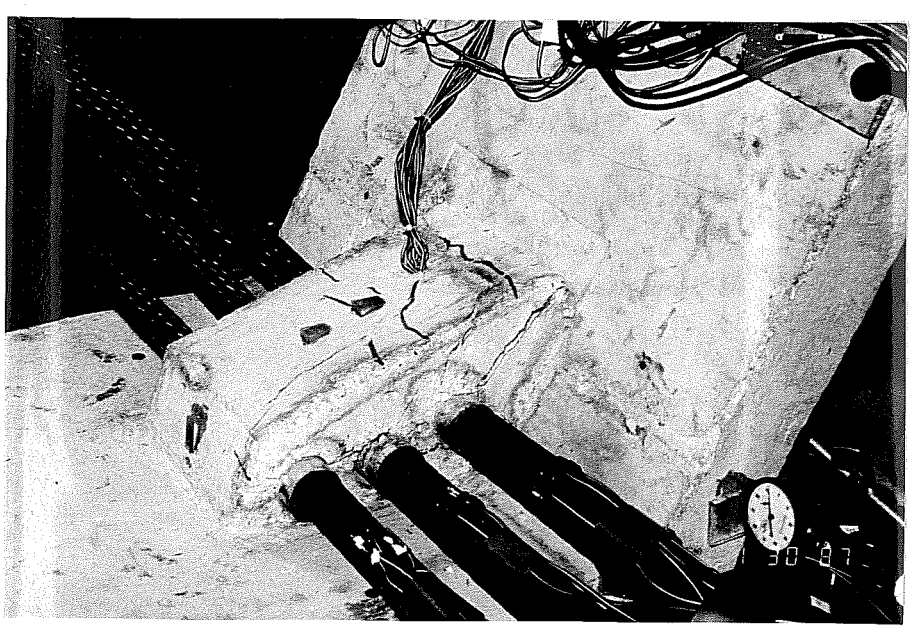

Figure 6.15 Block A: Advanced Cracking

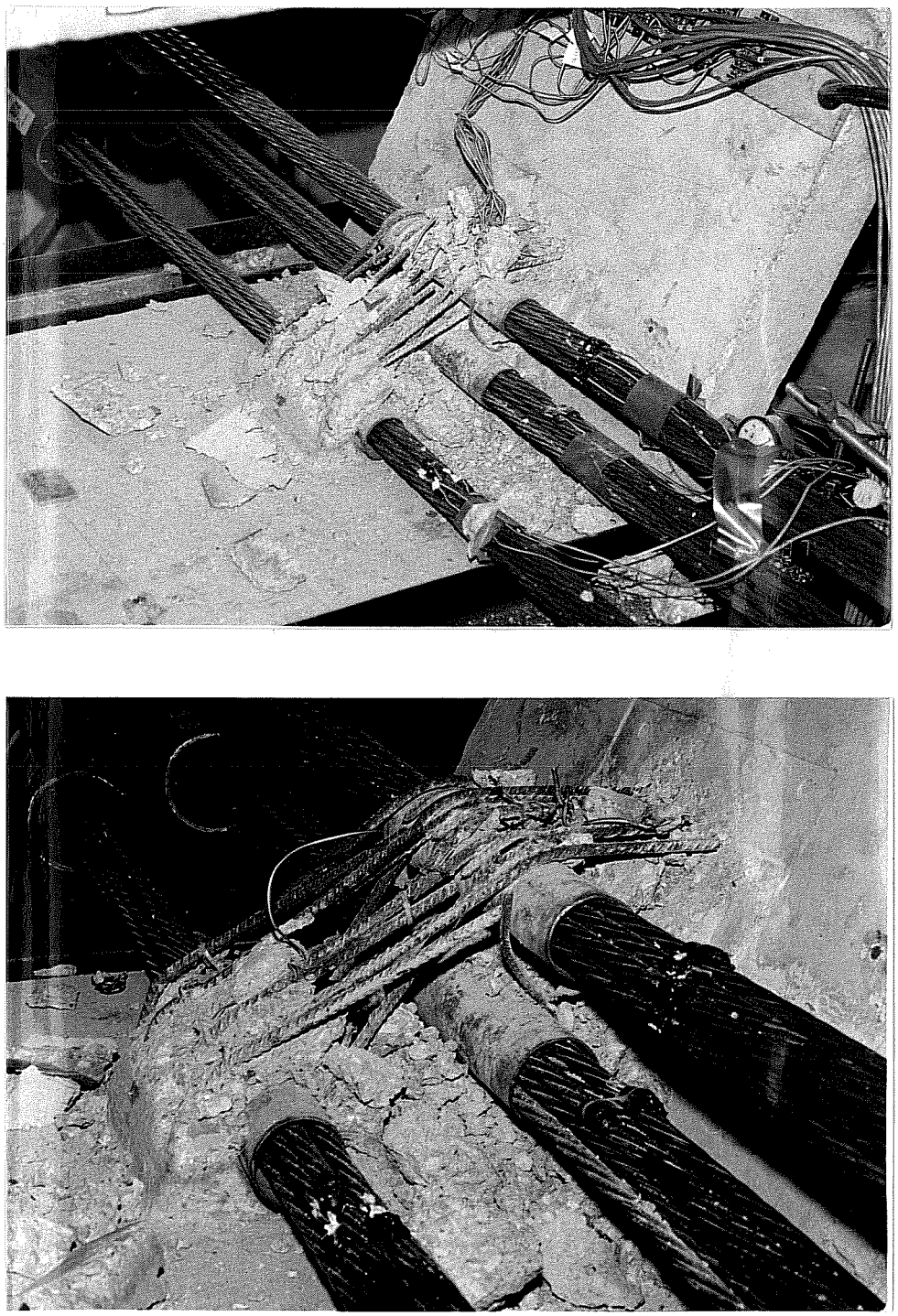

Figure 6.16 Block A: Immediately After Failure

After broken pieces of concrete had been cleared away, the photos in Fig. 6.17 were taken.

6.2.3 Comparison of Tests 1A and 1B. The primary difference between Block A and Block B was the direction of the total force vector on the deviator (refer to Fig. 6.2). In Test 1B this vector was directed approximately perpendicular to the top face of the deviation block. In comparison, the resultant force vector was more nearly parallel to the top face of Block A. In effect, Block B experienced a direct pullout, while Block A was subjected to more of a shear force. The total angle of deviation was smaller for Block A than Block B, but the depth of the concrete over the main vertically deviated tendon (Tendon 2 for Test 1B, Tendon 3 for Test 1A) was decreased for Block A. Although Block A had an additional tendon and duct, the reinforcement in both blocks was identical.

The differences in tendon geometry between blocks A and B may account for the dramatic difference in ultimate behavior between the two deviators. While Block B exhibited only minimal damage before failing catastrophically, Block A developed very large cracks and noticable displacements relative to the specimen box before breaking. Figure 6.18 shows both deviators as they appeared after failure with concrete rubble cleared away and tendons removed.

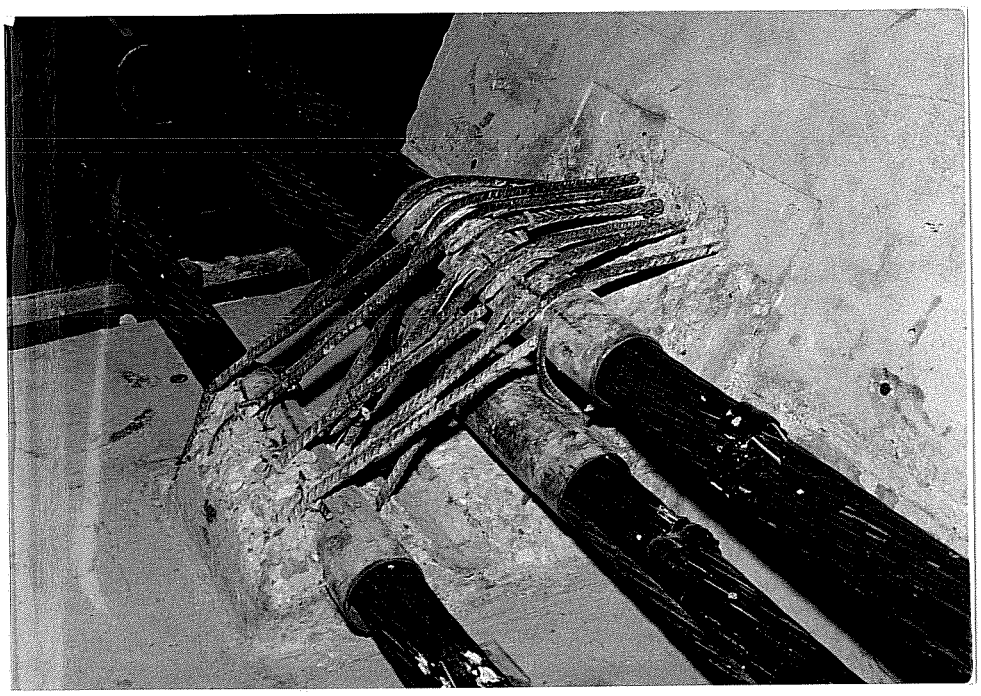

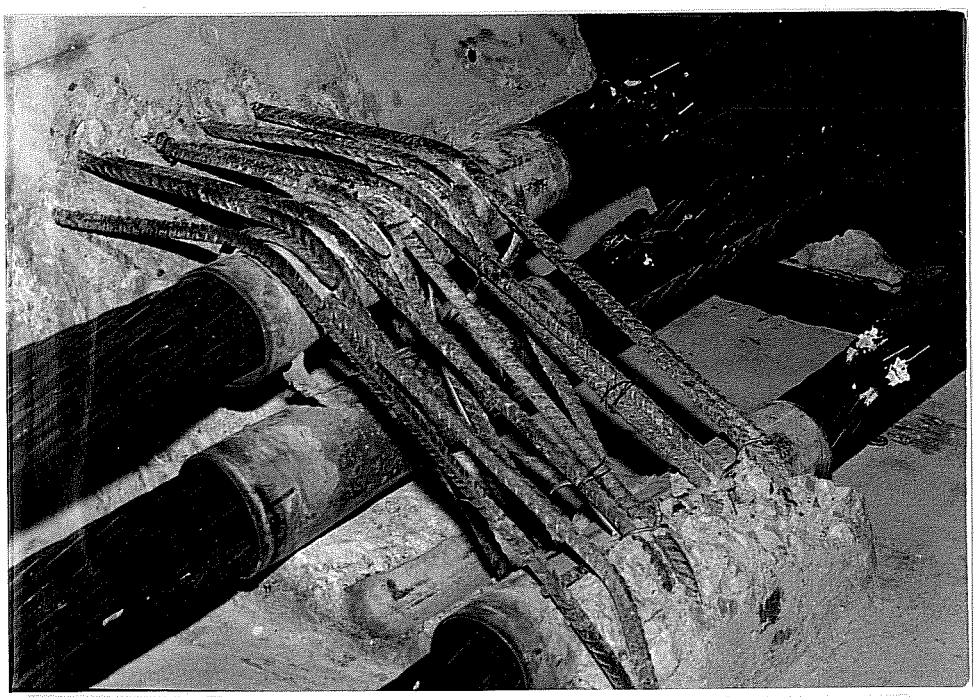

Figure 6.17 Block A Failure: Details

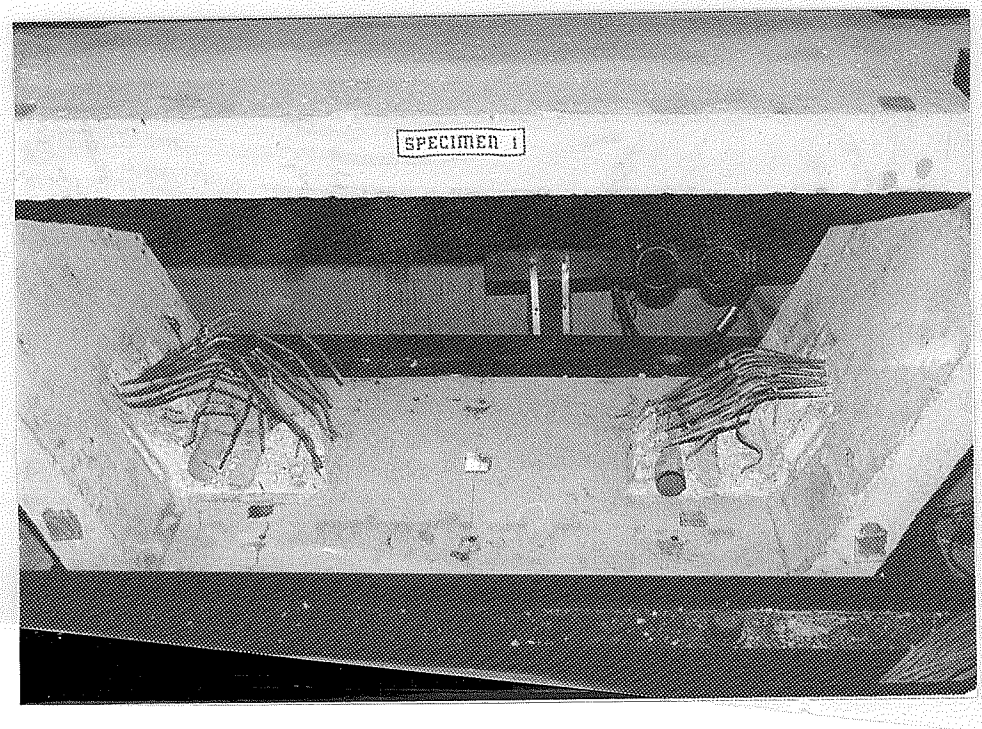

Figure 6.18 Failed Deviation Blocks A and B

The superior ductility of Block A, as compared to Block B, is further distinguished when the bar graphs from Figures 6.5 and 6.8 are compared (see Fig. 6.19). Even though each deviator failed at approximately 2.5 times its design load, D_o, the reserve capacity above first yield of the reinforcement was much greater in Test 1A. The strain and displacement data presented in the following section further attest to the differences in behavior.

6.3 Strain and Displacement Data

In this section, deviator reinforcement strain data and deviator and specimen box displacement data are presented.

6.3.1 Strain Data. Strain values for the various embedded gages on the principal deviator reinforcement are plotted with respect to the vector sum of forces on the deviator, D. Data are grouped on each plot to show results from multiple gages on individual bars or from gages in the same location on identical bars. Also indicated on each plot are the reference quantity D_o and the average yield strain of the reinforcement e_y.

6.3.1.1 Test 1B. Figures 6.20 through 6.26 are plots of deviator reinforcing steel strain versus the magnitude, D, of the vector sum of force components on the deviator. On each plot, the inset sketch shows the location of strain gages on the particular reinforcing bar and the location of the bar over the

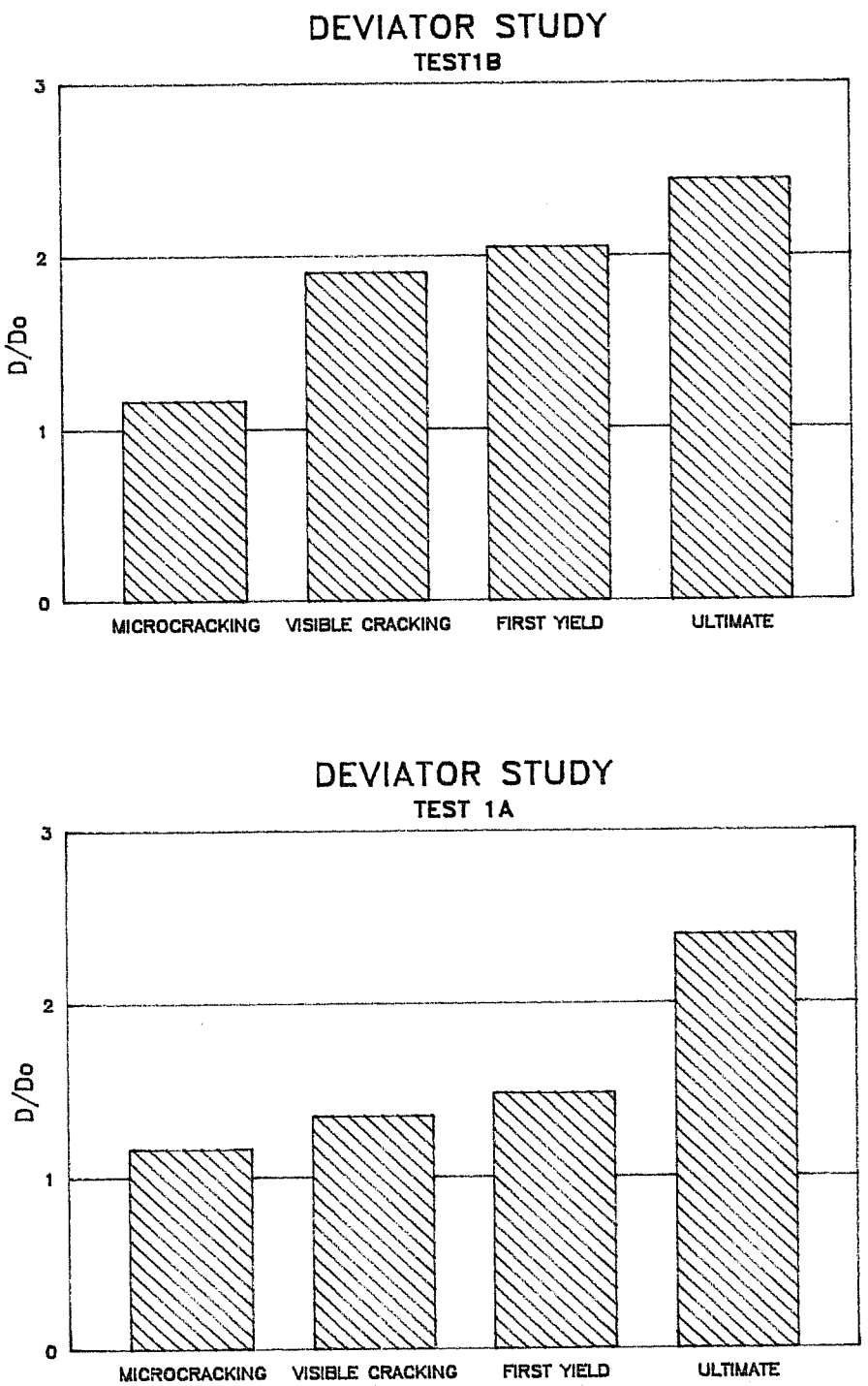

Figure 6.19 Tests 1B and 1A Force Comparisons

width of the deviator. In some cases, gages shown on the sketch are not represented in the plots because of a lost gage or a data acquisition channel malfunction. After the completion of Phase I, the deviator was completely unloaded in a single step. This unloading is indicated on the plots by a truncated line with an arrow at the end. Since Test 1B included two load cycles in Phase I and an additional load cycle in Phase II, the plots representing information from the entire test are sometimes difficult to follow. For clarity, some of these plots (for example, Fig. 6.20a of 6.20a-c) are broken down to reflect separate information from Phase I (6.20b) and Phase II (6.20c). Data from gages on the link bars will be discussed first, followed by discussions of the strain data from the outer loops, then the inner loops. A final plot shows comparative data from three different types of reinforcing bars which were located in approximately the same vertical plane of the deviator. Significant observations from Test 1B strain data plots are noted in the following paragraphs.

Figures 6.20a-c show the strain-load behavior for the fully instrumented link which was located near the center of the deviator on the A side. It can be seen from these plots that the legs of the links, monitored by Gages 1B-5 and 1B-6, developed more force than the top of the link, represented by Gage 1B-7.

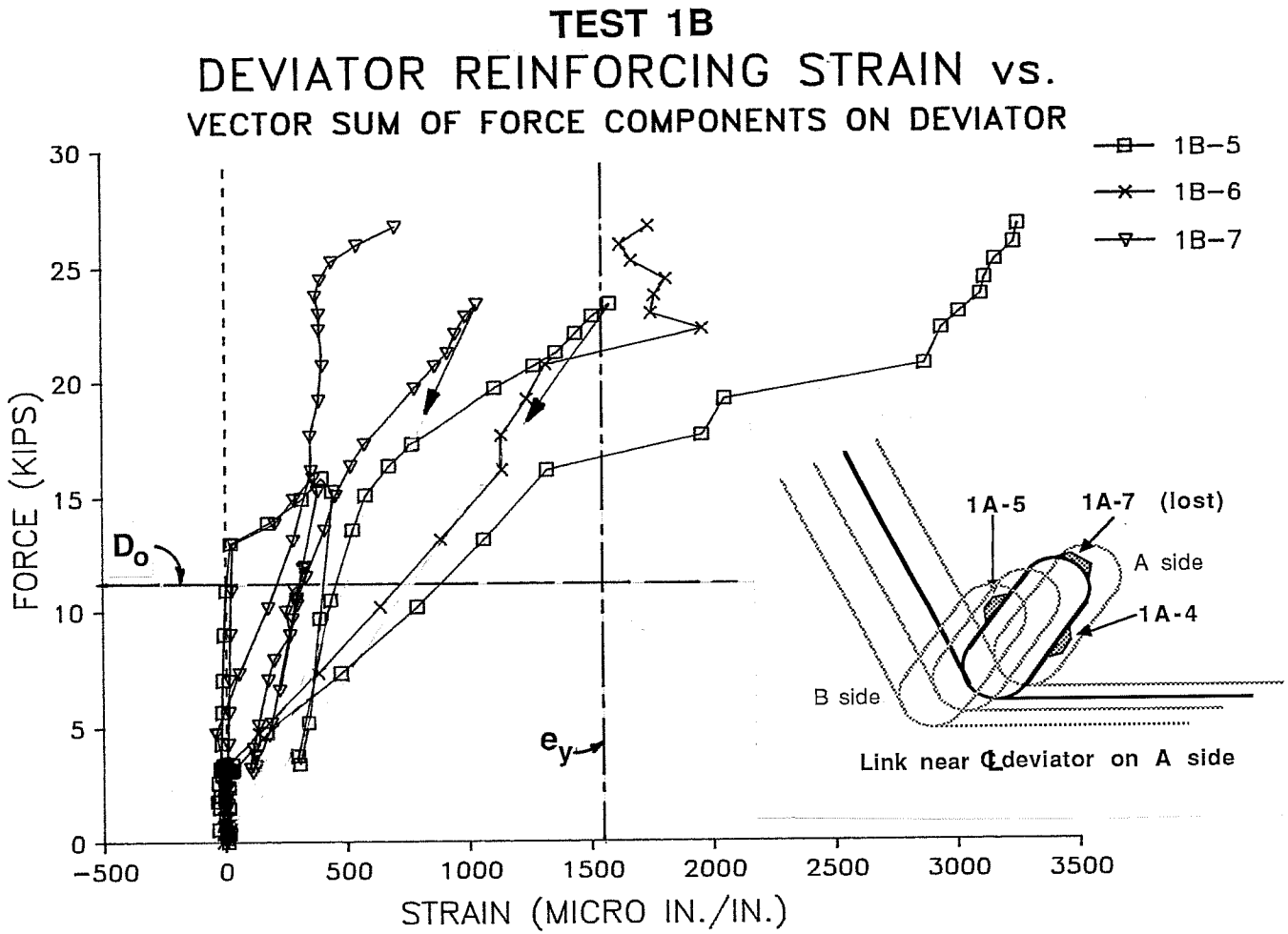

Figure 6.20a Test 1B Deviator Reinforcement Strain Gage Data

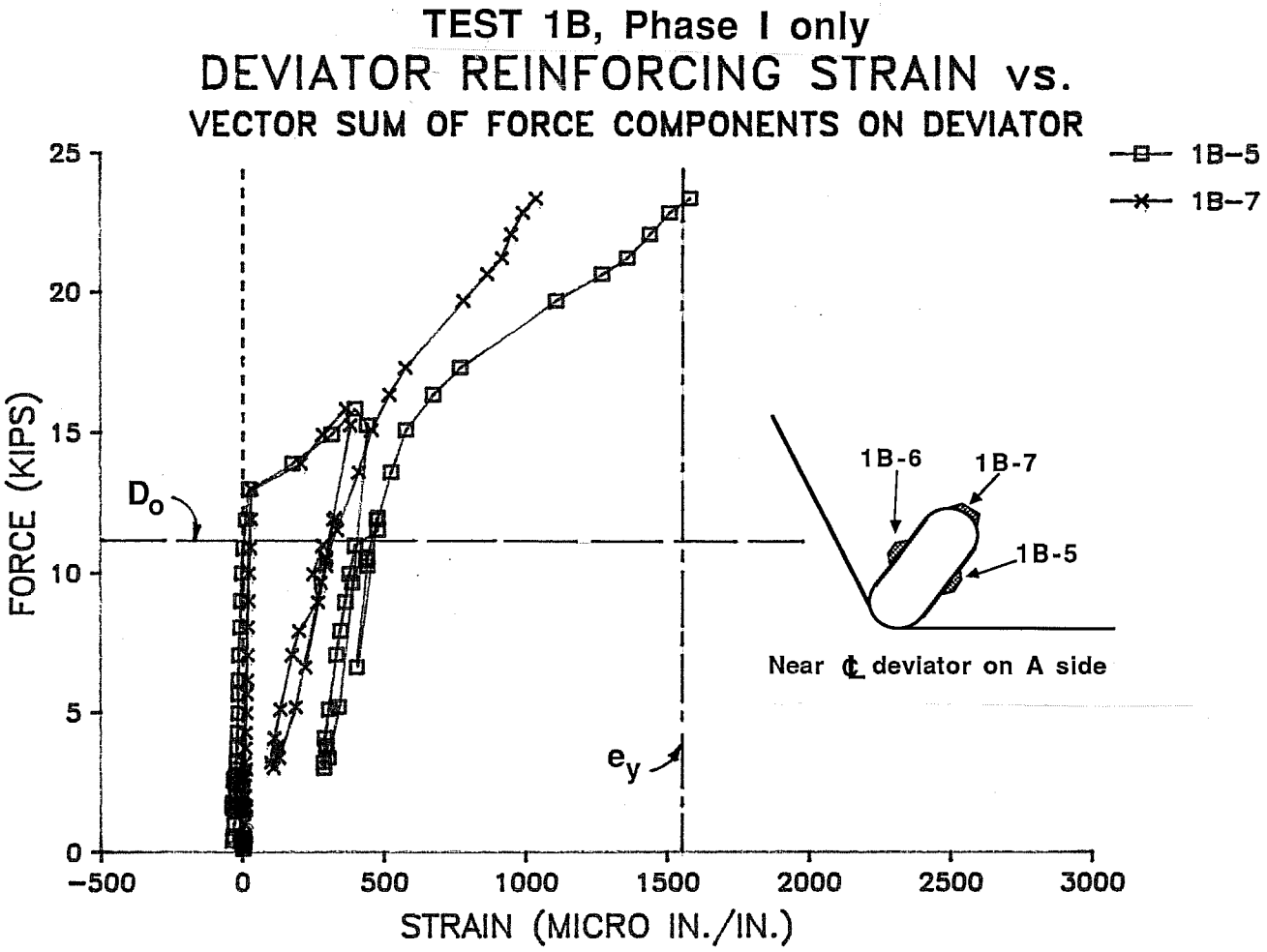

Figure 6.20b Test 1B Deviator Reinforcement Strain Gage Data

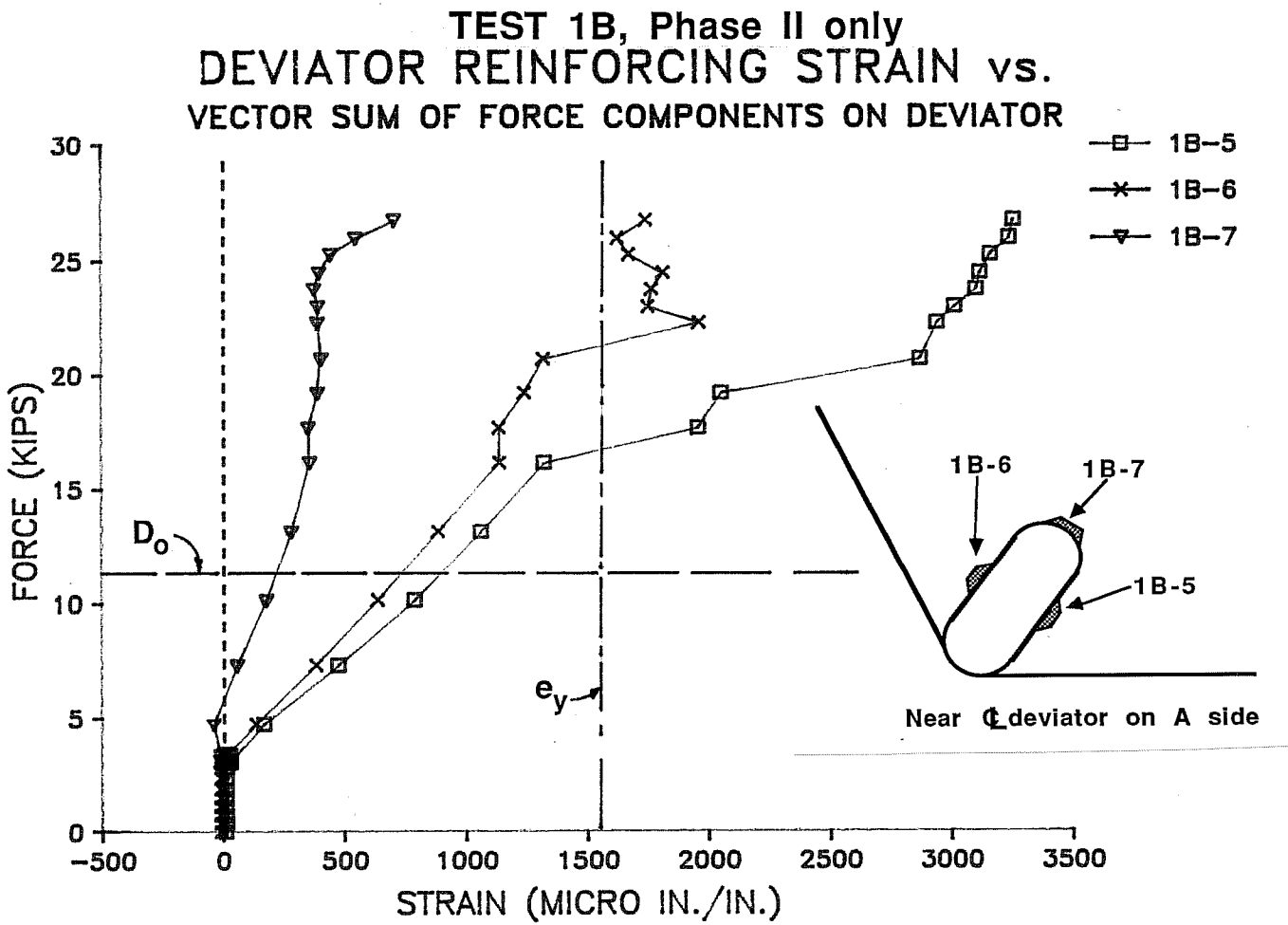

Figure 6.20c Test 1B Deviator Reinforcement Strain Gage Data

This would be expected since, if the bond was good at all points around the link, the part of the link which passed over the duct acted as a hook which developed the tensile force in the legs of the link. It is of interest to note that Gage 1B-7 saw even less strain in Phase II than in Phase I. This is probably due to a different distribution of strain in the pre-cracked section loaded in Phase II. Comparing Gage 1B-7 to Gages 1B-2 and 1B-12 which were located at the top of the two outermost links, however, reveals an apparent inconsistency in behavior (see Fig. 6.21). The tops of the two outer links developed strains more than twice yield strain during loading to failure in Phase II (Fig. 6.22). In trying to explain this inconsistency, another interesting correlation was made. The break points in the outer link bars occurred at the interface of the block and the bottom flange of the box, while the two inner links broke on the opposite side and closer to the top of the link, near the web-block junction. This behavioral trend was seen in both this test and Test 1A. Each link which exhibited very high strain at the top of the link broke at the interface of the block and the bottom flange of the box; those links which showed lower strain at the top of the link broke on the other side, near the web-block junction. Referring back to Fig. 6.20c, it is also apparent that the fully instrumented inner link experienced lower strain near the point where the bar actually broke, that is

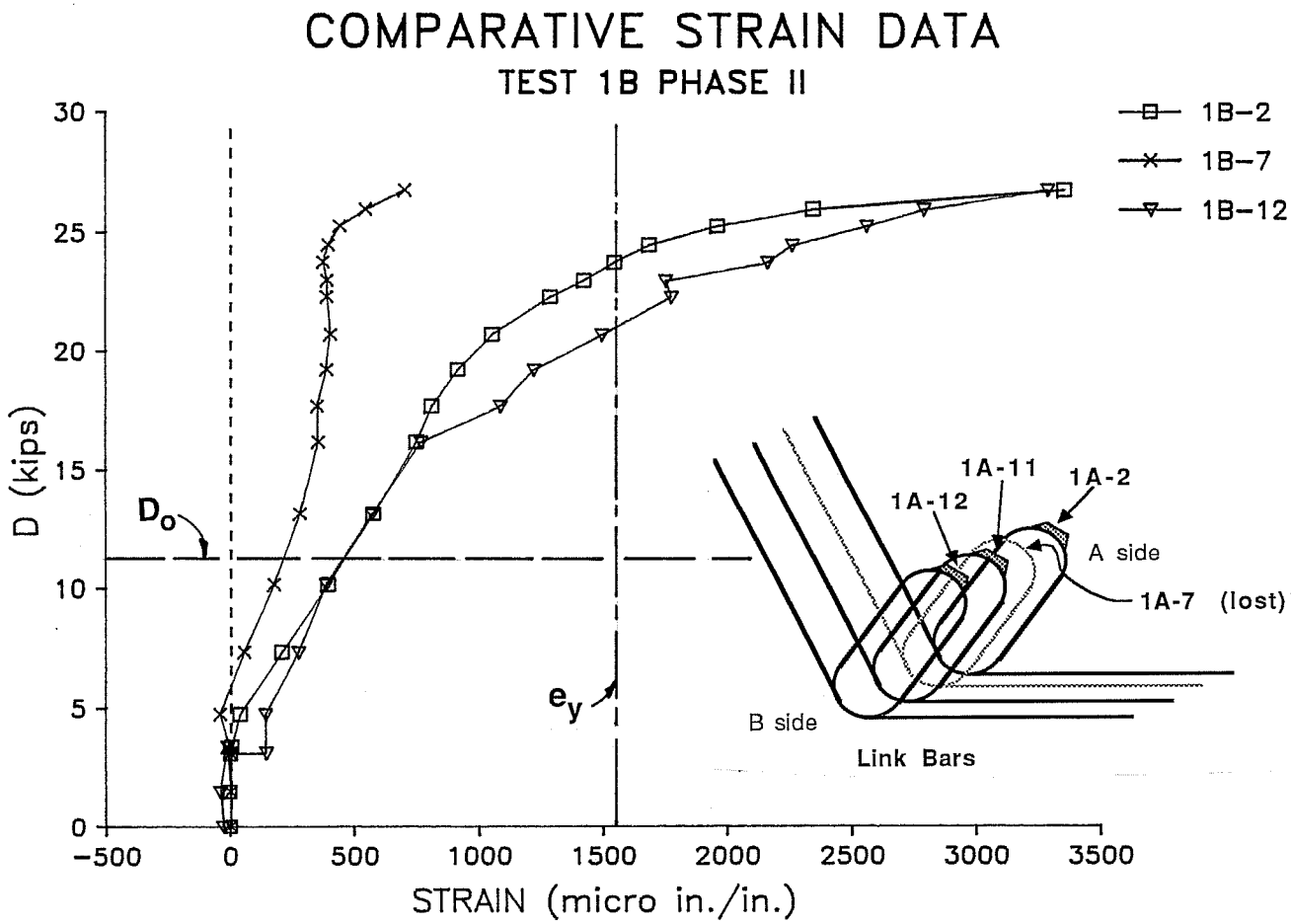

Figure 6.21 Test 1B Comparative Strain Data for Links

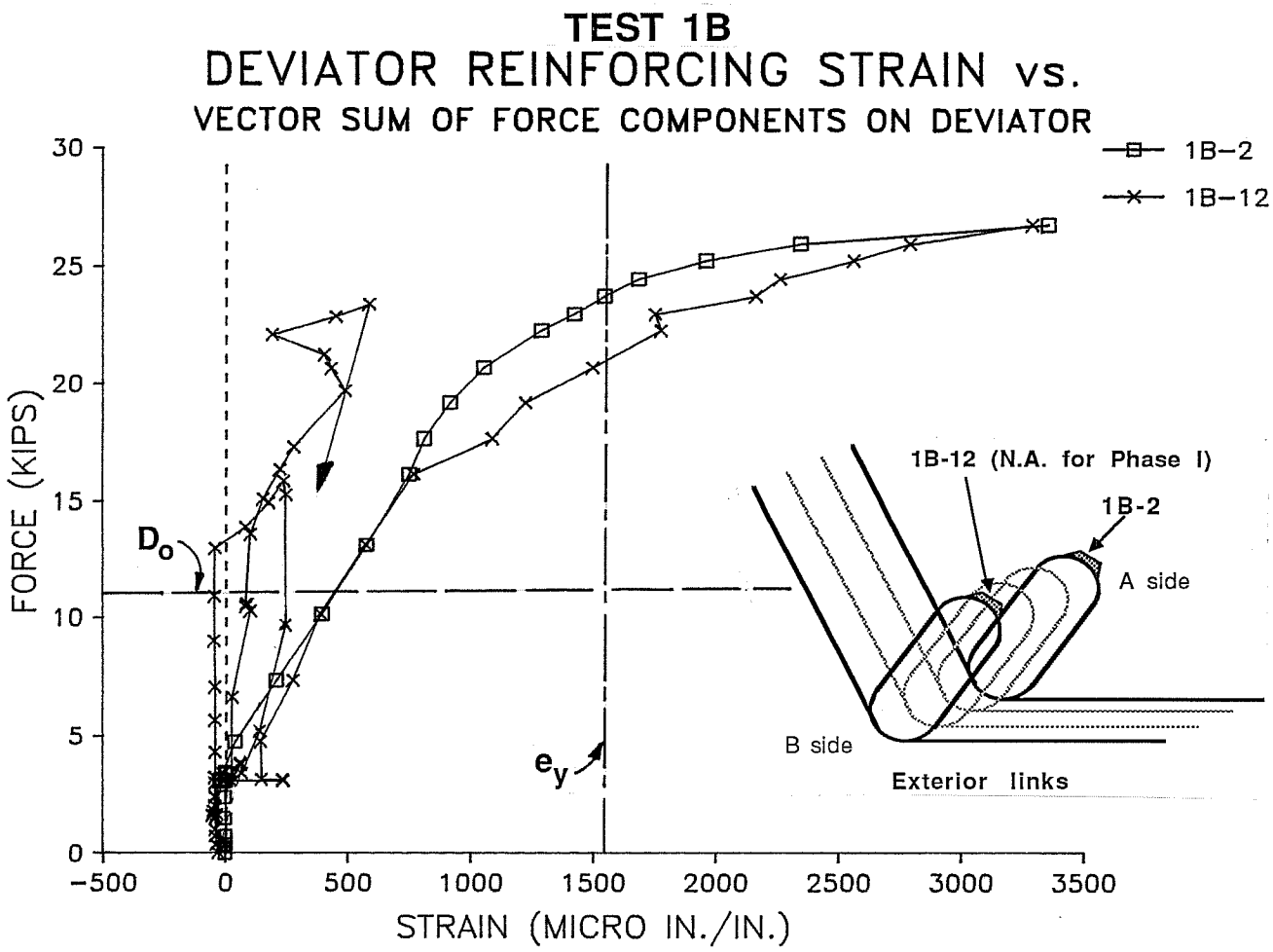

Figure 6.22 Test 1B Deviator Reinforcement Strain Gage Data

between gage points 1B-6 and 1B-7. It seems more reasonable that the break would have occurred in the vicinity of higher strains. The two outer links were not fully instrumented, so that the distribution of strain throughout the bar is not known. However, the trend of the link breaking in the leg which exhibited lower strain is also apparent in Test 1A data, which will be discussed in the following section. One possible explanation for this incongruous behavior is the fact that, at the moment of failure, force redistributions occur instantaneously, so that the location of breaking in the bars may not be significant with regard to any behavioral trends seen before failure.

Figures 6.23a-c and 6.24a-c present strain data from the two outer loops which were instrumented in Test 1B. Again, note that information from the complete test in the "a" figures is separated according to test phase in the "b" and "c" figures for clarity. Figure 6.23 presents data from a fully instrumented outer loop which was located in the interior region of the block, but closer to the "A" face. It is apparent from this figure that the front leg of the loop, instrumented by Gage 1B-4, picked up very little force, as expected, since this part of the bar was somewhat removed from the point of application of the load. The two gages on the upper and lower surfaces of the top part of the outer loop, 1B-3UP and 1B-3LO, maintained approximately equal

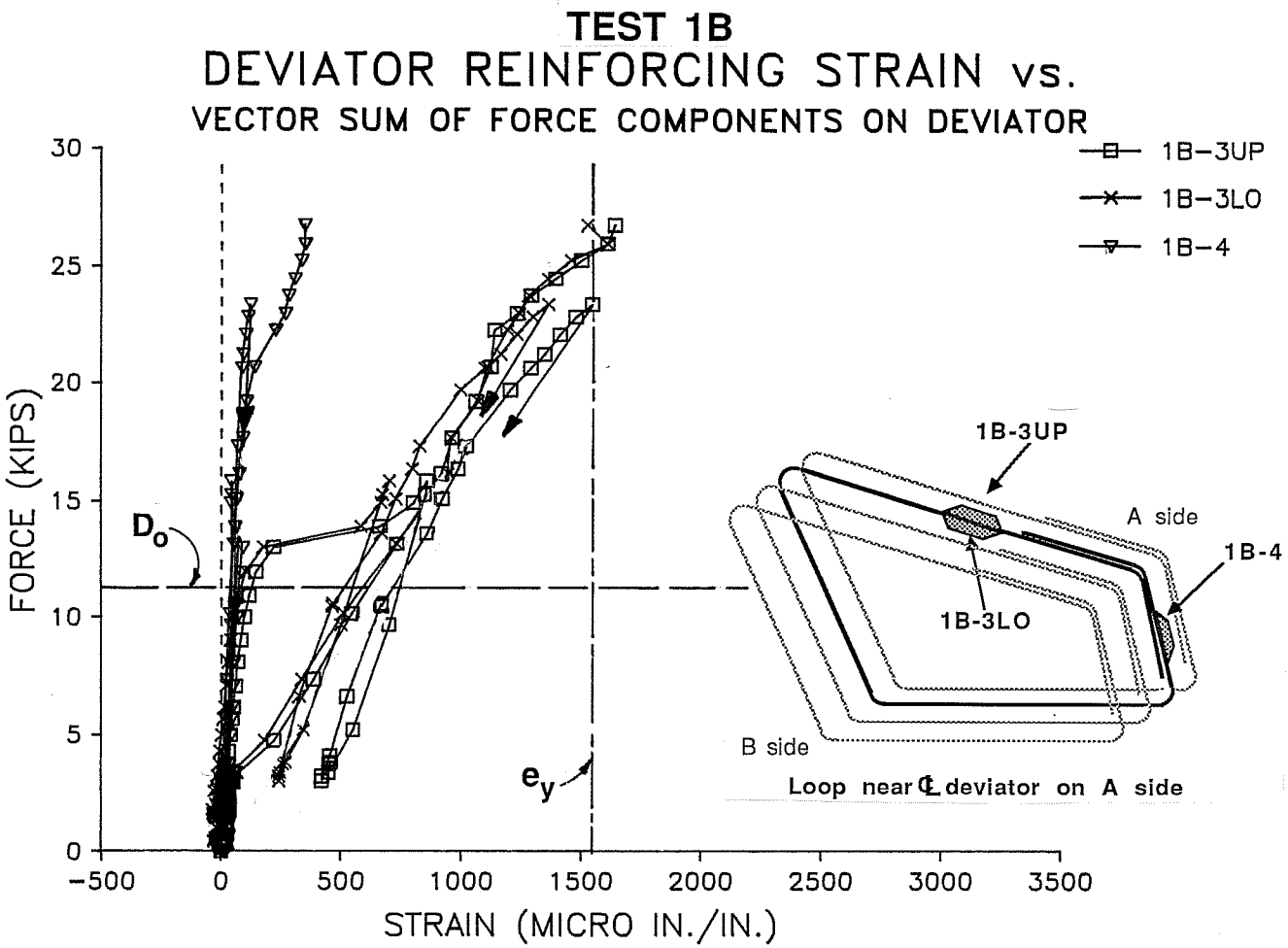

Figure 6.23a Test 1B Deviator Reinforcement Strain Gage Data

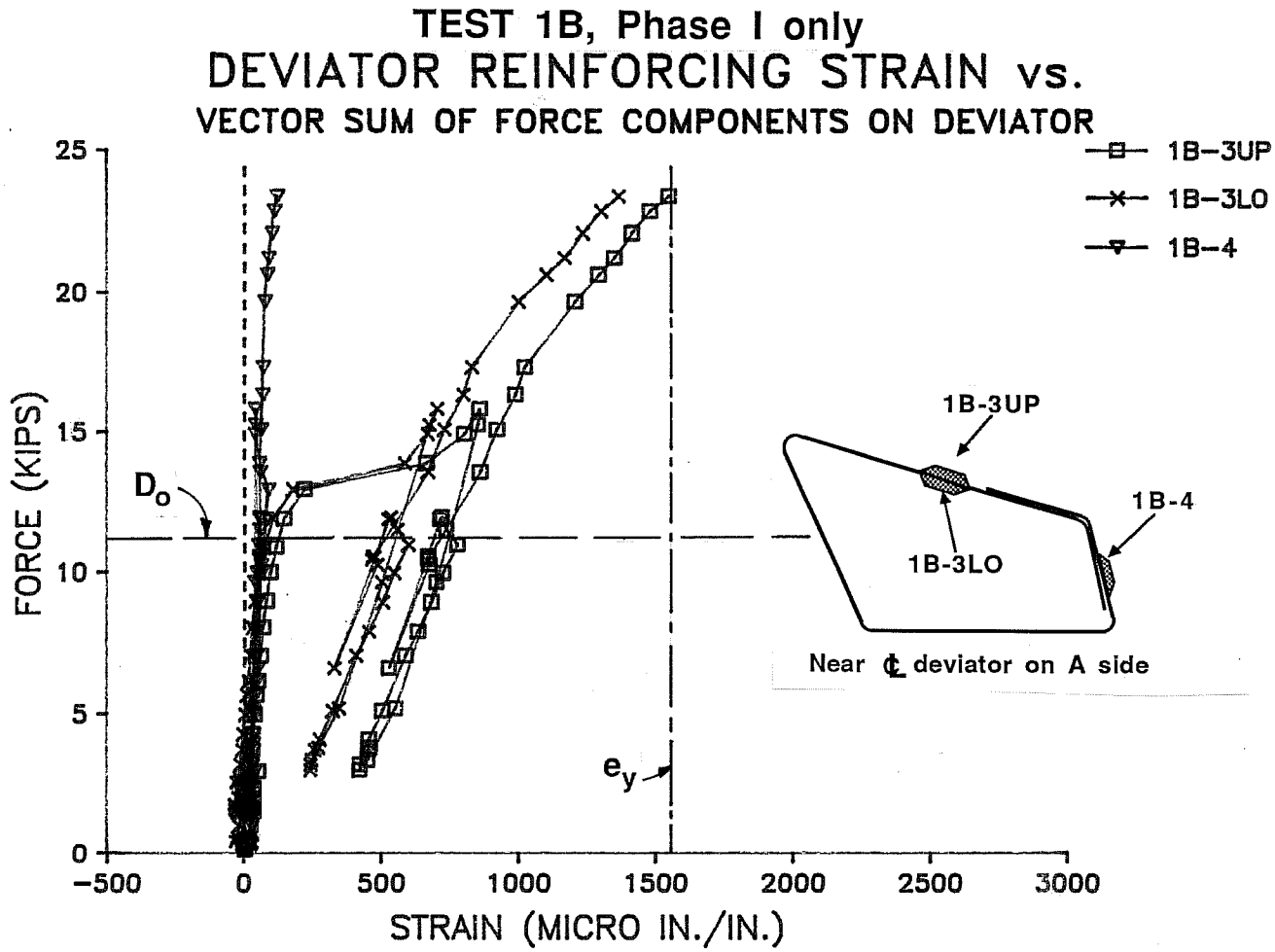

Figure 6.23b Test 1B Deviator Reinforcement Strain Gage Data

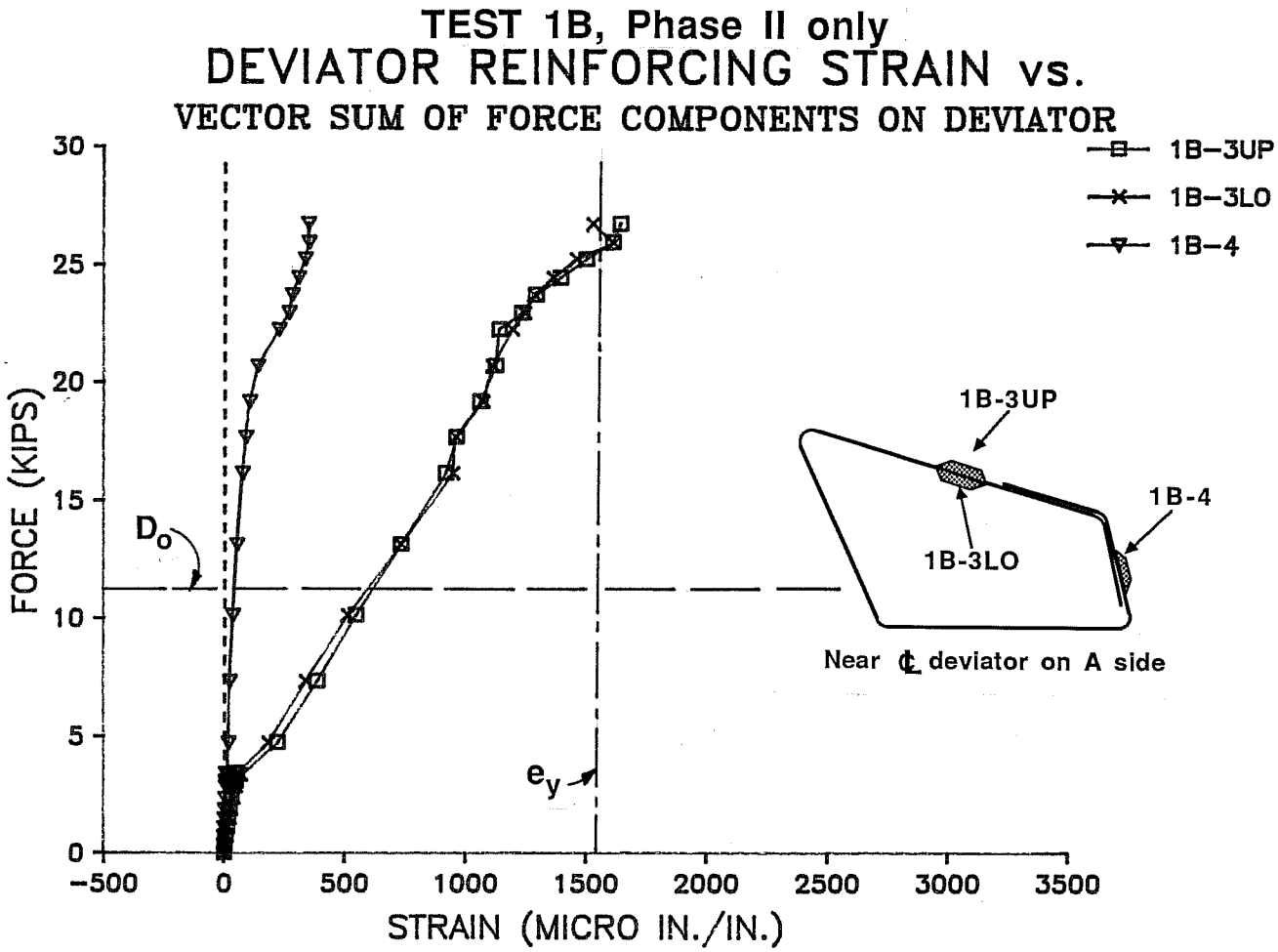

Figure 6.23c Test 1B Deviator Reinforcement Strain Gage Data

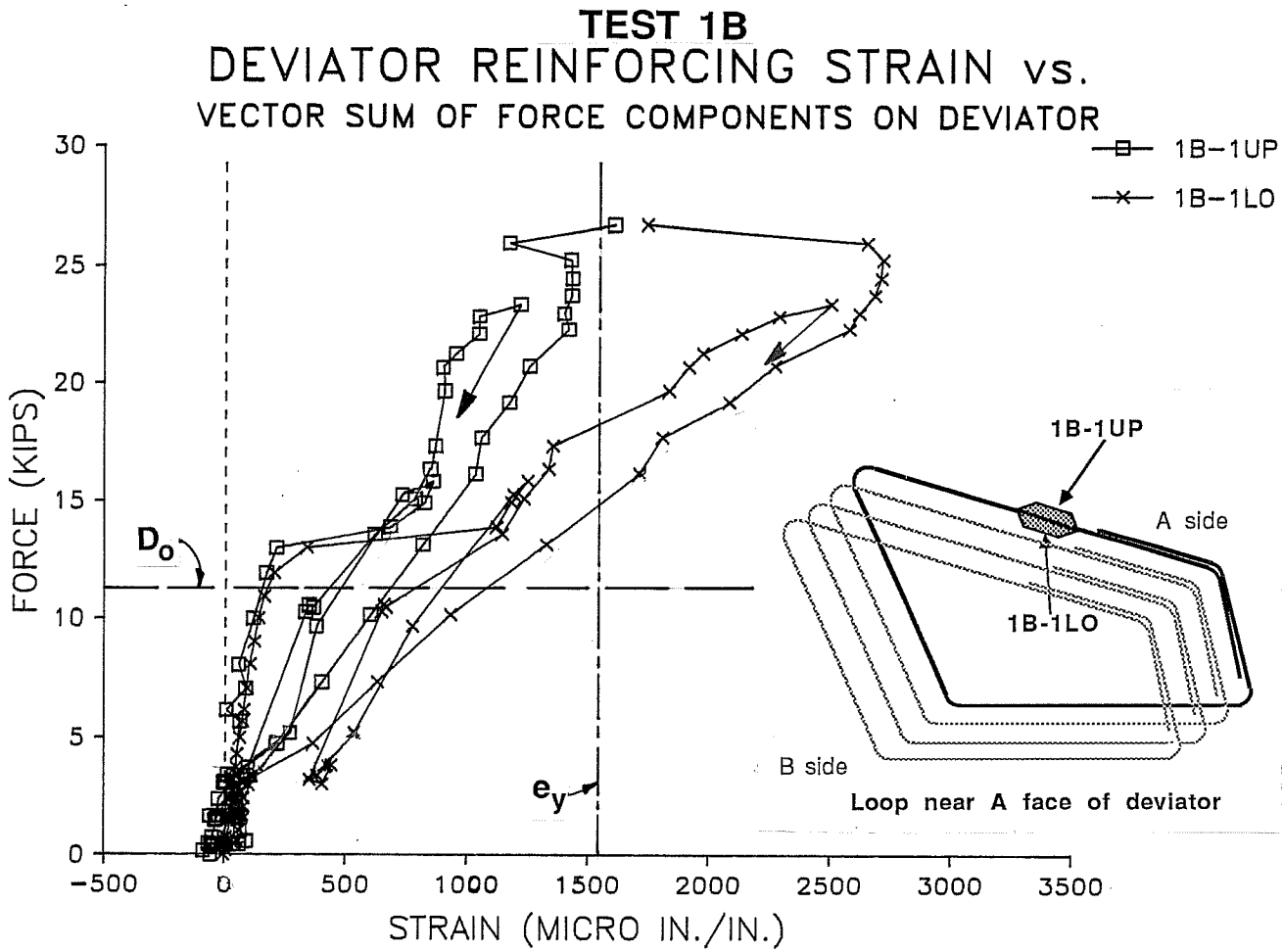

Figure 6.24a Test 1B Deviator Reinforcement Strain Gage Data

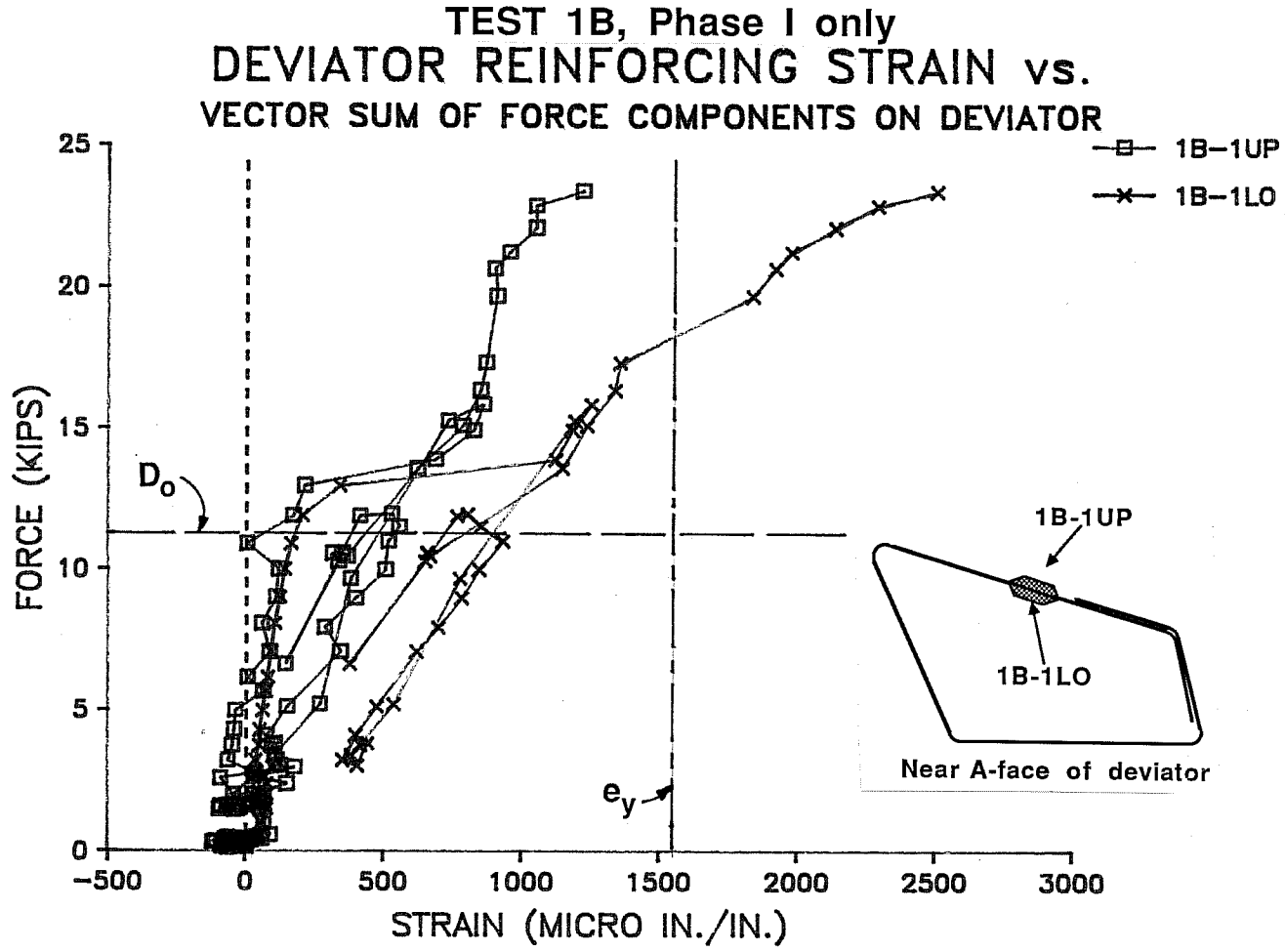

Figure 6.24b Test 1B Deviator Reinforcement Strain Gage Data

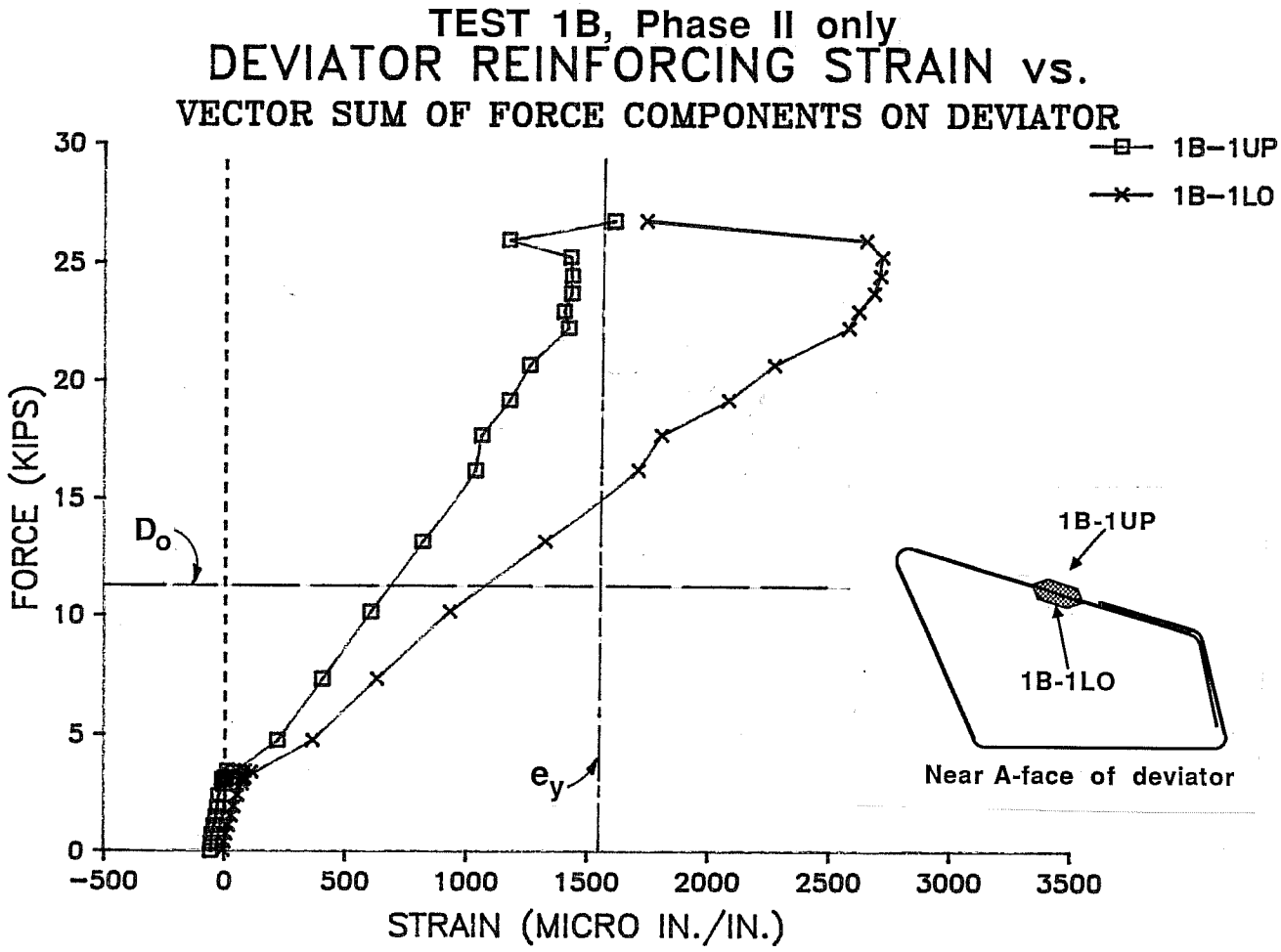

Figure 6.24c Test 1B Deviator Reinforcement Strain Gage Data

strain levels throughout the test. If the bar were being used in a primarily flexural capacity, a slightly lower strain level would be expected in the lower gage as is apparent in Phase I, since the bottom fiber of the bar was closer to the neutral axis of the strain gradient. However, this small differential over the 0.25 inch bar diameter could be easily affected by very localized behavior of the concrete in the vicinity of the gage. Corresponding gages, 1B-1UP and 1B-1LO, on the adjacent outer loop, located near the "A" face of the deviator (see Fig. 6.24a-c), did not exhibit the same expected behavior. The gage on the bottom surface of the bar indicated a significantly higher level of strain than did the top gage. Howver, this could be contributed to localized bending, since an average of these two strain curves, when compared with curves from Gages 1B-3UP and 1B-3LO, matches fairly well.

Strain data for the remaining instrumented bar, an inner loop which was located along the centerline of the deviator, is shown in Figures 6.25a-c. Note that the lower gage of the pair 1B-9UP and 1B-9LO, at the top arm of the inner loop, saw less strain than the top gage, possibly due to bending action. The front leg of the inner loop, represented by Gage 1B-10, probably picked up its force in resisting pullout of the vertically deviated tendon. If the top of the deviator behaved as a beam element, then this part of the inner loop probably provided part

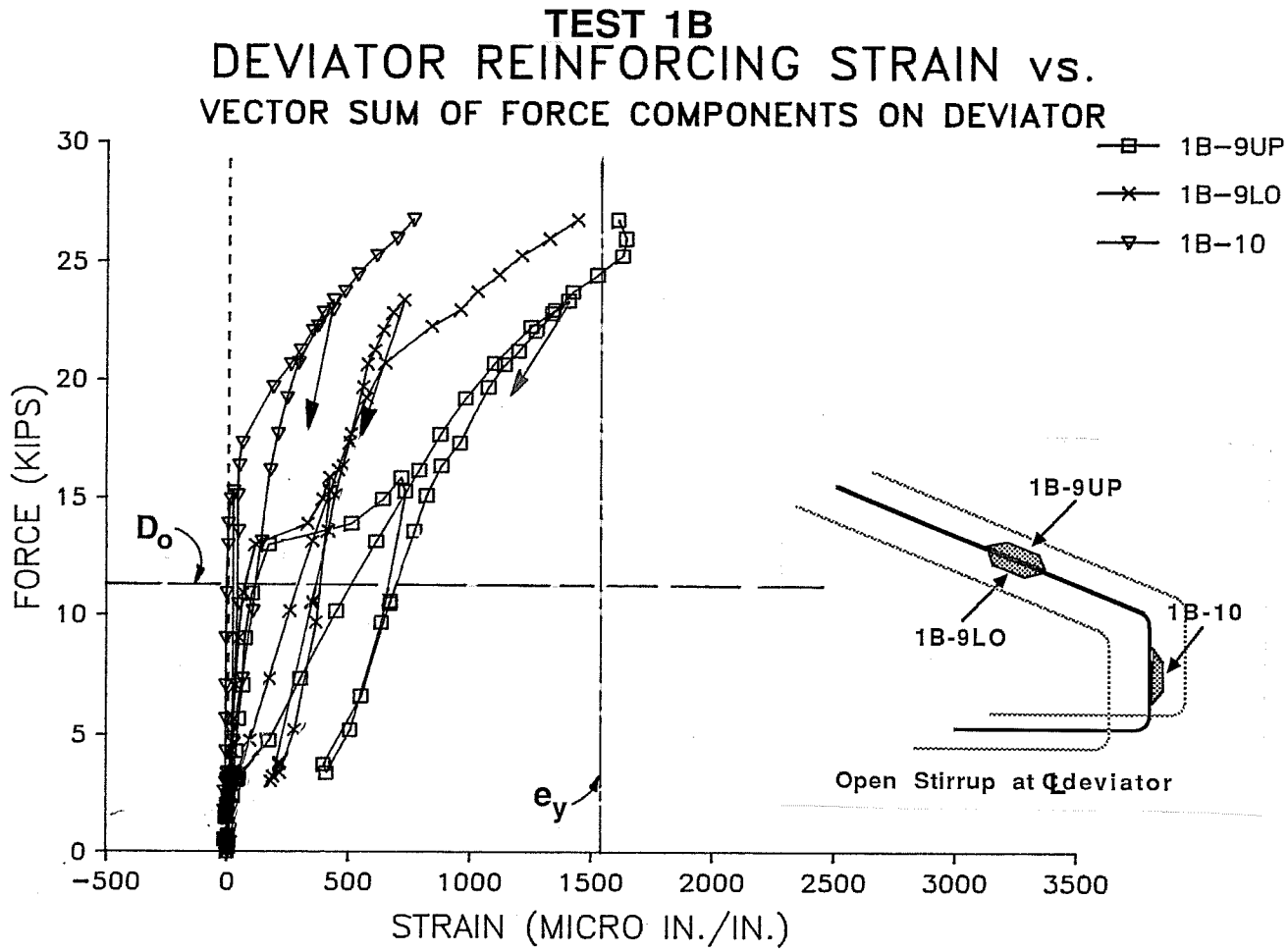

Figure 6.25a Test 1B Deviator Reinforcement Strain Gage Data

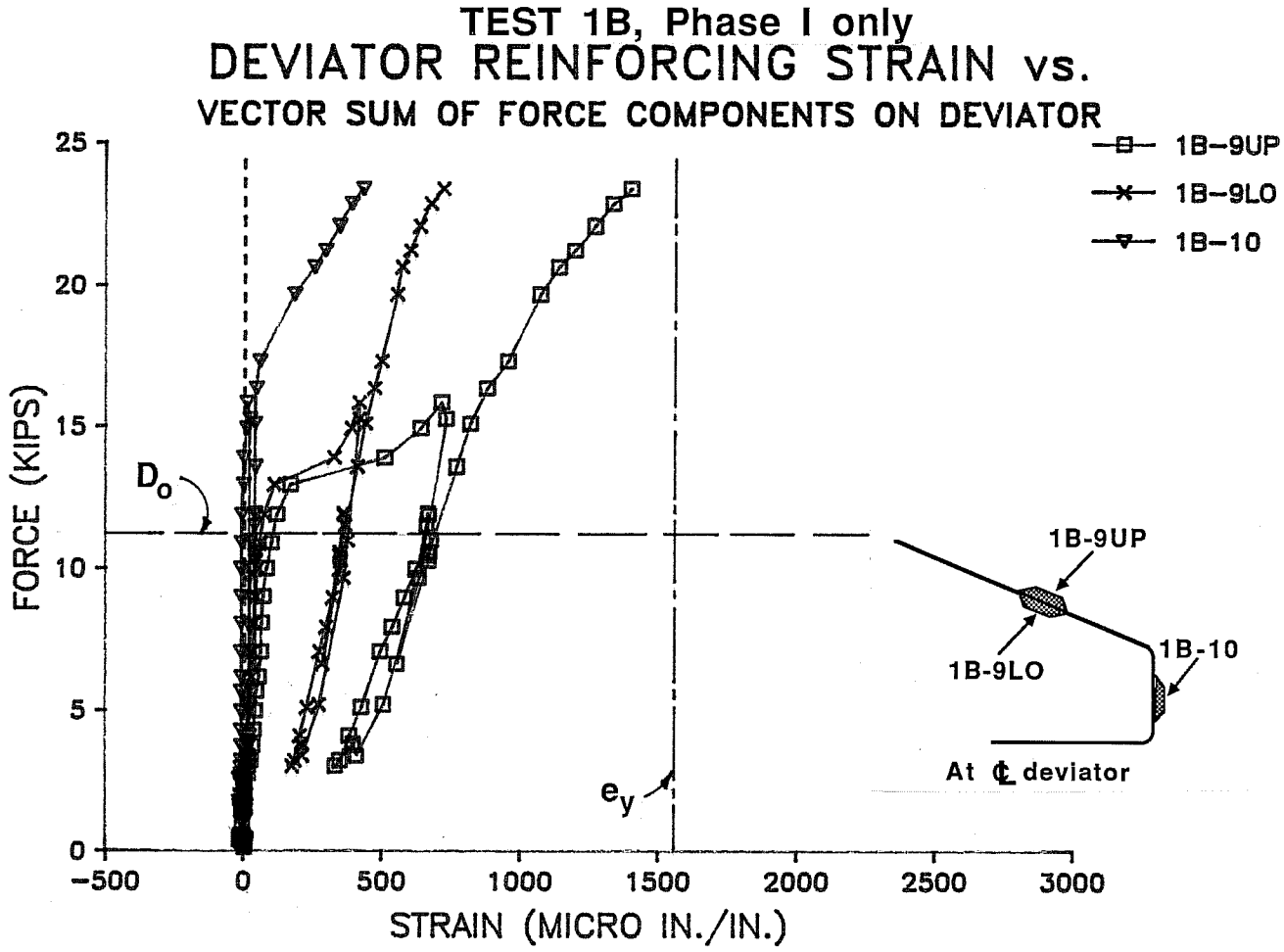

Figure 6.25b Test 1B Deviator Reinforcement Strain Gage Data

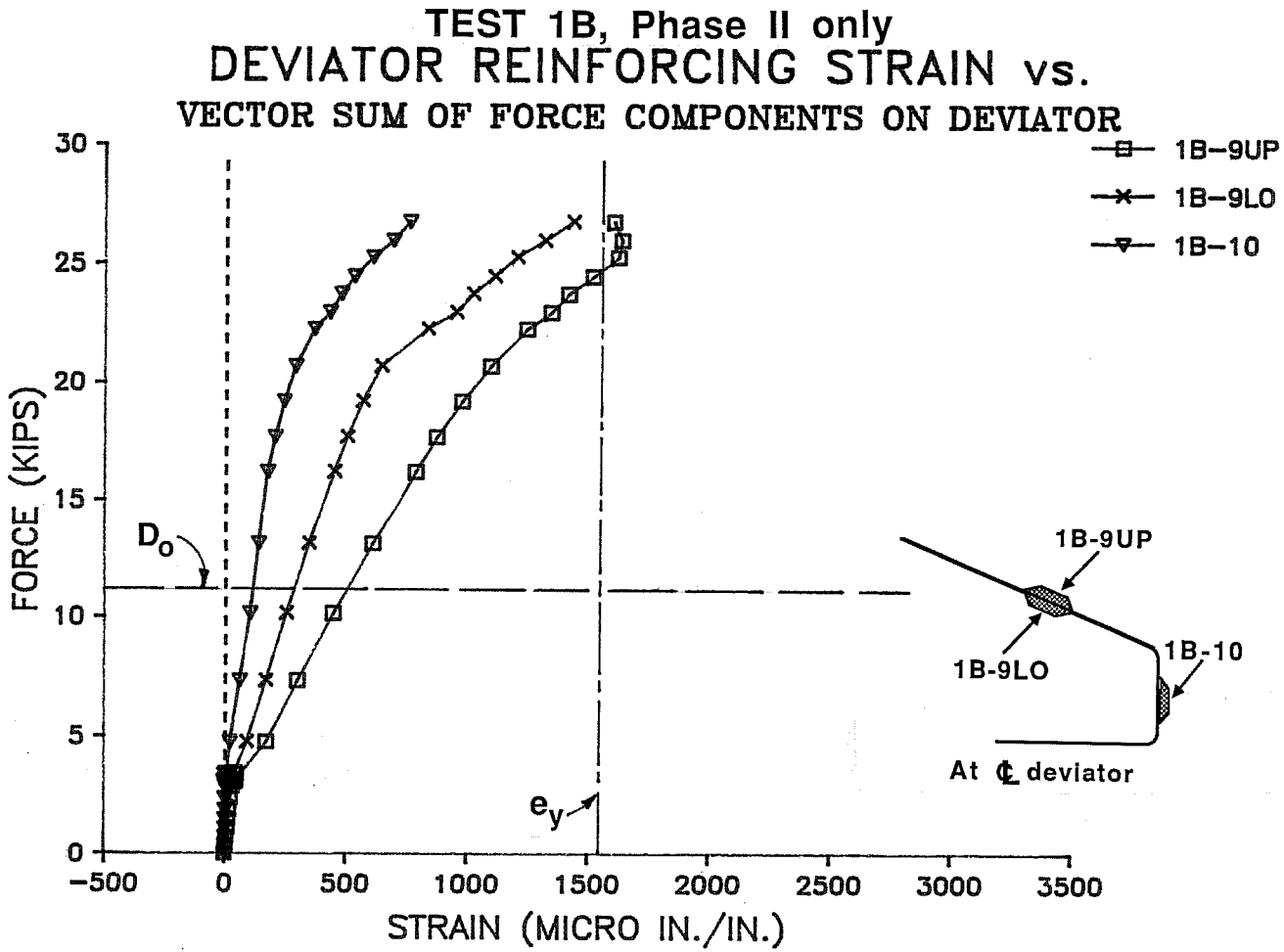

Figure 6.25c Test 1B Deviator Reinforcement Strain Gage Data

of the downward reaction necessary to restrain the end of the beam.

A final plot (Fig. 6.26) compares the load-strain behavior during Test 1B Phase II for three bars; one link, one outer loop and one inner loop. These three bars were all located in approximately the same vertical plane as shown in the accompanying figure (Fig. 6.27). The plot shows that the legs of the link bar, instrumented by Gages 1B-5 and 1B-6, underwent larger strains than did any other bar. Even the top of the bar, which saw relatively little strain over the course of the test, appears to have begun to pick up more strain just before ultimate, as evidenced by the sudden decrease in the slope of the curve three load stages before failure. The link bar, therefore, was used most efficiently to resist forces in the deviator block. This conclusion had been made intuitively before testing and was reaffirmed by the strain data. The next highest strains were experienced by the top arm of the outer loop, which ran along the top face of the deviator, followed closely by the top arm of the inner loop. The gage point for the inner loop was situated just below the gages on the closed outer loop. The behavior of these portions of the two bars indicates possible beam behavior, where steel closer to the neutral axis of the beam has lower strain. The gage on the front leg of the inner loop showed the next

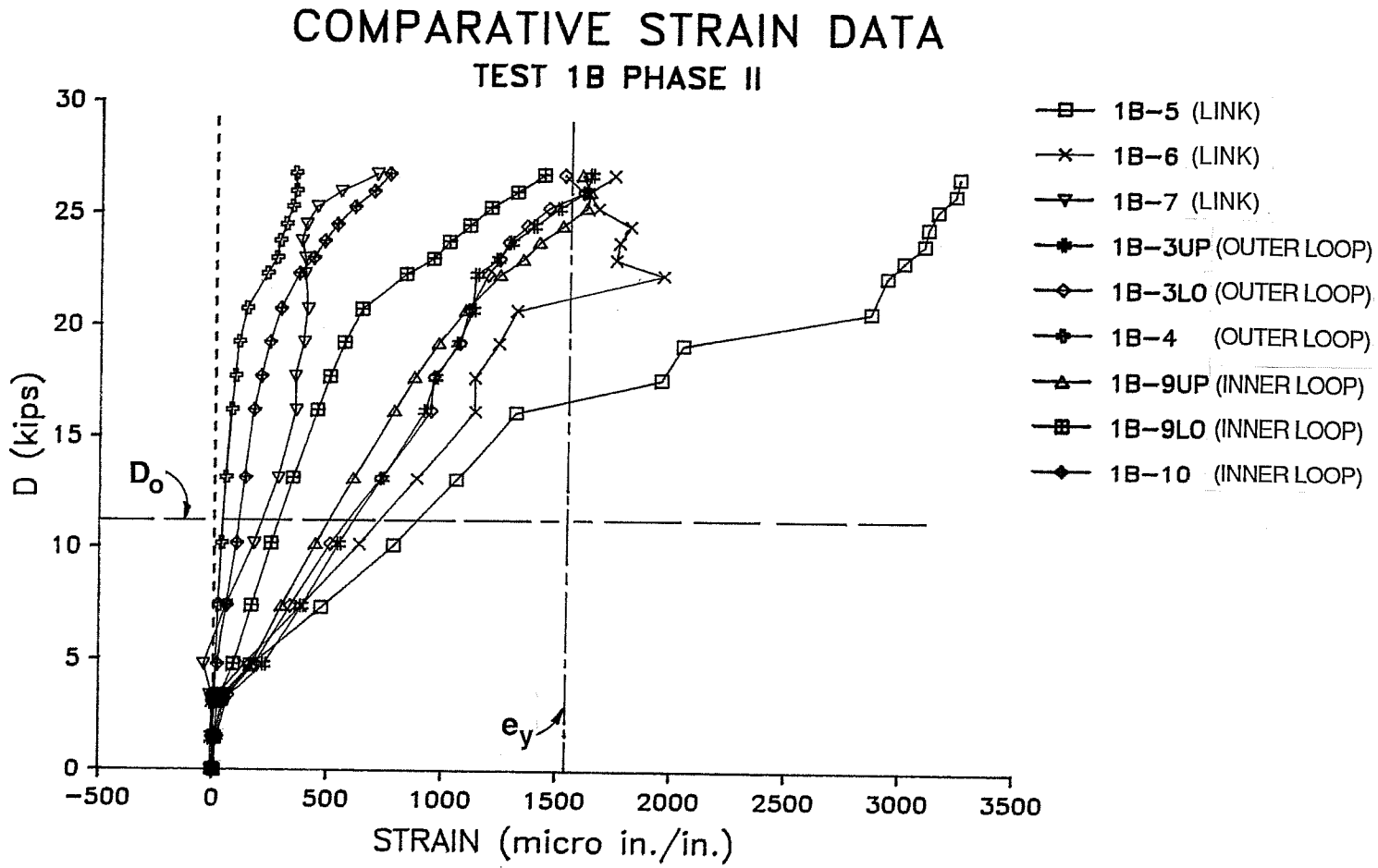

Figure 6.26 Test 1B Comparative Strain Data

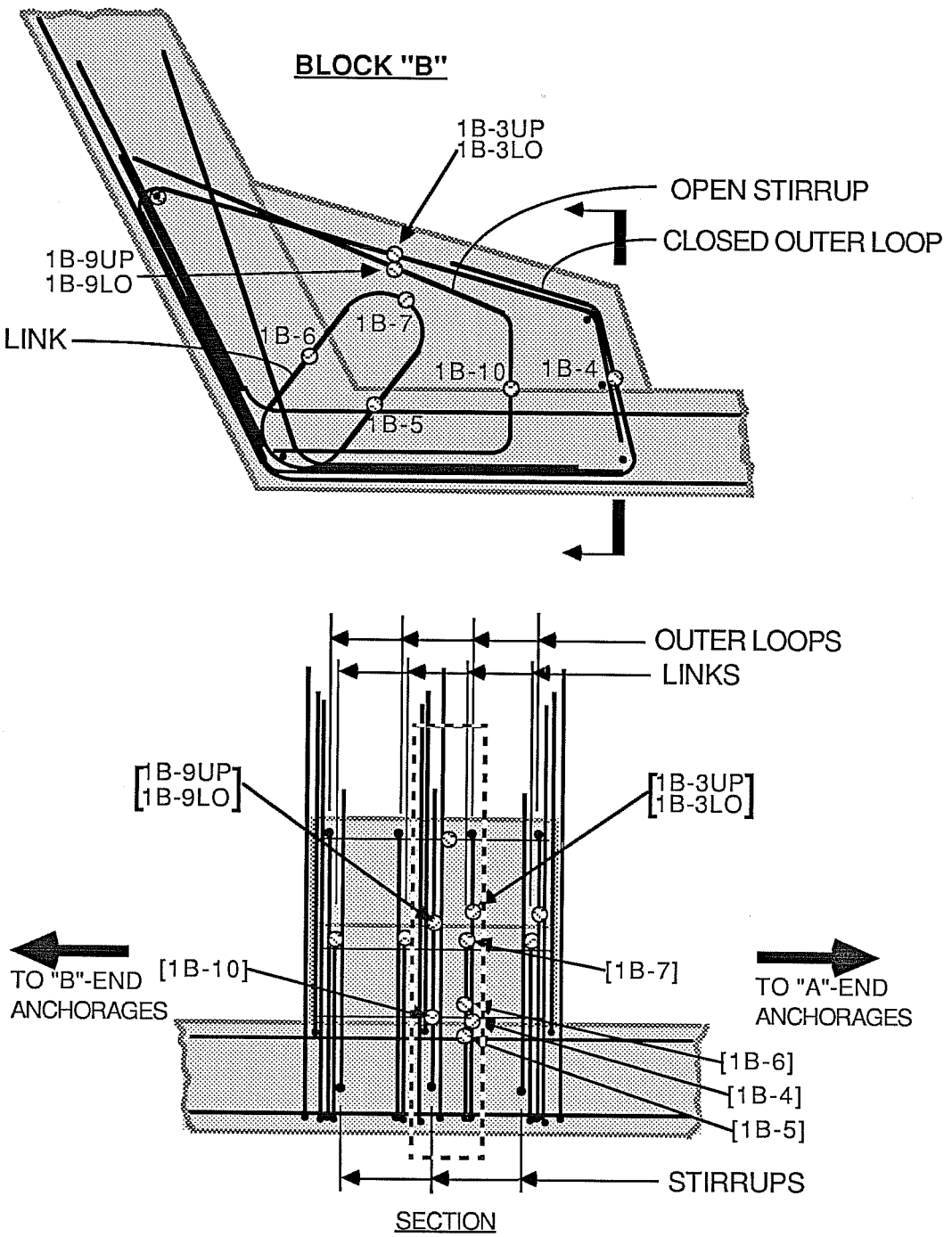

Figure 6.27 Block B: Gages in a Vertical Plane

highest strain, although it reached only about half yield strain just before ultimate. Finally, the gage showing the lowest level of strain was 1B-4 on the front leg of the closed outer loop. This could have been due to insufficient transfer of force through the lap, or to the fact that it is located far away from the point of application of vertical loads.

6.3.1.2 Test 1A. Figures 6.28 through 6.34 are plots of strain versus D for Test 1A. Again, each plot contains data from the entire test and indicates the reference quantities D_o and e_y. The discussion follows the same organization used in the previous section. In addition, comparisons between gages in similar locations in both test are made.

Figure 6.28 shows strain data for the fully instrumented link located in the interior region of the deviator to the "A" side of the centerline. Unfortunately, Gage 1A-7 at the top of the link did not function. The upper leg of the link, which was instrumented by Gage 1A-5, showed a significant increase in strain in the last load stages before failure. As was experienced in Test 1B, however, the break point for this link was near Gage 1A-4, which showed lower strain. Data for the remaining link bars, which were gaged at the tops only, are presented in Fig. 6.29. Gages 1A-2 and 1A-11 showed strains of more than twice yield only midway through Test 1A Phase II. (Figure 6.30 shows comparative data for the gages at the tops of

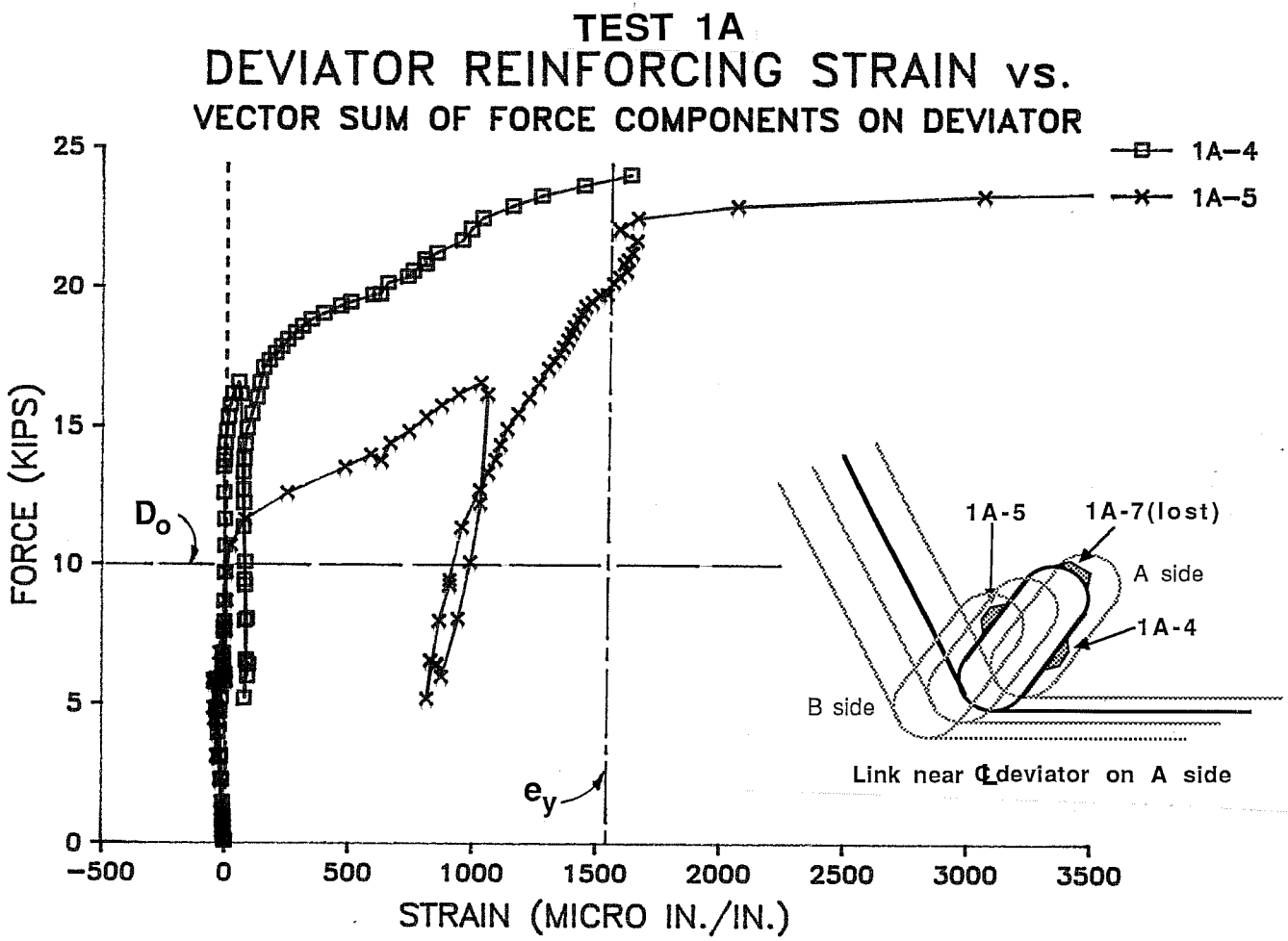

Figure 6.28 Test 1A Deviator Reinforcement Strain Gage Data

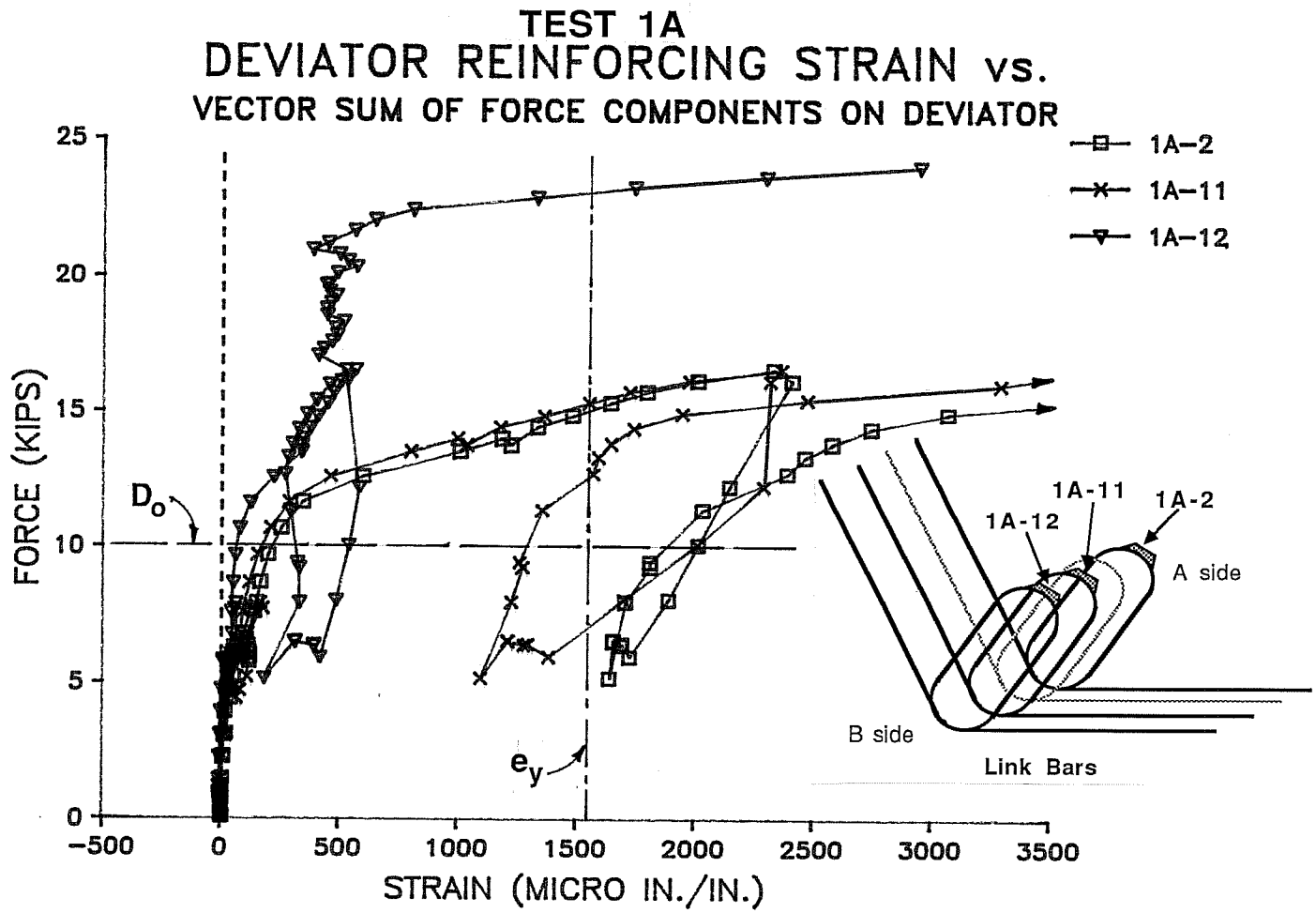

Figure 6.29 Test 1A Deviator Reinforcement Strain Gage Data

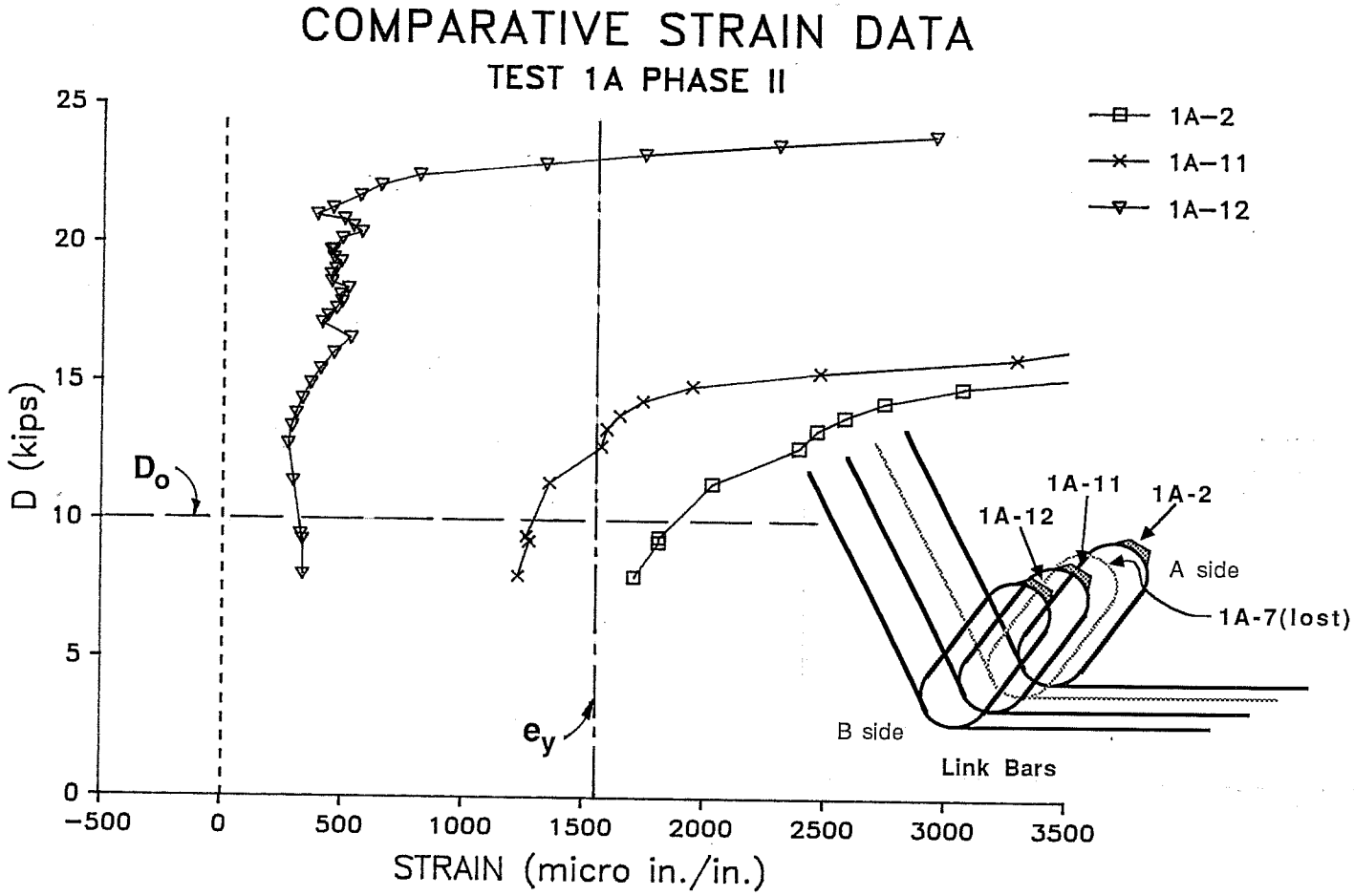

Figure 6.30 Test 1A Comparative Strain Data for Links

the link bars for Phase II only.) Maximum strains recorded for these gages exceeded 4500 micro in./in. before the gages failed. These two bars broke in the same location as the fully instrumented link, i.e. at the flange-block intersection. Gage 1A-12, on the other hand, maintained a relatively low strain level until a few load stages before the block failed. Again, this bar broke near the web, only an inch or so away from the gage point. This same pattern was outlined in the previous section; the break points for the bars occurred in regions of lower strain. Again, this may or may not be a relative point since instantaneous redistributions probably occurred at the moment of failure.

Only one outer loop was intrumented in Test 1A. Data from gages on this bar is presented in Fig. 6.31. This plot also includes data from the anchor bar which was located near the front edge of the deviator, inside and perpendicular to the four outer loops. Examining first Gage 1A-3LO (the gage on the top side of the bar did not function) up to a load level of about 17 kips (D/D_o=1.70), the strain-load behavior closely resembles that of gages in similar locations in Block B. At higher loads however, the level of strain at this gage begins to decrease, becoming compressive just before failure. One possible explanation for this apparent unloading could be that a shear mechanism began to control the behavior of the deviator. It seems

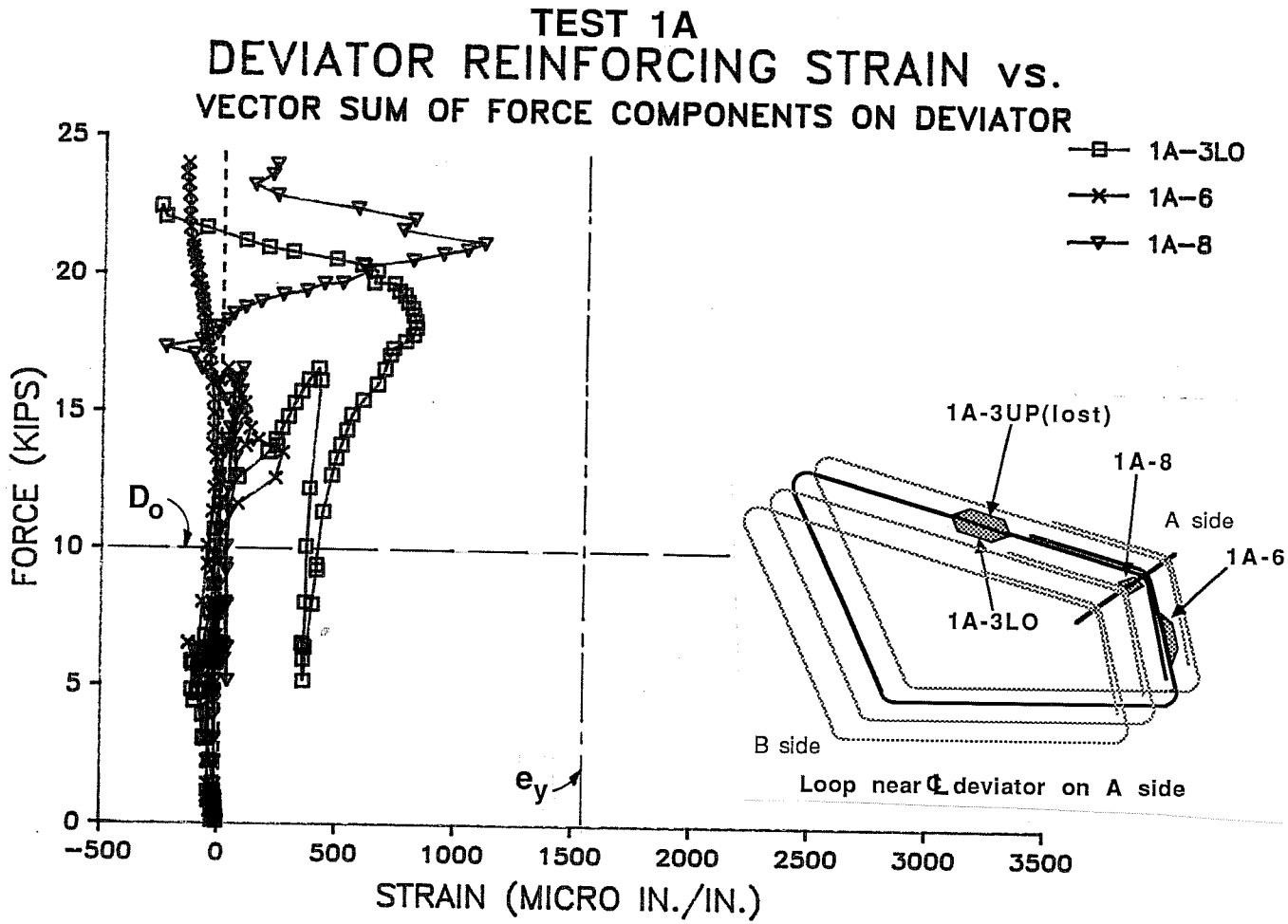

Figure 6.31 Test 1A Deviator Reinforcement Strain Gage Data

reasonable to assume that the top of the loop was first utilized as tension steel for a beam element formed by the top of the block. Then, as was observed during the test, cracking patterns formed a wedge of concrete which was pushed toward the web by the force of the two outer tendons which were deviated in that direction. It seems probable that, as this wedge began to move toward the web relative to the base of the block, the top of the outer loop, which had formerly developed tensile strains due to beam action, began to be compressed. The front leg of the outer loop, where Gage 1A-6 was located, did not appear to develop any tensile strain throughout the test, indicating that that portion of the bar was not utilized. This is consistent with data from Test 1B, in which a similar gage also maintained a very low strain level. Another point of interest is that the anchor bar, to which Gage 1A-8 was affixed at the center on the inside surface, picked up a considerable amount of strain, up to a level of D of about 21 kips. Then the strain level dropped off rapidly. This decrease could be attributed to the formation of a crack perpendicular to this bar (such a crack appeared on the top face of the deviator at about the same load level), and an accompanying redistribution of strain in the bar. The drop in strain also occurs at approximately the same time that the instrumented outer loop appeared to unload.

Figure 6.32 and 6.33 show the strain data from the two inner loops which were gaged for Test 1A. In Fig. 6.32, the same unloading phenomenon that was noted in the outer loop (as discussed in the previous paragraph) is evident in Gage 1A-9LO at the top part of the inner loop. During early stages of the test, this portion of the inner loop was probably utilized in a flexural capacity. When D reached about 17 kips, slope of the load versus strain curve increased. Then, at D of approximately 20 kips, the strain in Gage 1A-9LO sharply decreased, an indication of unloading in the upper portion of the strirrup. At the same time, Gage 1A-10 at the front leg of the inner loop showed a steadily increasing strain, reaching yield just before failure. A possible explanation for the considerable strain recorded for Gage 1A-10 could be that this part of the bar began to contribute to shear-friction action, as it tried to restrain the wedge of concrete being pushed toward the web. In Fig. 6.33, Gage 1A-1LO appears to begin to unload, but, unfortunately, the gage ceased to function when D reached approximately 19 kips, which was just before unloading began in Fig. 6.32. Gage 1A-1UP also failed five load stages earlier, before any unloading became apparent.

The final plot in this series, Fig. 6.34, shows comparative data for a group of bars located in approximately the same vertical plane of the deviation block (see Fig. 6.35). As

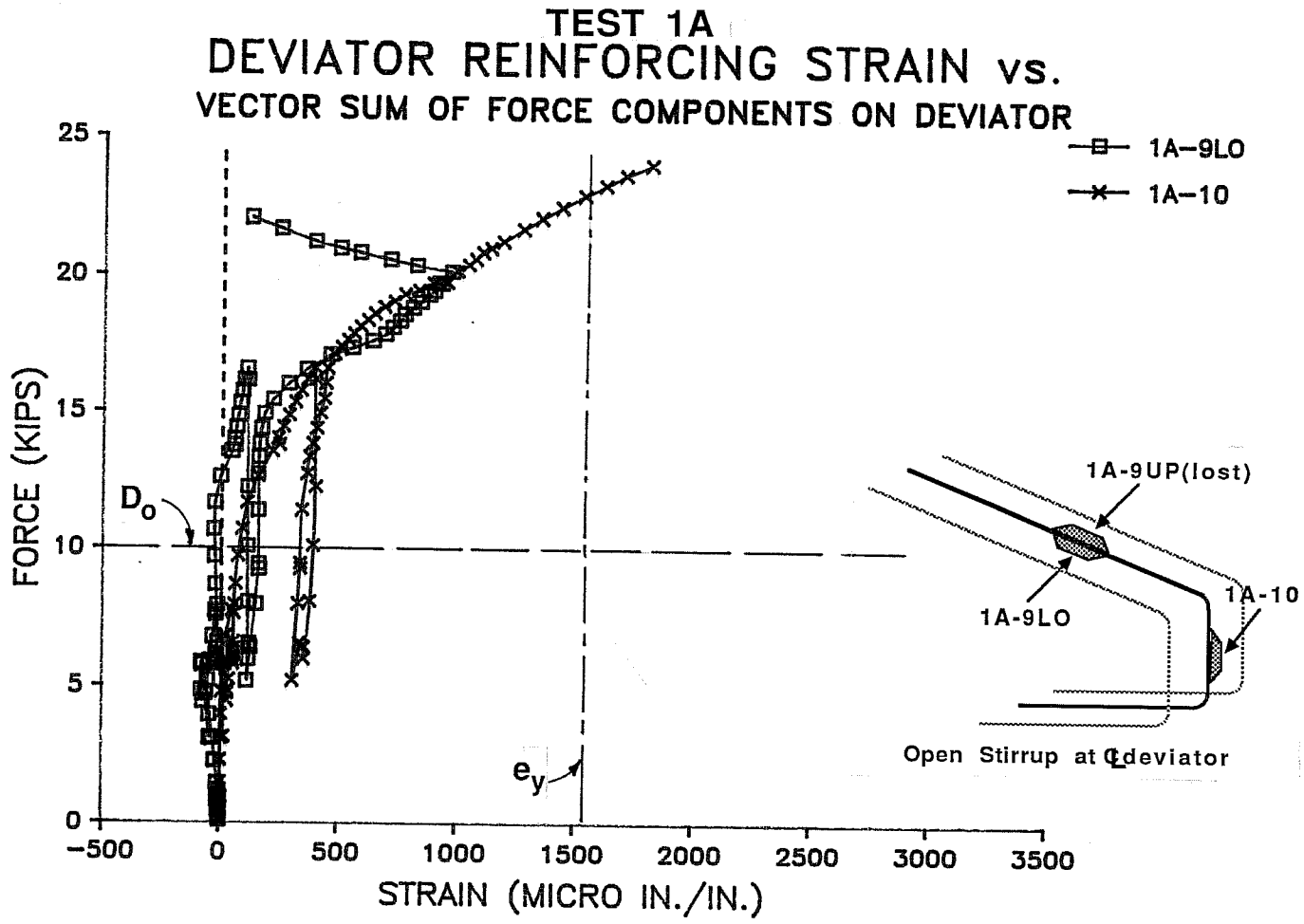

Figure 6.32 Test 1A Deviator Reinforcement Strain Gage Data

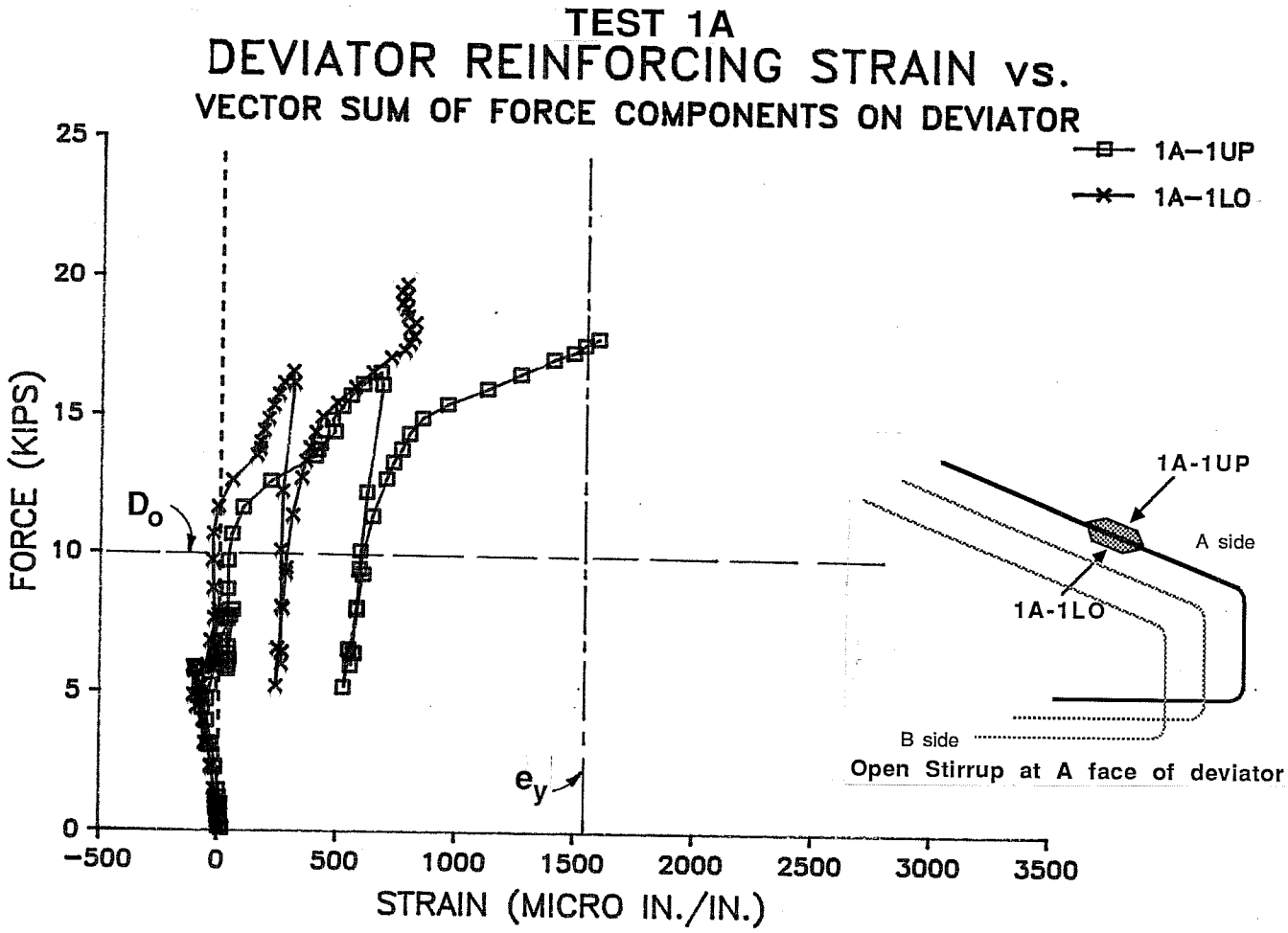

Figure 6.33 Test 1A Deviator Reinforcement Strain Gage Data

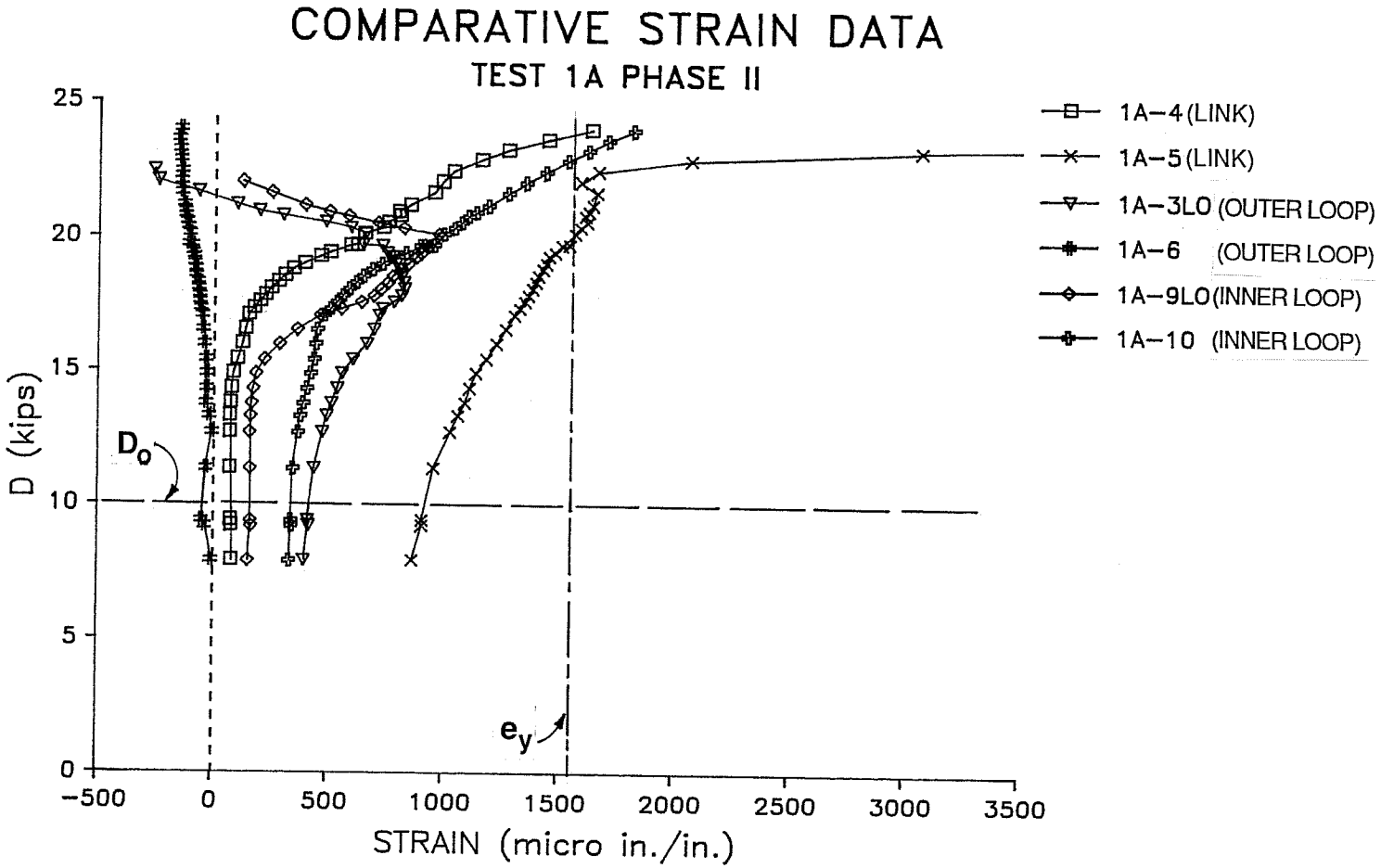

Figure 6.34 Test 1A Comparative Strain Data

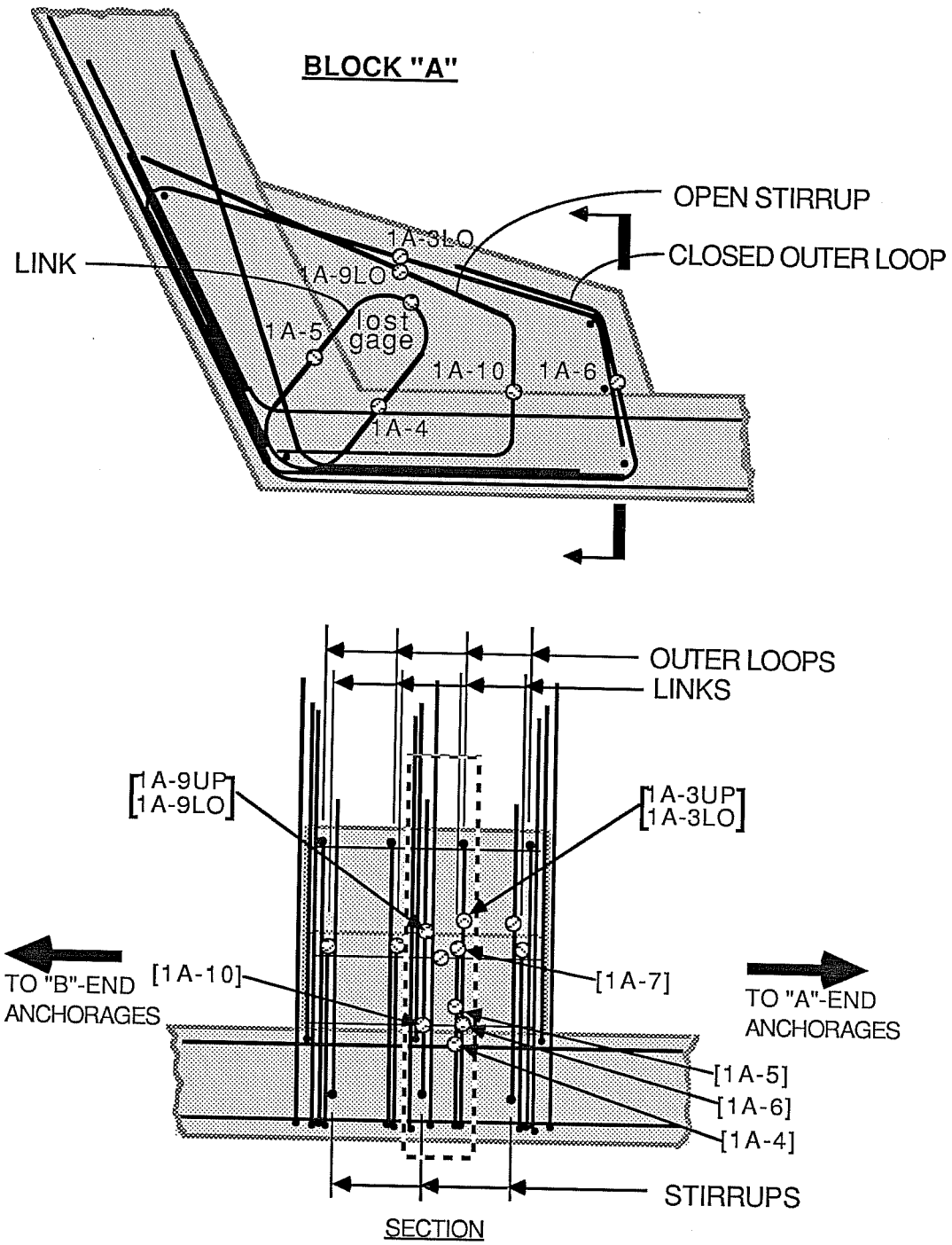

Figure 6.35 Block A: Gages in a Vertical Plane

in Test 1B, the link bar developed higher strain levels than any other bar, an indication that the link was being used more efficiently. Also similar to Test 1B, the upper parts of the inner loops and closed outer loops appeared to act as reinforcement for a beam element formed by the concrete at the top of the deviator. Comparing the data from Gages 1A-3LO and 1A-9LO during early stages of the test, 1A-3LO saw higher strain than 1A-9LO, which was closer to the neutral axis in the assumed beam strip at the top of the block. Both of these gages began to unload at roughly the same load level, possibly pointing again to the development of a shear mechanism. In contrast to Test 1B, the front leg of the inner loop was more active in resisting loads; this would stand to reason if it were utilized in Test 1A as shear-friction reinforcement. The trends observed in the strain data of this and Test 1B lend strong support to the hypothesis that a shear-friction mechanism played a much more dominant role in the behavior of the deviator in Test 1A.

6.3.2 Displacement Data. The dial gages and potentiometers located at points around the box girder specimen (see Fig. 5.3) were used to assess the rigid body motion of the box as loads were being applied to the deviator. Components of displacement due to translation and rotation of the box were subtracted from the global displacements of the deviation block

to determine the displacement of the deviator with respect to the box. However, the resulting values for deviator displacement are at best a rough estimate. It is likely that the very small displacement values, especially in the horizontal or east-west direction, include components reflecting the elastic deformation of the box. It was not feasible to provide the extensive intrumentation which would have been required to monitor the box deformations. Moreover, the small vertical and horizontal deviator displacements estimated for the two deviator tests are only significant as an indirect indication of the relative ductilities of Block A and Block B.

Figure 6.36 is a history of vertical displacement for Block B during Phase II of Test 1B. This curve represents readings from Potentiometer P-1B-V, which was located on the top face of the deviator, minus the total upward displacement of the specimen box at that level. The almost insignificant relative displacement of 0.03 inches just before failure reinforces the observation that the block had not deformed perceptibly before reaching ultimate capacity. An estimate of horizontal or east-west displacement of the front face of the deviator is shown in Fig. 6.37. Relative displacement toward the center of the specimen is taken as positive. This amount of displacement seems artificially high, but probably includes some component of box deformation, as discussed earlier.

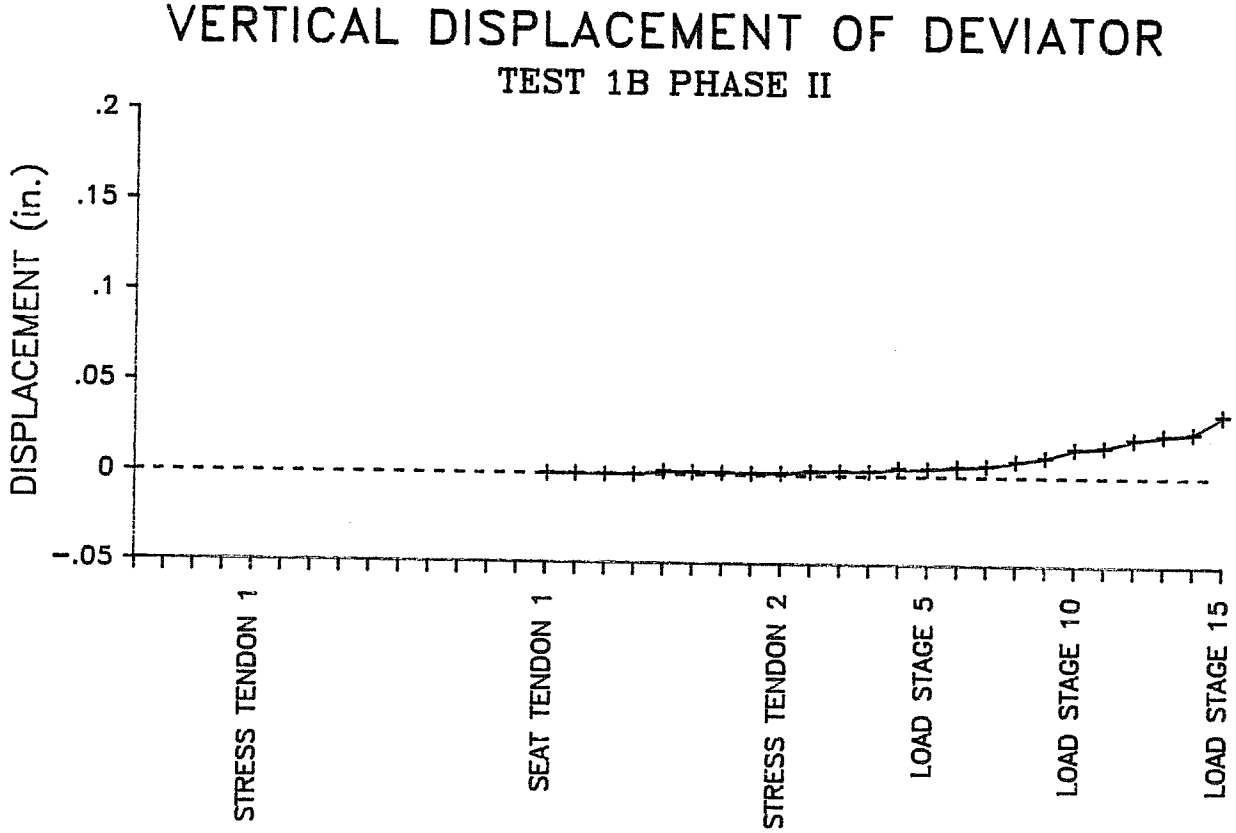

Figure 3.36 Test 1B: Vertical Displacement of Deviator

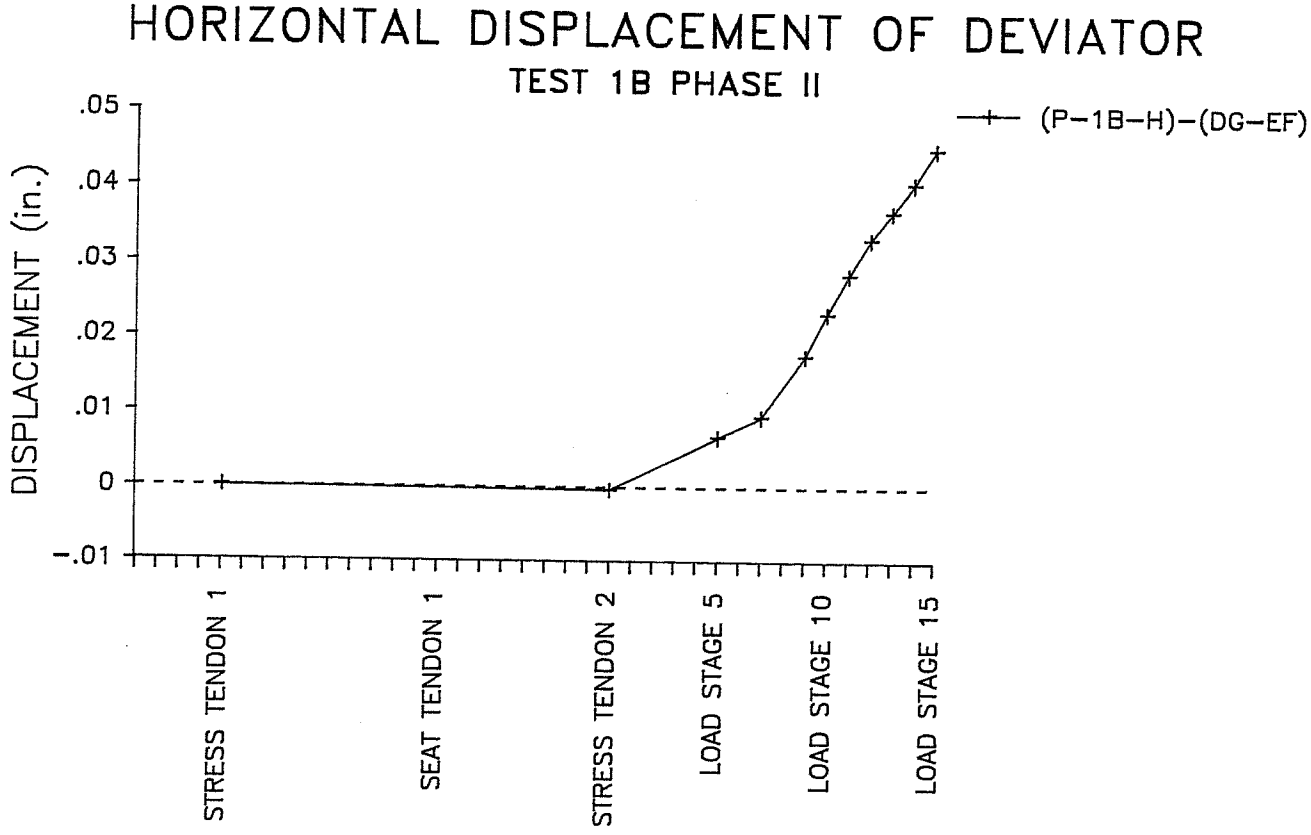

Figure 3.37 Test 1B: Horizontal Displacement of Deviator

Figures 6.38 and 6.39 show similar information for Test 1A Phase II. As expected, significant vertical displacements were recorded for Block 1A, reflecting the advanced state of noticible distress and deformation in Block A before it failed. Again, the horizontal displacements are probably inaccurate because box deformations were not accounted for, and should be viewed only as a relative indicator.

6.4 Comparison of Test Results with Simple Analysis Models

The strain gage data and crack patterns observed in the deviator tests suggest three dominant behavioral mechanisms that interact to form the overall behavior of the deviator. These three mechanisms, as illustrated in Fig. 6.40, are: 1) Direct tension action of the link reinforcement, 2) Beam action of the top portion of the deviator, and 3) Shear-friction along a plane of weakness at the level of the ducts. Isolating three simple models, each mechanism will first be considered individually; then their possible interactions will be discussed. The models chosen for investigation are simplified due to the limited data availible to refine them.

6.4.1 Direct Tension Model. The calculation of direct tension capacity for the deviator is relatively straightforward. The only reinforcement that realistically can contribute direct tension resistance to the pullout force of the vertically

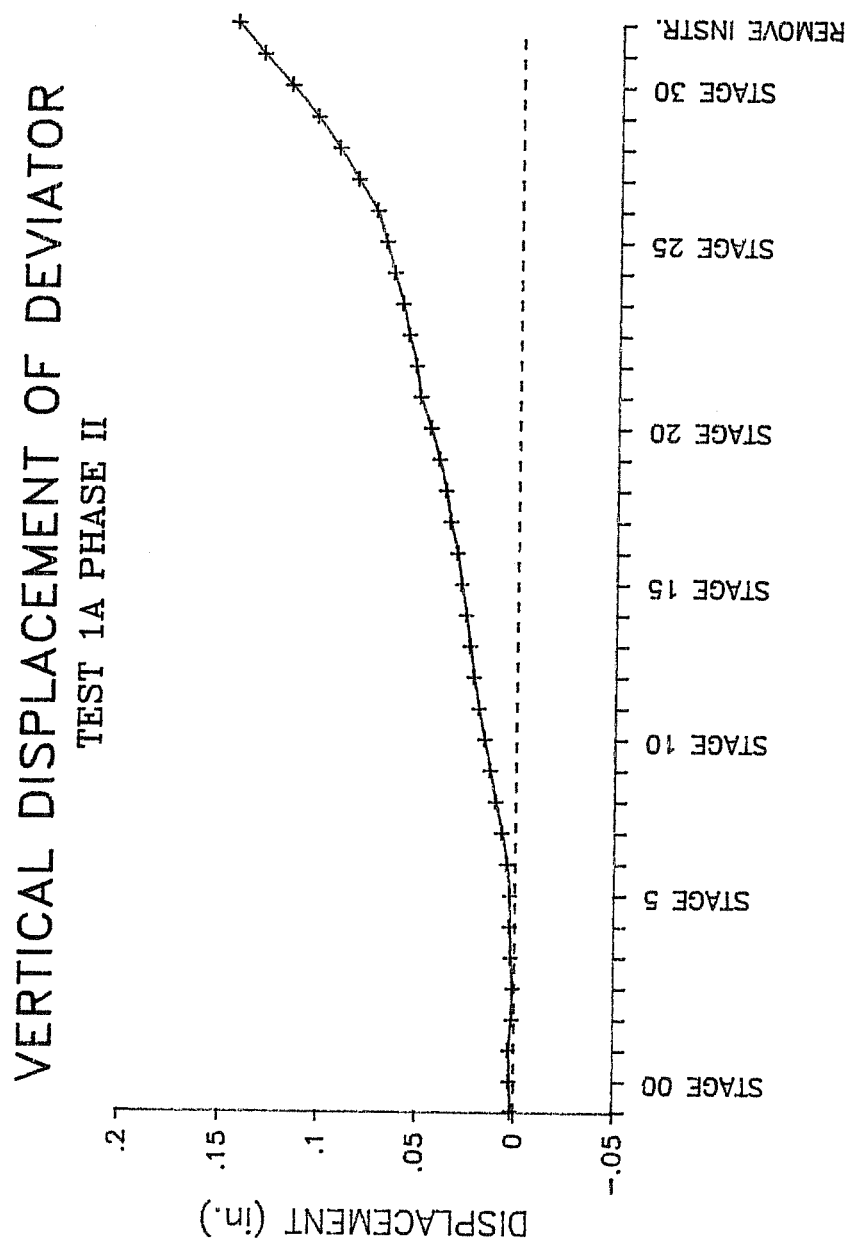

Figure 3.38 Test 1A: Vertical Displacement of Deviator

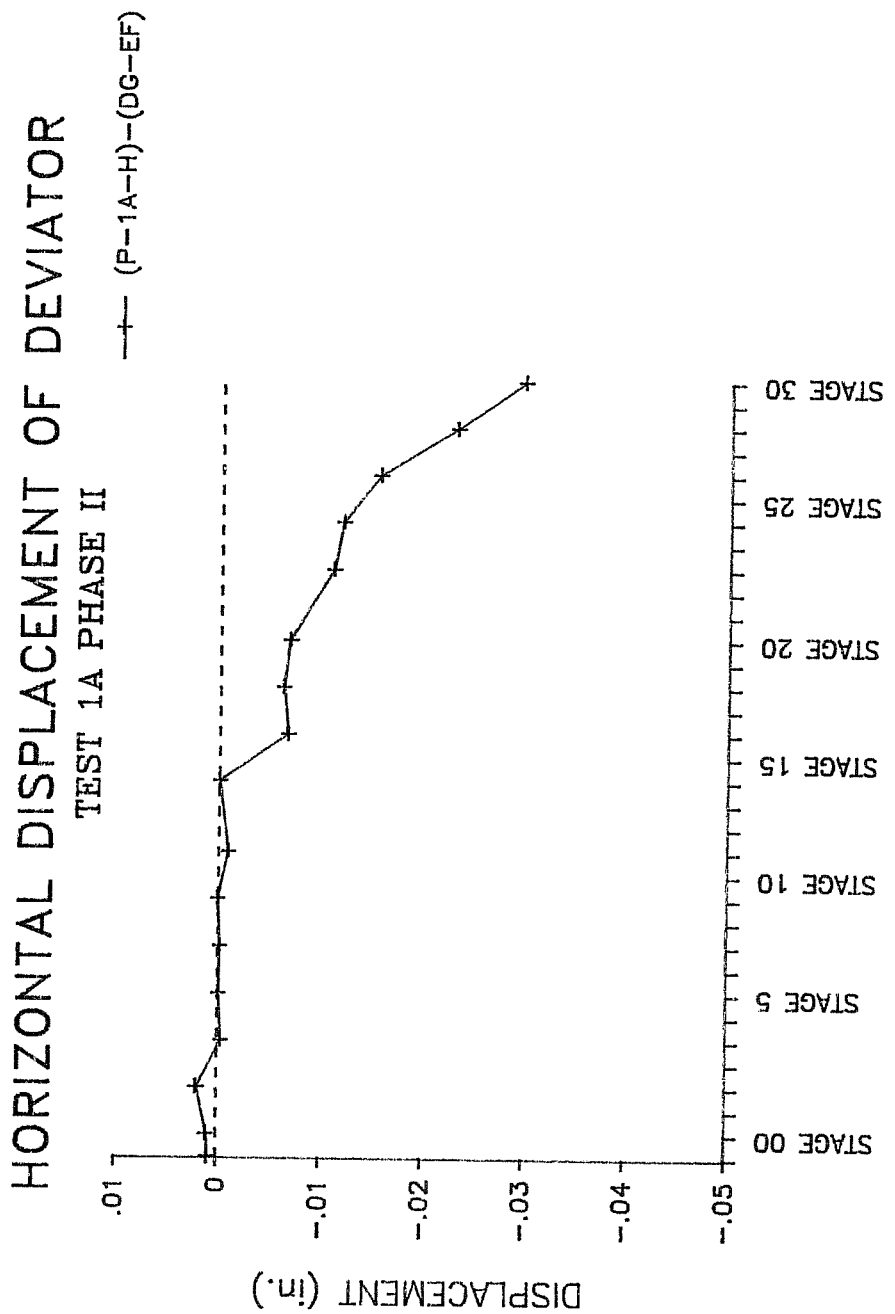

Figure 3.39 Test 1A: Horizontal Displacement of Deviator

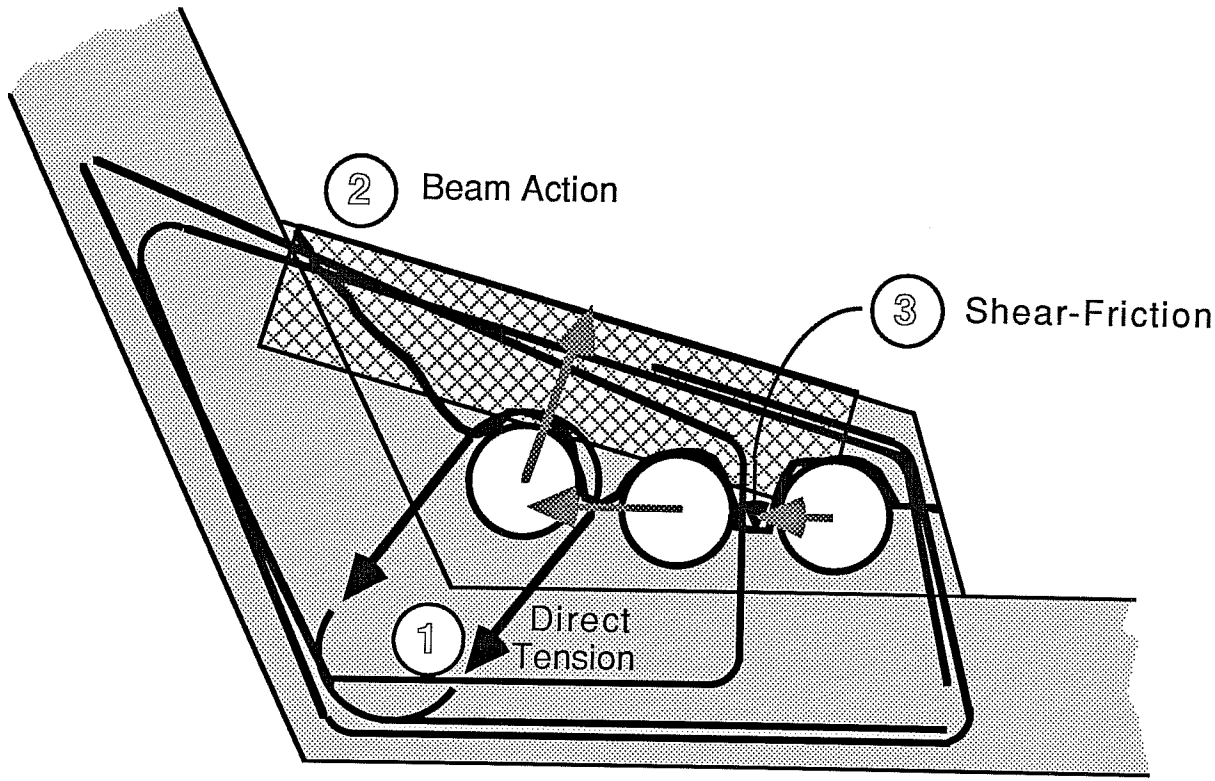

Figure 6.40 Behavioral Models

deviated tendon are the four link bars that tie the tendon back to the box section. The nominal and ultimate direct tension capacities of the links are calculated as shown in Fig. 6.41. The nominal capacity, denoted F_y, is the capacity that the designer can rely upon when proportioning the direct tension reinforcement. In a laboratory environment, however, the ultimate stress of the reinforcing steel is well known from material tests. Access to this information makes it possible to calculate the absolute ultimate tensile capacity of the bars, denoted F_{ult}. In other words, the links would not be expected to break until the force component directed along the link axis reached F_{ult}.

Figure 6.42 illustrates the relationship between link capacity and tendon force in the two deviators. Only the vertically deviated tendon in each deviator is considered in this relationship. The calculations show that approximately 92 kips in Tendon 2 would correspond to the failure load for Block B if the direct tension capacity of the links provided sole resistance to the pullout force of the deviated tendon. A force in Tendon 2 of 66 kips corresponds to the nominal capacity of the links for design purposes. In Block A the deviation angle is smaller, so 139 kips in Tendon 3 would be required to produce an ultimate force for the links alone. A maximum force in Tendon 3 of 99

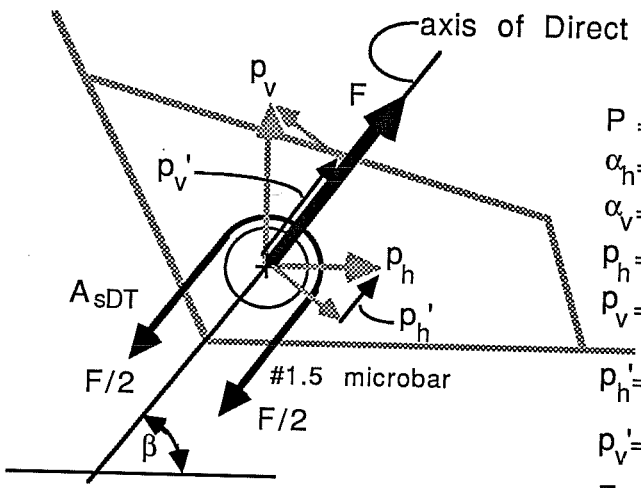

P = Tendon Force
α_h = Horizontal Deviation Angle
α_v = Vertical Deviation Angle
$p_h = P\sin\alpha_h$
$p_v = P\sin\alpha_v$
$p_h' = p_h\cos\beta$
$p_v' = p_v\sin\beta$
$F = p_h' + p_v'$

$\beta = 50°$
$A_{sDT} = 4 \times (2 \times 0.0276 \text{ sq.in.}) = 0.2208 \text{ sq.in.}$
$f_y = 45$ ksi $\quad f_u = 63$ ksi

F_y = Nominal Direct Tension Capacity of Link Bars
$= A_{sDT} \times f_y$
$= 0.2208$ sq.in. $\times$ 45 ksi
$= 9.94$ kips

F_{ult} = Ultimate Direct Tension Capacity of Link Bars
$= A_{sDT} \times f_u$
$= 0.2208$ sq.in. $\times$ 63 ksi
$= 13.91$ kips

Figure 6.41 Direct Tension Model

• CALCULATE TENDON FORCES CORRESPONDING TO LINK CAPACITIES:

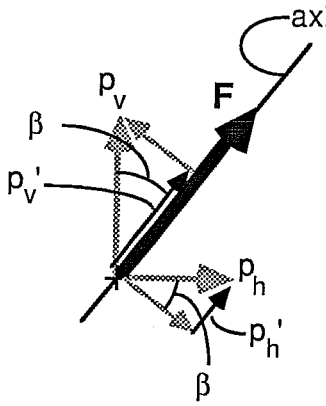

$F = p_h' + p_v'$

$= P[(\sin \alpha_h \cos\beta + \sin \alpha_v \sin\beta)]$

$\beta = 50°$

Test 1B

Given: $\alpha_h = 3.87°$ and $\alpha_v = 8.1°$

$F = P_2 [(\sin 3.87°)(\cos 50°) + (\sin 8.1°)(\sin 50°)]$

$= 0.1513P_2$

$F_y = 9.94$ kips

--> $P_2 = 65.7$ kips

= Force in Tendon 2 when links yield.

$F_{ult} = 13.91$ kips

--> $P_2 = 91.9$ kips

= Force in Tendon 2 when links fail.

Test 1A

Given: $\alpha_h = 0.84°$ and $\alpha_v = 6.8°$

$F = P_3 [(\sin 0.84°)(\cos 50°) + (\sin 6.8°)(\sin 50°)]$

$= 0.1001P_3$

$F_y = 9.94$ kips

--> $P_3 = 99.3$ kips

= Force in Tendon 3 when links yield.

$F_{ult} = 13.91$ kips

--> $P_3 = 91.9$ kips

= Force in Tendon 3 when links fail.

Figure 6.42 Direct Tension Calculations

kips corresponds to the nominal design capacity of the link reinforcement.

6.4.2 Beam Model. Test data, especially that of Test 1B, indicated that beam action contributed significantly to the behavior of the deviator. Crack patterns on the deviator resembled typical cracking in a simple beam loaded at the center. Strain data also suggested that the reinforcement along the top face of the block was utilized in a flexural capacity. However, calculating the contribution of beam action to the ultimate capacity of the deviator involves a considerable degree of uncertainty. Unknowns include the exact location and dimensions of the beam element and the support conditions for the ends of the beam. Reasonable simplifying assumptions must therefore be made.

The assumed beam element runs parallel to the top face of the deviation block as illustrated in Fig. 6.43. The top arms of the outer loops and the inner loops form the tension reinforcement for the beam. The principal load on the beam is applied at the top of the innermost duct by the vertically deviated tendon. Only the force component perpendicular to the beam is considered in the beam model. Since the diameter of the duct is significant with respect to the beam length, the force is distributed over a length equivalent to 75 percent (chosen as a reasonable estimate) of the duct diameter, rather than applied as

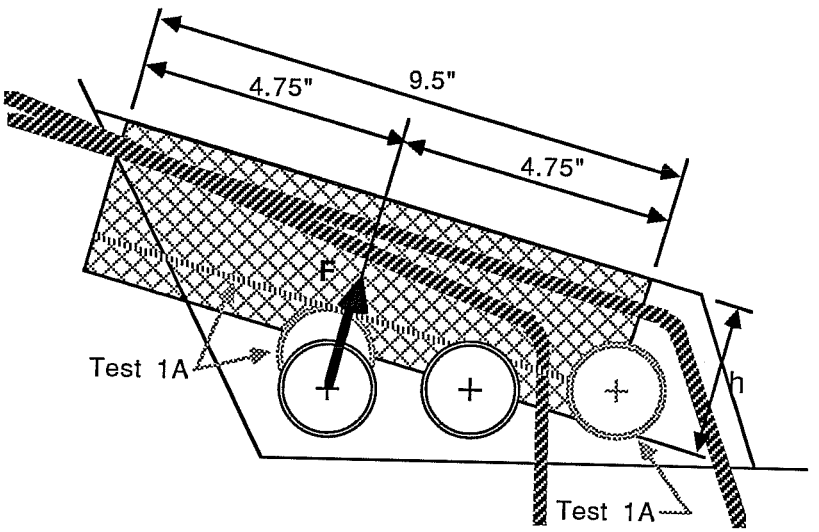

BEAM MODEL:

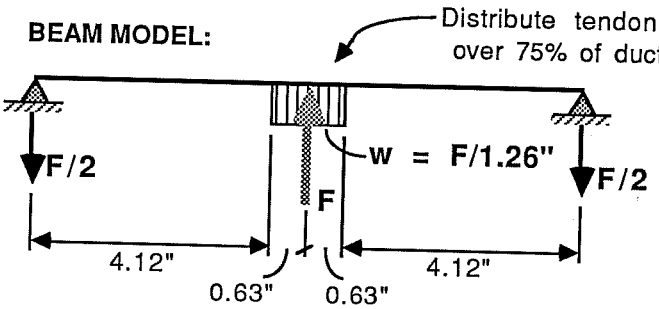

M_{max} = F/2(4.12+(1.26/4))
= 2.217F (at midspan)

CROSS SECTION:

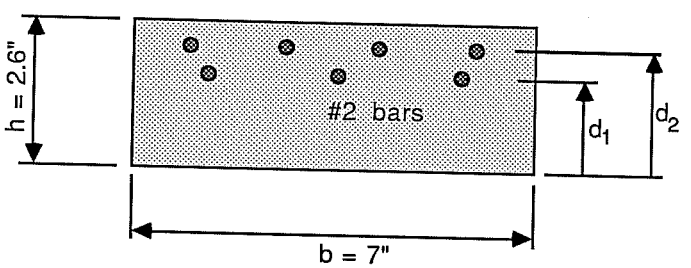

f'c = 5650 psi
fy = 45 ksi

$d = (d_1 x4 + d_2 x3)/7$

As = 7 x 0.0496sq.in.
= 0.3472sq.in.

M_n = As x fy(d-a/2)
a = (As x fy)/(.85 x f'c x b) = 0.465in.

Figure 6.43 Beam Model

a point load. The beam is assumed to be simply supported at both ends. The basis for this conservative assumption lies in the fact that early cracking near the ends of the proposed beam element (as observed in the tests) allows rotation. At the end of the beam near the front face of the deviator, the front legs of the inner and outer loops must provide the downward reaction for the assumed beam element. For this reason the end of the beam is taken as midway between the inner loop legs and the outer loop legs. At the opposite end, near the web, the beam is assumed to stop at the intersection of the tension reinforcement with the web-block interface. The overall length of the beam is 9.5 inches as indicated in the figure. Given these assumptions, the maximum moment on the beam is found (Fig. 6.43), in terms of the force component, F, perpendicular to the beam.

Figure 6.43 also shows the generalized cross section for the beam element. The point of maximum moment for the beam occurs at the point of application of the load, that is, at the top of the duct for the vertically deviated tendon. The depth of the concrete section at this point extends from the face of the deviator to the top of the duct. Therefore, the depth of the assumed beam in Block B is 2.6 inches. In Block A, Duct 3 is closer to the top of the block, so the beam depth is reduced to 1.8 inches. Values of concrete compressive strength and steel

yield strength are indicated, as well as total reinforcing steel area.

Figure 6.44 presents the calculation of nominal flexural capacity for each deviator. The force component, F, which is perpendicular to the beam, is related to the tendon force, P, in the vertically and horizontally deviated tendon. These calculations show that the flexural capacity of the beam element at a section over the duct corresponds to P_2 (i.e. the force in Tendon 2) of 72.4 kips for Block B and P_3 (force in Tendon 3) of 52.7 kips for Block A.

6.4.3 Shear-Friction Model. The tendon geometry for Test 1A produced relatively large shear forces which were directed toward the web of the specimen box. Cracking and strain gage data indicated that shear-friction action played a significant role in the behavior of Block A. In modelling shear-friction in the block, however, several uncertainties exist. First, the exact location and inclination of the shear plane is not well defined. A plane of weakness is assumed to exist along a surface which runs over and between the ducts, since along this surface the least area of concrete is available to participate in a shear transfer mechanism. The crack map from Test 1A (refer to Fig. 6.14) gives a good indication of the actual surface, but a predictable thoeretical shear plane is not obvious. A second area of uncertainty concerns the participation of the existing

• CALCULATE CAPACITIES OF BEAM ELEMENTS AND CORRESPONDING TENDON FORCES :

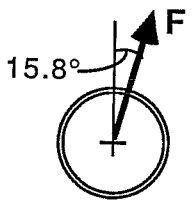

F = Component of Tendon Force, P, Perpendicular to Beam

$= P[(\sin\alpha_v)(\cos 15.8°) + (\sin\alpha_h)(\sin 15.8°)]$

where α_v = Vertical Deviation Angle, and

α_h = Horizontal Deviation Angle

TEST 1B

Given:

$\alpha_v = 8.1°$ --> $F = P_2[(\sin 8.1°)(\cos 15.8°)+(\sin 3.87°)(\sin 15.8°)]$

$\alpha_h = 3.87°$ -->$F = 0.154P_2$

h = 2.6" = beam height

d = 2.6"-0.625" = 1.975" --> d = (1.975 x 4 + 1.6 x 3)/7

d = 2.6"-1.0" = 1.6" = 1.814"

Then: M_n = .3472" x 45ksi(1.814 - 0.465/2)

= 24.7kip-in.

$M_n = M_{max}$ --> 24.7kip-in. = 2.217F

--> F = 11.15kips

F = 0.154P --> 11.15kips = $0.154P_2$

--> P_2 = 72.4kips

TEST 1A

Given:

$\alpha_v = 6.8°$ --> $F = P_3[(\sin 86.8°)(\cos 15.8°)+(\sin 0.84°)(\sin 15.8°)]$

$\alpha_h = 0.84°$ -->$F = 0.118P_3$

h = 1.9" = beam height

d = 1.9"-0.625" = 1.275" --> d = (1.275 x 4 + 0.9 x 3)/7

d = 1.9"-1.0" = 0.9" = 1.114"

Then: M_n = .3472" x 45ksi(1.114 - 0.465/2)

= 13.8kip-in.

$M_n = M_{max}$ --> 13.8kip-in. = 2.217F

--> F = 6.21kips

$F = 0.118P_3$ --> 6.21kips = $0.118P_3$

--> P_3 = 52.7kips

Figure 6.44 Beam Calculations

reinforcement in the shear transfer mechanism. Related to this, the third unknown is the area of concrete which can be considered to contribute to shear transfer.

Three mechanisms contribute to shear transfer across a crack: 1) friction between crack faces provided by a clamping force from reinforcement crossing the crack, 2) interlock of protrusions along the crack faces, and 3) dowel action of the reinforcement crossing the crack (26). The ACI Commentary (26) gives a modified shear-friction relationship which more closely reflects the contributions from these mechanisms than the design equations given in the ACI Code. This empirical relationship also incorporates the possibility of reinforcement inclined to the crack which produces tension in the reinforcement.

Figure 6.45 illustrates the assumed shear-friction model for Block A. Regarding this model, several assumptions were made. First, the crack across which shear transfer must occur was chosen as shown in the figure. This crack pattern appeared on the north face of the deviator in Test 1A (see Fig. 6.14). Next, the only effective reinforcement for shear-friction was assumed to be the front legs of the outer loops and inner loops. Third, the effective concrete area for shear-friction calculations is limited to the two regions dimensioned in the

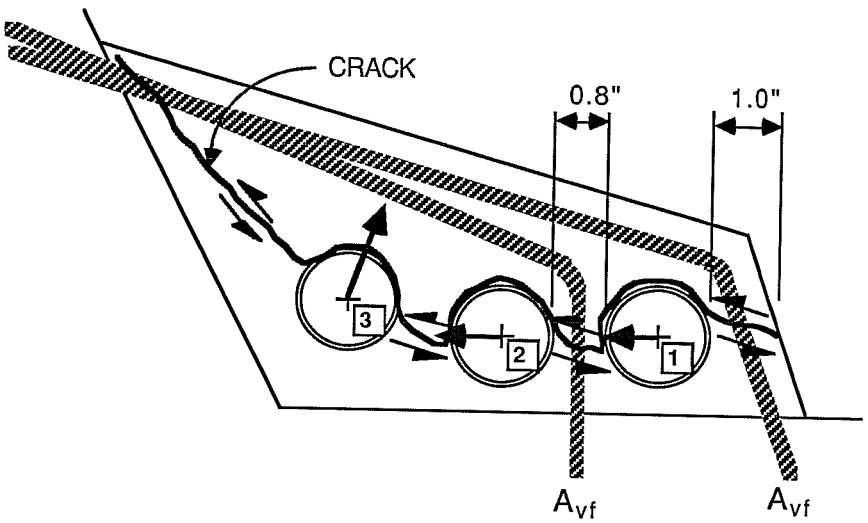

For a lower bound of shear-friction capacity, assume shear-friction reinforcement is perpendicular to crack so that the equation:

$$V_n = 0.8A_{vf}f_y + A_cK_1 \quad \text{(ACI Commentary Equation)}$$

is applicable. Then, substituting:

A_{vf} = .0496sq.in. x 7 = .3472sq.in.
f_y = 45 ksi
A_c = (0.8" + 1.0") x 7" = 12.6 sq.in.
= concrete area effective for shear-friction
and K_1 = 400 psi ,

The shear-friction capacity, V_n = 17.5 kips .

Assuming the direction of the crack to be parallel to the top face of the deviator, and taking into consideration the angle of the shear-friction reinforcement with the shear plane, the applicable ACI Commentary equation becomes:

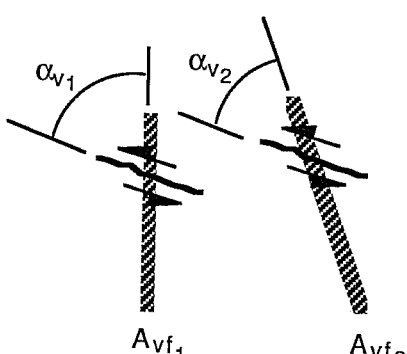

$$V_n = A_{vf}f_y(0.8\sin\alpha_v + \cos\alpha_v) + A_cK_1\sin^2\alpha_v .$$

Substituting:

α_{v_1}=74° $\quad$ α_{v_2}= 56°
A_{c_1}=0.8"x7" = 5.6sq.in. $\quad$ A_{c_2}= 1.0"x 7" = 7.0sq.in.
A_{vf_1}= 3x0.0496 = 0.15sq.in. $\quad$ A_{vf_2}= 4x0.0496 = 0.20sq.in.

The shear-friction capacity, V_n = 21.0 kips .

Figure 6.45 Shear-Friction Model and Calculations

figure. Justifications for the second and third assumptions are outlined in the following paragraphs.

The link reinforcement is fully engaged in resisting the pullout force from Tendon 3. It is this pullout force which probably instigates the formation of the crack. Once the crack grows wide enough to allow relative displacement due to shear forces, the link reinforcement more than likely has reached its yield strength and therefore cannot provide the additional clamping force necessary for shear transfer. Consequently, the link bars cannot be considered to contribute to the shear-friction capacity of the block.

The top arms of outer loops and inner loop bars cross the upper part of the crack near the intersection of the top face of the deviator and the box web. This reinforcement cannot provide shear-friction resistance in this region, however, since the bars are inclined to the crack in a direction which would induce compressive forces in the bars.

At the opposite end of the crack, near the front face of the deviator, the participation of the front legs of the outer loop seems reasonable. Even though the point of application of the shear force is behind these bars, relative displacement of the block of concrete above the ducts which is formed by the crack would induce shear in this region as well. It could be speculated that a vertical crack could form above Duct 1 which

would affect the transfer of shear to the front portion of the block. Even so, the presence of the outer loop bars across this speculated crack should develop enough force to transfer the shear to this region. In any case, no such crack was evident in the test. The limited strain data for the outer loop bars do not support the assumption that the front leg of the outer loop works in shear-friction. The single gage that was affixed to the front leg of one loop maintained near zero strain throughout Test 1A. The possibility exists, however, that this gage did not represent the actual state of stress in the vicinity of the shear plane. For example, the gage point may have been too far away from the crack (it was located near the block-flange intersection), the presence of the lap splice may have affected the stress distribution, or the gage may have malfunctioned. Also, there were no gages on the legs of the other three outer loops. Seeing that the experimental evidence is not conclusive, the assumption holds that the front legs of the outer loops fully participate in shear-friction action.

There is little question that the front legs of the inner loops contribute to shear-friction resistance. The bars cross the shear plane at a critical location and are well anchored to develop the neccessary clamping force. Strain data support this conclusion.

The third assumption concerns the area of concrete to be considered active in shear transfer. It stands to reason that the only concrete area along the shear plane that can be effective in shear transfer is that with effective shear-friction reinforcement crossing it. So, it follows that this effective concrete area occurs over the seven-inch width of the deviator, between Duct 2 and Duct 1 and from Duct 1 to the front face of the deviator.

Figure 6.45 presents two alternate calculations of shear-friction capacity based on the modified shear-friction formulas given in the ACI Commentary (26). The first calculation disregards inclination of the shear-friction reinforcement to the crack, while the second includes it. The results of these calculations provide rough bounds for shear-friction capacity since the actual inclination angle is not well known. The results predict shear-friction capacity between 17.5 and 21.0 kips.

6.4.4 Interaction and Comparison of Results. In order to compare theoretical capacities to actual forces on the deviator at first yield and at failure, the total force vector on the deviator, D, is resolved into components which are perpendicular and parallel to the top face of the deviation block. The component of force perpendicular to the top face of the block (and to the assumed beam element) is assumed to be

carried by beam action and direct tension. The component of D which is parallel to the top face of the deviator (and parallel to the assumed shear plane) is assumed to be carried by shear-friction.

Since the direct tension capacity and the flexural capacity of the block depend on unrelated reinforcement and carry forces in roughly the same direction, these capacities are additive. There is an interaction, however, between the combined beam/tension capacity and the shear-friction capacity. The lower of the two should control the failure of the block. In the following sections, the forces on each deviator at failure are compared with calculated capacities based on the simplified behavioral models.

6.4.4.1 Test 1B. Only direct tension and beam models were investigated for Block B, since it was apparent from test observations and data that shear-friction did not play a significant role in the overall behavior of the deviator. Figure 6.46 shows the total force vector on Block B at first yield of the deviator reinforcement and at failure of the block. The vector is defined by the magnitude, D, and the direction, θ, with the subscripts "y" and "f" denoting yield and failure respectively. The vector is resolved into components along a set of axes, denoted x' and y', which are directed parallel and

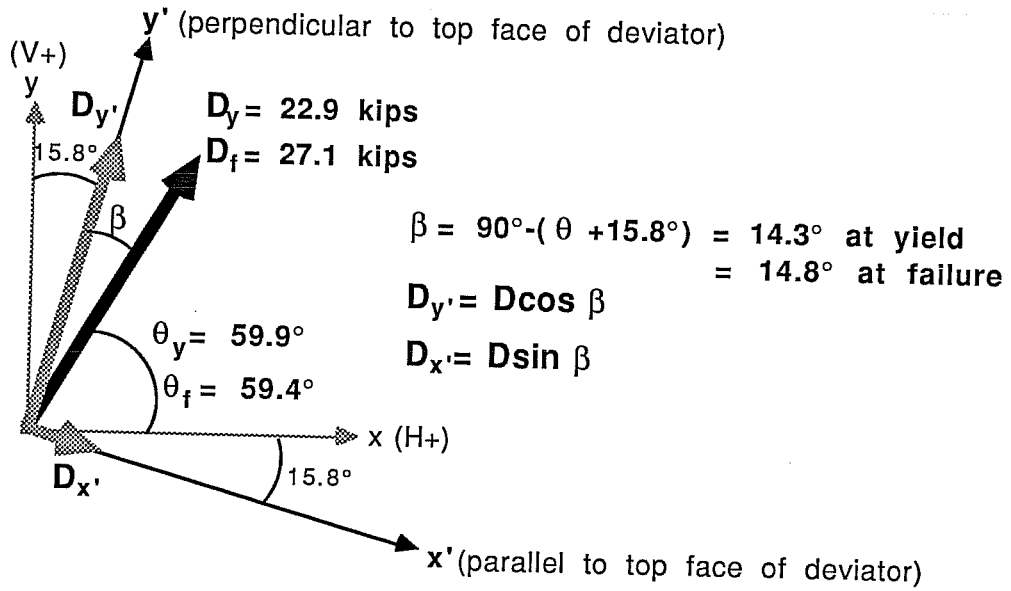

$D_{y'} = D\cos\beta = 22.9 \times \cos(14.3°) = 22.1$ kips
$D_{x'} = D\sin\beta = 22.9 \times \sin(14.3°) = 5.6$ kips
} FROM TEST 1B DATA: FORCE COMPONENTS AT FIRST YIELD

$D_{y'} = D\cos\beta = 27.1 \times \cos(14.8°) = 26.2$ kips
$D_{x'} = D\sin\beta = 27.1 \times \sin(14.8°) = 6.9$ kips
} FROM TEST 1B DATA: FORCE COMPONENTS AT FAILURE

F_{DT} = 13.9 kips (9.94 kips nominal capacity)
F_{BEAM} = 11.2 kips
$F_{COMB} = (.91 \times 9.94) + 11.2 = 20.3$ kips (nominal)
$F_{COMB} = (.91 \times 13.9) + 11.2 = 23.9$ kips (ultimate)
(Shear-Friction does not control)
} CALCULATED CAPACITIES BASED ON BEHAVIORAL MODELS

COMPARE $D_{y'}$ WITH F_{COMB} :

$D_{y'}$ = 22.9 kips
F_{COMB} = 20.3 kips
} 8.5 % DIFFERENCE AT FIRST YIELD

$D_{y'}$ = 26.2 kips
F_{COMB} = 23.9 kips
} 8.8 % DIFFERENCE AT FAILURE

Figure 6.46 Test 1B: Comparison of Theoretical and Experimental Results

perpendicular to the top face of the deviation block. The resulting components are denoted $D_{x'}$ and $D_{y'}$. The component of interest, in this case, is $D_{y'}$ which is equal to 22.1 at first yield and 26.2 kips at failure. Values for ultimate direct tension capacity of the link reinforcement, denoted F_{DT}, and flexural capacity of the assumed beam element, denoted F_{BEAM}, are repeated here from previous calculations as 13.9 kips (9.94 kips nominal capacity) and 11.2 kips respectively. Since the inclination of the direct tension reinforcement is not exactly perpendicular to the top face of the deviator, the value for direct tension capacity is adjusted accordingly (0.91 corresponds to the cosine of the angular difference) for the purpose of comparison. Combining direct tension and beam capacities gives 20.3 kips nominal capacity and 23.9 kips ultimate capacity for Block B. When compared to the force components on the deviator in the y'-direction at first yield and at failure, the calculated capacities underpredict the yield condition by just 8.5 percent and the failure condition by only 8.8 percent.

6.4.4.2 Test 1A. Similar information for Test 1A is presented in Fig. 6.47. For Block A, $D_{x'}$ equals 15.0 kips at failure (8.7 kips at first yield) and $D_{y'}$ is 18.7 kips at failure (11.5 kips at first yield). The reduced depth of the beam element in Block A results in a combined flexural/direct tension ultimate capacity of 18.9 kips (15.9 kips nominal capacity). The

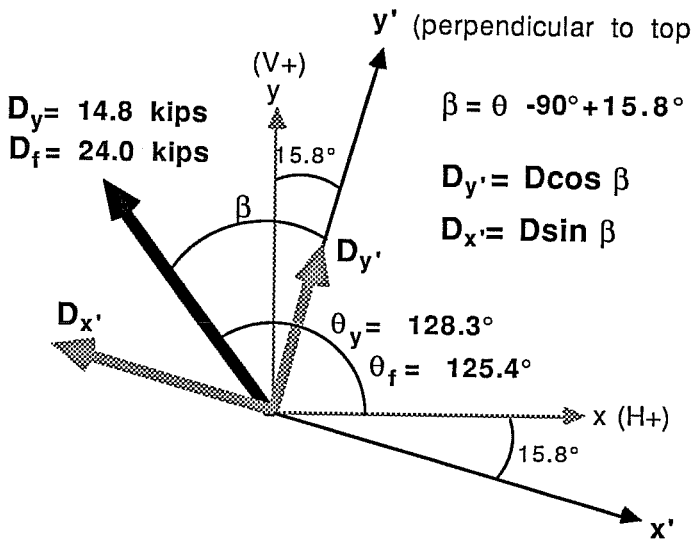

$\beta = \theta - 90° + 15.8°$ = 54.1° at first yield
= 51.2° at failure

$D_{y'} = D\cos\beta$

$D_{x'} = D\sin\beta$

$D_{y'} = D\cos\beta = 14.8 \times \cos(54.1°) = 8.7$ kips
$D_{x'} = D\sin\beta = 14.8 \times \sin(54.1°) = 11.5$ kips
} FROM TEST 1A DATA: FORCE COMPONENTS AT FIRST YIELD

$D_{y'} = D\cos\beta = 24.0 \times \cos(51.2°) = 15.0$ kips
$D_{x'} = D\sin\beta = 24.0 \times \sin(51.2°) = 18.7$ kips
} FROM TEST 1A DATA: FORCE COMPONENTS AT FAILURE

F_{DT} = 13.9 kips (9.94 kips nominal capacity)
F_{BEAM} = 6.2 kips
$F_{COMB} = (.91 \times 9.94) + 6.2 = 15.2$ kips (nominal)
$F_{COMB} = (.91 \times 13.9) + 6.2 = 18.9$ kips (ultimate)
V_{SF} = 17.5 kips to 21.0 kips (range)
} CALCULATED CAPACITIES BASED ON BEHAVIORAL MODELS

COMPARE $D_{y'}$ WITH F_{COMB} :

$D_{y'}$= 8.7 kips
F_{COMB}= 15.2 kips
} CALCULATED CAPACITY EXCEEDS FORCE AT FIRST YIELD BY 75%

$D_{y'}$= 15.0 kips
F_{COMB}= 18.9 kips
} CALCULATED CAPACITY EXCEEDS FORCE AT FAILURE BY 26%

COMPARE $D_{x'}$ WITH V_{SF} :

$D_{x'}$= 18.7 kips
V_{SF}= 17.5 to 21.0 kips
} FORCE AT FAILURE FALLS WITHIN RANGE OF CALCULATED CAPACITIES

Figure 6.47 Test 1A: Comparison of Theoretical and Experimental Results

shear-friction capacity, as calculated in Fig. 6.45, is in the neighborhood of 17.5 to 21.0 kips. The combined beam and direct tension nominal capacity is shown to be almost twice the actual pullout force on the deviator when first yielding of the deviator reinforcement occurs. This large difference between predicted yield and actual yield is probably due to the interaction of resistance mechanisms for forces in opposing directions. Comparing the calculated ultimate capacities to the actual failure loads shows that the combined beam/tension capacity exceeds the actual failure load in the y'-direction by 26 percent. The shear force on the block at failure, however, falls within the predicted range.

6.4.5 Conclusions. Analytical results based on simple models of the mechanisms controlling the behavior of the deviator agree fairly well with the actual loads on each deviator at failure. Reiterating, the models are necessarily simplified since the available experimental data for refining the models are limited to these first two tests. However, the assumptions made regarding the models are reasonable. Useful information from further experimental studies could include more extensive strain data to better define the distribution of stresses throughout the deviator reinforcement. In addition, isolation of the behavioral mechanisms (direct tension, beam action, shear-friction) in

individual tests could help to reinforce or refine the assumptions made regarding the behavioral models.

6.5 Effectiveness of Deviator Reinforcement Patterns

Based on experimental and analytical results, a few basic conclusions can be drawn regarding the effectiveness of each type of deviator reinforcement in contributing to the overall load carrying capacity of the deviator. The direction of the total force vector on the deviator is an important consideration when determining the effectiveness of each bar, since the same bar may act differently under different loading conditions.

6.5.1 Link Reinforcement. The link reinforcement is well detailed. The continuous hoop shape confines the critical tendon and provides excellent anchorage to tie the pullout force back to the strongest part of the box section (i.e. the web-flange intersection). The area of steel provided by the links is utilized efficiently; strain data indicate that these bars always develop beyond their yield points. For resistance to pullout, the links should be designed as the primary load carrying element, since the links carry the pullout forces directly and effieciently.

6.5.2 Outer Loop. The outer loops provide tension reinforcement for the flexural element formed by the top of the

block. The detailing of the loop is somewhat faulty because of the lap splice that is located at the top front edge of the loop which corresponds to a critical region of the block. This situation could be easily improved by relocating the lap so that it is anchored in the bottom flange of the box section. The outer loop, which more or less frames the outer surface of the block, probably limits cracking at the surface to a large extent, especially when pullout forces control the behavior of the deviator. This can account for the apparent lack of ductility in Test 1B. For these reasons, the outer loop reinforcement should probably be designed as a secondary load carrying element.

6.5.3 Inner Loop. For tendon geometries which induce significant shear forces in the deviation block, the inner loop bars work well as shear-friction reinforcement. When pullout forces dominate, these bars provide secondary beam reinforcement. Since beam reinforcement should probably be secondary to the link bars for pullout situations, and if the links bars are proportioned adequately, then the contribution of the upper arm of the inner loop to beam reinforcement is not really necessary. Instead, the shape of the inner loop could be modified to maximize its effiency as shear-friction reinforcement. If the upper arm of the inner loop were bent down to cross the block-bottom flange interface, forming a loop around the middle duct, then the area of shear-friction reinforcement would be doubled.

A 90 degree bend at the end of the bar, in the bottom flange, would provide the necessary anchorage. Such a modification should be investigated in future tests.

C H A P T E R 7

CONCLUSIONS AND RECOMMENDATIONS

7.1 Brief Summary

7.1.1 Literature Review. An extensive literature review traced the history and development of the technology connected with the use of external post-tensioning systems for bridges. The first known use of tendons external to the concrete section was in a German road bridge designed by Dischinger in 1928. The inavailability of high strength post-tensioning steel, and the then unknown effects of creep, shrinkage and relaxation rendered early post-tensioned structures ineffectual. Several externally post-tensioned bridges were built in France in the post WWII era. The use of external tendons evaded the Freyssinet prestressing patents and resulted in a number of successful and innovative structures. In the 1970's in France, considerable refinements in external post-tensioning technolgy were made through extensive use of external tendons for retrofit and repair of bridges. External tendons were first introduced in American concrete bridge construction in the Florida Keys bridges in 1980.

The use of external tendons poses inherent advantages as well as disadvantages. Advantages include the omission of tendon ducts from the concrete cross section which reduces congestion and avoids interference of the ducts with the reinforcing cage.

The accessability of external tendons ameliorates stressing and grouting procedures and allows the possibility of tendon replacement. Friction due to wobble is eliminated with external tendons and some fatigue advantages are apparent as well. The use of external tendons in segmental span-by-span construction has proven to save time and materials. Some disadvantages associated with the external post-tensioning include potential vibration problems for long unrestrained tendon lengths and limitations on available tendon eccentricity. In addition, unbonded, external tendons may result in reduced flexural efficiency and reduced ductility relative to comparable systems with internal tendons. Distribution of concentrated forces produced by external tendons at attachment points pose additional problems.

Deviators are required to create draped profiles for external tendons. Typical deviators for box girder bridges can be classified by shape into three catagories: blocks, ribs and diaphragms. The detailing of external tendon ducts embedded in deviators (and in anchorage zones) warrants special attention. The recommended minimum duct diameter corresponds to a duct area of 2.5 times the tendon area, an increase over requirements for internal tendons. The minimum radius of curvature for external tendon ducts varies from 10 to 20 feet depending on location (i.e, in anchorages or deviators) and tendon size. In addition,

since aligning ducts to meet the spatial geometry of the deviated external tendon is often difficult, special measures must be taken to avoid problems due to duct misalignment.

Design criteria which have been used to proportion and detail deviator reinforcement are not well known. Traditional design approaches do not directly treat the design or required safety of saddle or block type deviators. No generally accepted models exist for determining the diffusion of concentrated forces at deviators.

Problems have occurred with deviators in several existing bridges. The most common form of damage has been spalling and local cracking around misaligned external tendon ducts. Structural cracking has also been reported for both block and diaphragm type deviators.

The most significant experimental research projects concerning external post-tensioning currently known include two simple-span girder test series. One of these was performed at the Laboratory at Saint-Remy-les-Chevreuse, France, by SETRA-CEBTP, while the other was performed at the PCA Construction Technology Laboratories in Illinois. A scale model test of a three-span box girder bridge with external tendons is currently in preparation at the Ferguson Structural Engineering Laboratory. The only other known experimental research concerning deviators

is currently ongoing at the Saint-Remy laboratory, although the scope of that project seems limited to the behavior of the tendon in the deviator and not to the behavior of the deviator itself.

7.1.2 Experimental Study. Experimental investigation of deviator behavior was initiated by two tests of typical deviation blocks. A generalized test setup was designed and constructed. The setup adapts to accomodate a variety of specimen sizes, tendon layouts and loading alternatives. A typical structure was chosen from among existing U.S. bridges with external tendons to serve as a prototype for initial testing. A basic box girder section (minus the cantilevered wings), modelled goemetrically after the prototype cross section, was designed and reinforced in accordance with AASHTO minimum specifications. The 1/3 scale box section was chosen as a basic test unit which would be adaptable to a variety of deviation details.

Two deviation blocks from adjacent segments in the prototype bridge were chosen for the 1/3 scale model tests. The reinforcement in the two deviators was identical. The scaled reinforcement in the test deviators was provided by microbars having an average yield strength of 45 ksi. The primary reinforcement, which consisted of three bent bar types (labeled link, outer loop and inner loop), were instrumented with a number of embedded strain gages. Secondary deviator reinforcement,

which included additional web and flange reinforcement for the box section, was not instrumented. The tendon layout differed in the two test deviators. "Block A" deviated three tendons. The deviation forces produced a pullout component (directed perpendicular to the top of the deviation block) which was nearly equal to the lateral shear component (directed parallel to the top of the deviator) on the deviator. "Block B" contained only two external tendons. The tendon layout for Block B produced predominantly pullout forces on the deviator.

The deviation blocks were subjected to a full range of loading by incrementally increasing the stress in the deviated tendons. Deviator deflections, deviator reinforcing strains, and cracking patterns were monitored continuously throughout both tests. The mode of failure observed in the two tests differed markedly. Block B exhibited a relatively brittle failure. Visible cracking on the exterior of the block was not particularly excessive when the deviator exploded violently and unexpectedly. In contrast, Block A experienced a relatively ductile failure. The block developed sizable cracks and noticible deformations before finally rupturing in an explosive manner.

Cracking patterns and strain data suggested the influence of three behavioral mechanisms on the overall behavior

of the deviation blocks. These mechanisms included direct tension action provided by the link reinforcement, beam action of the top portion of the block, and shear-friction action across a plane of weakness through the level of the ducts. It was apparent from test data and observations that the behavior of Block B was governed by a combination of the direct tension and beam mechanisms, while the shear transfer mechanism controlled the ultimate behavior of Block A.

Three behavioral models (a direct tension model, a beam model, and a shear-friction model) were investigated analytically and compared with test results. Based on test data and model assumptions, the effectiveness of each pattern of primary deviator reinforcement was evaluated.

7.2 Conclusions

Based on the limited test data available from the two deviator tests, the following conclusions may be drawn:

1) The typical deviation detail which was tested safely carried the design load. The apparent factor of safety (ratio of actual ultimate capacity to nominal maximum design load) was approximately 2.4 in both tests.

2) The direction and the magnitude of the total force component on the deviator are equally important in determining the load resistance capabilities of the deviator reinforcement.

3) The link reinforcement was well detailed. It provided the most efficient resistance to the pullout force from the deviated tendon which was confined by the link.

4) Beam action contributed significantly to the resistance of the deviators to pullout forces.

5) Shear-friction transfer mechanisms became critical for the test with tendon geometry which produced significant lateral shear forces on the deviator (Block A).

6) The apparent ductility of the deviator (ratio of ultimate load to yield load) depended on the predominant failure mechanism.

7) Relatively simple models could be used to predict the approximate ultimate capacity of the deviator.

7.3 Interim Design Recommendations

Based on the preliminary results of the deviator study, some qualitative recommendations can be made regarding the design and detailing of deviators which are similar to the typical deviation detail tested.

1) The direction of the total force component on the deviator is an important consideration in the proportioning of deviator reinforcement. The same bar may behave quite differently under different loading conditions and must be

detailed considering direction as well as magnitude of the deviation forces.

2) Link reinforcement should be designed as the primary load carrying element for resisting pullout forces. Nominal design capacity is computed as the total bar area times the nominal yield strength of the reinforcement. Ideally, the inclination of the link axis should correspond to the direction of the force component from the tendon which is restrained by the link. However, for standardizing a deviator design, a less efficient axis perpendicular to the top face of the block is a practical choice.

3) Even though transverse beam action above the deviated tendons has been shown to provide a significant contribution to pullout resistance (i.e., resistance to forces perpendicular to beam element), until refinements in modelling can be made with information from further test data, the designer should not count on significant beam action. However, light reinforcement patterned after the outer loop bars used in this study should be provided for deviator crack control. Also, any lap splices of the deviator loop reinforcement should be anchored in the box girder section and not made in the deviator itself.

4) Resistance to transverse shear forces should be provided by well distributed shear-friction reinforcement. Shear-friction reinforcement should be additive to the direct tension

reinforcement. The weak plane for shear transfer should be taken through the level of the ducts, where the least area of concrete is available to contribute to shear-friction.

7.4 Future Research

Continued experimental investigation should address the uncertainties which were encountered in the first two deviator tests.

Due to limited data, several assumptions and simplifications were necessary for analytical modelling. Isolation of the behavioral mechanisms and more extensive strain intrumentation in future specimens could provide additional information for refining these models. Other parameters which appear to affect deviator behavior include variation in deviation angle combinations and possibly bond characteristics of the deviator reinforcement. These parameters should be investigated in future testing. In addition, reinforcement patterns could be reproportioned and/or modified to test potential improvements in efficiency.

As more experimental data become available, other analysis methods should be investigated. Finite element analysis leading to the development of a strut and tie model should prove interesting.

APPENDIX

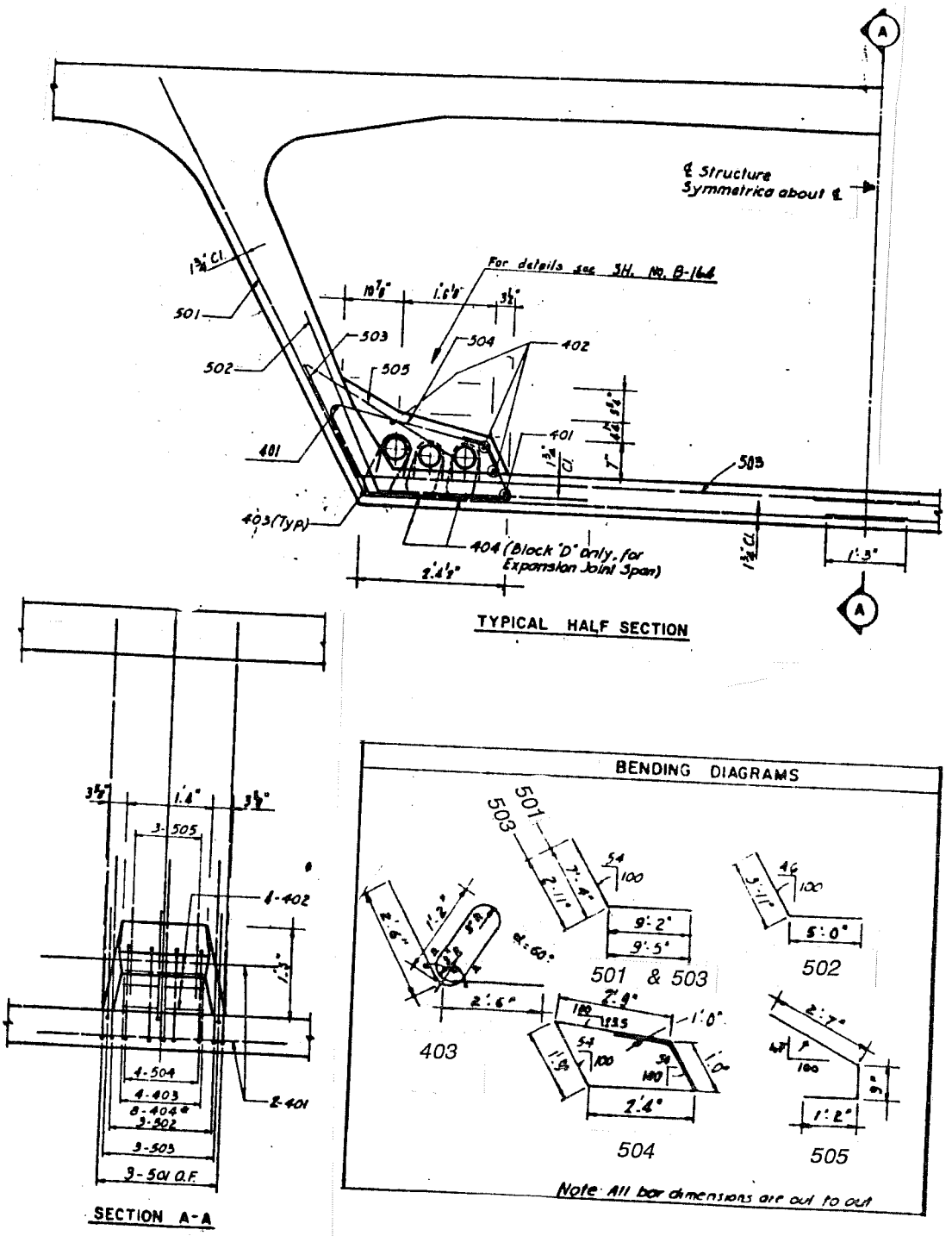

Figure A.1 Prototype Deviator Reinforcing Details

REFERENCES

1. Billington, D. P., The Tower and the Bridge, Basic Books, Inc., New York, 1983.

2. Peters, T. F., Billington, D. P., and Dubas, P., et al, The Development of Long-Span Bridge Construction, Eidgenossische Technische Hochschule (ETH), Zurich, Third Ed., 1981, p. 93.

3. Virlogeux, M., "La Precontrainte Exterieure," Annales de l'Institut Technique du Batiment et des Travaux Publics, December, 1983.

4. Chatelain, J., "Bilan de Sante des Anciens Ouvrages a Precontrainte Exterieure," Formation Continue La Precontrainte Exterieure au Beton, June, 1984.

5. Leonhardt, F., "Procede de Construction Par des Cycles de Betonnage en Coffrage Fixe et Cycles de Poussage," Annales de l'Institut Technique du Batiment et des Travaux Publics, January 1973.

6. Lossier, H., "Le Pont de Villeneuve-Saint-Georges: Conception de l'Ouvrage et Problemes Poses par sa Realisation," Supplement aux Annales de l'Institut Technique du Batiment et des Travaux Publics, July-Aug. 1953.

7. Menn, C., Stahlbeton-brucken, Springer-Verlag, Wien, 1986, pp. 28-29.

8. LeCroq, P., "Precontrainte Additionelle," Renforcement, Reparation des Structures, Annales de l'Institut Technique du Batiment et des Travaux Publics, Jan. 1983, pp. 96-109.

9. Podolny, W. and Muller, J., Construction and Design of Prestressed Concrete Segmental Bridges, John Wiley and Sons, Inc., 1982.

10. Combault, J., Poineau, D., et al, "Le Viaduc de Saint-Agnant," Extrait de la revue Travaux, Jan. 1985, pp. 1-13.

11. Thao, P., Piron, V., and LeCroq, P., "Le Viaduc de Sermanez," Extrait de la revue Travaux, Jan. 1985, pp. 15-22.

12. Causse, G., Duclos, T., et al, "Construction du Deuxieme Pont sur la Moselle a Pont-a-Mousson," Extrait de la revue Travaux, Jan. 1985, pp. 23-36.

13. Podolny, W., "The Cause of Cracking in Post-Tensioned Concrete Box Girder Bridges and Retrofit Procedures," Journal of the Prestressed Concrete Institute, Vol. 30, No. 2, March/April 1985, pp. 82-139.

14. Virlogeux, M., "Evolution de la Conception des Ponts de Portee Moyenne," Proceedings of the Ninth Congress of the Federation Internationale de la Precontrainte, Volume 1, Seminar Papers, June 1982, pp. 7-30.

15. Lin, T. Y., and Burns, N. H., Design of Prestressed Concrete Structures, Third Ed., John Wiley and Sons, Inc., New York, 1981, pp. 173-174.

16. Hoang, L. H., and Pasquignon, M., "Essais de Flexion sur des Poutres en Beton Precontraintes par des Cables Exterieurs," Volumes 1 and 2, Contrat SETRA-CEBTP 1985, Dossier de Recherche 91017, November 1985.

17. Sowlat, K., and Rabbat, B. G., "Testing of Segmental Girders," Final Report to Figg and Muller Engineers, Inc., Project No. 0217, July 1984.

18. Florida Department of Transportation, "Criteria for Bridge Construction and Design," Chapter 4: Design Criteria for Segmental Bridges, January, 1987, pp. 27-28.

19. Foure, B., and Hoang, L. H., "Essais de Traction sur des Cables Appuyes sur un Deviateur," Etude Preliminaire, Contrat SETRA-CEBTP 1983, Dossier de Recherche 91.024, March, 1984.

20. Figg and Muller Engineers, Inc., "Segmental Report No. 15, Sunshine Skyway Update," February, 1986.

21. Building Code Requirements for Reinforced Concrete, (ACI Standard 318-83), Detroit, American Concrete Institute, 1983, pg. 318-82.

22. Standard Specifications for Highway Bridges, Thirteenth edition, American Association of State Highway and Transportation Officials (AASHTO), 1983.

23. Post-Tensioning Manual, Fourth edition, Post-Tensioning Institute, Pheonix, Arizona, 1985.

24. Figg and Muller Engineers, Inc. - correspondence

25. Precast Segmental Box Girder Bridge Manual, Post-Tensioning Institute (PTI) and Prestressed Concrete Institute (PCI), Chicago, Illinois, 1978, pg. 22.

26. Commentary on Building Code Requirements for Reinforced Concrete (ACI Standard 318R-83), Detroit, American Concrete Institute, 1983, pp. 71-73.

VITA

Lisa Louise Carter was born in Baltimore, Maryland, on June 22, 1961, the only daughter of Louise Lubinski Carter and Robert Earl Carter. She graduated with honors from Perry Hall Senior High School, Perry Hall, Maryland in June of 1979. While attending the Georgia Institute of Technology, she worked for the Duke Power Company in Charlotte, North Carolina as a co-op student. She graduated with highest honors in May, 1984 and was awarded the degree of Bachelor of Science in Civil Engineering, Co-operative Plan. In September, 1984, she entered the Graduate School of the University of Texas at Austin, as the Phil M. Ferguson Graduate Engineering Fellow.

Permanent Address: P.O. Box 522
18 Cypress Court
Grand Island, Florida

This thesis was typed by Lisa L. Carter